MODELLING AND CHARACTERISATION OF CONDUCTING POLYMER CHEMORESISTORS

by

Paul Ingleby

School of Engineering

University of Warwick

A thesis submitted to the University of Warwick

for the degree of Doctor of Philosophy

March 1999

Contents

Heading	Page

List of Figures

List of Tables

Summary

Concerns that some respiratory diseases may be related to the level of urban air pollution have added to the call for renewed interest in the monitoring of air quality. Most air pollutants originate from industrial, domestic or automotive combustion processes. The monitoring of such processes, using either multi–component gas sensing or 'electronic noses', has become an important issue for the alleviation of environmental problems. Unfortunately, arrays of sensors based on conducting polymer technology suffer with interference of their baseline and response characteristics due to changes in temperature or humidity.

The problems associated with such device characteristics can be ameliorated either by the employment of sampling systems that can regulate the exposure conditions of the sensors, improvements in the nature of the sensor materials, or through parametric compensation routines in the data analysis and pattern recognition stages of such instruments. Mathematical models can be employed in all three of these stages for humidity and temperature compensation of the sensors. Such models would help in the optimisation of the analyte delivery system, the understanding of the sensor elements and in the mathematical compensation of sensor signals.

The aim of this thesis is to build models (either physical or empirical) of the response of poly(aniline) and poly(pyrrole) based sensors when exposed to example types of environmental pollutants. The target analytes for this study were chosen to represent an example of a volatile organic compound (i.e. ethanol) and a redox inactive gas (i.e. carbon dioxide). Although carbon dioxide is normally considered a greenhouse gas rather than an environmental pollutant, the more traditional targets such as carbon monoxide, ozone and compounds of nitrogen or sulphur oxides, have previously been detected using metal oxide sensors that do not respond to CO_2. The target species were exposed to the sensors at a range of humidities and temperatures and the resulting sensor characteristics were modelled.

The research objectives have been fulfilled in that detailed results have been obtained for the magnitude of the static response of typical poly(pyrrole) and poly(aniline) sensors when exposed to both ethanol and carbon dioxide. Theoretical or empirical models have been developed characterising these effects and also the influence of humidity and temperature. These models demonstrate good correlation to the experimental data. A dynamic model of the transient response of the polymers to ethanol has also been investigated. Although further work developing models based entirely on the theory of the interaction between a species and the polymers is required, the results and theories presented in this study provide an useful contribution in this research area.

Acknowledgements

Declaration

The work described in this thesis is entirely original and my own, except where otherwise indicated.

Parts of this work have been presented at international conferences:

1. *Eurosensors X, 8–11 September, 1996, Leuven, Belguim,* Dual resistance–mass polymeric sensor for improved gas sensing, P. Ingleby, J. A. Covington, J. W. Gardner and P. N. Bartlett.

2. *Eurosensors XII, 13–16 September, 1998, Southampton, UK,* Effect of micro–electrode geometry on the response of thin–film poly(pyrrole) and poly(aniline) chemoresistive sensors, P. Ingleby, J. W. Gardner and P. N. Bartlett.

Parts of the work contained in this thesis have also been published in the scientific literature:

3. J. W. Gardner, M. Vidic, P. Ingleby, A. C. Pike, J. E. Brignell, P. Scivier, P. N. Bartlett, A. J. Duke and J. M. Elliott, Response of a poly(pyrrole) resistive micro–bridge to ethanol vapour, *Sensors and Actuators B,* **48**, (1998) 289-295.

4. P. Ingleby, J. W. Gardner and P. N. Bartlett, Effect of micro–electrode geometry on the response of thin–film poly(pyrrole) and poly(aniline) chemoresistive sensors, *Accepted for publication in Sensors and Actuators.*

5. P. Ingleby, J. W. Gardner, P. N. Bartlett and J. M. Elliott, A competitive binding model for the response of poly(pyrrole) and poly(aniline) chemoresistors, *Under Preparation.*

Selected Abbreviations and Acronyms

TERM	DEFINITION
ADC	Analogue to Digital Converter
ASIC	Application Specific Integrated Circuit
ANN	Artificial Neural Network
BAW	Bulk Acoustic Wave
BSA	Butanesulfonate in acid
DAC	Digital to Analogue Converter
DAQ	Data Acquisition
DIO	Digital Input/Output
DSA	Decanesulfonate in acid
EMC	Electromagnet Compatibility
ESR	Electron Spin Resonance
HpSA	Heptanesulfonate in acid
HxSA	Hexanesulfonate in acid
I.C	Integrated Circuit
I.D	Inside Diameter
LED	Light Emitting Diode
LPCVD	Low Pressure Chemical Vapour Deposition
LUT	Look Up Table
MFC	Mass Flow Controller
MFM	Mass Flow Meter
MHP	Micro Hotplate
MOS	Metal Oxide Semiconductor
O.D	Outside Diameter
OSA	Octanesulfonate in acid
Pan	Poly(aniline)
PARC	Pattern Recognition
P.C	Personal Computer
PCB	Printed Circuit Board
Ppy	Poly(pyrrole)
PSA	Pentanesulfonate in acid

PTFE	Polytetrafluoroethylene
PM$_{10}$	Particulate Matter (diameter <10 µm)
R.H	Relative Humidity
R.T	Room Temperature
SAD	Sensor Array Device
SAW	Surface Acoustic Wave
SCE	Saturated Calomel Electrode
SCS	Single Crystal Silicon
SEM	Scanning Electron Microscope
SPCO	Single Pole Change Over
SRL	Sensors Research Laboratory
TTL	Transistor–Transistor Logic
UV	Ultra–Violet
VI	Virtual Instrument
VOC	Volatile Organic Compound

_____

CHAPTER 1

Introduction

The aim of this chapter is to briefly introduce the concept of gas and odour detection, and to outline the ideal characteristics of a gas sensing system. Typical applications of chemical sensors will be discussed and the concept of electronic noses will be introduced. Particular emphasis will be placed on the nature and suitability of conducting polymers for use in novel gas and vapour sensors.

The research objectives of this study and an outline of the thesis contents are given at the end of this chapter.

1.1 Characteristics and Applications of Chemical Gas Sensors

The basic function of any sensing device is to convert a quantity about which information is sought, or the measurand, into a signal which can be usefully processed or examined, called the sensor output. The measurands can be crudely divided into six forms [1.1]: chemical; electrical; magnetic; mechanical; radiant; and thermal. Each of these forms of signal input can also be employed as the form of sensor output. However, the most common form of output signal from a sensor is electrical. In the case of gas sensors, the input signal is normally a physical gas concentration. This concentration is converted by the sensor to an electrical signal such as resistance, voltage or frequency, which can then be communicated to the operator, usually via

_____

some type of signal processor or modifier and output signal actuator. The type of signal

modifier depends on the sensor technology employed and the information required.

The output actuator can take many forms ranging from the screen of a computer

monitor to an alarm bell. A block diagram of a typical sensor system [1.2] is shown in

Figure 1.1.
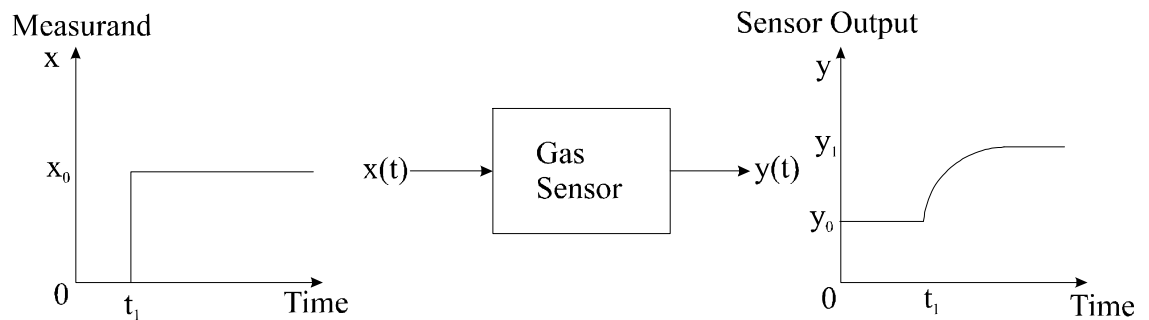
Figure 1.1 A block diagram of a simple gas sensor system with typical input (left) and output (right) signals shown (power supply not shown).

In a basic gas sensor system such as shown above, the measurand is usually the

concentration of some target species. At all times prior to the exposure of this analyte

(when the time is less than t_1) the sensor output should be equal to its baseline value

(y_0), which is shown here as non–zero. There are a number of factors which can effect

the baseline signal of typical gas sensors, these include pressure, humidity and

temperature. At a time, t_1, the sensor is exposed to a step in the input gas concentration

(from 0 to x_0). This exposure results in a response from the gas sensor, which alters its

output from y_0 to y_1. The steady–state magnitude of the response is equal to the

difference between the two signals (i.e. $\Delta y = y_1 - y_0$ as $t \rightarrow \infty$). Many research groups

now describe the static response of a gas sensor either by the dimensionless parameter

associated with the sensors fractional response ($\Delta y/y_0$) or by the absolute sensitivity of

the sensor, which is the ratio of the change in output signal due to the change in the measurand (dy/dx). The dynamic response of a sensor system is exponential for a first order system and the response time is generally defined as the time required for the output signal to achieve a certain percentage of its steady–state value. The percentage employed for these measurements are usually 63% (τ_{63}) or 90% (τ_{90}).

It is now possible to discuss some of the attributes required in an ideal sensor system. Most importantly, the sensors must give large, reproducible responses to the target species. The sensitivity of the sensors should therefore be constant over the range of the input measurand, and the removal and re–introduction of an input signal should yield identical system outputs. In an ideal gas sensing system the sensors would also be very selective, responding only to the target species and not being effected by other factors, such as humidity and temperature. The maximum size of the sensor response would be calibrated to be equal to the maximum possible output signal. In this way the resolution of the system would also be maximised. In a model sensing arrangement, the relationship between the magnitude of the measurand and the magnitude of the sensor output is ideally linear. This means that the static response of the sensor system would always be proportional to the size of the input signal within the intended measuring range. It is also important that the output signal from the system should return to its original baseline value, y_0, when the measurand is removed (all other conditions remaining constant). The response can then be described as completely reversible. There should be no drift in the characteristics of either the baseline or the response of the sensors either due to ageing or due to poisoning. Finally, the response and recovery times of an ideal detection system would be zero (i.e.: both τ_{65} and τ_{90} would be zero). This means that the ideal system would be zeroth order and so respond instantaneously when exposed to a target measurand.

_____

In real gas sensor systems these ideal characteristics are not observed. Some of the more common problems encountered include non–linear responses, where the output signal is not proportional to the input, low sensitivity, slow response times, interference due to external conditions, and drift in both the response and the baseline characteristics of the system. These problems can be combated through improvements in either the sensing elements (by changing the chemistry or the architecture of the active sensor elements) or the signal modifiers (by improving the interface electronics or data processing algorithms).

The number of possible applications of lightweight, portable gas sensing systems is huge. Perhaps the most common application of chemical gas sensors is in the area of domestic gas detectors. These simple and inexpensive systems are used in the prevention of gas explosions by triggering alarms when a given gas concentration is attained. In most domestic gas detection systems a thermistor is included in the circuit in order to compensate for humidity and temperature fluctuations. Similar systems can be employed in automatic ventilation applications. Gas detection systems are also now being employed in the monitoring of alcohol concentration in the blood (alcoholaemy). These systems monitor the level of alcohol vapours found in human breath [1.3].

A summary of other important fields in the application of chemical gas sensors with some typical examples [1.4] is shown in Table 1.1.

Table 1.1 Typical applications of chemical gas sensors.

Field of application	Typical example
Automotive	Engine control, air quality in car emissions

_____

Aerospace	Engine control, air quality in cabin, emissions
Agriculture	Fertiliser and pesticide control
Chemical analysis	Laboratory testing of materials
Safety (fire)	Fire warnings in mines, buildings, houses etc.
Process control	Production of chemicals, foodstuffs, etc.
Environmental monitoring	Detection of pollutants in the air, water or soil
Medicine	Anaesthetic gases, diagnostics, biochemistry
Customs	Illegal and dangerous substances
Quality control	Smell/flavour of drinks, foodstuffs tobacco

One of the most significant and constantly growing areas for the application of gas sensors is in the monitoring of air pollution. Advances in the sensitivity and selectivity of thin film sensors has initiated research into the possibility of introducing this type of technology to aid in the detection and measurement of low concentrations of environmental pollutants in the atmosphere. In the 1950s and 1960s the problems of air pollution in the UK were immense. In one incident in December 1952, 4000 excess deaths in London were attributed to the high levels of air pollution [1.5]. At this time the main pollutants were smoke particulates and sulphur dioxide (SO_2). Although the clean air acts of 1956 and 1968 combined with the switch of most domestic heating systems to gas reduced these particular pollutants to acceptable levels, recent studies have shown that other pollutants, principally associated with traffic emissions, are having serious effects on urban air quality. Concerns that some respiratory diseases may be related to the level of urban air pollution have led to renewed interest in the monitoring of air quality. Current air quality monitoring techniques vary for the diverse array of pollutants which have to be monitored. Some typical techniques are shown in Table 1.2.

Table 1.2 Current detection techniques for common urban atmospheric pollutants.

Pollutant	Technique
NO_2	Photomultiplier tube detects light emitted in a chemiluminescent reaction between ozone and NO (produced by NO_2 thermal decomposition)
SO_2	Gas phase fluorescence using an excitation wavelength of 216 nm and measuring fluorescence in the range 240-420 nm
CO	IR absorption at 4.6 μm or pellistors
Ozone	UV absorption at 254 nm, or semiconducting oxides
Hydrocarbons	Cryogenic preconcentration and subsequent gas chromatography with flame ionisation detection
PM_{10}	Particulate matter (10 μm diameter and less) drawn through a size selective inlet onto a filter which is attached to a oscillating microbalance

These techniques can require complex and cumbersome equipment that could certainly be assisted if not replaced by simple gas sensor systems based on either metal oxide or polymer sensors.

Other species of air pollutant which are of particular interest include CO_2 and volatile organic compounds such as benzene, toluene and ethanol. The monitoring of CO_2 is vital due to its role as a greenhouse gas and consequent effect on climate change. The detection of redox inactive gases such as CO_2 cannot be accomplished using commercially available sensors based on oxidation or reduction mechanisms. There is therefore a need for a low–cost, portable, reproducible CO_2 sensor. The detection of volatile organic compounds is important due to their role in ozone formation. Although much work has been published on the effects of this type of compound on conducting

polymer sensors [1.6, 1.7 and 1.8], a full characterisation and model of its interaction with the polymers has not yet been published. It is these categories that form the target analytes in this study.

1.2 Electronic Noses

A novel and comparatively recent application of gas sensors is in the production of artificial olfactory systems or 'electronic noses'. These instruments aim to mimic the mammalian olfactory system by using arrays of chemical sensors. Such systems exhibit a high degree of sensitivity for odours and are also able to discriminate between different odour types. One of the first artificial noses based on the electrochemical effects of odorants was produced in 1964 by Wilkens and Hartmann [1.9]. Since this early work, advances in the development of artificial noses has paralleled work on the understanding of biological olfactory systems [1.10]. In a typical mammalian nose a sensing mucosa has tens of millions of sensing cells. These receptors (primary neurones) demonstrate responses to a wide variety of odorous stimuli. Between 10 and 20 thousand of the primary neurones communicate signals to each of the secondary neurones contained within the olfactory bulb. The signal from the secondary neurones then passes through the higher olfactory pathways to the olfactory cortex. In order to recreate such a sensing system, artificial replacements for each of the three main olfactory sections have to be employed. A model nose would therefore use chemical gas or vapour sensors in order to obtain the initial odour signals (mimicking the primary neurones), electronic signal processing (to replace the secondary neurones) and data processing algorithms or neural networks (to imitate the olfactory cortex). Basic

experimental systems based on this model architecture have been investigated since Persaud and Dodd published a seminal paper in 1982 [1.11].

Figure 1.2 shows the basic stages of signal processing in a typical electronic nose system [1.12]. The sample space is determined by the chemical composition of the samples and can take the form of either a single compound (for a simple odour $j = 1$) or a number of compounds (in a complex odour $j > 1$), at a concentration of X_j.
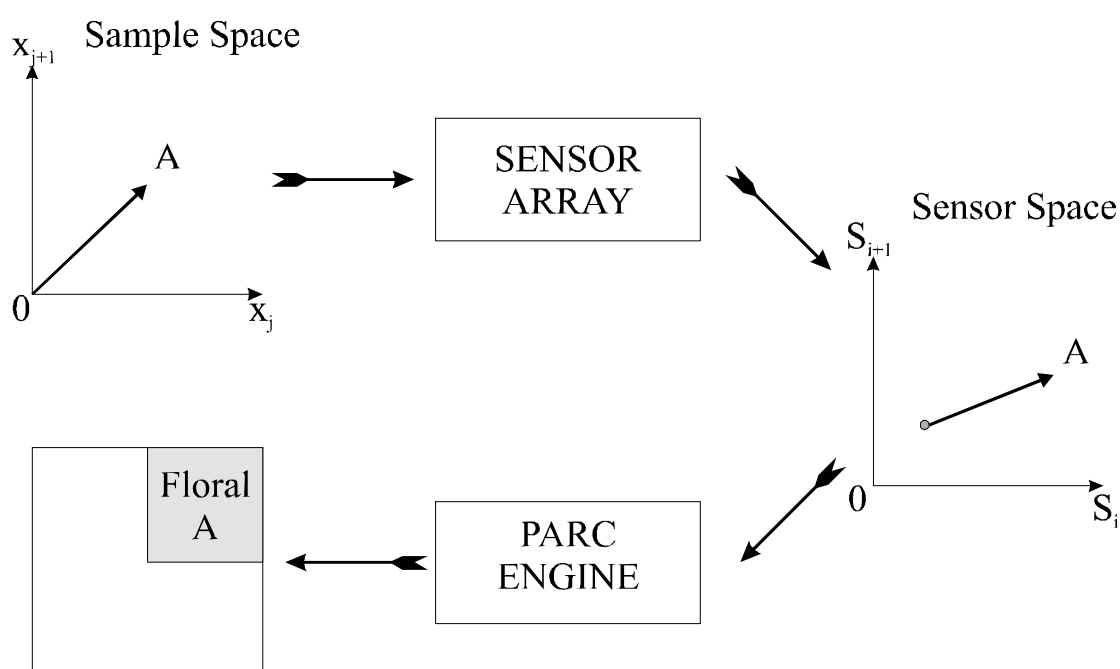
Figure 1.2 Signal processing in an electronic nose.

An array of i: 1 to n sensors responds to the sample and therefore maps one point in sample space into one in sensor space. This is the most important stage in the production of current electronic nose and generally determines its resolving power. Ideally the sensors should respond, with broadly overlapping sensitivities to a range of simple volatile organic molecules. Therefore, not all of the sensors in an array would respond in the same manner to an identical odour. This technique enables

_____

discrimination between odours with as little as 3 sensor elements i.e. i = 3 [1.11],

although the number of sensors employed at this stage is also significant. Amrani et al.

have demonstrated that the discriminating power of a sensor can also be improved

through the type of interrogation method employed [1.13]. They have shown that

multi–frequency measurements of the a.c. response of conducting polymer sensors

could lead to powerful, discriminating instruments with few sensor elements [1.14,

1.15].

The sensitivities of the sensors employed in electronic noses must be matched to

the typical concentration of the volatiles for which detection is required and ideally

response times of the sensors must be fast. Other requirements of the sensors employed

in an electronic nose are similar to those discussed for the application to general gas

detection (section 1.1).   These include reversibility, and reproducibility in both

manufacture and response characteristics.

The development of sensors for use in electronic noses has been aided by

research interest in multi–component gas sensing using arrays of nonspecific chemical

sensors [1.16]. There is only a subtle difference between the two areas and therefore

research advances in one area are usually transferred into the other.   In multi–

component gas sensing an array of chemical sensors is employed to estimate

concentrations of gases or gas mixtures [1.17 to 1.20]. Electronic noses characterise

mixtures of odorant molecules sometimes containing hundreds or thousands of volatile

compounds.

If the resolution of the samples in sensor space are sufficiently distinct then the

pattern recognition (PARC) engine should be able to classify the odours using a range

of techniques (such as metric transformations, back–propagation techniques or self–

organising maps) [1.17, 1.21 to 1.26]. In reality, limitations in the performance of the

_____

pattern recognition techniques and the sensor characteristics hamper the overall efficiency of electronic nose systems. Particular problems occur due to the lack of sensitivity or selectivity of the sensor elements, and interference of their responses by environmental factors such as humidity and temperature.

There are many types of sensor that can be employed as the individual elements in an electronic nose, although a substantial amount of research has been directed towards sensors based on inorganic semiconducting materials such as oxides and catalytic metals. This type of device suffers from a high power consumption when employed as a thick film sensor. Integrated thin film versions have been made that require less power per device, but these tend to be more expensive to produce and generally suffer from poor stability [1.27, 1.28]. The employment of organic materials such as conducting polymers can therefore offer a number of advantages. Firstly, polymer sensors require far less power to operate and are cheaper to produce than their inorganic counterpart. There is also a much wider choice of materials that can be employed to produce diverse sensor arrays. The combination of organic materials with different functional groups in order to control their interaction with distinct classes of odorant molecule is also possible. Moreover, polymer sensors tend to give better reproducibility and are easier to process than oxides. Methods that can be used include electrochemical deposition, spin–coating, screen–printing and Langmuir–Blodgett techniques. The effects of humidity and temperature on the response of conducting polymer sensors is discussed in depth in this study.

1.3 Conducting Polymers as Gas Sensors

_____

The electrochemical production of polymer membranes has been widely investigated since the first electrochemically prepared polymer was reported by Dall'Olio [1.29] in 1968. However, the first detailed characterisation of electrochemically fabricated polymers was not possible until 1979 when Diaz et al. produced the first poly(pyrrole) films that were not only highly conductive, but were also stable in air [1.30]. The development of conducting polymers as gas and vapour sensors began when the materials demonstrated rapid reversible responses to a range of compounds at room temperature [1.31, 1.32 and 1.8]. The wide variety of monomer types that can be polymerised to give conducting polymer films [1.33 to 1.35] combined with the possibility of producing new substituted monomers, is one of the main attractions of employing conducting polymers as gas and vapour sensors. Examples of commonly studied conducting polymers are shown in Figure 1.3.

Poly(pyrrole)   Poly(aniline)   Poly(thiophene)
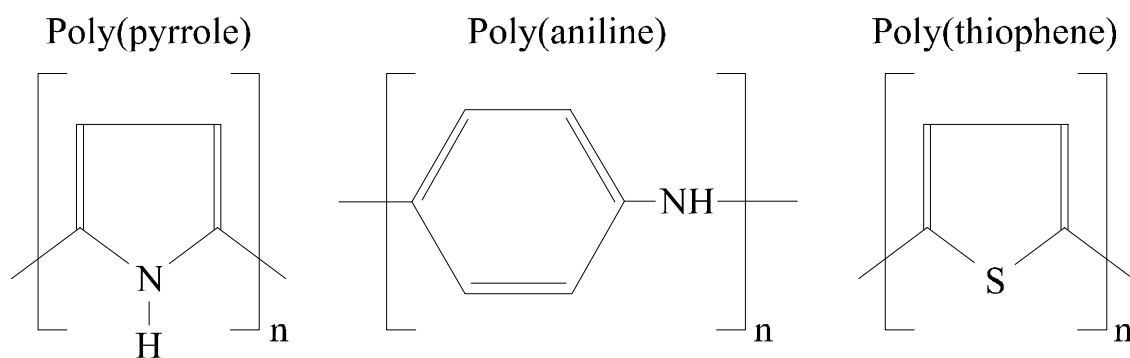
Figure 1.3 Examples of some commonly studied heterocyclic and aromatic conducting polymers.

Electro–active conducting polymer sensors can be fabricated by controlled electrochemical deposition of a film across a narrow gap between two inert electrodes. Micro–electrode structures are formed by photolithographic methods and are made of gold. However, some of the earlier polymer sensors were created by sputtering gold

_____

onto both sides of thin Mylar films and then encapsulating the resulting gold/Mylar/gold sandwich so that only the edge was exposed [1.6].

The deposition process for conducting polymers requires the monomer to react to form an extended conjugated system. This can be achieved either chemically or electrochemically. However, electrochemical techniques allow for precise control of the polymer deposition by varying the growth conditions such as the current employed and the time allowed for the growth to occur. In order to electrochemically grow a conducting polymer, the monomer must be dissolved in an appropriate solvent. The choice of solvent has a large effect on the morphology, electrical conductivity and electroactivity of the resulting polymer [1.36]. The technique employed during the deposition of the devices used during this study was identical to those developed previously [1.6, 1.37, 1.38] and known to yield reproducible, useful devices. Details of the deposition process can be found in Chapter 2 (section 2.4). Common deposition techniques normally begin with the generation of a radical cation formed by oxidisation at the surface of the electrode. This radical can then react either with a second radical to give a dimer, or with a neutral monomer followed by subsequent oxidisation to give the dimer [1.39, 1.40]. The result is growth of a polymer film on the working electrode. A schematic overview of the electropolymerisation process is shown in Figure 1.4. A polymer grown in such a manner would be oxidised and present as a polycation. The charge on the polymer is therefore balanced by the incorporation of anions from the solution as it grows. Typically a single polymer anion is associated with between 3 (trimer) and 6 (hexamer) monomer units in the polymer chain. The properties of the final polymer therefore depend, not only on the choice of monomer but also on the choice of counter–ion.
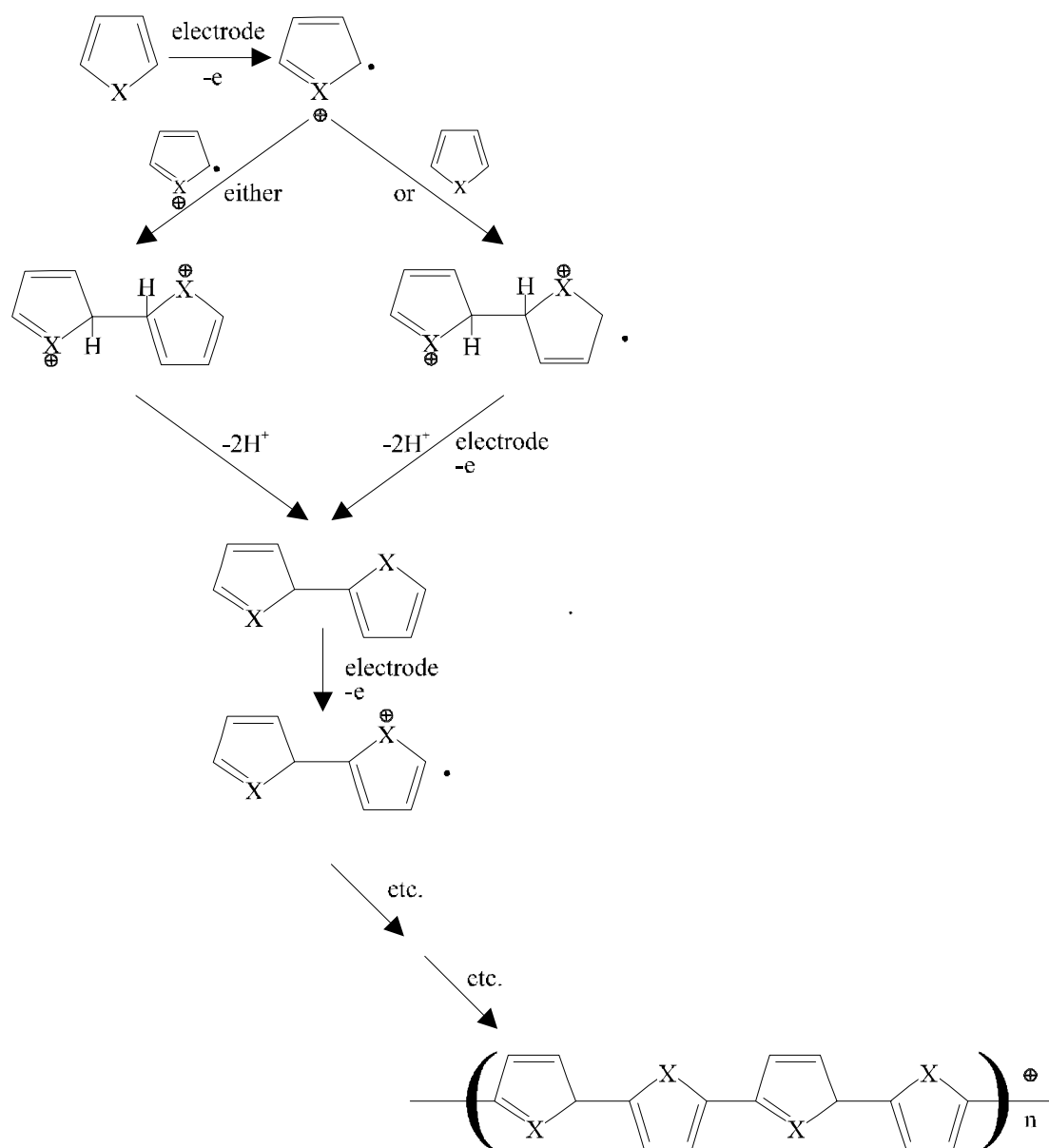
Figure 1.4 The general mechanism for the electropolymerisation of monomers such as pyrroles and anilines, (pyrrole tetramer shown here).

The range of conductivities that have been reported in polymeric membranes covers some 15 orders of magnitude, from the undoped polymers which have very low conductivities, to the extremely high conductivities which are found in the heavily doped regime. This large range has hampered investigations into the conduction

_____

mechanisms occurring within the films. Research has been further impeded through the alteration of the conductance mechanisms under different doping conditions.

The simplest view of the conduction mechanism occurring within a polymer [1.41] is that radical cations are produced due to a charge transfer process that occurs between the polymer backbone and the doping ions. The radical cations are thought to be delocalised π–electrons that have been removed from the polymer backbone. A single radical cation is sometimes termed a polaron and has a relatively unstable spin of ½. Two nearby polarons may therefore form a bipolaron which has been shown by Electron Spin Resonance (ESR) studies to be a more stable, spinless charge carrier [1.42]. The polaron or bipolaron charge carriers can then travel along the conjugated backbone of the polymer. In this way the polymer film will conduct when an electric field is applied. Pfluger et al. have completed a great deal of research into the physical structure of conducting polymer films and how this can affect the conduction mechanisms. They conclude that there is a large degree of cross–linking occurring between polymer chains. This increases the structural disorder within the films and therefore affects the distance a charge carrier can travel along the polymers backbone [1.43 and 1.44].

In terms of the electronic band gap structure of the polymer, the creation of polarons or bipolarons can be perceived as the introduction of electronic states between the valence and conduction bands. The subsequent formation of intermediate bands between the conducting and valence bands is shown in Figure 1.5. Figure 1.5(a) shows the conditions in an undoped conducting polymer material where there are no intermediate states. The creation of polarons is depicted in Figure 1.5 (b) where electronic states with a spin of ½ have been created. In Figure 1.5 (c) the spin of the polaron states is removed due to the formation of bipolarons. Finally, further charge

_____

removal due to increasing dopant level results in the broadening of the bipolaron states

to form the intermediate band gaps (Figure 1.5 (d)). This is accompanied by an overall

increase in the band–gap since the bipolaron states have emerged from the conduction

and valence bands.
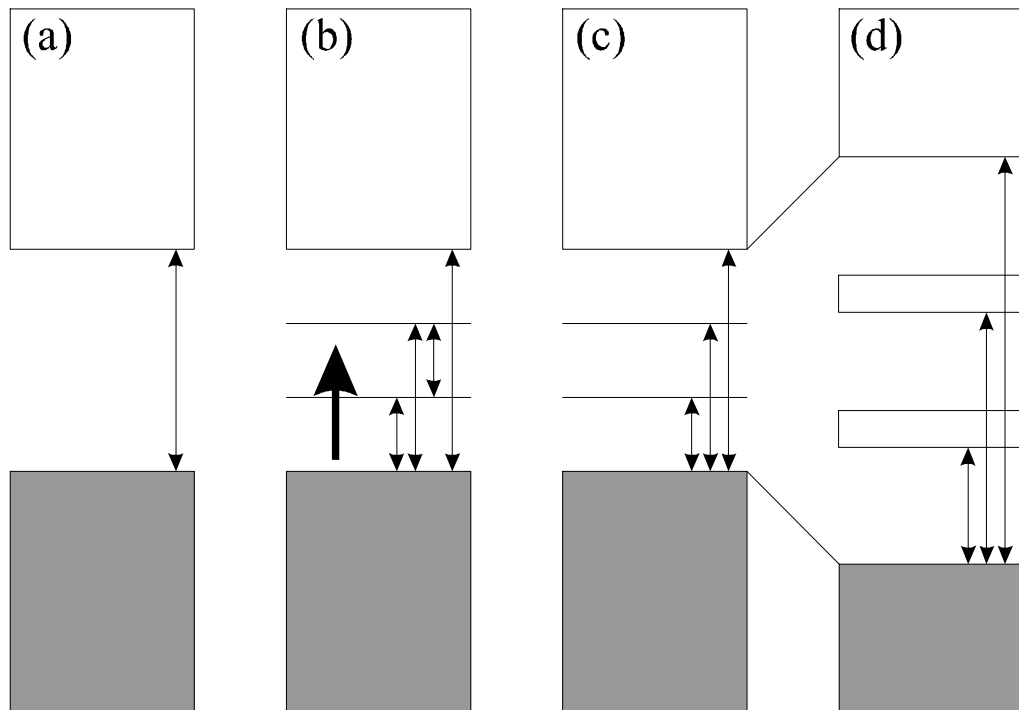
Figure 1.5 Energy level diagram for poly(pyrrole): (a) undoped; (b) polaron formation after removal of a single charge; (c) bipolaron formation after the removal of another unit of charge; (d) further charge removal causes broadening of bipolaron bands [1.37]. Double headed arrows are used to indicate transitions that have energies in the optical region of the electromagnetic spectrum.

On a macroscopic level it is thought that the charge carriers travel along the

backbone of the polymer film (intrachain transport). The conductivity of the material

therefore depends on several physical properties of the membrane:

- the conjugated chain length (i.e.: the distance a delocalised charge carrier

   can travel before it encounters a defect).

- the overall chain length.

_____

- interchain hopping of the charge carriers (i.e.: the distance a charge carrier has to jump in order to transfer from one polymer chain to the next).

There is some evidence that this final point is the limiting factor in the determination of the conductivity of a conducting polymer film. This supposition is supported by the temperature sensitivity of the polymers which has demonstrated characteristics consistent with a variable range hopping model developed by Mott to describe the temperature sensitivity of inorganic semiconductors [1.45]. It is clear that further research is required in order to completely understand the conduction mechanisms occurring within conducting polymer films.

Some conducting polymer sensors have been shown to reversibly respond to gaseous and vaporous species. The simplest method of monitoring this reaction is by observing the resistance of the polymer sensor. However, the way in which the vapour or gas interacts with the polymer membrane is not yet fully understood. Preliminary research into the interaction mechanisms suggested that oxidising or reducing agents in atmospheric gases either donate or accept electrons from the polymer membranes. Blackwood and Josowicz employed UV/visible spectroscopy and Kelvin probe techniques to study the interaction between poly(pyrrole) and various organic vapours [1.46]. Their results relate to the polaron and bipolaron concentrations, and work function modulations of the polymers upon exposure to the target analyte. They conclude that the interaction between the polymer and the vapour results in reversible changes in the bipolaron and polaron concentrations due to an electron transfer complex between the backbone of the conducting polymer and the organic vapour. Subsequent work noted that there were also plasticisation effects at high vapour concentrations [1.47, 1.48]. Studies of the changes in mass and resistance of poly(pyrrole) to a

_____

selection of gases and vapours by Slater et al. [1.49] suggests a dual mechanism where the response is effected by both a charge transfer and a swelling of the polymer film.

Bartlett et al. have studied the interaction between methanol and both poly(pyrrole) and poly(aniline) [1.7 and 1.8]. They conclude that the characteristics of the polymers were consistent with a simple binding isotherm and that there was no evidence for diffusion limitation. Gardner et al. have proposed a basic model of conducting polymer sensors [1.50] where approximate analytical solutions to diffusion and adsorption equations [1.51] are combined with a semiconductor model of electronic conduction in gas sensors [1.52]. The resulting model identifies six different types of behaviour and their characteristic responses. Inverse gas chromatography has been employed by Bailey and Persaud [1.53] in order to characterise the effects of a range of alcohols, alkanes and other polar samples on the surface of poly(pyrrole). They conclude that the adsorption interaction of the polymer is influenced by the basic nature of its surface. Clearly, further work is required to investigate all of the possible interactions between conducting polymers and gas or vapours. A summary of all of the possible interaction methods is shown in Figure 1.6 [1.39].

The first way in which interaction between a polymer and a species may occur is through the direct generation or removal of charge carriers (as discussed above) through the oxidation or reduction of the polymer. A second possibility is if the target species reacts with the polymer to change the mobility of the charge carrier along the polymer backbone (intrachain mobility). Interaction of the gas or vapour with the counter–ion is the third method that may result in a change in the conductivity of the polymers. This interaction would occur either through alterations in the charge transfer process occurring between the counter–ion and the monomer, or by the modification of the orientation of the polymer chains.

1) Carrier generation (removal) by oxidation (reduction)

Ads -

X-

X-

5) Change in interfacial charge transfer

Ads

+

+

+

2) Change in intrachain carrier mobility

Ads

4) Change in interchain hopping

Ads

+

+

+

Ads

X-

3) Interaction with the counter-ion

X-

POLYMER   **METAL**
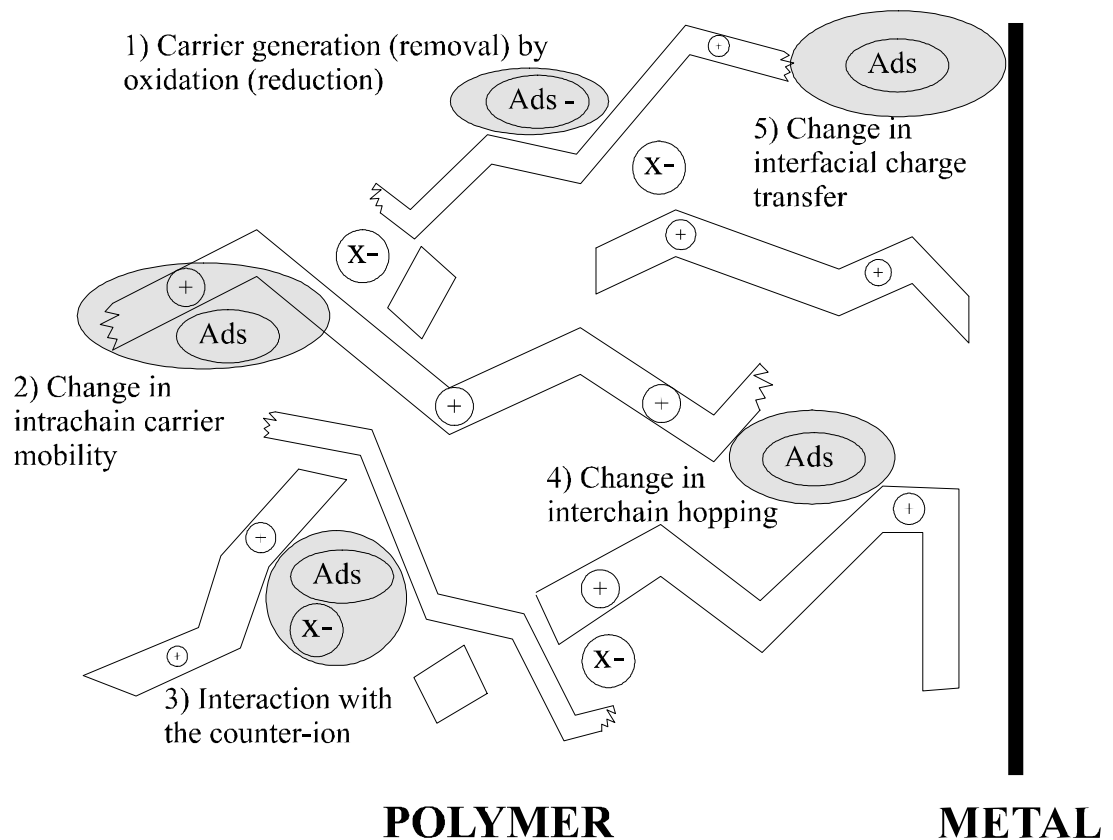
Figure 1.6 Five possible mechanisms explaining the gas sensitivity of conducting polymer chemoresistor devices.

The fourth area in which the target species may interact with the charge carriers is through changes in the interchain hopping distance. As it is accepted that this hopping mechanism is the principal determining factor in the magnitude of the polymer's conductivity, any modulation of this hopping barrier will result in large changes in the sensor's conductivity. Finally, the fifth mechanism for the interaction between the gas or vapour and the polymer is through alterations in the interfacial charge transfer. The exact method with which a polymer attaches to an electrode is not fully understood. It is possible that a target species may affect this interface between the polymer and the surface on which it has been deposited.

_____

Although the effects of both temperature and humidity on the conductivity of polymers have been studied, there has been little work published on the effects of these parameters on the response characteristics of the sensors. A number of groups have studied the temperature dependence of the conductivity of conducting polymers [1.45, 1.54 to 1.57, and 1.7]. All the groups have concluded that the temperature dependence of the polymers is best described by a three dimensional random hopping model of the Mott kind [1.45],

$$\sigma = A \exp\left[\left(-B/T^{1/4}\right)\right] \qquad (1.1)$$

where σ is the d.c. electrical conductivity, T is temperature, A is a constant and B is given by,

$$B = 2\left(3/2\pi\right)^{1/4}\left[\alpha^3/k_b N(E_F)\right]^{1/4} \qquad (1.2)$$

where α describes the spatial extent of the localised wavefunction, $N(E_F)$ is the density of states at the Fermi energy level and k_b is the backward reaction rate constant. Bartlett et al. [1.7] are one of the few groups to also investigate the effect of temperature on the response characteristics of the polymers. They have reported on the effect of temperature on the response of poly(pyrrole) to methanol vapour and conclude that the sensitivity of the polymer arises from a change in the pre–exponential factor, A. However, a detailed investigation of the effects of temperature on the response of

_____

conducting polymer sensors at a range of target analyte concentrations has not been reported.

There has been very little work published on the effect of water vapour on the characteristics of conducting polymers. Timofeeva et al. [1.58] have reported on the interaction of water vapour with poly(aniline) and poly(pyrrole) thin films. They have shown that the presence of water increases the electrical conductivity of poly(aniline) films. Casalbore-Miceli et al. [1.59] suggests that the water sensitivity of poly(thioaphtheneindole) results from the polymer being a proton conductor and undergoing an acid–base interaction between the water and NH^+ ions. However, the polymers employed during these experiments had been doped with the ions in order to specifically take advantage of this type of interaction. Details of the effects of humidity on the response of polymers to other gases and vapours have not been published and, although it is critical, models of the effects of both humidity and temperature on conducting polymers do not exist.

The interaction between polymers, target gases or vapours, and the effects of temperature and humidity on the sensor's response is the subject of this study.

1.4 Research Objectives

The main objectives of this research are:

- To investigate the response of a selection of conducting polymers to an organic vapour at a range of temperatures and humidities. Little data has been reported on the effects of either temperature or humidity on the response of such polymers.

- To develop novel theoretical or empirical models of both the static and dynamic response of the polymer films.

- To investigate the basic response of poly(pyrrole) (Ppy), poly(aniline) (Pan) and a modified form of Pan sensor to low concentrations of CO_2 at a range of humidities and temperatures. The basic concept is new and so never reported.

- To produce a mathematical model describing the novel CO_2 response characteristics.

- Where possible, to combine the modelling expressions in order to propose unique equations defining the response of conducting polymer sensors to both an organic vapour and a target gas, at a range of humidities and temperatures.

1.5 Outline of Thesis

This thesis describes the modelling of both the static and dynamic responses of Ppy and Pan conducting polymer sensors. Target analytes employed for the vapour and gas models were ethanol and CO_2, respectively. These species were chosen to represent an example of an environmental pollutant and a greenhouse gas. The sensors were exposed to these species in a variety of temperatures and humidities in order to incorporate these environmental effects in the final models. The thesis is therefore divided into two sections. The first two chapters are concerned with the fabrication and testing of the polymer sensors. The next 4 chapters describe the results obtained from the testing procedure and the development of both empirical and theoretical models of the polymer's response.

Chapter 2 addresses the types of sensor substrates required for the interrogation of the physical properties of the polymers, the techniques employed in the sensors fabrication and also briefly discusses the electrochemical deposition of the polymer films. This chapter supplies basic information about the sensors that have been employed in the subsequent modelling chapters. In order to characterise the polymers

_____

they have to be exposed in a controlled manner to a range of vapour and gas concentrations. This was achieved through the employment of a dynamic headspace testing station which is described in Chapter 3. The system was modified from existing equipment that was designed specifically for the analysis of beers [1.10, 1.60]. Different types of sensor were accommodated by the inclusion of a generic sensor head which could be altered (or replaced) according to the type of sensor employed. This dynamic system provided the means to collect all of the experimental data presented in this study.

Chapters 4 and 5 discuss the static modelling of the effects of ethanol vapour and CO_2, respectively. In Chapter 4 the effect of ethanol on Ppy and Pan sensors is explored at a range of humidities. Due to the similarity of the two types of polar molecule (ethanol and water), the model assumes that there is competition between for the available binding sites within the polymer. The characterisation of the effect of humidity on the response of polymer sensors and the development of a mathematical model to describe the effects are entirely original and can lead to a better understanding of the interaction mechanisms occurring between the polymers and the target analyte. In Chapter 5 a model is developed of the effects of CO_2 on Ppy, Pan and a novel, modified Pan sensor. The concept of the interaction between this type of polymer and CO_2 is unique and may offer an inexpensive and reliable method for the monitoring of this greenhouse gas. In both chapters the effects of temperature on the models are also explored.

In Chapter 6 a dynamic model of the effects of ethanol on the Ppy and Pan sensors is developed by employing sensor substrates with a variety of electrode separations. Again, the effects of both humidity and temperature on the dynamic responses is investigated. Although the dynamic model has been published by Gardner

_____

et al. [1.50], a full characterisation of the dynamic response of the polymers and the effects of temperature and humidity on the response has never been reported. This characterisation supplies valuable information in determining the interaction mechanisms occurring within the polymer and whether the response is limited by the diffusion–rate of the analyte or the reaction process. Chapter 7 discusses the final model of the response of the polymer sensors. Where possible the expressions developed in earlier chapters are combined yielding a unique, final model of the effects of both a polar vapour and a redox inactive gas on the response of the sensors. The final model will again include the effects of humidity and temperature on the characteristics of the polymers. Such a model would help in the in the optimisation of sensor systems, the understanding of the characteristics of conducting polymers and in the mathematical compensation of sensor signals.

1.6 References

1.1   J. W. Gardner, *Microsensors,* John Wiley and Sons Ltd, 1994.

1.2   A. C. Pike, Design of chemoresistive silicon sensors for application in gas monitoring, *Ph.D. Thesis, University of Warwick, UK, 1996.*

1.3   P. Ciureanu and S. Middelhoek (eds.), *Thin Film Resistive Sensors,* Institute of Physics Publishing Ltd, 1992.

1.4   W. Göpel, T. A. Jones, M. Kleitz, I Lundström and T. Seiyama (eds.), *Sensors: A Comprehensive Survey, Vol. 2/3: Chemcial and Biochemical Sensors,* VCH Publishers, Weinheim, Germany, 1991.

1.5   R. M. Harrison, A fresh look at air, *Chemistry in Britain,* (1994) 987-1000.

_____

1.6   P. N. Bartlett, P. B. M. Archer, and S. K. Ling-Chung, Conducting polymer gas sensors. Part I: Fabrication and characterisation, *Sensors and Actuators*, **19**, (1989), 125-140.

1.7   P. N. Bartlett and S. K. Ling-Chung, Conducting polymer gas sensors. Part II: Response of polypyrrole to methanol vapour, *Sensors and Actuators*, **19**, (1989), 141-150.

1.8   P. N. Bartlett and S. K. Ling-Chung, Conducting polymer gas sensors. Part III: Results for four different polymers and five different vapours, *Sensors and Actuators*, **20**, (1989), 287-292.

1.9   W. F. Wilkens and J. O. Hartmann, An electronic analog for the olfactory processes, *Annals of the New York Academy of Science,* (1964), **116,** 608-612.

1.10   S. Deutsch, *Models of the nervous system,* John Wiley and Sons Ltd, 1967.

1.11   K. Persaud and G. Dodd, Analysis of discrimination mechanisms in the mammalian olfactory system using a model nose, *Nature*, **299**, (1982), 352-355.

1.12   J. W. Gardner and P. N. Bartlett, Performance definition and standardisation of electronic noses, *Technical Digest, Transducers '95 - Eurosensors IX,* (1995), 1-4

1.13   M. E. Hassan Amrani, K. C. Persaud and P. A. Payne, High–frequency measurements of conducting polymers: development of a new technique for sensing volatile chemicals, *Meas. Sci. Technol.,* **6**, (1995), 1500-1507.

1.14   M. E. Hassan Amrani, R. M. Dowdeswell, P. A. Payne and K. C. Persaud, An intelligent gas sensing system, *Sensors and Actuators B,* **44**, (1997), 512-516.

1.15   M. E. Hassan Amrani, R. M. Dowdeswell, P. A. Payne and K. C. Persaud, Pseudo–random binary sequence interrogation technique for gas sensors, *Sensors and Actuators B,* **47**, (1998), 118-124.

_____

1.16   T.C. Pearce, Sensor–based machine olfaction: Instrumentation for the analysis of beer, *Ph.D. Thesis, 1997.*

1.17   J. W. Gardner and P. N. Bartlett, Pattern recognition in gas sensing, in *Techniques and mechanisms in gas sensing,* P. T. Moseley, J. Norris, and D. E. Williams (eds.), Adam Hilger, UK (1991) 347-380.

1.18   C. Hierhold and R. Müller, Quantitative analysis of gas mixtures with non–selective gas sensors, *Sensors and Actuators,* **17,** (1989), 587-592.

1.19   G. Hörner and C. Hierhold, Gas analysis by partial model building, *Sensors and Actuators B,* **2**, (1990), 173-184.

1.20   R. Müller, High electronic selectivity obtainable with nonselective chemosensors, *Sensors and Actuators B,* **4**, (1991), 35-39.

1.21   J. W. Gardner, Detection of vapours and odours from a multisensor array using pattern recognition. Part 1. Principle component and cluster analyses, *Sensors and Actuators B,* **4,** (1991), 109-116.

1.22   J. W. Gardner, E. L. Hines and H. C. Tang, Detection of vapours and odours from a multisensor array using pattern recognition. Part 2. Artificial neural networks, *Sensors and Actuators B,* **9,** (1992), 9-15.

1.23   M. S. Nayak, R. Dwivedi and S. K. Srivastava, Application of iteration technique in association with multiple regression method for identification of mixtures of gases using an integrated gas–sensor array, *Sensors and Actuators B,* **21,** (1994), 11-16.

1.24   C. Chatfield and A. J. Collins, *Introduction to multivariate analysis,* Chapman and Hall, London, (1980).

1.25   J. W. Gardner and E. L. Hines, Integrated sensor array processing in an electronic nose, *Proc. IEE Coll. Digest,* **83,** (1987), 1-3.

_____

1.26   J. W. Gardner, E. L. Hines and M. Wilkinson, Application of artificial neural networks to an electronic olfactory system, *Meas. Sci. Technol.,* **1,** (1990), 446-451.

1.27   J. V. Hatfield, P. Neaves, P. J. Hicks, K. Persaud and P. Travers, Towards an integrated electronic nose using conducting polymer sensors, *Sensors and Actuators B,* **18-19**, (1994), 221-228.

1.28   J. W. Gardner and P. N. Bartlett, A brief history of electronic noses, *Sensors and Actuators B,* **18-19**, (1994), 211-220.

1.29   A. Dall'Olio, G. Dascoia, V. Varacca and V. Bocchi, Electron paramagnetic resonance and conductivity of an electrolyte oxypyrrole (pyrrole polymer) black, *C. R. Acad. Sci., Paris Ser. C,* **267** (1968) 433-435.

1.30   A. F. Diaz, K. K. Kanazawa and G. P. Gardini, Electropolymerisation of pyrrole, *J. Chem. Soc. Chem. Commun.,* **5** (1979) 635-636.

1.31   J. J. Miasik, A. Hooper and B. C. Tofield, Conducting polymer gas sensors, *J. Chem. Soc., Faraday Trans.* **82** (1986) 1117-1126.

1.32   C. Nylander, M. Armgarth, I. Lundsröm, An ammonia detector based on a conducting polymer, *Anal. Chem. Symp. Series,* **17** (1983) 203-207.

1.33   A. F. Diaz, J. F. Rubinstein and H. B. Mark, Electrochemistry and electrode applications of electroactive/conductive polymers, *Advances in Polymer Science,* **84,** (1988) 113-139.

1.34   J. Heinze, *Topics in Current Chemistry,* **152,** Springer, Berlin, 1990.

1.35   A. F. Diaz and J. Bargon, in T. A. Skotheim (ed.), *Handbook of Conducting Polymers,* **1,** Marcel Dekker, New York 1986.

_____

1.36   K. Imanishi, S. Masaharu, Y. Yasuda, R. Tsushima and S. Aoki, Solvent effect on electrochemical polymerization of aromatic compounds, *J. Electroanal. Chem.,* **242** (1988) 203-208.

1.37   N. Blair, The development and characterisation of conducting polymer based sensors for use in an electronic nose, *Ph.D. Thesis, University of Southampton, UK,* 1994.

1.38   P. N. Bartlett, J. W. Gardner and R. G. Whitaker, Electrochemical deposition of conducting polymers onto electronic substrates, *Sensors and Actuators A,* **21-23,** (1990) 911-914.

1.39   P. N. Bartlett and J. W. Gardner (ed), *Sensors and Sensory Systems for an Electronic Nose,* Kluwer Academic Publishers, Dordrecht, 1992.

1.40   G. K. Chandler and D. Pletcher, The electrochemistry of conducting polymers, *Specialist Periodical Reports, Electrochemistry,* **10,** Royal Society of Chemistry, London 1985.

1.41   R. R. Chance, D. S. Boudreaux, J. L. Bredas and R. Silbey, in T. A. Skotheim (ed.), *Handbook of conducting polymers,* Marcel Dekker, New York (1986).

1.42   J. C. Scott, P. Pfluger, M. T. Kroundbi, and G. B. Street, Electron spin resonance studies of pyrrole polymers, *Phys. Rev. b., Condens. Matt.,* **28**, (1983) 2140-2145.

1.43   G. B. Street, S. E. Lindsey, A. I. Nazzal and K. J. Wynne, the structure and mechanical properties of polypyrrole, *Mol. Cryst. Liq. Cryst.,* **118**, (1993) 137-148.

1.44   A. I. Nazzal and G. B. Street, Molecular weight determination of pyrrole based polymers, *J. Chem. Soc. Commun.,* **1**, (1984) 83-84.

1.45   N. F. Mott and E. A. Davies, *Electronic processes in non–crystalline materials,* Clarendon Press, Oxford, 1979.

1.46   D. Blackwood and M. Josowicz, Work function and spectroscopic studies of the interactions between conducting polymers and organic vapours, *J. Phys. Chem.* **95**, (1991), 493-502.

1.47   M. Josowicz and P. Topart, in J. W. Gardner and P. N. Bartlett (ed.), *Sensors and Sensory Systems for an Electronic Nose,* Kluwer Academic Publishers, Dordrecht, 1992, 117-129

1.48   P. Topart and M. Josowicz, Characterisation of the interaction between poly(pyrrole) films and methanol vapour, *J. Phys. Chem.* **96**, (1992), 7824-7830.

1.49   J. M. Slater, E. J. Watt, N. J. Freeman, I. P. May and D. Weir, Gas and vapour detection with poly(pyrrole) gas sensors, *Analyst,* **117**, (1992), 1265-1270.

1.50   J. W. Gardner, P. N. Bartlett, and K. F. Pratt, Modelling of gas–sensitive conducting polymer devices, *IEE Proc.–Circuits Devices Syst.*, **142**, (1995), 321-333.

1.51   P. N. Bartlett and J. W. Gardner, Diffusion and binding of molecules to sites within homogeneous thin films, *Trans. Roy. Soc. London A*, **354**, (1996), 35-57.

1.52   J. W. Gardner, A diffusion–reaction model of electrical conduction in tin oxide gas sensors, *Semicond. Sci. Technol.*, **4**, (1989), 345-350

1.53   R. A. Bailey and K. C. Persaud, Application of inverse gas chromatography to characterisation of the Ppy surface, *Analytica Chimica Acta,* **363**, (1998), 147-156.

1.54   Y. Shen, K. Carneiro, C. Jacobsen, R. Qian and J. Qiu, Characterisation of the transport properties of conducting polypyrrole films, *Synthetic Metals,* **18**, (1987), 77-83.

_____

1.55   J. P. Parneix and M. El Kadiri, in H. Kuzmany, M. Mehring and S. Roth (eds.),
        Springer series in solid state sciences, Springer, Germany 1987, 23-26.

1.56   M. Rotti, H. Krikor and P. Nagels, in H. Kuzmany, M. Mehring and S. Roth
        (eds.), *Springer series in solid state sciences,* Springer, Germany 1987, 27-30.

1.57   S. Yueqiang, K. Carneiro, W. Ping and Q. Renyuan, in H. Kuzmany, M.
        Mehring and S. Roth (eds.), *Springer series in solid state sciences,* Springer,
        Germany 1987, 31-35

1.58   O. N. Timofeeva, B. Z. Lubentsov, Ye. Z. Sudakova, D. N. Chernyshov and M.
        L. Khidekel, Conducting polymer interaction with gaseous substances I. Water,
        Synthetic Metals, **40**, (1991) 111-116.

1.59   G. Casalbore-Miceli, M. Campos, G. Beggiato, Effect of relative humidity on
        the electrical transport properties of poly(thioaphtheneindole), *Solid State
        Ionics,* **80**, (1995) 239-244.

1.60   J. W. Gardner, T. C. Pearce, S. Friel, P. N. Bartlett and N. Blair, A multisensor
        system for beer flavour monitoring using an array of conducting polymers and
        predictive classifiers, *Sensors and Actuators B,* **18 - 19,** (1994) 240-243.

CHAPTER 2

Sensor Design and Fabrication

2.1 Introduction

The aim of this chapter is to describe the design criteria and fabrication processes involved in the production of the sensors used during this study. A brief overview is also included of the electrochemical deposition processes used to grow the active membranes. The three different types of substrate technology employed are summarised in Table 2.1 with details of the electrode gap size, substrate material and the application for which the sensor technology is intended. Each of the sensor layouts requires different design considerations and fabrication methods in order to obtain a structure supplying the attributes required by the particular application. To identify the sensors, a Sensors Research Laboratory (SRL) reference code has been used.

The SRL123 and SRL127 sensor configurations were designed and fabricated by Dr A. C. Pike and formed part of his PhD thesis [2.1] in which the design and fabrication of several types of substrate was documented. The SRL123 consists of a basic, two electrode structure whilst the SRL127 differs only by the inclusion of a planar heating element. These layouts were intended to provide a basic conducting polymer configuration to be employed in the production and testing of large numbers of devices. Sensors created on these structures would be employed both in the characterisation of active membranes and in the development of electronic nose

instruments. In order to allow the mass production of these devices, silicon was employed as the substrate material. The use of this material allows a reduction in the fabrication costs and also improves in the reproducibility of sensor characteristics.

Table 2.1. Details of the sensor technologies employed, their electrode gap size, substrate material and an indication of the application for which the sensor is intended.

SRL Device Number	Electrode Gap Size (μm)	Substrate Material	Application Details
101	Variable (10 to 45)	alumina (Al_2O_3)	Investigating the effect of electric field distribution on the response of CPs
123	10	silicon (si)	General characterisation of conductance in polymers (no micro–winding heater)
127	10	silicon (si)	General characterisation of conductance in polymers (with micro–winding heater)

The variable gap devices (SRL101) were designed by Ms S. Friel whilst employed at Warwick University. This type of device was intended to be used purely in experimental work for investigating the effect of electrode geometry on the characteristics of polymeric sensors. The experimental nature of this device combined with the limited number of sensors required for this application, allowed the devices to be fabricated on 0.5" alumina tiles. The ceramic substrate not only acts as an insulating element but also has very useful thermal properties which include a low coefficient of linear expansion which reduces the stress on the sensors during thermal experiments.

2.2 Design and Fabrication of Variable Gap Resistive Arrays

_____

Variable gap devices (SRL101) were designed in order to allow the investigation of the effects of electrode geometry on both the static and dynamic responses of conducting polymer films. The design had to create a range of electrode gaps on a sensor substrate which was compatible with the electrochemical deposition techniques employed for polymer growth (outlined in section 2.4). The electrode structure chosen created a device with a common ground separated from eight electrodes by a range of gaps (from 10 to 45 μm). The resolution required in order to generate such an electrode geometry made the employment of photolithographic techniques essential in the fabrication of the device.

Alumina tiles (Materials Research Society) were employed as the substrate for the SRL101 devices because this material offers a number of properties useful for this sensor application. This type of substrate material had also previously demonstrated a compatibility with the electrochemical deposition process to be employed for polymer growth [2.2]. Particular benefits could be obtained due to the good adhesion demonstrated between the alumina substrate and gold electrodes. This reduced the number of stages required in sensor fabrication by allowing the omission of a seeding layer. The thermal properties of alumina were also an important consideration as they allowed the sensors to quickly reach equilibrium with the surrounding environment. This reduced the time required for experiments aimed at characterising the thermal effects on the properties of the active membrane.

A schematic diagram of the electrode structure to be formed on the substrate is shown in Figure 2.1. The structure consists of the alumina substrate, a gold electrode layer and a photoresist passivation layer which is employed in order to restrict the areas

_____
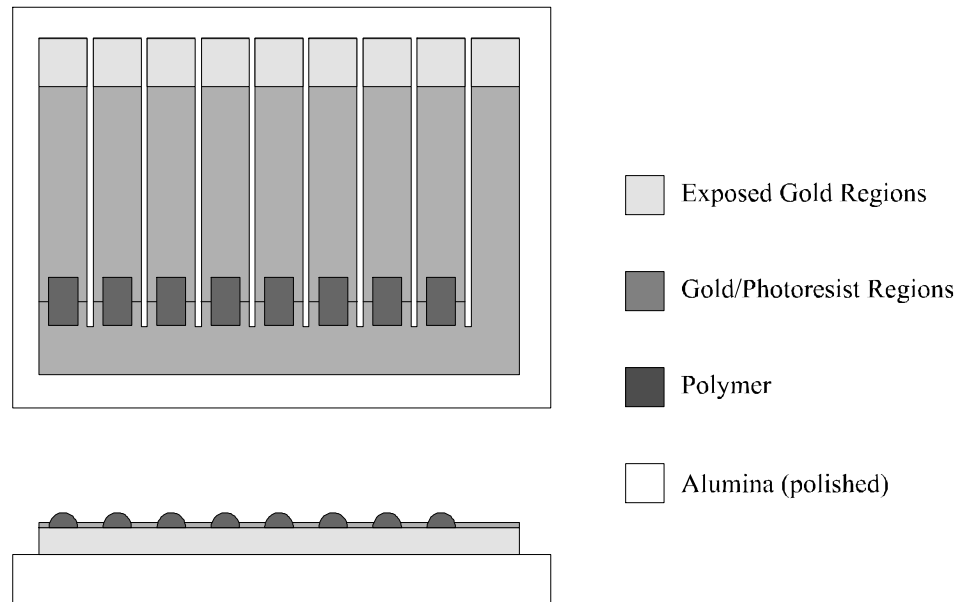
Figure 2.1 Schematic of variable gap devices showing the layout of the device and the areas of polymer deposition (this diagram is not to scale).

of polymer growth. The exposed gold regions at the top of this diagram are used for

electrical contacts employed during both the growth of the polymer membranes and

throughout the sensors life for monitoring the performance of the device.

The fabrication of a variable gap device commences with a 100 nm thick layer

of gold being thermally evaporated onto the substrate using a modified Edwards E306A

electron–beam evaporator. This thickness of gold demonstrated good adhesion to the

substrate and was sufficient to allow the micro–bonding of electrical contacts to the

structure. Photolithographic techniques are then employed to pattern the gold layer.

This process employs two stages; the production of a mask design and the transfer of

this image to the substrate. The SRL101 device required two masks to be employed

during fabrication. The first was used to define the geometry of the electrodes formed in

the 100 nm gold layer. A second mask was then employed to outline the required

structure in the photoresist passivation layer used to limit the areas of polymer growth.

_____

Both masks were designed using L–Edit^TM (Tanner Tools Ltd) and produced using photographic developing facilities at Warwick University.

The transfer of the mask image to the gold surfaced substrate is achieved through spin–coating a layer of Shipley Microposit 1813 onto the gold face. This layer is selectively exposed to ultra–violet light using the first source mask. The photoresist contains radiation–sensitive groups which chemically respond to the exposed light, forming a latent mask image. This is then developed to pattern the relief image in the photoresist. The areas of photoresist remaining protect the underlying gold structure during a subsequent chemical etch. The wet etchant used during this stage is one part "Gold Etch, Isoclean" (Micro Image Technology Ltd) diluted with two parts deionised water and the etching procedure is carried out at room temperature. Using this method the 8 electrode gaps varying from 10 to 45 µm in steps of 5 µm are generated on the variable gap devices in the gold layer.

When the required electrode structure has been formed, the second mask is used to develop the remaining photoresist, generating the contact pads and exposing the areas of gold where polymer deposition is required. A photograph of a variable gap device substrate is shown in Figure 2.2. This clearly shows the areas where the photoresist layer has been removed exposing the gold electrode structure beneath. The final substrate structure is then soft baked at 100 °C for 2 hours. This hardens the photoresist layer to ensure that no chemical interference occurs during the polymer deposition process.

_____
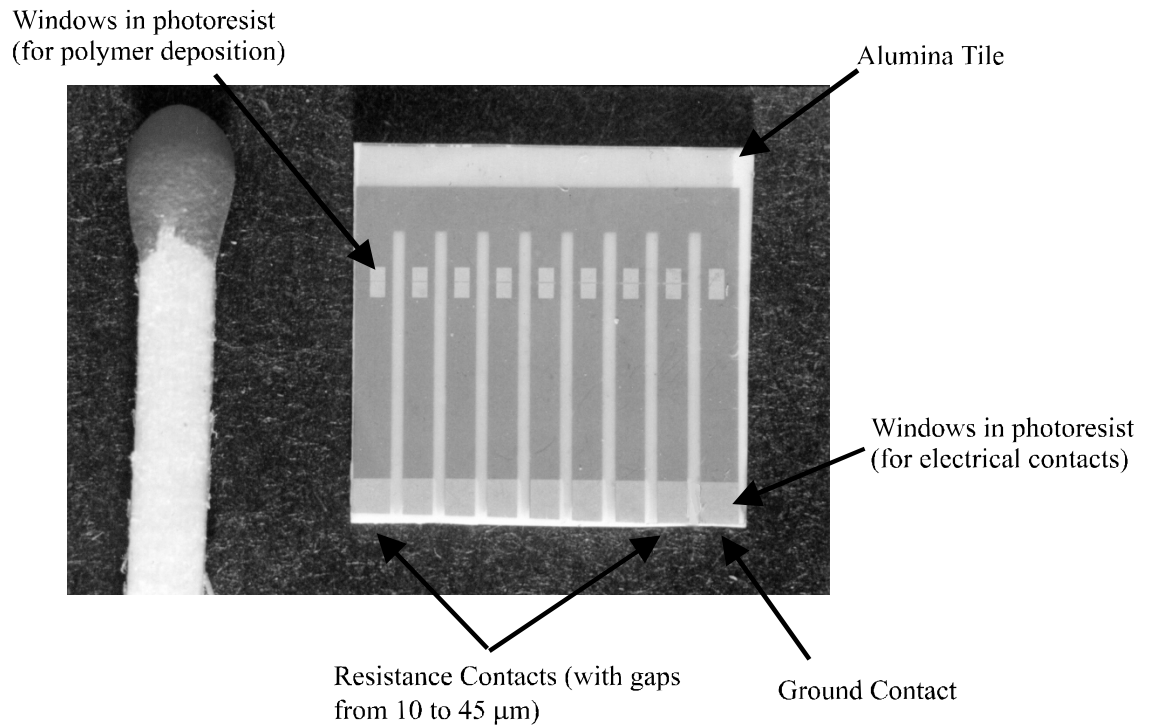
Figure 2.2 Photograph of a variable gap substrate showing the layout of the device and also a matchstick head for dimensional comparison.

When the sensor substrates have been fabricated they need to be prepared for polymer deposition (which is described in detail in section 2.4). The deposition process involves using the sensor substrate as one electrode in a three electrode cell, which is immersed in a solution of the required electrolyte. The substrate therefore has to be mounted on a printed circuit board (PCB) that can be used to supply reliable electrical connections to the gold electrodes during deposition. This board can then be used to dip the device into the growth solution. The layout of a typical circuit board used for this purpose consists of a 100 to 120 mm long PCB, which supplies up to nine copper tracks on to which electrical connections can be made. These tracks are exposed at either end of the board and covered with a protective lacquer in areas where the contacts should not be revealed. The substrates are attached to the boards using a commercially available dental wax which is employed as a temporary adhesive. Thin

gold wires with a diameter of 25 μm are then ultrasonically bonded between the substrate contacts and the exposed regions of the circuit board. The micro–bonded wires are covered with further dental wax to prevent the growth of polymer on the contact pads.

When the polymer deposition process is completed the devices are removed from their mounts and all traces of the dental wax is removed. Each completed device is then mounted on smaller PCBs that allow wires to be micro–bonded between the sensor's contact pads and the boards themselves. These circuits are employed to supply good electrical contacts between the polymer devices and commercially available 0.1" gold plated, square–pin through headers. This type of arrangement allows the sensors to be easily interfaced with the chambers used in the dynamic headspace testing station.

2.3 Design and Fabrication of Discrete Resistive Sensors

Discrete resistive sensors (SRL123 and SRL127) were designed to be extensively used in the characterisation of conducting polymer membranes and also for use as the individual devices in multi–element arrays. To cater for the large number of devices that would be required for these applications, both types of device were designed in order to ease mass production and increase reproducibility. The SRL123 and SRL127 devices therefore contain several features that were excluded from the SRL101 design of sensor substrate.

A silicon substrate was employed for the fabrication of the sensors replacing the alumina tile configuration used by the SRL101 devices. This allowed multiple layers to be generated by using commercially available fabrication methods, enabled a large number of sensors to be created for every silicon wafer processed and also reduced the

_____

resistance of the deposited tracks due to the silicon's lower surface roughness. The

SRL127 sensor design was also developed to incorporate a micro–hotplate structure.

This consists of a micro winding track that is generated in the same layer as the

electrodes employed for monitoring the resistance of the polymer films. The structure

of this type of device is shown in Figure 2.3. Such an arrangement allows rapid and

accurate temperature control over the polymer membrane. However, in all of the

experiments documented in this study, temperature control over the sensors was

maintained using the dynamic headspace testing equipment (described in Chapter 3)

and the planar heaters were not employed.
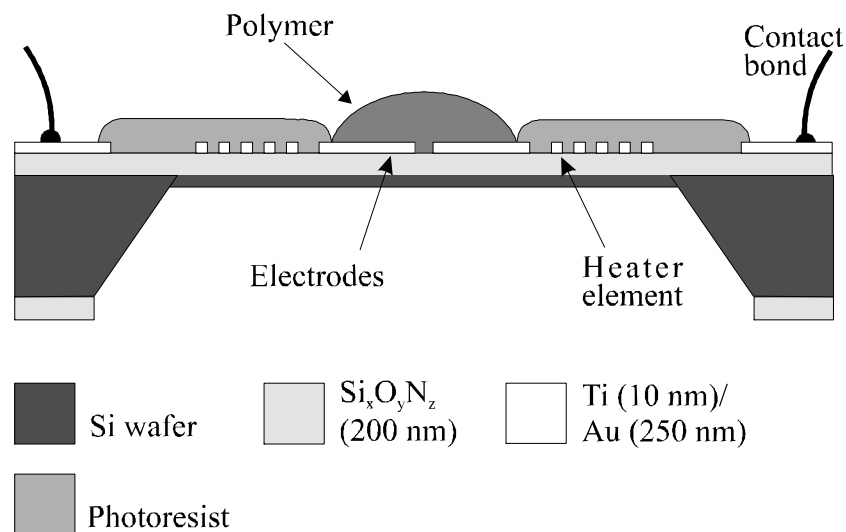
Figure 2.3 Schematic cross–section through the silicon–micromachined conducting polymer gas sensor
(SRL127).

The fabrication of the SRL127 devices involves the use of three masks: the first

is used to pattern the gold metalisation layer; the second to pattern the protective

photoresist layer; and the third to protect the device during a back–etch procedure. To

reduce the mechanical stress in the devices, a standard cleaning procedure is carried out

between each of the processing steps.   The substrate employed for these devices consists of a 3", 350 μm thick, double–sided, polished, single crystal silicon (SCS) wafer. A silicon oxynitride ($Si_xO_yN_z$) [2.3] layer is deposited onto the wafer by low pressure chemical vapour deposition (LPCVD) using controlled flow–rates of dichlorosilane, ammonia and nitrous oxide. The properties of this membrane layer allow the structure of the device to be mechanically stable, with low stress, and also provide the appropriate thermal properties to minimise power loss.

During the first stage of device fabrication an adhesion layer consisting of 10 nm of titanium is deposited onto the substrate followed by a 250 nm thick layer of gold. Both layers are sputtered onto the substrate and patterned using the first mask. The gold etchant used during this stage was identical to that used during the fabrication of the variable gap devices (SRL101) and consists of one part "Gold Etch, Isoclean" (Micro Image Technology Ltd) diluted with two parts deionised water. The titanium etchant was composed of 2 parts ammonium fluoride, 8 parts nitric acid (70%) and 90 parts deionised water. Both etching procedures were carried out at room temperature. The mask used during this stage creates the gold electrode structure and also the device's heating elements. Use of a planar heating element created out of the same metalisation layer as the electrode structure reduced the number of steps required to fabricate this type of device. The heater geometry is split into two regions of meandering track on both sides of the electrodes. This design increases the thermal uniformity along the inter–electrode gap.

The wafer top–side is then spun coated with Shipley Microposit 1813 photoresist coating and patterned with the second mask. This procedure defines the areas where polymer deposition is required, opens contact pads in the photoresist and also offers some protection to the wafer top–side during the final etching stage. The

_____

photoresist was hardbaked for 1 hour at 180 °C after development. Finally, a potassium

hydroxide (KOH) anisotropic silicon etch is used to produce the desired membrane

structure and snap grooves. The wafer back–side $Si_xO_yN_z$ layer was patterned using the

third mask and a plasma etch was employed in order to form a KOH resistant mask.

This was then mounted in a protective jig in order to shield the wafer top–side from

KOH attack. The etching speeds of different crystallographic planes in the SCS is

accurately documented [2.4, 2.5]. Using this information a timed etch can be used to

leave the required SCS thickness to increase the strength of the $Si_xO_yN_z$ membrane.

The SCS thickness varies from approximately 1 to 20 μm across the wafer due to

uneven solution agitation and a ±5 μm wafer thickness tolerance. Figure 2.4 shows the

fabrication procedure employed in the manufacture of SRL127 sensor substrates.

(a) Coat Si substrate with 200 nm of $Si_xO_yN_z$

(b) Deposit Ti/Au (10/250 nm) metallisation and
     pattern with Mask 1

(c) Pattern underside $Si_xO_yN_z$ with Mask 2
     to create KOH back-etch mask

(d) Deposit photoresist and pattern with Mask 3
     to form passivation layer

(e) Timed KOH back-etch to realise membrane
     structure and snap grooves

Si wafer $Si_xO_yN_z$ Ti/Au

Photoresist
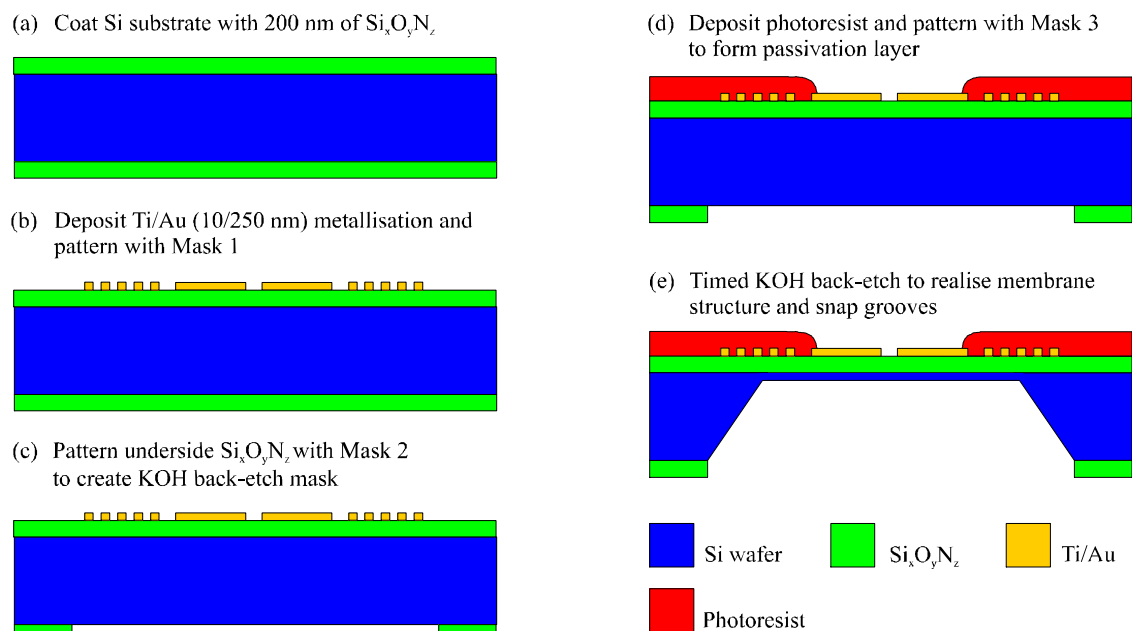
Figure 2.4 Schematic of fabrication procedure for the SRL127 sensor substrates. These views only
indicate processing steps and do not relate to a specific cross–section and are not drawn to scale.

_____

The fully fabricated wafer is diced and mounted on custom designed PCBs. Gold wires are ultrasonically bonded onto the contact pads allowing electrical contacts to be made between the device and commercially available 0.1" pitch, gold–plated through headers. The completed device is then ready for the polymer membranes to be deposited. This design of sensor substrate enables the circuit board employed during polymer deposition to be used throughout the device life for controlling the planar heating element and for monitoring the performance of the membrane. A photograph of a completed device is shown in Figure 2.5.
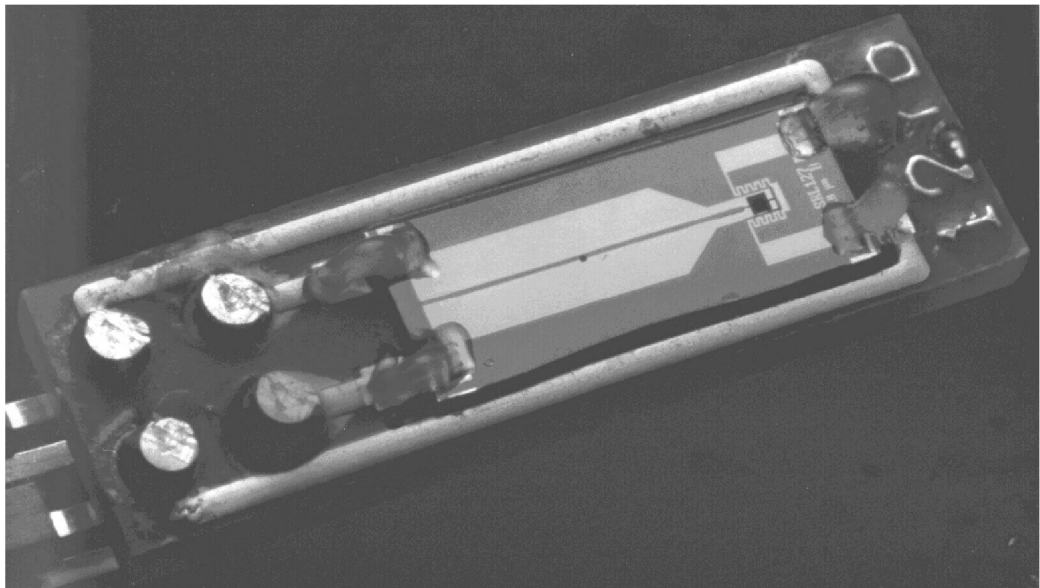
Figure 2.5 Photograph of SRL127 silicon–micromachined conducting polymer gas sensor.

The SRL123 discrete polymer devices are similar in structure to the SRL127. However, the substrate for this type of device has been simplified by the removal of the micro–winding heating element therefore eliminating the need for a KOH back–etch. The sensor can therefore be processed using only two dark field masks employing Shipley Microposit 1813 in a procedure identical to that employed for the SRL101

devices. The first mask is used for patterning the gold layer and forming the electrode structure. A second is then employed to expose areas for polymer deposition and contact pads through the photoresist passivation layer. The devices are again mounted on custom designed PCBs with ultrasonically bonded gold wires allowing electrical contacts to easily created.

2.4 Electrochemical Conducting Polymer Deposition

The electrochemical production of polymer membranes has been widely investigated since the first electrochemically prepared polymer was reported by Dall'Olio [2.6] in 1968. However, the first detailed characterisation of electrochemically fabricated polymers was not possible until 1979 when Diaz et al. produced the first Ppy films that were not only highly conductive, but were also stable in air [2.7]. The development of conducting polymers as gas and vapour sensors began when the materials demonstrated rapid reversible responses to a range of compounds at room temperature [2.8, 2.9]. The wide variety of monomer types that can be polymerised to give conducting polymer films [2.10, 2.11, 2.12] combined with the possibility of producing new substituted monomers, is one of the main attractions of employing conducting polymers as gas and vapour sensors.

The work presented in this study has concentrated on polymers derived from two types of monomer unit: pyrrole and an emeraldine form of aniline[1]. Details of the fabrication of sensors based on this type of conducting polymer are given elsewhere [2.2, 2.13, and 2.14], however, the exact reaction mechanisms involved do vary from

---

[1] There are three forms of aniline: leucoemeraldine; emeraldine; and pernigraniline. Only the protonated form of emeraldine conducts.

_____

monomer to monomer.   Generally, in the formation of a conducting polymer, the

monomer must react to form an extended conjugated system.   This reaction may be

generated either chemically or electrochemically.   The benefits of using the

electrochemical method employed in the fabrication of the sensors reported in this

study, is due to the greater control that can be sustained over the polymer growth. The

potential applied to the sensor substrate and the time of growth can both be accurately

regulated to enable the physical properties of the produced polymer to be considerably

altered.

In order to electrochemically grow a conducting polymer the monomer must be

dissolved in an appropriate solvent.   The choice of solvent has a large effect on the

morphology, electrical conductivity and electroactivity of the resulting polymer [2.15].

The technique employed during the deposition of the devices used during this study

were identical to those developed previously [2.2, 2.13, 2.14] and known to yield

reproducible, useful devices. This technique normally begins with the generation of a

radical cation formed by oxidisation at the surface of the electrode.   This radical can

then react either with a second radical to give a dimer, or with a neutral monomer

followed by subsequent oxidisation to give the dimer [2.16, 2.17]. The result is growth

of a polymer film on the working electrode.   A schematic overview of the

electropolymerisation process is shown if Figure 2.6.   A polymer grown in such a

manner would be oxidised and present as a polycation. The charge on the polymer is

therefore balanced by the incorporation of anions from the solution as it grows.

Typically a single polymer anion is associated with between 3 and 6 monomer units in

the polymer chain. The properties of the final polymer therefore depend, not only on

the choice of monomer but also on the choice of counter–ion.

_____

All of the electrochemical experiments employed for polymer growth are carried out using a laboratory–constructed potentiostat in a three electrode configuration, where the gold regions of the device onto which the polymer is to be deposited form the working electrode. The counter and reference electrodes are a large area platinum gauze and a saturated calomel electrode (SCE), respectively. During polymer growth the potential between the working electrode and the reference electrode
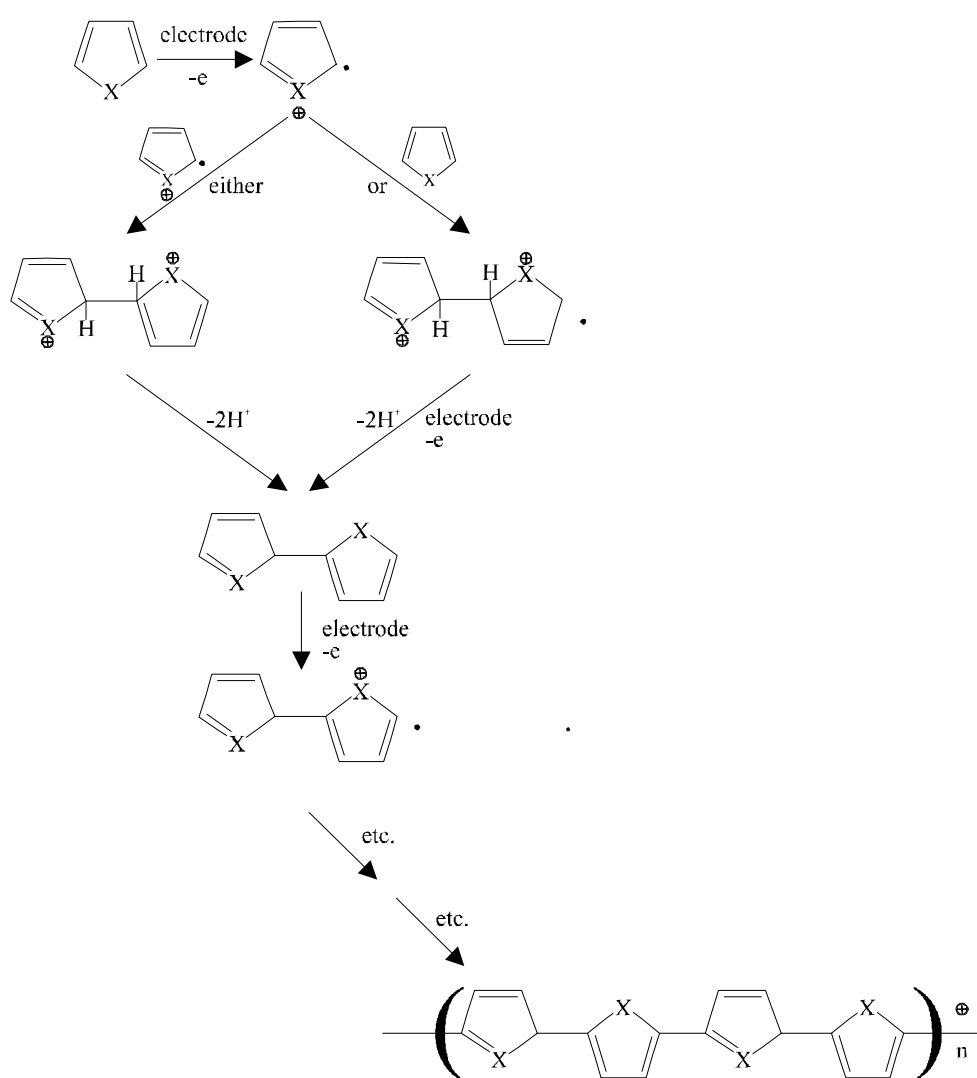
Figure 2.6 The general mechanism for the electropolymerisation of monomers such as pyrroles and anilines, (pyrrole shown here).

_____

is held constant, while the current flowing from the working electrode to the counter

electrode is measured. The reference electrode therefore provides a stable potential

from which the voltage across the working electrode/solution interface is controlled.

Most of the applied potential creates a high field at the electrode surface [2.18]. This

field can be employed to control the addition or removal of electrons from molecules in

the solution near to the electrode surface. It is this oxidation or reduction process that

leads to the growth of a polymer on the exposed gold regions.

All solutions employed for polymer growth are freshly prepared using reagent

grade water produced by a Whatman water purification system (Whatman WR50

deioniser and Whatman Stillplus units). Glassware is cleaned by soaking overnight in a

3% solution of Decon 90 and thoroughly washed with purified water before use. In

order to ensure consistent, uniform polymer growth onto the devices it is essential to

ensure that the gold is clean before use. This is achieved by electrochemical cleaning of

the devices immediately before the polymer deposition process is initiated. The

electrodes are cleaned by cycling the potential three times between -0.3 V and 1.8 V in

2 mol/dm^3 sulphuric acid. Figure 2.7 shows a typical voltammogram obtained for a

clean device under these circumstances.

The anodic current, starting at a working electrode potential of approximately

1.3 V indicates the formation of an oxide layer at the gold surface. The corresponding

cathodic current at ~0.9 V registers the removal of this oxide layer. The charge passed

in stripping the oxide layer can be use to estimate the real surface area of the exposed

gold. Only devices that show well–behaved voltammetry and reproducible oxide

stripping currents are used in device fabrication. After cleaning, the sensor substrates

are rinsed with reagent grade water and then kept under water until they are ready for

use. This prevents any contamination of the surface by material from the laboratory

atmosphere. The gas sensor response and the base resistance of the conducting polymer based devices depend on the selection of monomer, the choice of counter–ion used to dope the polymer, the solvent used to grow the film and the precise conditions used in the deposition. It is therefore essential to carry out the deposition of the different polymers onto the substrates under well–defined conditions.
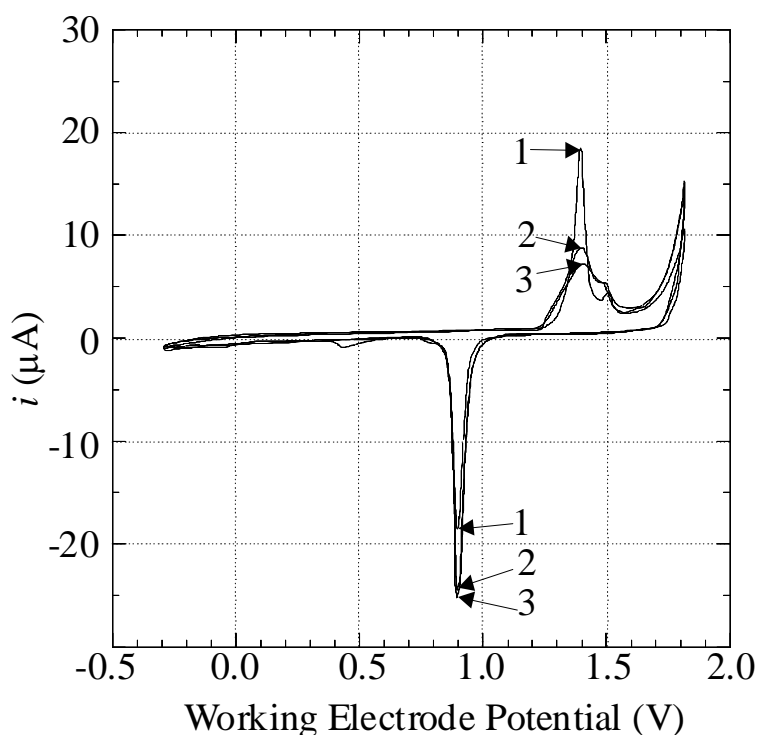
Figure 2.7 Typical cyclic voltammograms for a clean, uncontaminated gold surface in 2 mol dm^{-3} sulfuric acid solution recorded at 100 mV S^{-1}. The first 3 scans are shown. The cathodic peak indicates polymer growth and the area it encloses can be used to estimate the real surface area of the electrode. The anodic peak may be related to the reduction of the water which has been employed as a solvent.

Ppy and Pan with different alkylsulfonate counter–ions, can be electrochemically deposited onto cleaned substrates from an aqueous solution containing pyrrole/aniline and sodium salt of the appropriate alkylsulfonate. This is achieved by stepping the potential of the gold electrodes (from approximately 0 to 0.85

_____

V for Ppy and 0 to 0.9 V for Pan) and holding it there for two minutes. At the end of

this time the potential is stepped back to 0 V and the current allowed to decay for two

minutes. Figure 2.8 shows a typical current/time growth transient for the deposition of

Ppy onto the required devices. This figure shows the current flowing through the

polymer when different alkysulfonates are employed as the counter–ion.
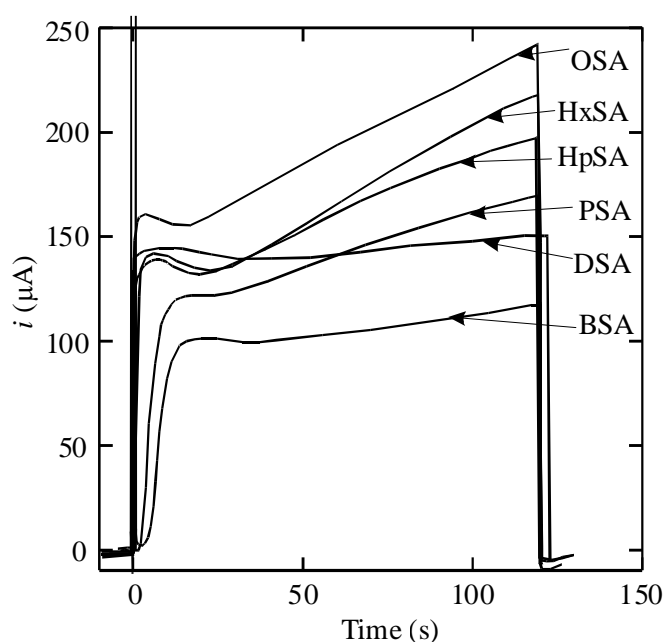
Figure 2.8 Potential step growth transients for Ppy films grown with six different alkylsulfonate counterions in aqueous solution.   The counter–ions shown are butanesulfonate in acid (BSA), pentanesulfonate in acid (PSA), hexanesulfonate in acid (HxSA), heptanesulfonate in acid (HpSA), octanesulfonate in acid (OSA) and decanesulfonate in acid (DSA). The polymer films were grown by stepping the potential of the electrodes from 0 to +0.85 V.

Following the potential step the oxidation of the monomer in solution leads to

the deposition of the conducting polymer onto the electrode surface. The current at any

point in the deposition is a measure of the rate of polymer development and the total

charge passed is related to the total amount of polymer grown onto the device.

Following deposition of the polymer films the devices were washed with water and allowed to dry at room temperature before use.

The large variety of conducting polymer types that can be fabricated make an in–depth study of all polymers impossible. For the purpose of this research a small selection of the broad range of polymer types had to be made. This selection represented a typical cross–section of the full range of polymers available. For the characterisation of the affect of ethanol vapour on the sensors (Chapters 4 and 6) four types of polymers were used: Pan pentane sulfonic acid; Pan decane sulfonic acid; Ppy pentane sulfonic acid; and Ppy decane sulfonic acid. These represent the two types of monomer available combined with two different lengths of counter–ion, pentane sulfonic acid (five units) and decane sulfonic acid (ten units). When investigating the affects of CO_2 (Chapter 5) the polymers employed were Pan butane sulfonic acid. These sensors are modified after deposition by a treatment which involves soaking the polymer membrane in water for 10 minutes, followed by immersion in an aqueous solution of $NaHCO_3$ for 1 minute and finally in water for another 10 minute period. This modifies the ionic structure of the polymers and therefore permits the detection and measurement of CO_2. Brief experiments on the affect of CO_2 on the polymer types employed during ethanol characterisation without any post–deposition modifications were also completed.

2.5 Conclusion

This chapter has given an overview of the fabrication processes required in the creation of conducting polymer sensors. The development of the three types of sensor substrate employed during this study have been discussed and relative merits of the sensor

technologies employed have been compared. A brief summary of the electrochemical growth of conducting polymers has also been supplied with details about which types of polymers were used during the characterisation stages of this study.

2.6 References

2.1 A. C. Pike, Design of chemoresistive silicon sensors for application in gas monitoring, *Ph.D. Thesis, University of Warwick, UK*, *1996.*

2.2 N. Blair, The development and characterisation of conducting polymer based sensors for use in an electronic nose, *Ph.D. Thesis, University of Southampton, UK,* 1990.

2.3 V. S. Nguyen, S. Burton and P. Pan, The variation of physical properties of plasma–deposited silicon nitride and nxynitride with their composition, *J. Eletrochem. Soc.,* **131**, No. 10, (1984), 2348-2353.

2.4 K. E. Bean, Anisotropic etching of silicon, *IEEE Trans. Electron. Devices,* **ED-25** (1978) 1185-1193.

2.5 H. Seidel, L. Csepregi, A. Heuberger and H. Baumgärtel, Anisotropic etching of crystalline silicon in alkaline solutions, *J. Electrochem. Soc.,* **137**, No. 11 (1990) 3612-3626.

2.6 A. Dall'Olio, G. Dascoia, V. Varacca and V. Bocchi, Electron paramagnetic resonance and conductivity of an electrolyte oxypyrrole (pyrrole polymer) black, *C. R. Acad. Sci., Paris Ser. C,* **267** (1968) 433-435.

2.7 A. F. Diaz, K. K. Kanazawa and G. P. Gardini, Electropolymerisation of pyrrole, *J. Chem. Soc. Chem. Commun.,* **5** (1979) 635-636.

_____

2.8   J. J. Miasik, A. Hooper and B. C. Tofield, Conducting polymer gas sensors, *J. Chem. Soc., Faraday Trans.* **82** (1986) 1117-1126.

2.9   P. N. Bartlett and S. K. Ling-Chung, Conducting polymer gas sensors. Part III: Results for four different polymers and five different vapours, *Sensors and Actuators,* **20** (1989) 287-292.

2.10   A. F. Diaz, J. F. Rubinstein and H. B. Mark, Electrochemistry and electrode applications of electroactive/conductive polymers, *Advances in Polymer Science,* **84,** (1988) 113-139.

2.11   J. Heinze, Electronically conducting polymers, *Topics in Current Chemistry,* **152,** Springer, Berlin, 1990.

2.12   A. F. Diaz and J. Bargon, in T. A. Skotheim (ed.), *Handbook of Conducting Polymers,* **1,** Marcel Dekker, New York 1986.

2.13   P. N. Bartlett, J. W. Gardner and R. G. Whitaker, Electrochemical deposition of conducting polymers onto electronic substrates, *Sensors and Actuators A,* **21-23,** (1990) 911-914.

2.14   P. N. Bartlett, P. B. M. Archer and S. K. Ling-Chung, Conducting polymer gas sensors, Part I: Fabrication and characterisation, *Sensors and Actuators,* **19** (1989) 125-140.

2.15   K. Imanishi, S. Masaharu, Y. Yasuda, R. Tsushima and S. Aoki, Solvent effect on electrochemical polymerization of aromatic compounds, *J. Electroanal. Chem.,* **242** (1988) 203-208.

2.16   P. N. Bartlett and J. W. Gardner (ed), *Sensors and Sensory Systems for an Electronic Nose,* Kluwer Academic Publishers, Dordrecht, 1992.

_____

2.17   G. K. Chandler and D. Pletcher, The electrochemistry of conducting polymers, *Specialist Periodical Reports, Electrochemistry,* **10,** Royal Society of Chemistry, London 1985.

2.18   J. W. Gardner and P. N. Bartlett, Potential applications of electropolymerized thin organic films in Nanotechnology, *Nanotechnology,* **2,** (1991) 19-32.

CHAPTER 3

Dynamic Headspace Testing Station

3.1 Introduction

Conducting polymer sensors have previously demonstrated responses to a variety of gases and vapours [3.1]. Our own research has indicated that the polymers are affected not only by the concentration of analyte to which they are exposed but also by the ambient conditions in which they are accommodated. The development of a model to describe these effects would therefore require the exposure of the polymer sensors to a range of concentrations of an analyte whilst control is maintained over a number of operating conditions in the sensor chamber, such as the ambient temperature, absolute humidity and gas flow–rate. In order to achieve this, a dynamic headspace testing station was assembled with the aim of creating a controlled simulation of the type of conditions encountered in the atmosphere. The system allows the delivery of a range of concentrations of volatile organic compounds (VOCs) whilst control is maintained over the environmental conditions that affect the characteristics of the sensors.

The system was modified from existing equipment that was designed specifically for the analysis of beers [3.2, 3.3]. Different types of polymer device are accommodated by the inclusion of a generic sensor head which can be altered (or replaced) according to the type of sensor employed. The chemical and electronic equipment enables computer control over sampling, data collection and data storage

using custom written virtual instrumentation. The system is versatile enough to allow modification of the hardware for the delivery of gases rather than vapours. This is achieved through alterations to the compressed gas sources and the simultaneous by–passing of the VOC sample storage vessels. For example, if the compressed air sources employed as carrier gases were replaced by pre–calibrated concentrations of CO_2 the affects of this type of gas could be investigated. This dynamic system provided the means to collect all of the experimental data presented in this study.

The development of fully automated test systems has been reported previously by several workers. Many systems possess similar characteristics, such as microcomputer control, compressed gas sources, and both temperature and humidity control. The major differences between these systems is in the type of sensor employed (e.g. MOS chemoresistor [3.4-3.6], SAW devices [3.7, 3.8]) and the type of analyte of interest (e.g. vapours [3.5, 3.6, 3.8], gases [3.4, 3.7, 3.9] and odours [3.3]).

3.2 System Objectives and Design

The aim of the dynamic headspace system is to deliver a range of concentrations of volatile organic compounds to a variety of sensors while controlling both the temperature of the sensors and the water content of the headspace. The system should also be versatile enough to permit modifications allowing the VOC samples to be replaced by gases. The equipment would then allow testing to be carried out on several types of sensor (i.e. discrete resistive sensors, integrated resistive sensors, variable gap devices and mass sensitive devices) using an assortment of target analytes. It is also important to have the capability of automating the chemical hardware and data collection procedure through microcomputer control. This allows the system to collect

data over long periods of time with minimum user intercourse, reducing both the amount of inconvenience to the user and also eliminating errors associated with human interaction. A schematic overview of the gas/vapour test system that has been developed is shown in figure 3.1. The equipment can be divided into three catagories; vapour/gas flow hardware, signal conditioning and test sequence software. The gas flow hardware and signal conditioning electronics employed for polymer chemoresistors are identical to those used in previous experiments performed on the odours generated by beer samples [3.2, 3.3]. The electronic interface for the chemical hardware is contained in the same Eurorack system that also houses all of the resistive signal conditioning electronics.
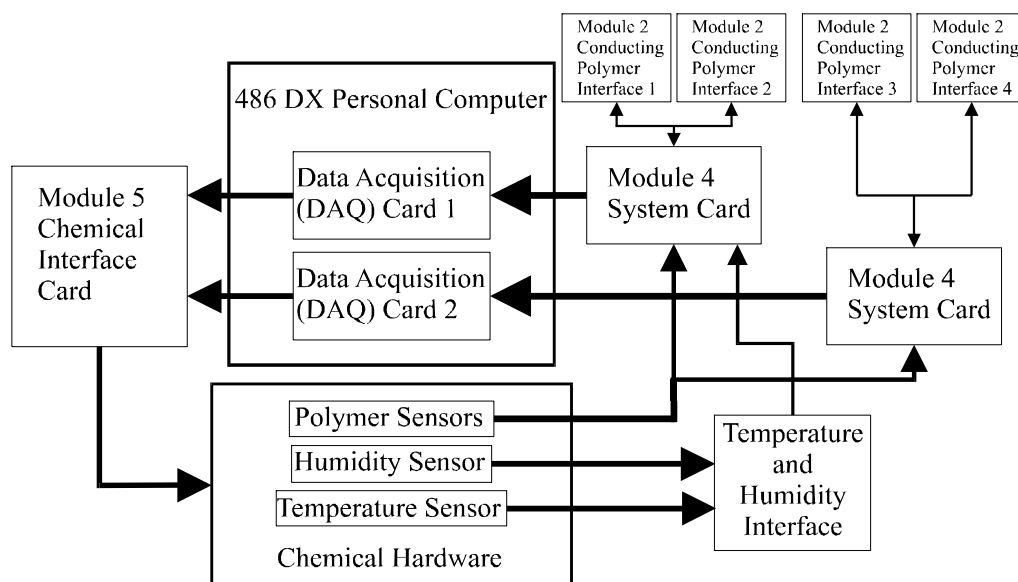
Figure 3.1 Schematic of the sensor test system used for discrete polymeric sensors and variable gap devices.

In order to control valve states and flow–rates in the chemical hardware both analogue and digital control signals are required. The signal conditioning electronics will then return analogue signals proportional to the resistance of the sensors. The generation and monitoring of these signals is achieved using two National Instruments®

AT-MIO-16-XE-50 data acquisition (DAQ) cards. The signals used for the control of the chemical hardware and the monitoring of chemoresistive responses are generated using a single microcomputer operating these two cards.

The software used to control the chemical hardware system and monitor the responses of the polymer chemoresistors was custom written in the National Instruments® high level programming language LABVIEW® for Windows, Version 4.0. This package allows the generation of virtual instruments (VIs) which are used to obtain real–time control over the sampling system and the monitoring and recording of signals over long sampling periods.

3.3 Chemical Hardware

Figure 3.2 shows a schematic layout of the sampling system with the elements shown using BS 2917/ISO 1219 symbols where possible. The principal aim of the system is to generate three gas lines: a dry air line; a line containing a high relative humidity; and a sample line containing a known concentration of the target analyte. By mixing each of these sources in user controlled ratios, a constant relative humidity may be generated and a range of concentrations of the analyte can be injected to the mixture without changing this level of water content. A key to the chemical apparatus employed, suppliers and specifications is shown in table 3.1.
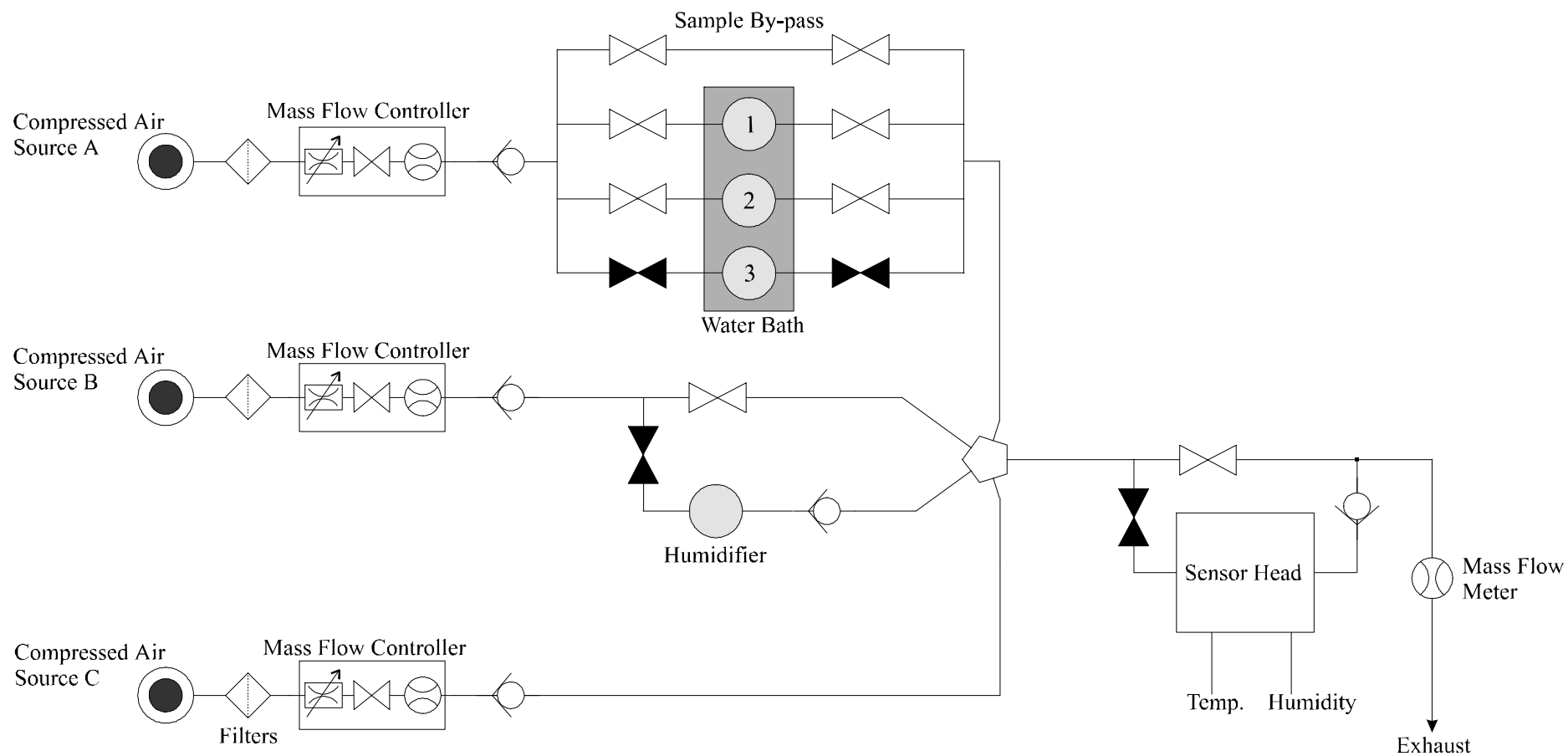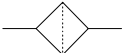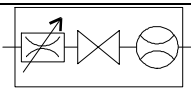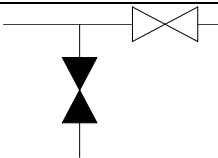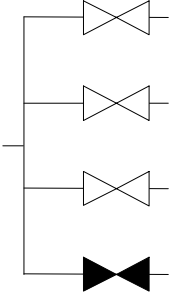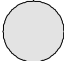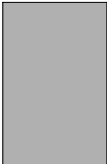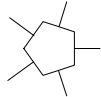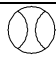
Figure 3.2 Schematic Of Chemical Hardware of the Injection Flow Analyser - showing from left to right, compressed gas bottle sources, line filters, mass flow controllers, non–return valves, quad NC valves, sample vessels (contained in a water bath), humidifier by–pass valve, humidifying bubbler with non–return valve, five way mixing chamber, sensor head by–pass valve, sensor head housing the temperature, humidity and polymer sensors, non–return protection valve and the final flow meter.

Table 3.1 Chemical hardware parts key

Symbol	Part	Supplier	Details
⬤	Compressed Air Source	BOC Gases Ltd.	Compressed cylinder containing low grade dry air. Pressure is controlled by a single stage regulator.
⬤	500 PPM CO_2/Air Mixture Compressed Source	BOC Special Gases Ltd.	Gas cylinder containing 500 PPM CO_2 in dry air. Concentration accuracy; filling tolerance $\pm 1\%$. Supply pressure controlled by a brass single stage gas regulator.
◇	Particulate Matter Filter	Lee Products Ltd.	Filters which trap particles with diameter greater than 35 μm.
	Mass Flow Controller (1, 2 and 3)	Brooks Instruments B.V.	Model TR 5850. 0 to 300 ml/min flow range. Each MFC consists of a flow controller, override valve and flow meter.
	Non–return Value	Lee Products Ltd.	Used after each MFC to prevent backward flows in the system due to pressure differentials or empty gas cylinders.
	3/2 Solenoid Activated, Solenoid Return Valves	Lee Products Ltd.	Low power solenoid values with 5 $V_{d.c.}$ switching voltage.
	Quad Manifold Valves	Neptune Research	Software configurable normally closed manifold valves. These are used either to split a single input into four outputs or to converge 4 inputs into a single output.
◯	Bubbler	Fisons Scientific Equipment Ltd.	250 ml Drechsel (gas washing) bottle and head with grade 3 sinter.
▮	Hakke Water Bath	Fisons Scientific Equipment Ltd.	

_____

	Mixing Chamber	N/A	Brass mixing chamber manufactured at Warwick University to allow the mixing of 4 input gases and the delivery to a single output.
	Flow Meter	Brooks Instruments B.V.	
	PTFE Tubing	Economatics Ltd.	4 mm O.D (2 mm I.D) tubing used wherever possible within the equipment.
	Fittings	Economatics Ltd.	Brass Compression fittings for use with 4mm O.D tubing.
Sensor Head	Sensor Chamber		Custom designed and manufactured sensor chambers.
	Dri–block® heater	Techne Ltd.	Dri–block heater Model DB-2P allowing 3 pre–set temperatures to be set in a range from room temperature to 110 ºC, with long–term stability within 0.1 ºC.

Compressed air was employed as the carrier gas during experiments on vaporous analytes. The sources delivered air to the Mass Flow Controllers (MFCs) via microbiological filters (Part NO. TCFA1201035A, Lee Products Ltd.). These filters are employed to reduce the amount of unexpected particles entering the MFCs, thereby avoiding distortion of the flow–rate measurements and eliminating long term contamination. The MFCs (Model No. 5850 TR, Brooks Instruments B.V.) are fully programmable and incorporate a flow–rate control valve, an override stop valve and a flow–rate meter to supply feedback signals. Three MFCs each with a range of 0 to 300 ml/min (i.e. 5 ml/s) and an accuracy of 1% of full scale, are employed to independently regulate the flow through each of the three supply lines.

_____

PTFE tubing and brass compression fittings were used throughout the system to connect together the integral pieces of chemical hardware. Both materials demonstrate negligible reactions with the compounds studied in our experiments and therefore should undergo no long term poisoning effects. A non–return valve is positioned directly after each mass flow controller to prevent any pressure differentials within the system which could cause a back flow. This would be particularly damaging to controllers positioned after vapour or water bubblers as it would lead to contamination of the controller with the associated fluid.

Mass flow controller C is used as a source of dry air and is therefore connected directly to a brass mixing chamber. This chamber was produced at Warwick University and is used to mix four input lines before delivering a single source which is exposed to the sensor head. Mass flow controller B delivers air to a solenoid activated, solenoid return 3 way valve. This valve directs flow either through a 250 ml Drechsel (gas washing) bottle containing water or through a by–pass line to enable cleaning or testing of samples in zero humidity. When the humidifier is enabled we can predict the concentration of water vapour contained in the air being emitted from the vessel by bubbling the gas through the fluid using a fine sinter (Grade 3). This technique allows us to make the assumption that the concentration of water is equal to the saturated concentration that would be found in a static headspace system. The concentration can then be accurately calculated using Antoine vapour equation [3.10, 3.11] and is dependent only on the temperature of the source and physical constants associated with the vapour.

$$\log P = A - \frac{B}{C + T} \tag{3.1}$$

where P is the partial pressure of the vapour, A, B, and C are constants associated with an individual vapour, and T is the temperature of the vapour. If we assume an ideal gas behaviour, which is sufficiently accurate for vapour and air mixtures, then we can calculate the concentration of vapour from the partial pressure using equation 3.2

$$C = \frac{P(vap)}{P(air)} \times 10^6 \tag{3.2}$$

where C is the concentration of vapour in PPM, $P(vap)$ is the partial pressure of the vapour and $P(air)$ is assumed to be equal to atmospheric pressure. Both the humid air flow and the humidifier by–pass are connected directly to the mixing chamber.

Mass flow controller A delivers the compressed air carrier gas to a quad Normally Closed (NC) manifold valve (Model No. 225T07, Neptune Research). This valve is used to route the flow through any of three sample vessels or through a by–pass line. A second valve of the same type is used to connect the selected sample vessel or by–pass to the mixing chamber. In this manner up to three vapours can be tested in an automated manner with a sample by–pass facility making it easier to clean the majority of piping in order to reduce contamination. Concentrations of analyte can again be predicted using equations 3.1 and 3.2 and employing the constants shown in table 3.2.

The output from the mixing chamber is connected to the sensor head via a solenoid activated, solenoid return 3 way valve. This allows the sensor head area to be by–passed during cleaning or purging of the equipment. The output of the sensor head area is recombined with the by–pass before passing through a final mass flow meter (Model No. 5850 TR, Brooks Instruments B.V.). This final piece of equipment is used

for comparison with the flow inputs in order to check for leaks in the system. The

vapours then pass to a fume cupboard where they are vented to atmosphere.

Table 3.2 Constants for use in the Antoine equation for the prediction of the partial pressure of the saturated headspace above fluid at equilibrium. Values for several volatile organic compounds and also water vapour are shown. The temperature range for which these values are valid is also indicated. Constants documented in [3.11] except water which was derived from data found in [3.12].

Chemical	Constant A	Constant B	Constant C	Temperature Range / °C
Water	10.12	1686.0	229.7	0.85 to 106
Toluene	6.96	1346.8	219.7	6 to 137
Benzene	6.90	1211.0	220.8	8 to 103
Ethylene Glycol	8.09	2088.9	203.5	50 to 200
Ethanol	6.95	1344.8	219.5	6 to 137

The sensor chamber is located within a Dri–block heater (Model DB-2P, Techne

Ltd.) allowing 3 pre–set temperatures to be fixed in a range from room temperature to

110ºC, with long–term stability within 0.1ºC. This gives accurate and stable

temperature control over the sensor area. There were two types of sensor chamber used

during this study. The first system was used in the collection of static data from

Warwick discrete polymer devices (code–named SRL 127). This system consisted of a

glass jar with a PTFE cap through which a custom designed printed circuit board was

positioned. The board was held in place and sealed using a thermally conductive epoxy

encapsulant and made inert using a PTFE spray. Connections to input and output

tubing were made using brass 1/8 inch British standard pipe connectors. The signals

from the polymer sensors were interfaced to the electronic conditioning circuitry using

the sensor mounting circuit board and 25 way D–type connectors. Temperature and humidity sensors (LM35DZ, National Semiconductor Ltd and Minicap 2, Panametrics, respectively) were also mounted on the circuit board within the chamber. Conditioning of these signals was carried out on the board and the resulting signals were connected to an interface card (Module 4, described in section 3.4) using 6 way Mini DIN connectors. The humidity sensor gives a quick, linear response between 5% and 95% R.H, and has negligible temperature dependence between 0 °C and 50 °C. The temperature sensor gives a linear response between 0 °C and 100 °C with a response of 10 mV per degree centigrade. The glass jars gave ample space (120 ml) for mounting up to 12 discrete polymer sensors, 2 sensor arrays on integrated packages, or a combination of both discrete and integrated sensors. A rubber O–ring wrapped in PTFE tape was used to improve the seal between the jar and lid.

Significant design improvements can be made to this sensor chamber through the reduction of dead–volume around the sensors, the production of a heat exchanging system to ensure the gas/vapour entering the chamber is at the same temperature as the sensors and through the reduction of leaks encountered. For these reasons a second sensor chamber was designed and manufactured by Mr Ian Talbot as part of a third year undergraduate project [3.13]. This second generation chamber was made in three parts; a bottom section that included a meandering track heat exchanging system, a middle section supplying a deadspace area for sensor exposure and finally the sensor mounting head. A photograph of the three parts of the sensor chamber is shown in figure 3.3. The sensor mounting head shown in figure 3.3 has the capability of mounting up to 12 discrete sensors (such as SRL127), a single array of sensors mounted on integrated packages (up to 16 pin dual–in–line packages) or 2 variable gap devices on alumina

tiles. This head can be replaced by similar designs catered to hold a variety of sensor types such as quartz crystal microbalance or resistive micro–bridge sensors.
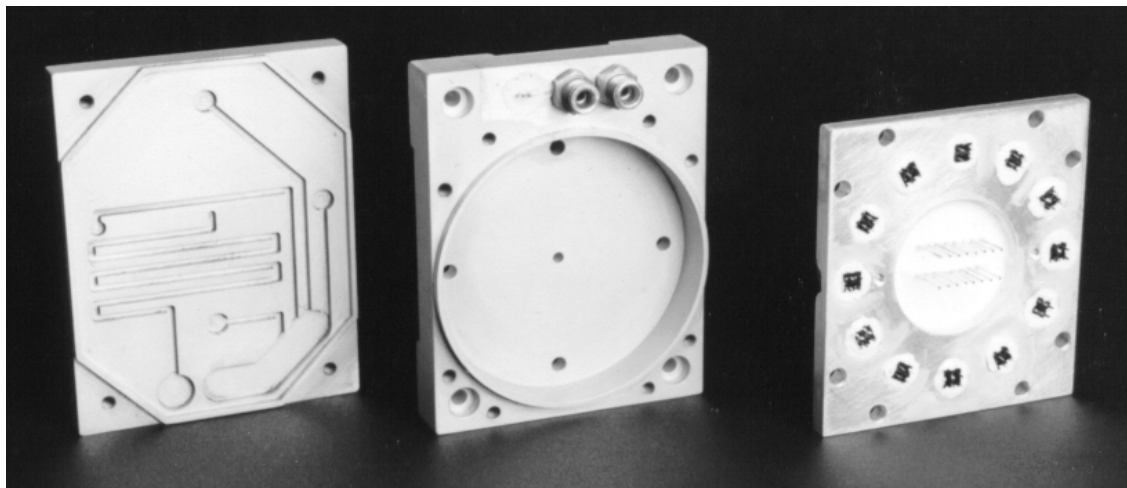
Figure 3.3 A photograph of a second generation sensor header showing the meandering track heat exchanging system (left), sensor exposure area (centre) and sensor mount (right) with the capability of interfacing up to 12 discrete sensors and/or 16 pin D.I.L package.

This second generation sensor chamber has a dead–volume of less than 38 ml. The length of the heat exchanger determines the thermal time response of the chamber and is dependent on a number of factors including:

- the type of gas/vapour employed

- the gas/vapour flow rate

- the input temperature of the gas/vapour

- the temperature of the sensor chamber

The length of the heat exchanging channel therefore has to reflect the operating conditions expected for the chamber. However, the length is also limited by the physical dimensions of the chamber. The channel employed for this chamber has a length of 264 mm and a cross–sectional area of 4 mm^2. When modelled using a forced convection heat transfer theory these dimensions are shown to be of sufficient length to

heat a variety of gases and vapours over range of temperatures and flow rates beyond

the normal operating conditions of this system [3.13].

Figure 3.4 shows how the three parts of the sensor head connect together to

form a single sensor chamber. The dimensions of the blocks allow two chambers to be

contained within a single Dri–block heater.
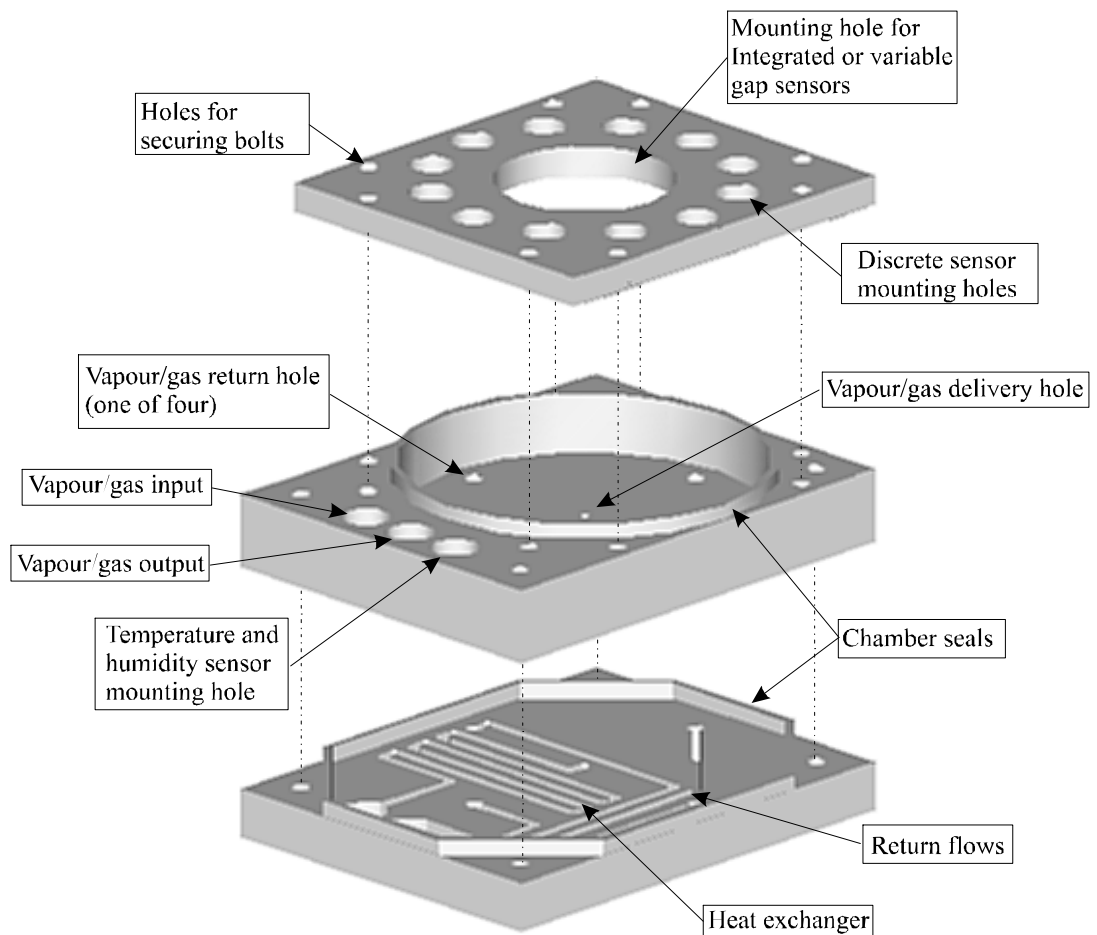
Figure 3.4 An exploded view of the second generation sensor chamber showing the location of connectors, heat exchanger, screw holes, chamber seals and vapour delivery/return holes. Indications of the way in which the blocks can be connected together is also given.

By connecting the chambers input and output connections either in series or in parallel

simultaneous tests on up to 24 discrete sensors, 4 variable gap sensor arrays or 2

integrated sensor arrays can be carried out. The heat exchanger is sufficiently long to

_____

enable flow–rates of up to 500 ml/min of most VOCs to be heated by approximately

100°C. This ensures that there is no possibility of the sensor responses being

influenced by thermal shocks due to the input vapour cooling the sensors to which it is

exposed. The chamber was produced in aluminium and coated with a thin PTFE film

to ensure no long term contamination occurred. Sealing grooves between the three

sections of the chamber were combined with rubber O–rings wound in PTFE tape to

ensure leaks were minimised when the sections were bolted together.

3.4 Electronic Interfaces

The electronic hardware used both in the control of the chemical equipment employed

in the dynamic headspace testing system and the interfacing of the polymer

chemoresistive sensors to the PC–based DAQ cards was designed and produced by Dr.

T. C. Pearce and formed part of his PhD thesis [3.3]. Three types of custom designed

PCB Eurocard™ modules were employed; a polymer chemoresistor interface card

(Module 2), a system interface card (Module 4) and driver circuitry for the chemical

hardware (Module 5). Interfacing for the temperature and humidity sensors was carried

out either on the PCB used to mount the polymer sensors in the gas flow, or on a

external interface card. Both methods supplied voltages proportional to the temperature

and humidity to the Module 4 card to be interfaced to the PC.

The PC–based DAQ cards (National Instruments, Model No. AT-MIO-16-

XE50) each provide 16 single–ended analogue inputs (ADC) with 16 bit accuracy, 2

single–ended analogue outputs (DAC) with 12 bit accuracy and 8 TTL digital

input/output signals (DIO). The analogue inputs to the DAQ cards are used for the

monitoring of the polymer sensor array voltages, the temperature and humidity sensors

and the returned voltages from the mass flow controllers and the mass flow meter. Three of the four analogue outputs are used to control the flow–rate settings of the MFCs with the final output left spare. The digital input/output signals are used to control the states of the valves throughout the chemical hardware. The noise demonstrated by the system generates a 20 unit, peak to peak signal at the 16–bit (65536 unit) ADC.

3.4.1 Eurorack System

All of the custom designed PCB Eurocard™ modules have been incorporated into a standard KM6 Eurocard™ (VERO–BICC Electronics) compliant with DIN 41494 part 5, IEC 297 section 3 and IEC subcommittee SC 48D. This system incorporates all of the module cards required to interface up to 24 polymer chemoresistors and the required driver circuitry for the chemical hardware. The backplane connectivity routes signals from the two Module 4 system cards through to the four Module 2 and the single Module 5 cards.

A front view of the Eurocard™ system is shown in figure 3.5 (a). To the right of the rack is the single Module 5 card with MFC ribbon connectors (top) and discrete valve connections (bottom). Next to this are the two Module 4 system interface cards with connections to the sensor heads and the four Module 2 sensor interface cards with channel scale settings. Finally, to the left of the rack are the three linear power supplies (Model No. LK 35, VERO–BICC Electronics). This split–mode power supply eliminates the possibility of switching noise passing from the Module 5 card to the
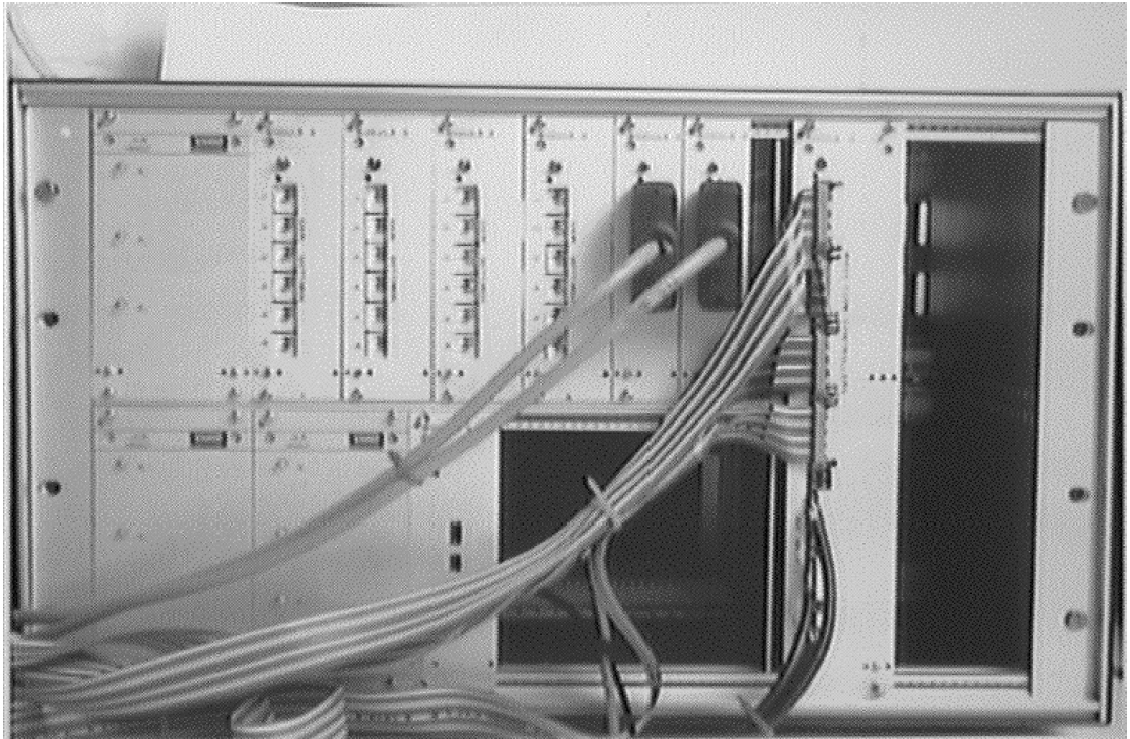
(a)
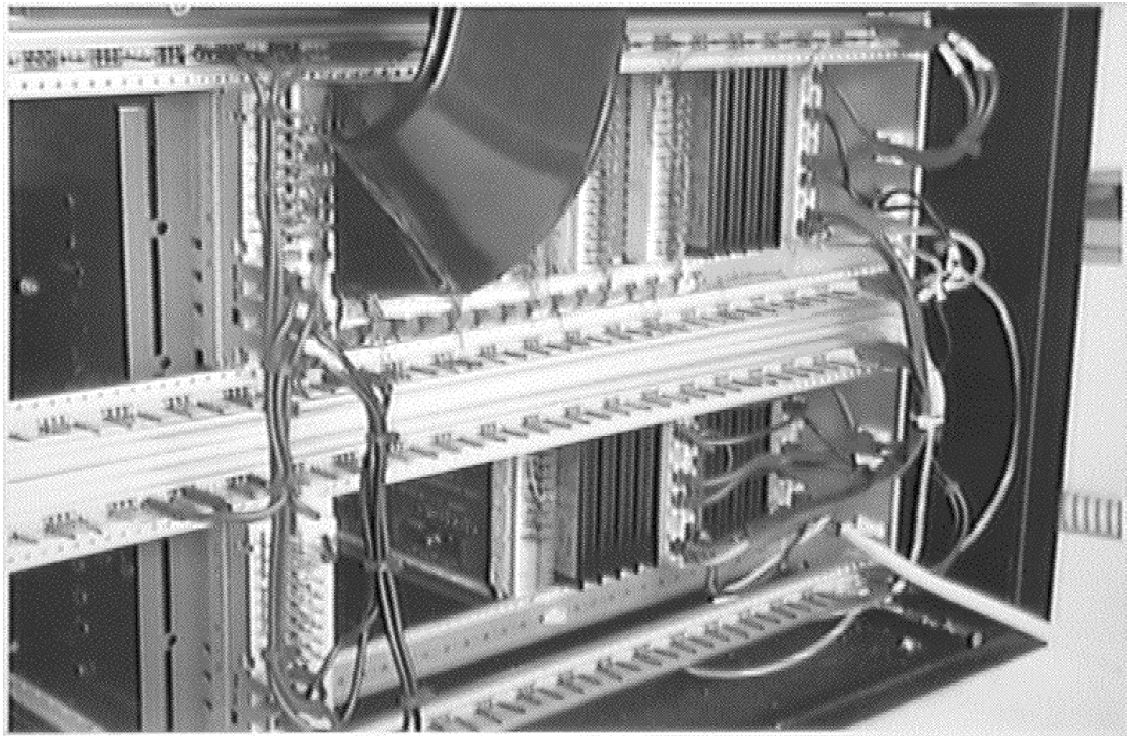
(b)

Figure 3.5 Photographs of the Eurorack™ system - (a) front, and (b) rear.

_____

sensor interfaces by providing separate sources for the analogue instrumentation associated with the sensors and those that power the chemical hardware. A rear view of the Eurocard™ is shown in figure 3.5 (b). Connections are made using wire–wrapping as this system was initially designed as a prototype version. However, this technique could easily be replaced using a custom designed back–plane PCB when necessary. The distribution of power to the modules is provided by the bus–bar shown at the top and bottom of each card section, with power connections to the individual cards made using local wire–wrapping. For Electromagnetic Compatibility (EMC) and safety reasons the entire rack and casing of the system are connected to mains earth.

3.4.2 Polymer Chemoresistor Interface

The Module 2 polymer interface (Module 2) converts the DC–based resistance of each polymer film into a voltage compatible with the ADC input stage of the DAQ cards. It does this by utilising the near ohmic response of CP's over the operating voltage range of the interface circuitry. The I–V characteristics of electrochemically prepared conducting polymers have been studied by Blair [3.14]. The behaviour of the films was shown to be close to ohmic at low voltages, however at voltages greater than ± 0.5 V the polymers became non–linear. It was suggested that the non–linear characteristic could be due to variable range hopping. Pearce [3.2] also studied the I–V characteristics of poly(pyrrole) devices when designing the Module 2 polymer interface card. Again a near ohmic response was found in the range ± 0.15 V.

We can therefore say that for the voltage range employed in the Module 2 polymer interface the devices investigated possess a linear I–V characteristic. This allows us to employ a constant current source and monitor the voltage dropped over the

polymer, with the response directly proportional to the resistance of the polymer film as shown in figure 3.6.

During the design of the Module 2 cards a number of features were considered to be vital to the successful operation of the system. The functionality of the cards
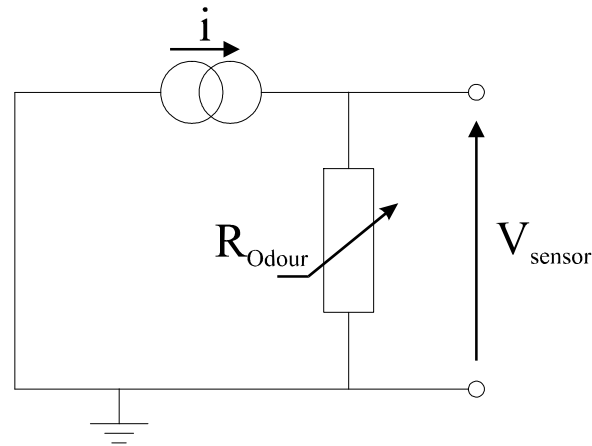
Figure 3.6 Measurement principle used for a conducting polymer interface.

would therefore have to include capabilities, such as the ability to measurement a wide range of resistance values, the capacity to detect small changes in baseline value, an output scaled between 0 and 5 V, a low noise output (nominally lower than 1 mV$_{pp}$) and good long–term stability to reduce the need for re–calibration.

A simplified diagram of a single conducting polymer interface channel is shown in figure 3.7. The polymer sensor is connected between point A and the ground, G of the circuit. The first op–amp circuit drives a constant current through the sensor because of the action of the precision reference diode (D_Z). The diode sets a constant voltage of 2.5 V between one side of the scaling resistor (R_{scale}) B and the non–inverting input, A, to the op–amp at virtual ground. The magnitude of the constant current is then defined by the size of the scaling resistor and its value given by equation 3.3

_____

$$I_{sensor} = \frac{2.5V}{R_{scale}}$$

(3.3)
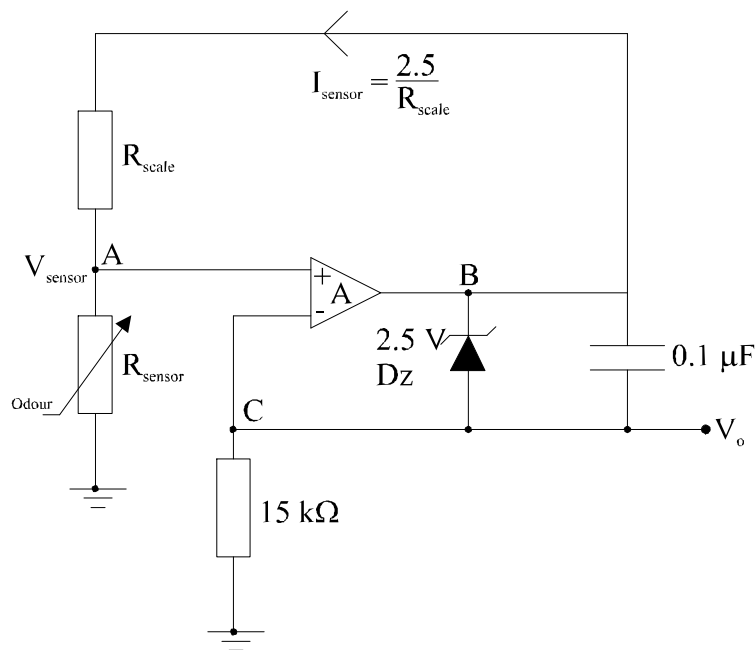
Figure 3.7 Simplified schematic diagram of a single conducting polymer sensor interface circuit, which acts as a linear ohmeter. The output, V_o, is amplified by a second stage circuit, providing offset and gain settings.

A selection of R_{scale} values were chosen to provide a range of currents through the sensor of 1μA, 10 μA, 100 μA, or 1 mA to 0.1% accuracy. The resistance of the device, R_{sensor} can be given by,

$$V_{Sensor} = R_{Sensor} \times I_{Sensor}$$

$$= R_{Sensor} \times \frac{2.5V}{R_{Scale}}$$

(3.4)

where V_{sensor} is the voltage dropped across the device. The first stage of this circuit is designed to generate a voltage drop of less than 100 mV across the polymer device, which is well below the value required in order to ensure the response of the sensors is in the ohmic region of their I–V characteristic. The scale settings therefore correspond to full scale readings of the sensor resistance's up to 100 Ω, 1 kΩ, 10 kΩ and 100 kΩ, with R_{scale} being 2.5 kΩ, 25 kΩ, 250 kΩ and 2.5 MΩ.

The second stage of the circuit amplifies the full scale sensor signal, V_{sensor} to 5 V at the output V_o. A standard non–inverting amplifier provides the required gain of +50 in order to generate an output voltage compatible with the input stage of the DAQ cards. This stage also provides voltage offset control and gain setting capabilities although these are not shown in figure 3.7. Full design documentation, schematics, parts lists and revisions are provided by Pearce [3.3].

3.4.3 System Interface Cards

The system interface card, Module 4, is required to distribute signals from the four Module 2 sensor interfaces, the Module 5 flow system controller and the temperature and humidity instrumentation to the two PC–based DAQ cards. This module provides:

- Synchronisation of data acquisition duty cycles of separate Module 2 polymer interface cards;

- Distribution of backplane connections to other hardware modules;

- Distribution of sensor signals to other hardware modules;

- Distribution of DAQ card signals to and from other hardware modules.

Connections to the DAQ cards are made via two 50 way SpeedBlock™ connectors using fully shielded ribbon cables. Backplane connections are made via standard 96

way system connectors. High specification 25 way D–type sockets are used to interface the polymer device signals, while the supply of power and the monitoring of temperature and humidity devices was carried out using 6 way mini DIN connectors. Full design documentation, schematics, parts lists and revisions are provided by Pearce [3.3].

3.4.4 Chemical Hardware Controller Card

Control of the chemical hardware was maintained using a single PCB, the Module 5. This module supplies circuitry for driving the MFCs, controlling the sample vessel valves and controlling the by–pass valves with associated TTL conditioning on–board. The drive circuitry for the MFCs gives regulation over the three parts of this equipment: the flow sensor, control valve and the electronic control system. This circuitry also allows four important features to be implemented:

I. **Soft Start –** configures the flow control system using a suitable damping factor to reduce gas over/under shoot.

II. **Remote Programming –** allows a single analogue voltage to set the flow–rate passing through the control valve.

III. **Valve Override –** overrides the flow control setting to obtain a fully open or fully closed condition.

IV. **Flow–rate Measurement –** supplies a single analogue voltage related to the flow–rate passing through the instrument. This can be used for feedback in flow control instrumentation.

Three of the analogue outputs from the DAQ cards are used for controlling the flow–rate settings of the MFCs. These voltages are directly connected to the controllers via the Module 5 card. The units provide an accuracy of ±1% full scale and give excellent rejection of fluctuations in the pressure of the supply source. Double–pole Butterworth filters using single operational amplifiers are used to condition the return signals relating the actual flow through the equipment. These are then connected to analogue inputs to the DAQ cards. The override valves included in the MFCs are controlled by TTL outputs from the DAQ cards and a Single Pole Change Over (SPCO) relay driven by a transistor stage.

In the chemical hardware flow was routed through the sample vessels using two quad manifold valves and a further two valves were required for by–passing both the humidifying vessel and the sensor head itself. An SPCO relay driven by a transistor stage is again used to allow digital signals from the DAQ card to control this equipment. In addition to this circuitry, a simple RC network has been included to increase the operating life of the valves. An initial d.c. switching voltage of 12 V used to activate the valves is subsequently decreased to a holding voltage of only 4 V. An LED has also been incorporated on each channel and these are grouped at the front panel of the Module 5 for diagnostic purposes. Full design documentation, schematics, parts lists and revisions are provided by Pearce [3.3].

3.4.5 Temperature and Humidity Interface

Each sensor head produced contains both a temperature and a humidity sensor. The temperature sensor (LM35DZ, National Semiconductor Ltd.) is a three pin integrated device that provides a linear voltage output of 10 mV / °C. The device requires power and ground to be supplied and returns a voltage which is conditioned using unity gain

_____

operational amplifiers as buffer circuitry. The returned voltage is then connected via the system interface card to spare analogue inputs on the DAQ card.

The humidity sensor (Minicap 2, Panametrics Ltd.) is a capacitive sensor designed for monitoring relative humidity. The device relies on the sensitivity of the dielectric constant of a polymeric membrane to water vapour. The signal conditioning of such a device involves the use of two astable multi–vibrators with the capacitive device controlling the frequency of the first stage. Unfortunately the use of this kind of device has a number of disadvantages. Firstly, the sensitivity of the dielectric constant to fluctuations in humidity was found to have a strong temperature dependence. For accurate readings of either absolute or relative humidity the signals from this sensor would have to be combined with the returned temperature signals. A model of the characteristics of the sensor would then have to be produced that could be used in a range of temperatures and humidity and software employed to convert the sensor readings to reflect the true humidity in the sensor chamber.

A second problem encountered when using this type of device was due to the polymer membranes sensitivity to the target analytes. The humidity sensor demonstrated a significant dependence on the VOCs entering the sensor head. The magnitude of the capacitance change was directly related to the concentration of the analyte to which it was exposed. This response was present at a range of humidity settings in the mass flow equipment, including a test in which dry air was used exclusively. This final test conclusively demonstrated that the humidity sensor was responding to both ethanol and toluene vapour. For these reasons the humidity sensor was used purely as a diagnostic device with only those readings obtained during baseline or purge periods being considered valid.

_____

3.5 Testing Protocol

An overview of the testing procedure used for all of the experiments reported in this study is shown in figure 3.8. The sequence begins with the user manually loading the polymer devices into the sensor head and setting up the interface ranges on the Module 2 sensor interface cards. A warm–up period of at least 24 hours is then given allowing the sensors to reach thermal equilibrium within the Dri–block heater. Diagnostic tests and leak checks are then carried out manually using real time control software. The operation of each of the MFCs is confirmed, the integrity of connections in the chemical hardware is checked and leaks in the system are minimised. The compressed gas source is then employed in a pre–clean phase. This ensures that no contamination of the equipment has occurred since the last testing sequence. High flow–rates are directed through all piping, control elements and glassware with impurities being carried out through the exhaust and vented to atmosphere. During the next stage the user loads the sample vessels with required solutions and the humidifier with water (or the required wetting mixture). A sample preparation phase is then initiated which employs high flow–rates of the carrier gas to extinguish all of the laboratory air and other contaminates that may have been trapped within the sample vessels and humidifier. These samples are then considered ready for testing. The main data acquisition phase is then completed with the sensor responses being stored either directly to hard disc or in the computer's transient memory and downloaded to disc when the phase is complete. If further tests are required on both the analytes and sensors installed in the chemical hardware this phase can be repeated indefinitely.

_____
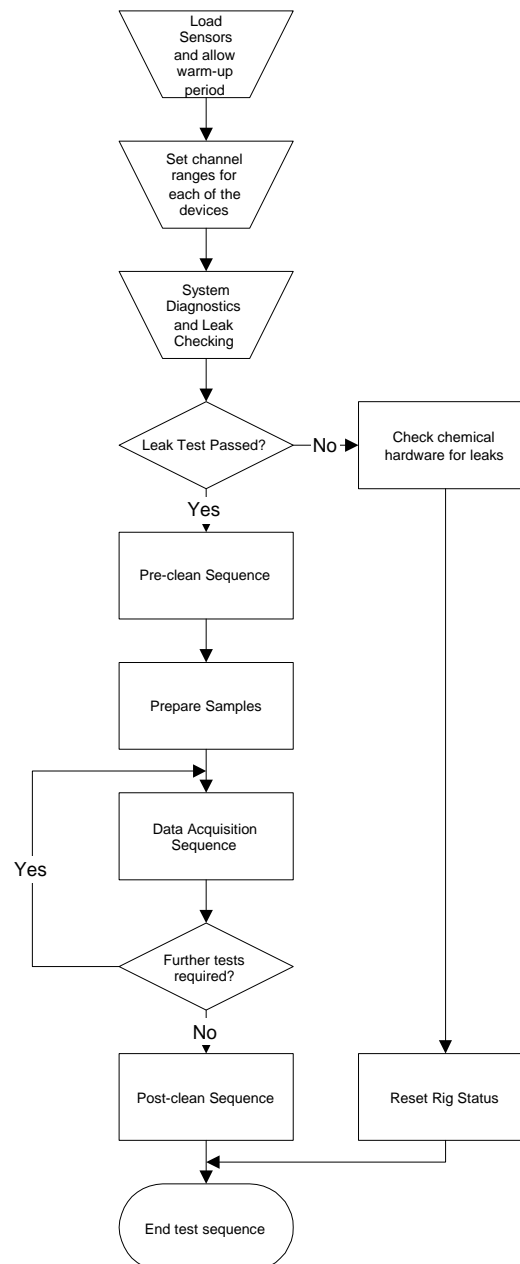
Figure 3.8 Overview flowchart of testing sequence.

When all of the required tests have been completed the samples and sensors are removed from the equipment and a post–cleaning phase is executed. This phase is identical to the pre–clean stage and fulfils a similar function by reducing cross contamination between successive tests.

3.5.1 Diagnostics and Leak Checking

_____

Diagrams for the diagnostic and leak checking phase are shown in figure 3.9 and figure

3.10. These phases are carried out manually following using real–time control over the

chemical hardware and stringently following the sequence shown. Each MFC is

checked individually to confirm that it is functioning correctly and that there are

negligible leaks in the associated piping and valves. The phase begins with the user

opening the three compressed gas sources and confirming that there is sufficient

pressure to complete the whole testing sequence. The rig status is then confirmed to be

at the default settings with no flow through the controllers by setting all of the control

signals from the software to zero. Each MFC is addressed sequentially with MFC 3

(controlling the dry air line) tested first because this has the lowest amount of

associated chemical hardware and is therefore useful for confirming the absence of

leaks both in the dry air line and in the sensor head by–pass and exhaust. If leaks are

found in these areas they would be common mode to all of the MFC tests and therefore

influence further checks. For this reason, if excessive leaks are confirmed from the first

MFC inspection, the testing sequence will terminate.

Each of the controllers undergo two diagnostic tests and a single leak check.

This procedure involves setting an individual arbitrary flow–rate (300 ml/min) to the

flow controller and confirming that the returned flow from the integral flow meter is of

equal magnitude. This flow is then diverted through the chemical hardware associated

with the MFC. By reading the returned signal from the output mass flow meter we can

Start Process

Open Gas Cylinders

Check 3 cylinders for pressure requirement

Sufficient gas pressure? —No→ Replace low gas cylinder

Yes

Set control signals to zero

Activate sensor head by-pass

Set MFC 3 (dry air) flow-rate to 300 ml/min

MFC 3 Flow Test

Does MFC 3 return flow = set flow? —No→ Report MFC 3 failed

Yes

Dry Air Line Leak Test

270 ml < output MFM < 300 ml? —No→ Report leak in dry air line, sensor head by-pass or output line

Yes

Reset MFC 3 flow-rate to zero

MFC 3 Zero Flow Test

Output MFM = zero? —No→ Report MFC 3 zero error

Yes

A

Reset rig status

Finish Sequence

A

Activate humidifier by-pass

Set MFC 2 (wet air) flow rate to 300 ml/min

MFC 2 Flow Test

Does MFC 2 return flow = set flow? —No→ Report MFC 2 failed

Yes

Wet Air Line Leak Test

270 ml < output MFM < 300 ml? —No→ Report leak in wet air line

Yes

Activate humidifier line

270 ml < output MFM < 300 ml? —No→ Report leak in humidifier

Yes

Reset MFC 2 flow-rate to zero

MFC 2 Zero Flow Test

Output MFM = zero? —No→ Report MFC 2 zero error

Yes

Reset by-pass valve

Reset rig status

B

Finish Sequence

Figure 3.9 Flow chart for diagnostic and leak checking phase - part 1.
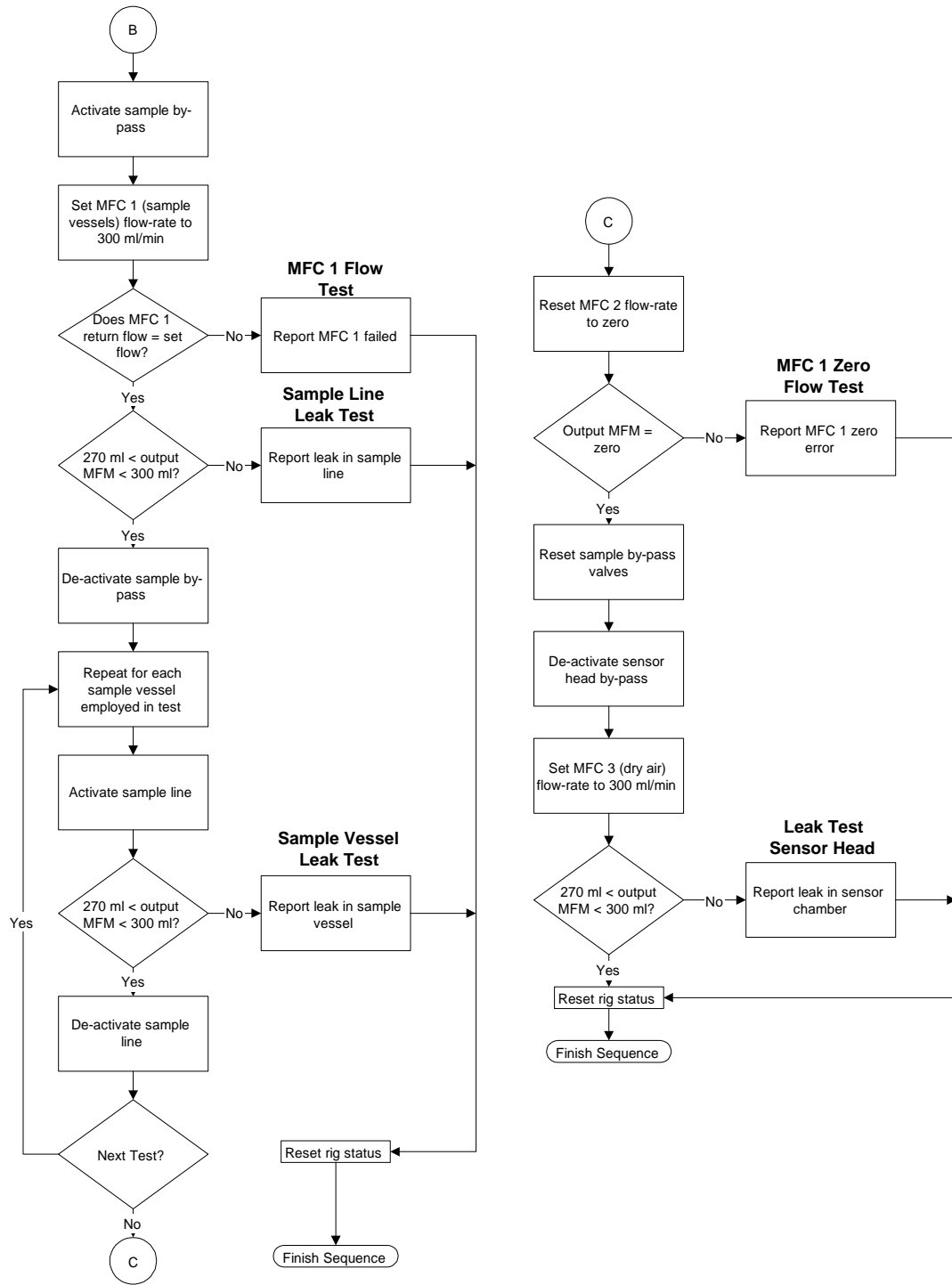
Figure 3.10 Flow chart for diagnostic and leak checking phase - part 2.

establish the extent of any leakage in the system and compare this with the allowed

tolerance. When inspection of all chemical hardware allied with the MFC is complete

the flow–rate control is set to zero and the integral flow meter is checked to confirm the

controller is closing correctly. These tests are carried out on each MFC sequentially.

3.5.2 Pre/Post Clean Phase and Sample Preparation

The pre/post clean phases allow the chemical hardware, including the sample vessels

and associated piping to be thoroughly cleaned before the samples are loaded and data

acquisition occurs or after data acquisition when the samples have been removed. This

phase requires both the sample vessels and humidifier to be empty and clean. High

flow–rates are set on the all three MFCs and the flow is directed through the sample

chamber by–pass and the humidifier before being re–combined and leaving the

equipment via the sensor head by–pass and exhaust system. These conditions are

maintained for 10 minutes to ensure thorough decontamination of all vessels and

associated pipes and valves. At the end of the 10 minute period flow is directed

through the humidifier by–pass and the first of the sample vessels. A 10 minute period

is again allowed for cleaning each of the sample vessels.

When used for cleaning the equipment following a series of tests the procedure

will be the final computer controlled sequence. The rig status should therefore be set to

default, the gas sources switched off and, if an extended period is expected before the

next test sequence, the sensors should be removed and stored correctly. If the sequence

has been applied as a phase prior to testing, then the next stage is to install and prepare

the target analytes. The installation of the analyte involves filling the 250 ml Dreschel

vessels with analyte sufficiently to cover the sintered gas wash bottle head. The

(a)

Start sequence

Reset rig status

Activate sensor head by-pass

Set all MFC's to 300 ml/min

Activate sample chamber by-pass

Activate humidifier

Wait for 10 minutes

Activate humidifier by-pass

For each sample vessel

Activate vessel

Wait for 10 minutes

Next vessel?

Yes

No

Reset rig status

End sequence

(b)

Start sequence

Reset rig status

Load analyte into sample vessels

Activate sensor head by-pass

Set MFC 1 to 300 ml/min

For each sensor vessel

Is this vessel used in test?

Yes

Active vessel

Wait for 5 minutes

De-activate vessel

Next test vessel?

Yes

No

Set MFC 1 to zero flow

Reset sample valves

Active humidity chamber

Set MFC 2 to 300 ml/min

Wait for 5 minutes

Reset rig status

End sequence

Figure 3.11 Flow chart for (a) pre/post–clean phase, and (b) sample set–up phase.

_____

objective of this procedure is to maximise the length of the mean carrier gas bubble path, causing the vapour/gas mixture leaving the chamber, even at high flow–rates, to be approximately equal to the atmosphere created in a static system. This increases the accuracy of equation 3.1 used for calculating the concentration of analyte in the sensor head.

When the samples are installed the preparation phase, shown in figure 3.11(b) is initiated. This sequence ensures that the samples are pure and contain no contaminates prior to the data acquisition phase which could interfere with the sensor's response. A high flow–rate (300 ml/min) is bubbled sequentially through each of the samples used in testing and also through the humidifier for a period of 5 minutes. This regime was found to be proficient in extinguishing all laboratory air contained during the filling of the vessels and also any other contaminants in the solutions. The sensor head is by–passed during this period to ensure the sensors are not poisoned during this phase. When this sequence is completed the analytes are prepared for the data acquisition phase and the rig status can be reset.

3.5.3 Data Acquisition Phase

This phase is run completely by a computer VI reading parameters from user written text files containing flow–rate and valve settings. The parameters are stored in transient memory and indexed to time. A running clock is created in the software and changes in chemical hardware settings are triggered when the system clock equals a setting in the text file. The remainder of the row allied with the sampling time contain the information required to set the flow–rates on all 3 MFCs and the 10 valves settings. Throughout all of tests documented in this study a constant combined flow–rate of 300 ml/min has been maintained through the sensor chamber. This parameter remained

_____

constant to due to the possibility of the sensors having a dependence on the flow–rate,

perhaps through the pressure created in the chamber, and also to simplify the modelling

of the systems flow dynamics (described in section 3.7.2).

The stage begins with the text file being read into the PC transient memory and

the confirmation of satisfactory operation of each of the MFCs used in the test. When

this is complete the user specified file paths, data acquisition rates, data acquisition

periods and data storage regime are read from the graphical user interface. The system

has the capability of storing the acquired data either in transient memory and

downloading to file at the termination of the test, or by writing the sensor signals

directly to disc as they are collected. The storage of data in transient memory allows

the software to manage higher sampling rates than when the data is written directly to

disc. However, when long tests are required, large amounts of data are to be stored or

data acquisition rates are low it is possible to write the data directly to disc. This

reduces the amount of data being carried in transient memory and also reduces the risk

of data loss due to a computer or system failure.

The software allows the user to set 4 files to which the signals from all of the

sensors will be stored, the period for which to use the specified file and also the data

acquisition rate to be employed for this file. This allows total command over the data

acquisition process giving the option to change the data acquisition rate during a test

and control over the size of the file created. When the system clock is greater than the

time parameter of the final row of the acquisition text file the test is complete. In the

transient memory data acquisition regime the contents of the memory are downloaded
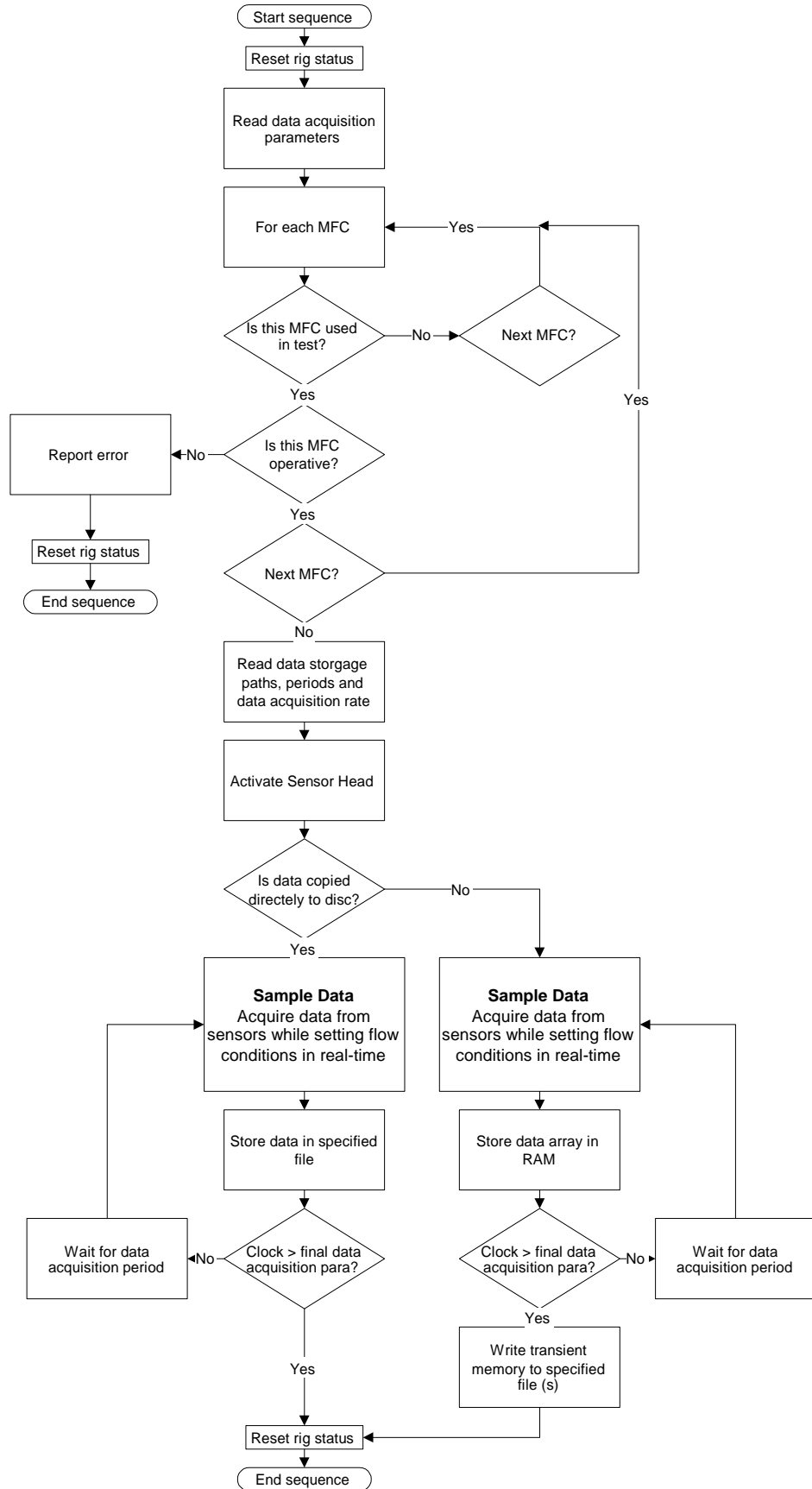
Figure 3.12 Flow chart for data acquisition phase.

to the specified file. In both cases the system now either initiates a post–clean process (during which the user would have to unload the analyte solutions) or resets all chemical hardware to default settings and is ready for the next data acquisition sequence.

3.6 Virtual Instrumentation

3.6.1 Introduction

Software control over the chemical hardware is achieved using National Instruments$^{®}$ data acquisition package LABVIEW$^{®}$ for Windows, Version 4.0. This software creates Virtual Instruments (VIs) which are defined as a layer of software and/or hardware added to a general–purpose computer in such a fashion that users can interact with the computer as though it were their own custom–designed traditional electronic instrument. The system consists of four elements: data acquisition; analysis of signals; presentation of data; and control. Data acquisition is carried out by the DAQ cards and the analysis and presentation of data by the software. Control over the system is maintained by a combination of both software and DAQ cards.

A VI is a hierarchical system consisting of two sections: the front panel and a wiring diagram. The front panel acts as a graphical user interface allowing the user to control the output of analogue and digital signals from the DAQ cards and also visually monitor the returned voltages. The wiring diagram is used to connect together the elements of the front panel, create procedure loops and communicate signals to and from the DAQ cards. Sub–VIs are employed to simplify tasks such as disc management, instrument input and output, and signal analysis. Theses sub–VIs can take the form of instruments distributed with the LABVIEW package or custom written

instruments designed to be application specific. The hierarchical structure of the instrument can be expanded by the incorporation of these instruments in a higher level VI.

Two types of VI were required for the dynamic headspace testing station. The first allows real time control over the status of the chemical hardware with the returned signals from the instrumentation relayed directly to the user interface. The second would be required for long–term tests and would therefore be controlled by pre–written text files. The data acquired from this system would have to be referenced to an internal clock and be saved to disc at a specified acquisition rate. Both systems would be required to interface arrays of either 12 or 24 sensor signals.

3.6.2 Real Time Chemical Hardware Control

Figure 3.13 shows the front panel user interface for the real time control (Look mode) VI. Two versions of the VI were created; one interfacing up to 12 sensors (shown), the other up to 24 signals. Control over the DAQ cards digital outputs was achieved using two banks of Boolean switches, shown at the top of the front panel. These permitted control over the 10 valve settings and also allowed override control over the MFCs. Beneath these Boolean switches are the numeric controls for the three MFCs are the displays for their returned signals and also the signal from the output flow meter. To the right of this is a display of the percentage leak in the system. This is calculated internally from the return flows from the MFCs and the output flow meter.

The main body of the panel is used for a graphical display of the state of the sensor signals. A horizontal slide gives an immediate indication of the sensor's

_____

Digital Output Controls (Card A)   Digital Output Controls (Card B)
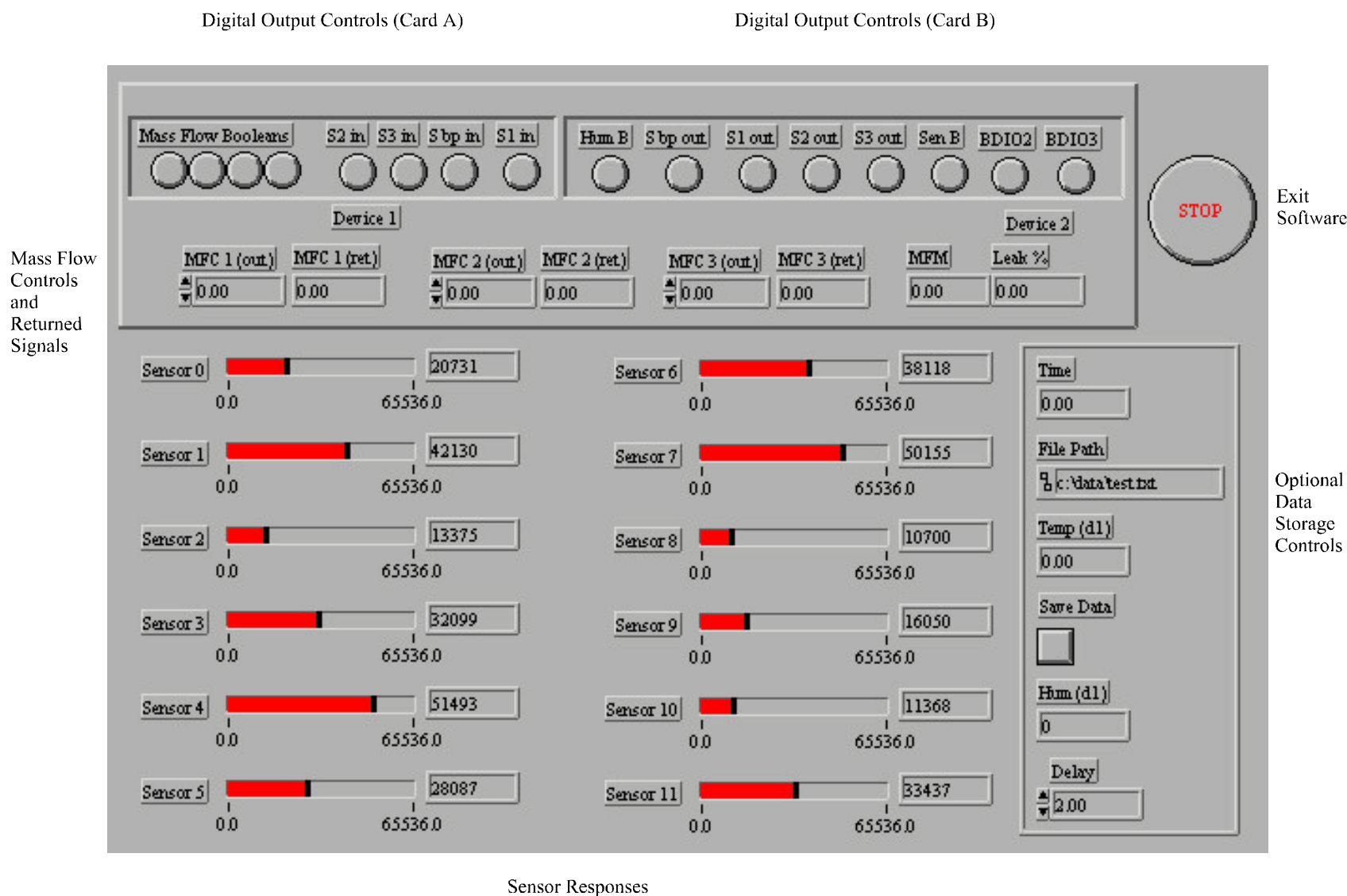
Figure 3.13 Front panel user interface for 'Look mode' software control returning signals from up to 12 polymer sensors

Sensor Channel Interface

Chemical Hardware Control Parameters

Test Status

MFC status

Data Storage Path Control

Data Acquisition Rate   Period of Storage at Specified Path   Start Acquisition
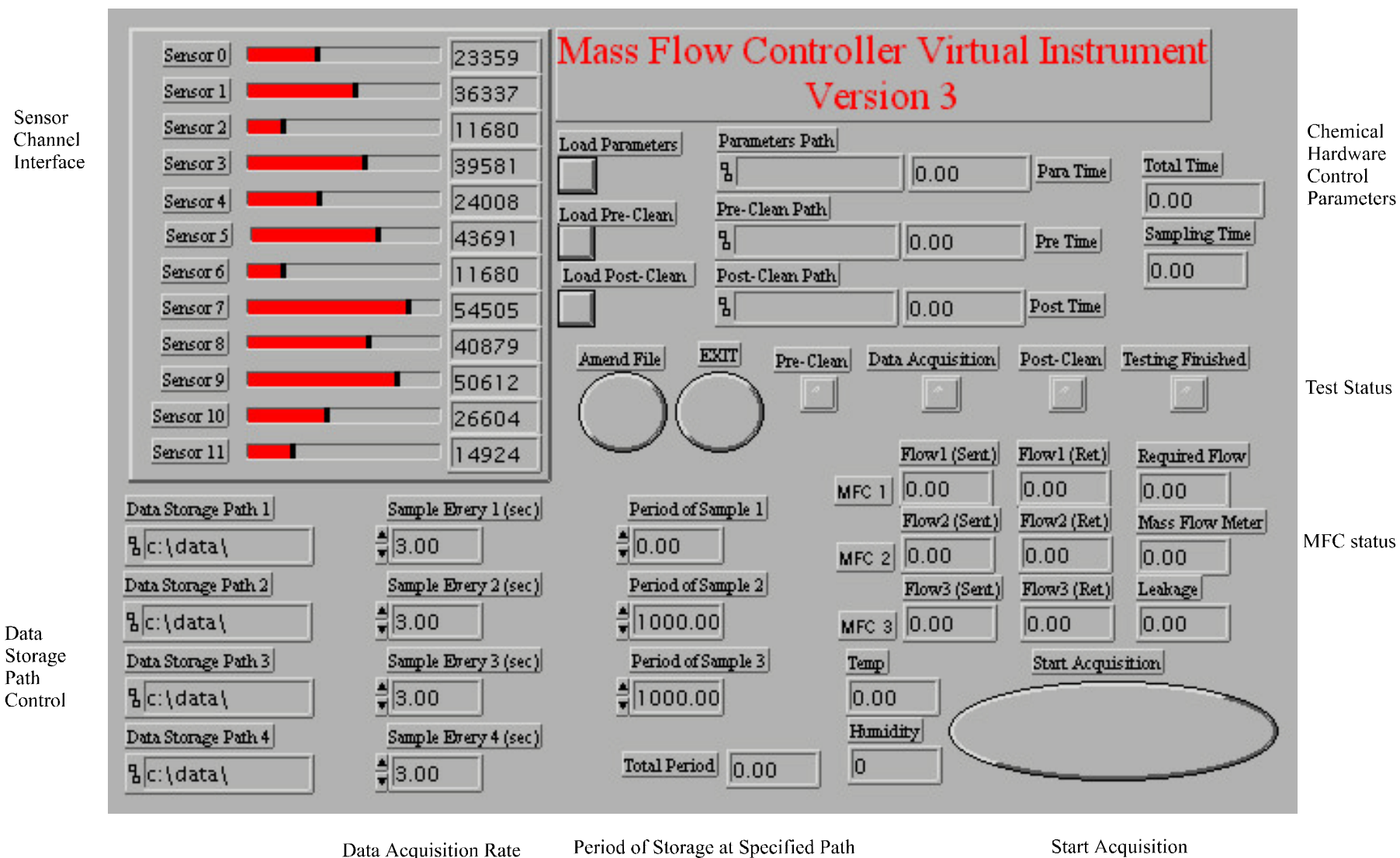
Figure 3.14 Front panel user interface for 'Data acquisition mode' software control returning signals from up to 12 polymer sensors.

response and a numeric display gives the exact value of the returned signal in ADC units. The signals are updated every second when there is no data being stored to file. To the right of the signal display is an optional data storage control. This allows the user to save the data from the sensors to a specified file at the acquisition rate indicated by the 'delay' control. The 'Time' indicator is a display in seconds showing the elapsed time since the data storage procedure was initiated. Humidity and temperature sensor data are also displayed in this area with the allied calibration routines executed on the incoming signals in the wiring diagram.

3.6.3 Data Acquisition Control

Figure 3.14 shows the VI used for the acquisition of data from an array of up to 12 polymer sensors. The sensor responses are displayed in the top left–hand corner of the panel again using a horizontal slide and numeric indicator. To the right of these (centre top) are the controls for importing text files containing the data acquisition parameters. The period of the imported file is shown to the right with the total time for the test to execute and the current sampling time also indicated. The 'sampling time' uses the system clock to calculate the period elapsed since a particular phase began. Below these are digital indicators showing the stage of testing and the rig conditions, including the required output flow, the current output flow and the amount of leakage in the equipment (ml/min). In the bottom left of the panel are the disc management controls. The instrument allows data to be sampled to any of up to four locations with the period to store data at a location and the data acquisition rate both controlled. To the right of these controls are the temperature and humidity displays the values of which are also stored in the data acquisition file. In the centre of the instrument are two digital controls. The first controls the type of data acquisition, either stored or transient

memory or amended to disc files, the other allows the current data acquisition phase to be shut down at any stage. If this switch is activated any data stored in transient memory is stored in a back–up file and the rig status is reset to default values.

3.7 Calibration and Commissioning

Commissioning of the chemical hardware is required to ensure that the controls set by user via the software are consistent with the physical variables being exposed to the sensors. Due to the sensor interface electronics having the facility for altering both the offset and gain parameters of the second stage amplifier, calibration of the sensor responses is also required. This ensures that the bit responses from the sensors can be converted in to an accurate observation of the resistance of the polymer device.

The temperature and humidity sensors housed in the sensor chambers are employed purely as diagnostic tools to show fluctuations in either of these physical parameters. Sufficient data has been collected using the dynamic headspace testing station to allow full calibration of these devices and the conversion of the signal received at the DAQ cards directly to humidity and temperature readings. However, the accuracy of such a procedure would be limited by the equipment with which it was calibrated. To use the sensors as anything except diagnostic tools would require independent calibration using precision equipment. If a sufficiently accurate device was employed the sensors could then be used as self–reliant transducers confirming both the temperature and humidity of the sensor head, and the accuracy of the vapour delivery system. Unfortunately, such an alternative system would be a dew–point hygrometer which is expensive and so was not available when data collection began. Therefore both types of sensor could only be used as diagnostic tools employed to show

unexpected fluctuations in the temperature and humidity in the sensor head, with absolute errors of about ± 1°C and ± 2% r.h.

The flow–rate, concentration and humidity of the analyte exposed to the sensors is determined by the accuracy of the MFCs and the feedback signals from the integral meter. Therefore the most critical calibration for the chemical hardware is that of the flow controllers. The specialised equipment required in the calibration procedure (outlined in section 3.7.2) of these sections of the equipment is not available at Warwick University. The calibration was therefore carried out by registered suppliers (Flotech Solutions Ltd.). The returned meters are accurate to 1% of full scale and have a range of 0 to 300 ml/min.

3.7.1 Sensor Interface Calibration

The Module 2 sensor interface cards (described in section 3.4.2) have the capability of altering both the offset and gain of the second stage amplifier. The 16–bit accuracy of the DAQ cards allowed these settings to be minimised and each channel of the interface to be calibrated for long–term use. Although, as expected, the calibration function takes the same form for each channel. The values obtained for the parameters used in the function does vary for individual channels. This can only be accounted for by the employment of different types of potentiometer on both the offset and feedback signals for the distinct channels.

Each channel was calibrated using a number of precision resistors (± 0.1%) and through monitoring the ADC bit value returned by the DAQ card. A linear model of the channels response could then be created. This procedure was repeated for all 24 sensor channels and for each of the 4 possible resistance ranges. The resulting equations were then employed to convert the ADC bit values recorded during data

acquisition to the physical resistance of each device. A typical calibration curve with a linear trendline is shown in figure 3.15 with the full table of sensor calibration equations and variants shown in table 3.3.

3.7.2 Modelling and Calibration of System Dynamics

In order to successfully model the characteristics of polymer sensors, the physical data obtained from the dynamic testing system have to reflect only the polymers' attributes and not those of the system itself. In the study of static responses, provided the system accurately controls the concentration of analyte, humidity and temperature, the sensors will reach an equilibrium value in a test environment when sufficient time is permitted to pass. The magnitude of the sensor response can then be calculated independently from the system dynamics. However, when transient attributes are being investigated, the time response and characteristics of the vapour delivery system need to be known in order to distinguish the real sensor characteristics from the received signals.

The effect of the flow system will be dependent on several factors but most critically the flow–rate settings and the combined volume of the pipe–work and the sensor chamber. To ensure the accuracy of the flow–rates within the system, calibration of the flow controllers and output meter were vital. A high degree of accuracy was ensured in these instruments by the employment of a registered Brooks Instrument suppliers (Flotech Solutions Ltd.) to calibrate the units using custom designed equipment. The procedure utilises a sophisticated system using volumetric calibrators to allow exact setting of the flow–rate control valve and to ensure the

_____
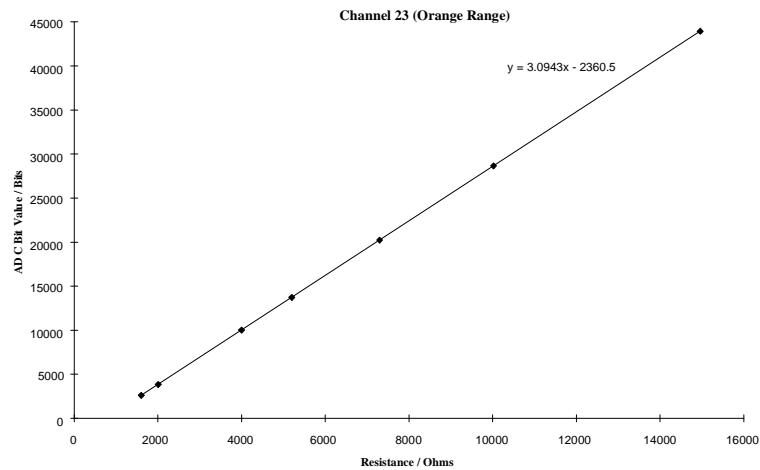
Figure 3.15 Typical sensor calibration chart (channel 23) on the Orange range setting (1 kΩ to 15 kΩ). A linear regression fit to the data is also shown.

Table 3.3 Table of linear calibration models for all 24 channels covering the 4 available range settings (variants indicate where individual channels differ from the normal calibration). The resistance, R is shown as a function of the ADC unit value x.

Sensors	Brown (10-100Ω)	Red(100-1k Ω)	Orange(1k-10k Ω)	Yellow(10k-100k Ω)
0 to 5	$R = \dfrac{x + 1841.9}{276.73}$	$R = \dfrac{x + 2979.5}{30.766}$	$R = \dfrac{x + 2079.4}{3.0278}$	$R = \dfrac{x + 2328.6}{0.3077}$
Variants	N/A	N/A	Ch 2 and 3 $R = \dfrac{x + 2499.7}{6.7523}$	N/A
6 to 11	$R = \dfrac{x + 2057.3}{275.99}$	$R = \dfrac{x + 2889.1}{30.716}$	$R = \dfrac{x + 1958.7}{3.0269}$	$R = \dfrac{x + 2172}{0.3077}$
Variants	N/A	N/A	N/A	N/A
12 to 17	$R = \dfrac{x + 2599.3}{279.63}$	$R = \dfrac{x + 2773.9}{31.032}$	$R = \dfrac{x + 2434.3}{3.0938}$	$R = \dfrac{x + 2511.6}{0.3088}$
Variants	N/A	N/A	N/A	N/A
18 to 23	$R = \dfrac{x + 2437.9}{278.98}$	$R = \dfrac{x + 2040.9}{30.766}$	$R = \dfrac{x + 2360.4}{3.0943}$	$R = \dfrac{x + 2403.7}{0.3093}$
Variants	Ch 22 and 23 $R = \dfrac{x - 1065}{278.87}$	N/A	Ch 22 $R = \dfrac{x + 23635}{2..5938}$	N/A

accuracy of the signal returned from the integral meter. Each of the flow controllers can be calibrated to user defined standards varying both the full scale range and the type of gas for which the calibration is accurate.

To simplify the dynamic modelling of the system, testing procedures maintained a combined flow–rate of all 3 MFCs through the sensor chamber at a constant 300 ml/min. However, variation in the flow through each of the elements of the system was required in order to change humidity and analyte concentrations. The dynamic modelling of a complex flow system such as this can be accomplished either by employing a very fast responding sensor system to detect fluctuations in humidity and analyte concentration within the sensor chamber, or through the use of input and output flow meters and basic fluid dynamics to model the vapour flow. As a fast sensor system was not available the latter approach has been taken. The full characterisation and modelling of the flow system is beyond the scope of this study. Therefore a number of assumptions have to be made which can be used to simplify the flow dynamics to give an approximate analytical model for the changes in concentration of analyte in the sensor chamber area. Firstly we have to consider the gas or vapour as an incompressible fluid and postulate that the concentration of analyte present in the vapour is determined by the ratio of flow–rates of the different input lines. We can then consider the chemical equipment and pipelines as a time delay between the input flow from the MFCs and the vapour arriving at the sensor chamber. This time delay will be dependent on both the volume of each line and the flow–rate passing through it. All of the tests completed for this study were under steady–state humidity conditions. Therefore we can simplify our modelling of this equipment by only considering the input line of interest (i.e. the sample line) as the influence of the other two lines during

transient responses would be negligible. The flow characteristics of the system can then

be dynamically modelled by the characterisation of the input MFC1
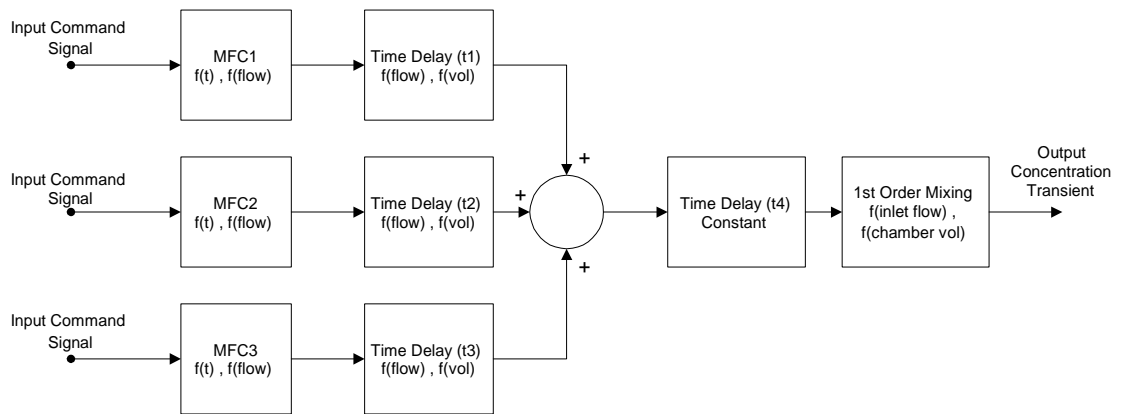
Figure 3.16 Overview of the system used for modelling the dynamic flow through the chemical equipment. Only the characteristic of MFC1 is modelled as MFC2 and 3 are used only to maintain a steady–state humidity.

The response of the flow profile of the system was modelled using a simple

exponential expression (equation 3.5). In this model the signal sent to MFC1 is

considered as the system input. For our purposes the dynamic flow response of the

sensor chamber can then be approximated to be equal to the response of the output flow

meter while the sensor head by–pass is active.

$$Flow(t) = A \times (1 - e^{-Bt}) \tag{3.5}$$

Where *Flow(t)* is the flow–rate at time *t*, *A* is the magnitude of the command signal in

ml/min and *B* is the response time coefficient. This expression allows accurate

prediction of the flow–rate transients occurring within the dynamic flow system within

the operating range of MFC1. A sample of the results obtained during the

characterisation of the flow profile are shown in figure 3.17. These results demonstrate

a time constant (τ) of no greater than 18 seconds.
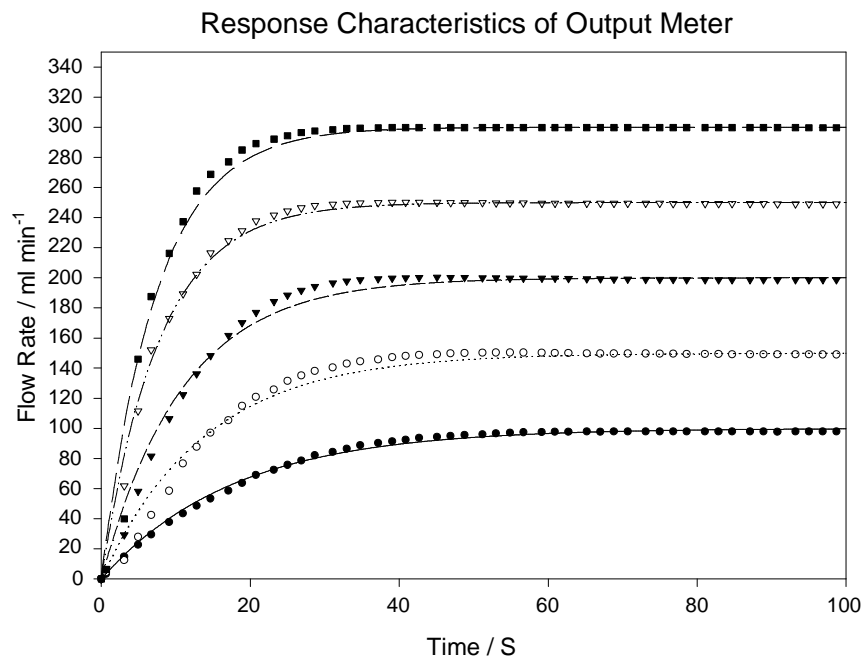
Figure 3.17 The response of the output mass flow meter to a step input signal from MFC1. Both the flow response and the values obtained from the system model using a non–linear regression fit are shown. Flow settings of 100, 150, 200, 250 and 300 ml/min are displayed.

The transient concentration characteristics of the sensor chamber can now be

modelled by combining the internal flow model with an expression defining the effect

this flow transient on the concentration incident to the polymers. For our purposes and

in order to keep the overall model as simple as possible the effects of mixing in the

sensor chamber will be assumed to be first order and related only to the input flow–rate

and the volume of the chamber itself. This assumption is valid provided that the sensor

chamber volume is kept at a minimum. The second generation chamber has such a

sufficiently low volume, however for experiments carried out in the larger 120 ml glass

jar the models accuracy decreases. For our purposes this error can be ignored as the

data gathered using the first generation chamber was used exclusively for investigating steady–state polymer responses and does not therefore require a transient model.

The model of the transient behaviour of the system can be further simplified due to the inlet flow–rate of the sensor chamber remaining at a constant 300 ml/min throughout all experiments executed on polymer membranes. This allows us to assume that the time constant of the sensor chamber is dependent only on the flow setting of MFC3. Using these all of these assumptions we can then create an approximate model describing the concentration transients within the sensor chamber.

The final model of the system as a whole has an absolute time delay describing the amount of time required for the vapour to travel from the sample vessel to the sensor chamber. The second part of the model shows how the concentration in the chamber varies with time. The model predicts that at a flow–rate of 300 ml/min the dynamic system takes approximately 30 seconds to develop the required concentration in the sensor chamber. Although the validity of this model has not been confirmed experimentally it does supply an indication of the dependence of the transient sensor chamber concentration on the input flow–rate and various other parameters associated with the chemical equipment. The model also allows us to distinguish absolute sensor responses from data containing components related to both the polymers and the dynamics of the chemical hardware.

3.8 Conclusions

This chapter has documented the design, construction and commissioning of a dynamic headspace testing system for Volatile organic compounds. Details of the chemical equipment employed, the electronic control systems and the interface used for

monitoring the sensor responses are also supplied. A model of the dynamic flow within the system is developed with particular attention to its effect on the concentration transients in the sensor chamber. Details of the custom written software used to control the flow system and store the returned signals from the electronic equipment are supplied and the testing protocol used throughout this study is documented.

3.9 References

3.1   P. N. Bartlett and S. K. Ling-Chung, Conducting polymer gas sensors. Part III: results for 4 different polymers and 5 different vapours, *Sensors and Actuators*, **20** (1989) 287 - 292.

3.2   J. W. Gardner, T. C. Pearce, S. Friel, P. N. Bartlett and N. Blair, A Multisensor System for Beer Flavour Monitoring Using an Array of Conducting Polymers and Predictive Classifiers, *Sensors and Actuators B,* **18 - 19** (1994) 240 - 243.

3.3   T.C. Pearce, Sensor–based Machine Olfaction: Instrumentation for the Analysis of Beer, *Ph.D. Thesis, 1997.*

3.4   I Harvey, G. Coles and J. Watson, The Development of an Environmental Chamber for the Characterisation of Gas Sensors, *Sensor and Actuators,* **16** (1989) 393 - 405.

3.5   V. Demarne, A. Grisel, R. Sanjines and F. Lévy, Integrated Semiconductor Gas Sensors Evaluation with an Automated Test System, *Sensors and Actuators B,* **1** (1990) 87 - 92.

3.6   T. Nakamoto, S. Ustumi, N. Yamashita, T. Moriizumi and Y. Sonoda, Active Gas/Odor Sensing Using Automatically Controlled Gas Blender and Numerical Optimization Technique, *Sensors and Actuators B,* **20** (1994) 131 - 137.

_____

3.7   M. Nieuwenhuizen and J. Harteveld, An Automated SAW Gas Sensor Testing System, *Sensors and Actuators A,* **44** (1994) 219 - 229.

3.8   J. Grate, D. Ballantine and H. Wohltjen, An Automated Vapour–Generation and Data Collection Instrument for the Evaluation of Chemical Microsensors, *Sensors an Actuators,* **11** (1987) 173 - 188.

3.9   H-E. Endres, H. Jander and W. Göttler, A Test System for Gas Sensors, *Sensors and Actuators B,* **23** (1995) 163 - 172.

3.10   N. A. Lange and John A. Dean, *Langes Handbook of Chemistry*, McGraw Hill, London, 1985.

3.11   T. Boublik, V. Fried and E. Hála, *The Vapour Pressure of Pure Substances*, Elsevier Publishing, 1990.

3.12   A. M. James and M. P. Lord, *Macmillan's Chemical and Physical Data,* The Macmillan Press Ltd, London, 1992.

3.13   I. Talbot, The design and Characterisation of a conducting polymer sensor chamber, *Project Thesis, 1996.*

3.14   N. Blair, The Development and Characterisation of Conducting Polymer Based Sensors for use in an Electronic Nose, *Ph.D. Thesis,* 1994.

CHAPTER 4

Static Modelling of Conducting Polymers

4.1 Introduction

This chapter describes the development of a steady-state (i.e. static) model to characterise the response of Ppy and Pan films to a mixture of ethanol and water vapours. Due to the similarity between the two types of polar molecule, the model assumes that there is competition for the available binding sites within the polymer film. The resulting analytical expression can be used to predict the effect of water vapour on the response of these polymers and, more importantly, may be used to ameliorate the problem of water-sensitivity in conducting polymer sensors through the development of parametric correction routines.

Ethanol vapour was chosen as the target species for the development of this model as the polymers had previously demonstrated fast response and recovery times when exposed to this type of volatile organic compound [4.1, 4.2 and 4.3] and, being a polar molecule, its response may be related to water sensitivity. The choice of polymer membranes to be employed during the investigation of this model was also significant. The characteristics of conducting polymers can be modified chemically and they can be deposited electrochemically in a reproducible and controlled manner [4.4] providing a large number of polymer types each with slightly different attributes. As only a limited number of this variety of polymer types could be employed during a test sequence, only

a fraction of the polymer types could be characterised. The types chosen for the steady-state characterisation represented each of the two major classes of monomer, pyrrole and aniline, with two types of counter-ion representing a five unit chain (pentane sulfonic acid) and a ten unit chain (decane sulfonic acid). This type of acid was chosen due to its hydrophobic properties and also because it has previously produced polymers with good long–term stability [4.5]. Three nominally identical polymer types were used to confirm the repeatability of the results giving a total array of 12 polymers.

4.2 Response to Ethanol Vapour

4.2.1 Theory

A model has been developed elsewhere in which it is assumed that a species, A, diffuses into a homogeneous thin film and undergoes adsorption to fixed sites described by a Langmuir adsorption isotherm [4.6]. In this model it is assumed that the film contains a uniform distribution of immobile sites, concentration Γ, with which the species can reversibly react and that this reaction does not alter the sites affinity for the species. It is further assumed that there are no interactions between molecules of A on different sites and that the species does not interact with any other analytes present. The reaction can now be described by the Langmuir adsorption isotherm,

$$A + \left\{ \ \right\}_{site} \underset{k_b}{\overset{k_f}{\Leftrightarrow}} \left\{ A \right\}_{site} \tag{4.1}$$

where k_f and k_b are the forward and backward reaction rate constants, respectively[1]. These constants are defined as the constants of proportionality in equations defining the forward and backward reaction rates within the polymers. The forward reaction rate, r_f, is proportional to the concentration of the target species, C, and the number density of free sites within the polymer

$$r_f = k_f CN(1 - \theta) \tag{4.2}$$

where N is the number density of sites and θ, is the fractional occupancy of the sites. The backward reaction rate, r_b, is proportional only to the concentration of sites containing the target species,

$$r_b = k_b N\theta \tag{4.3}$$

When considering the steady-state behaviour for this process we can ignore the details of the transport process because, at equilibrium, the forward and backward reaction rates are equal. The Langmuir model therefore describes the occupancy of the sites by,

$$\theta_\infty = \frac{K_a C_a}{\left(1 + K_a C_a\right)} \tag{4.4}$$

---

[1] It should be noted that, due to the steady–state nature of this model, the bulk transport mechanism is not included in this theory. This mechanism is assumed in later chapters to be a diffusion process.

where C_a is the concentration of species A, and the binding constant, K_a, is the ratio of the forward and backward reaction rate constants (k_f / k_b). If we now assume that the conductance[1] of the device is related linearly to the concentration of the bound species A by

$$G_f = G_i + a_a \Gamma \theta \tag{4.5}$$

where a_a is a sensitivity coefficient and G_f and G_i are the final (steady-state) and initial (base–line) device conductances of the polymers, respectively. This model is consistent with a basic model of the polymer as a doped semiconductor in which the electron mobility is weakly modulated by the sorbed molecule[2]. It is unlikely that the carrier density of the polymer will change on exposure to organic vapours because that would require charge transfer to take place.

Therefore, we assume that the change in device conductance, ΔG, to the concentration of vapour from Equations (4.4) and (4.5) is approximately given by,

$$\Delta G = \left(G_f - G_i \right) \approx \frac{K_a C_a a_a \Gamma}{1 + K_a C_a} \tag{4.6}$$

---

[1] An earlier empirical model [4.1] was based on a resistance model but the conductance model is a marginally better fit to the data and is more consistent with our conductance model for a semiconducting material [4.7].

[2] A more sophisticated exponential model is described later that extracts explicitly the temperature dependence of the electron mobility [4.8]

The initial and final values of device conductance can be obtained from measurements taken with the Dynamic Headspace Testing equipment (see Chapter 3) and the validity of the model can be tested.

4.2.2 Results

The initial experiments were run at a constant temperature (23.7 $\pm$ 0.1 °C) and a constant absolute humidity of 1,238 ppm in order to investigate the basic conductance model. An example of the type of results obtained from the Dynamic Headspace Testing Station is shown in Figure 4.1.
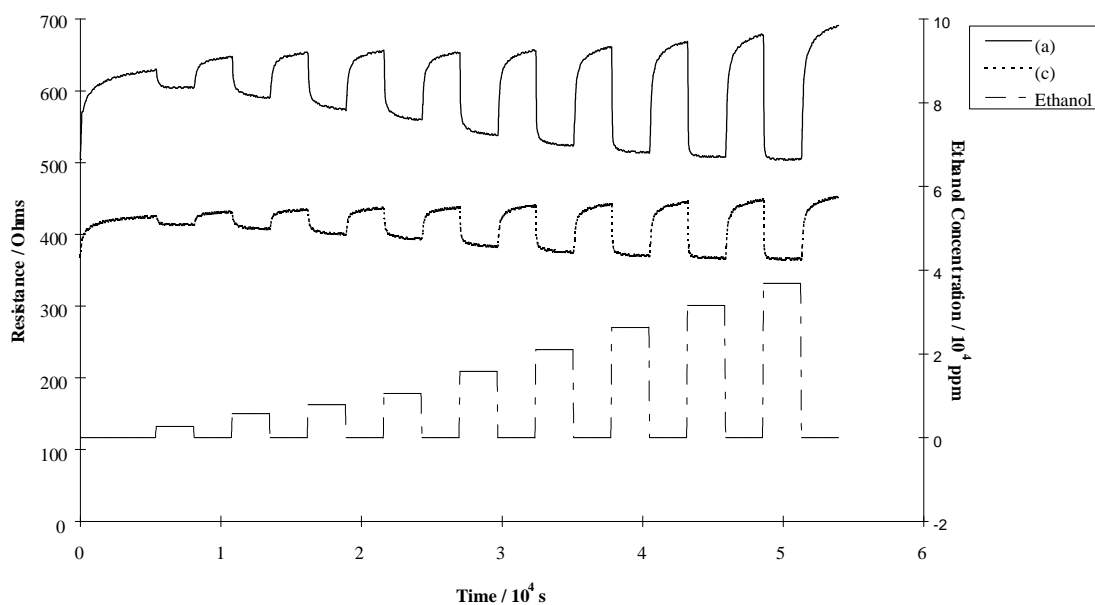
Figure 4.1 An example chart showing the form of the raw data as collected from the Injection Flow Analysis equipment. This graph shows two of the Pan/PSA/H_2O sensors (a and c) in terms of their resistance versus the sampling time at 23.7 ^{0}C and 1238 ppm of water. The ethanol concentrations to which the sensors are exposed is also shown.

These results show how the resistance of the sensors change with time when exposed to different ethanol concentrations at fixed humidity and temperature. The initial variation

in resistance of the sensors shown in Figure 4.1 is a characteristic of the change of humidity from ambient in the sensor chamber. When an equilibrium at the required humidity has been achieved a series of pulses of ethanol vapour are exposed to the sensors. After each pulse the sensors are allowed time to return to their original base–line resistance value in the target humidity. The change in conductance of the devices is calculated using the initial (R_i) and final (R_f) values of the sensor's resistance. These data are obtained by extracting the resistance of the polymers immediately prior to, and at the termination of an ethanol pulse.

Data gathered from all of the 12 polymer devices (3 replicates of each of the four types) tested here gave a good statistical fit to the model (i.e. Equation 4.6). The typical correlation coefficient calculated for the Ppy sensors was 0.970 for PSA and 0.936 for DSA. The Pan sensors had typical coefficients of 0.998 for both types of counter-ion. Results are shown for the response of Ppy in Figure 4.2 and Figure 4.3, and the response of Pan in Figure 4.4 and Figure 4.5, to ethanol vapour in the range of 2,000 to 40,000 ppm. It can be seen that Pan and Ppy films respond differently to the target analyte. Pan films show a significant increase in their conductance on exposure to ethanol (up to ~ +15%), while Ppy films show a smaller decrease (~ –5%). However, in both cases a non-linear regression (solid lines) of the model (Equation 4.6) onto the experimental data shows an excellent fit. The observed differences are explained by different signs and values computed for the sensitivity terms, $a_e\Gamma$.

The sensitivity term, $a_e\Gamma$, was found to be positive for all of the Pan films with the values obtained for the 3 sensors ranging between 8.347 mS and 2.78 mS for the sensors with PSA as the counter-ion, and between 0.45 mS and 4.77 mS for the polymers with DSA as the counter-ion. The Ppy films all demonstrated a negative
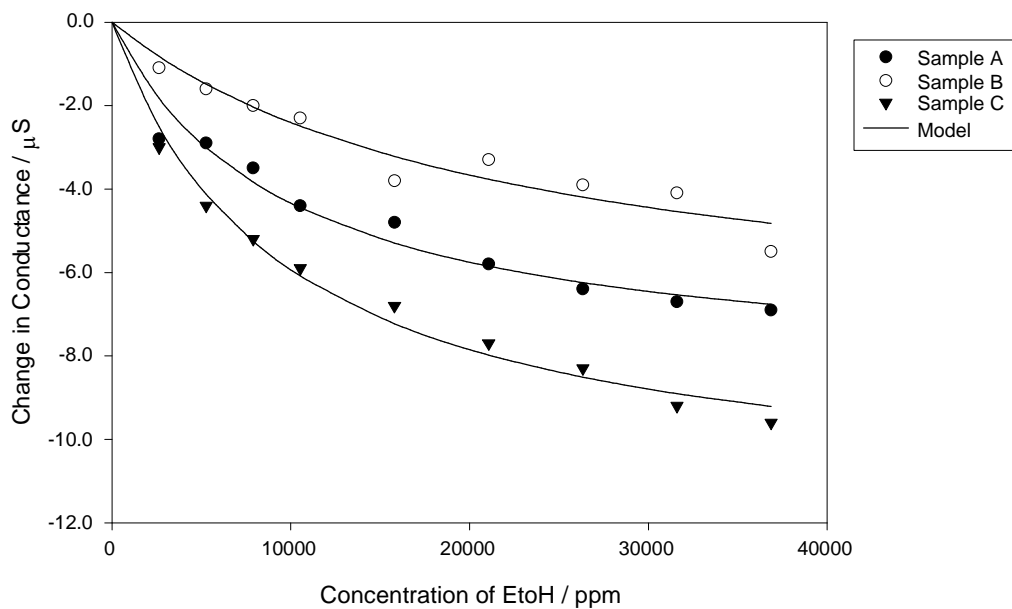
Figure 4.2 A plot showing the effect of ethanol vapour on the change in conductance of three replicates of Ppy/PSA/H_2O sensors. The sensors were maintained at a constant temperature of 23.7°C and an absolute humidity of 1,238 ppm.
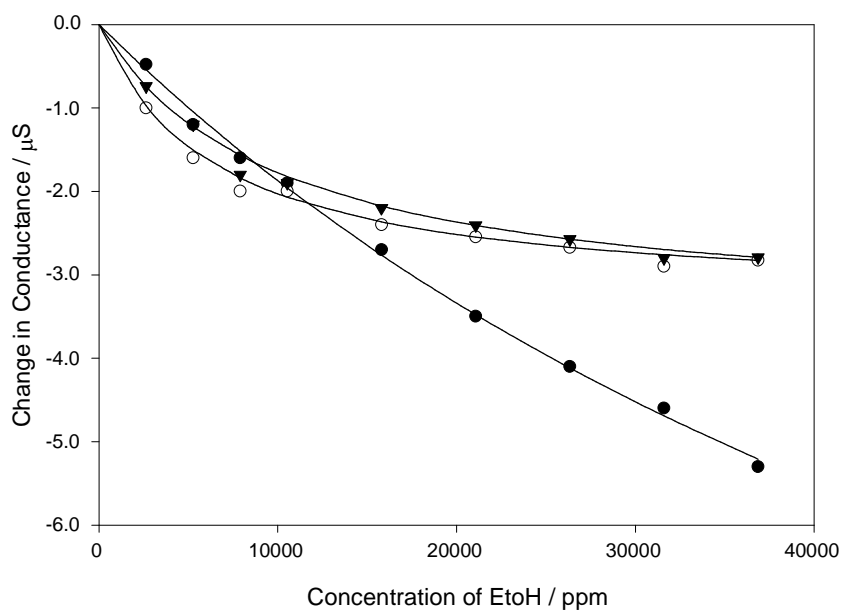
Figure 4.3 A plot showing the effect of ethanol vapour on the change in conductance of Ppy/DSA/H_2O sensors. The sensors were maintained at a constant temperature of 23.7°C and an absolute humidity of 1,238 ppm.
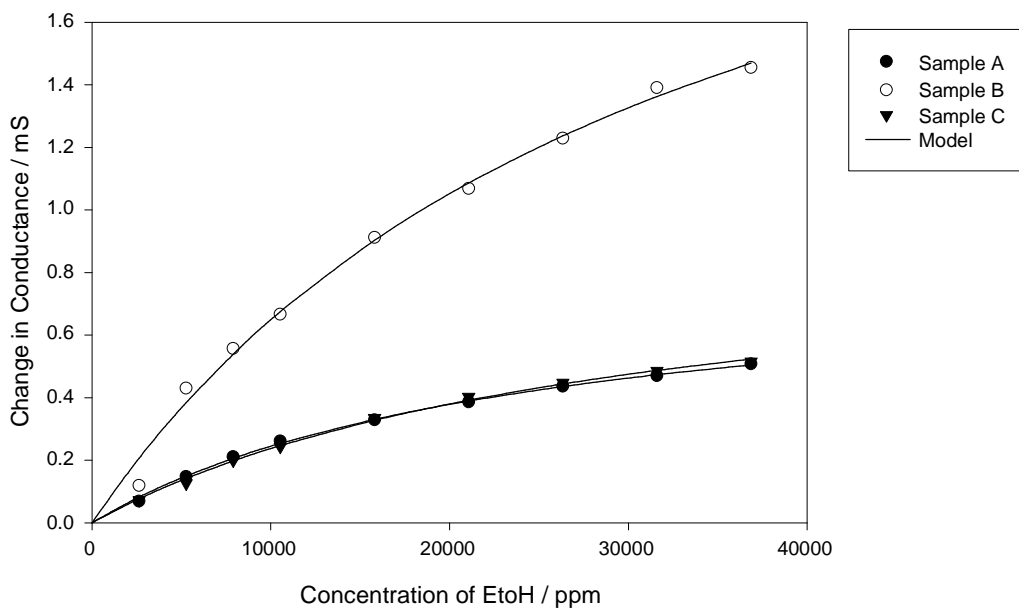
Figure 4.4 A plot showing the effect of ethanol vapour on the change in conductance of three replicates of Pan/PSA/H$_2$O sensors. The sensors were maintained at a constant temperature of 23.7°C and an absolute humidity of 1,238 ppm.
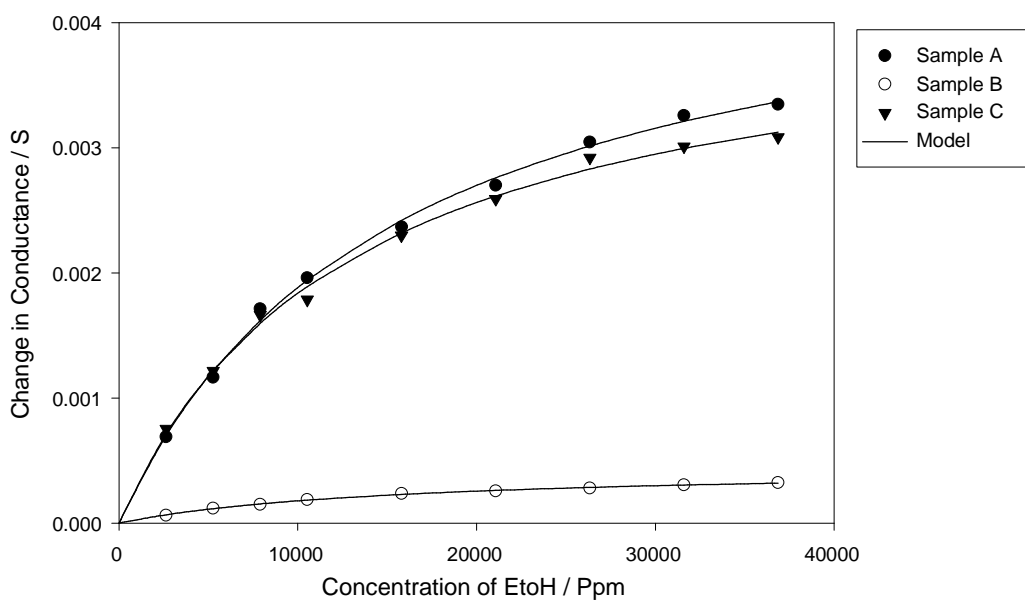
Figure 4.5 A plot showing the effect of ethanol vapour on the change in conductance of three replicates of Pan/PSA/H$_2$O sensors. The sensors were maintained at a constant temperature of 23.7°C and an absolute humidity of 1,238 ppm.

sensitivity term with values between -7.71 µS and -11.59 µS for PSA and between -

3.31 µS and -15.50 µS for polymers with DSA as the counter-ion. Full details of the

values obtained for each parameter are given in Table 4.1. It is interesting to note that

Pan gives a significantly larger absolute response to ethanol vapour and this is reflected

in the size of the sensitivity term with the value for Pan/PSA/H_2O being up to 360 times

larger than that for Ppy/PSA/H_2O. Clearly, the choice of monomer has a larger effect

on the gas-sensitivity of the sensor compared with that of the size of the counter-ion.

Table 4.1 Parameter values obtained using a non-linear regression fit to experimental data for the response of polymer sensors to ethanol vapour.

SENSOR	K_e (10^{-5} ppm^{-1})	$a_e\Gamma$ (µS)
Ppy/PSA/H_2O(a)	10.31 ± 2.30	-8.55 ± 0.66
Ppy/PSA/H_2O(b)	4.54 ± 1.77	-7.71 ± 1.47
Ppy/PSA/H_2O(c)	10.49 ± 1.37	-11.59 ± 0.53
Ppy/DSA/H_2O(a)	1.37 ± 0.19	-15.50 ± 1.57
Ppy/DSA/H_2O(b)	15.78 ± 6.24	-3.31 ± 0.39
Ppy/DSA/H_2O(c)	10.03 ± 3.36	-3.55 ± 0.43
Pan/PSA/H_2O(a)	4.14 ± 0.23	834.7 ± 23.9
Pan/PSA/H_2O(b)	3.05 ± 0.42	2779.0 ± 218.9
Pan/PSA/H_2O(c)	3.33 ± 0.26	950.4 ± 42.2
Pan/DSA/H_2O(a)	6.50 ± 0.39	4774 ± 125.0
Pan/DSA/H_2O(b)	6.48 ± 0.42	452.1 ± 12.5
Pan/DSA/H_2O(c)	7.67 ± 0.55	4230.0 ± 122.2

The value of the binding constant for ethanol (K_e) determines the degree of

curvature observed in the response plots shown in Figures 4.2 to 4.5. The values

computed for this term suggest that Ppy films have a lower binding constant to ethanol

than Pan films. The Pan PSA films gave values of K_e between 3.045×10^{-5} ppm^{-1} and

4.143×10^{-5} ppm^{-1}, while the DSA counter-ions gave values between 6.483×10^{-5} ppm^{-}

^{1} and 7.666×10^{-5} ppm^{-1}. The values determined for the Ppy films lay between $4.538 \times$

10^{-5} ppm^{-1} and 1.049×10^{-4} ppm^{-1} for PSA, and between 1.373×10^{-5} ppm^{-1} and $1.578 \times$

10^{-4} ppm^{-1} for the sensors with DSA counter-ions. The effect of a difference in the magnitude of this parameter is to make the response curves for Ppy much more linear than for Pan over the same concentration range. The significance of the size of the counter-ion on the binding constant seems to be marginal, with only Pan/DSA/H_2O consistently showing a slightly larger binding constant than Pan/PSA/H_2O.

4.3 Effect of Water Vapour

4.3.1 Theory

We can now extend the basic conductance model to take account of the affect of water vapour upon both the base–line conductance (i.e. conductance in ambient air) and the response to ethanol of a conducting polymer gas sensor. To do this we make a further assumption that there is only one type of active immobile site for which both the water and ethanol molecules actively compete. This seems reasonable as they are both small polar molecules. Thus, the polymer has an intrinsic sensitivity to water and we assume once again that the sites exhibit a Langmuir isotherm. Then the base–line device conductance is approximately given by,

$$G_i \approx G_0 + \frac{K_w c_w a_w \Gamma}{\left(1 + K_w c_w\right)} \qquad\qquad (4.7)$$

where G_0 is the conductance of the polymer in dry air, K_w is the water binding constant, a_w is the sensitivity coefficient for water vapour and Γ is again the concentration of sites within the film. Therefore, we can relate the conductance of our polymer sensor to the concentration of both the ethanol vapour and water vapour in air by,

$$G_f \approx G_0 + \frac{\left(K_w c_w a_w \Gamma + K_e c_e a_e \Gamma\right)}{\left(1 + K_w c_w + K_e c_e\right)} \tag{4.8}$$

Combining Equation 4.7 and 4.8 gives the response of a polymer gas sensor (defined now in terms of its fractional change in conductance) as,

$$\frac{\Delta G}{G_i} \approx \frac{\dfrac{\left(K_w c_w a_w \Gamma + K_e c_e a_e \Gamma\right)}{\left(1 + K_w c_w + K_e c_e\right)} - \dfrac{K_w c_w a_w \Gamma}{\left(1 + K_w c_w\right)}}{G_0 + \dfrac{K_w c_w a_w \Gamma}{\left(1 + K_w c_w\right)}} \tag{4.9}$$

This description of a conducting polymer film assumes that only water and ethanol are reacting with the available sites and that the vapours are directly competitive.

4.3.2 Results

The effect of water vapour on the base–line conductance, G_i, of the four types of polymer is shown in Figures 4.6, 4.7, 4.8 and 4.9. Once again the two types of polymer film exhibit a different sign of the sensitivity term ($a_w\Gamma$), with the conductance of Ppy sensors decreasing and those of Pan increasing as the water concentration is raised. A non-linear regression fit of Equation 4.7 to the experimental data is good and provides values for the three material parameters of the polymers: the water binding constant (K_w); the water sensitivity term ($a_w\Gamma$); and the conductance of the polymer in dry air (G_0). The $a_w\Gamma$ term was found to have a value between -11.97 μS and -816.10 μS for Ppy PSA and between -0.24 mS and -0.39 mS for the polymers with DSA counter-ions.
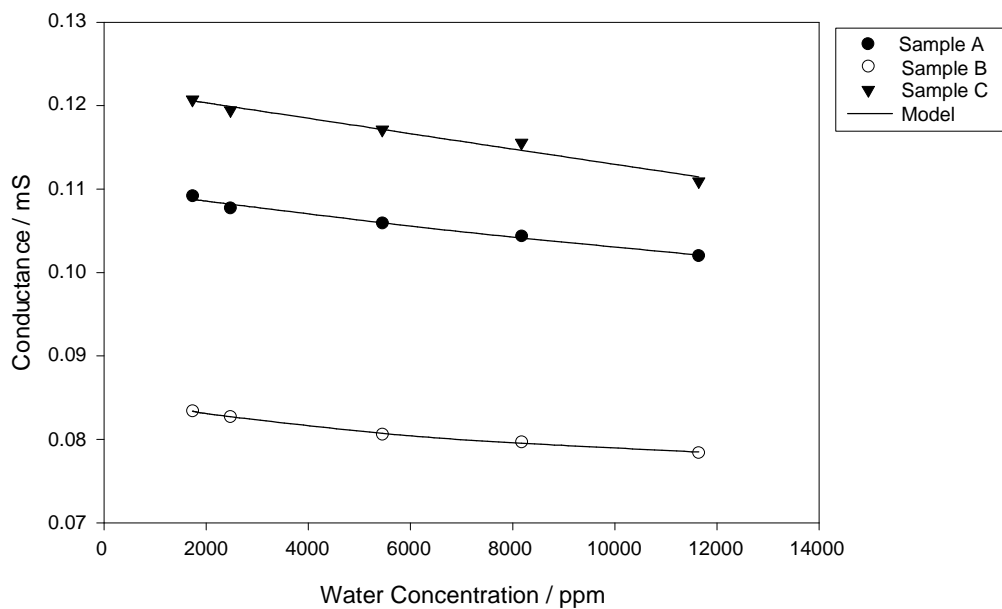
Figure 4.6 A plot showing the effect of water vapour on the base−line conductance of Ppy/PSA/H_2O gas sensors at 23.7°C.
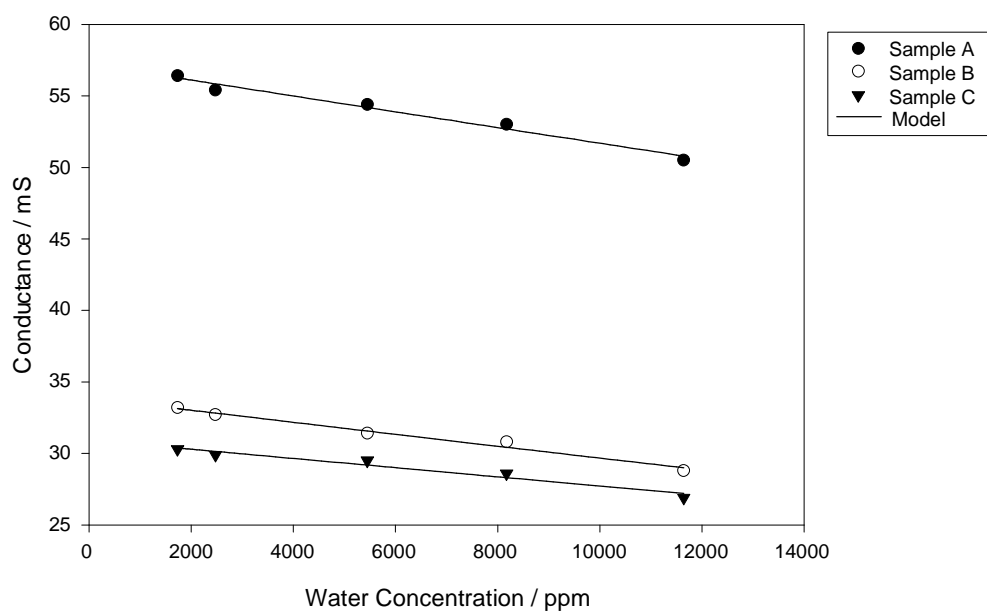
Figure 4.7 A plot showing the effect of water vapour on the base−line conductance of Ppy/DSA/H_2O gas sensors at 23.7°C.
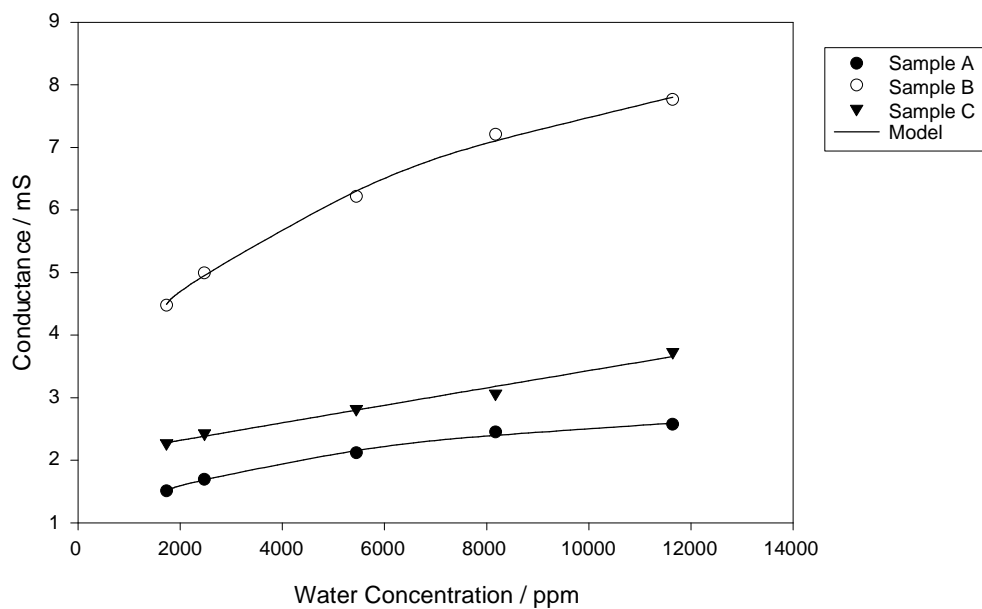
Figure 4.8 A plot showing the effect of water vapour on the base–line conductance of Pan/PSA/H_2O gas sensors at 23.7°C.
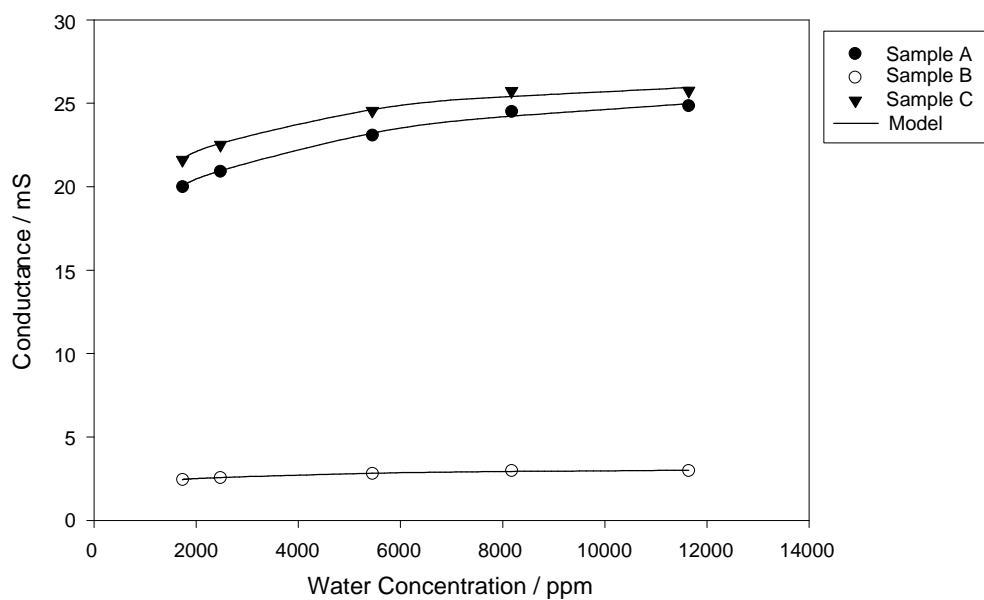
Figure 4.9 A plot showing the effect of water vapour on the base–line conductance of Pan/DSA/H_2O gas sensors at 23.7°C.

The Pan PSA and DSA sensors varied from 2.46 mS to 8.00 mS, and 1.38 mS to 12.01 mS, respectively. The magnitude of these values are consistently higher than those obtained in the earlier model of the response to ethanol for both Ppy and Pan. This seems to indicate that the polymers give a larger response to water than to ethanol at similar concentrations. The sensitivity values are shown in Table 4.2 in addition to the computed values of the dry-air conductance[1] (G_0) and the water binding constants.

The binding constant obtained for the water vapour also demonstrated a definite trend when compared to the results computed for ethanol in the earlier, non-competitive model. The Pan sensors all exhibit a higher value for the water binding constant than for the ethanol. This parameter is sometimes as much as 7 times greater for water in the same polymer sensor. As this parameter indicates the affinity of a binding site for the vapour, the Pan sensors seem to give a stronger reaction to water than to ethanol. However, the trend demonstrated by the Ppy sensors showed the opposite characteristic, with most polymers giving a larger absolute value for K_e than for K_w, indicating a higher ethanol sensitivity. The values predicted for the conductance of the polymers under dry, ethanol free conditions seem to be consistent with the base–line values of the polymers as measured during the experimental work.

The competitive nature of the model predicts that an increase in the concentration of water vapour in the air will result in a reduced magnitude of the response to the ethanol vapour. This effect was observed for both the Pan and Ppy sensors and can be seen clearly in the experimental results shown in Figures 4.10, 4.11, 4.12 and 4.13.

---

[1] This parameter is hard to measure because the long-term stability of the polymers in dry air is poor. Here it is estimated from the model.

Table 4.2 Parameter values obtained using a non-linear regression fit to experimental data for the response of polymer sensors to water vapour.

SENSOR	G_0 (mS)	K_w (10^{-5} ppm^{-1})	$a_w\Gamma$ (10^{-5} S)
Ppy/PSA/H$_2$O(a)	0.1103 ± 0.0008	2.316 ± 3.951	-3.853 ± 4.92
Ppy/PSA/H$_2$O(b)	0.08543 ± 0.0005	11.92 ± 4.382	-1.197 ± 1.23
Ppy/PSA/H$_2$O(c)	0.1222 ± 0.0012	0.1145 ± 0.394	-81.61 ± 173.50
Ppy/DSA/H$_2$O(a)	0.05723 ± 0.0007	0.1475 ± 0.377	-38.13 ± 84.89
Ppy/DSA/H$_2$O(b)	0.03387 ± 0.0005	0.1768 ± 0.355	-24.17 ± 42.62
Ppy/DSA/H$_2$O(c)	0.03094 ± 0.0006	0.08395 ± 0.256	-38.71 ± 25.20
Pan/PSA/H$_2$O(a)	0.8814 ± 0.242	19.68 ± 9.662	245.8 ± 14.84
Pan/PSA/H$_2$O(b)	3.071 ± 0.352	12.41 ± 4.314	800.4 ± 74.47
Pan/PSA/H$_2$O(c)	1.915 ± 0.158	8.735 ± 3.251	279.2 ± 152.80
Pan/DSA/H$_2$O(a)	15.73 ± 1.942	32.74 ± 17.630	1168.0 ± 112.40
Pan/DSA/H$_2$O(b)	1.858 ± 0.472	42.38 ± 38.970	138.0 ± 34.00
Pan/DSA/H$_2$O(c)	15.45 ± 4.891	59.38 ± 52.600	1201.0 ± 413.20

Again, each sensor gave a good fit to our conductance model (Equation 4.9) with the norm of the residual values obtained for each fit being typically less than 0.028 for the Ppy sensors and less than 0.15 for Pan. The data fitting process employed four parameters: $a_e\Gamma/G_0$; $a_w\Gamma/G_0$; K_e; and K_w. This method yielded the most accurate parameter values during the non-linear regression data fitting process. The full model (Equation 4.9) not only allows us to make direct comparisons between the effect of water and ethanol vapour on the polymer films, but also enables comparison with the trends and values established by the earlier independent water and ethanol only model.

Each of the sensors gave similar values for the ethanol and water binding constants, K_e and K_w. This indicates that neither vapour is dominating in the competition for sites occurring within the polymer film. The binding constants also showed a surprising degree of consistency between different types of polymer. Therefore, the differences observed between the response of Ppy and Pan sensors, as shown in Figures 4.10, 4.11, 4.12 and 4.13, can be attributed to the magnitude of both the ethanol and water sensitivity terms. Although the curvature of the models is similar

for the different polymeric types, the response of Pan will be affected to a greater extent. This implies that, although the Pan sensors gave a larger response to the ethanol vapour at a low humidity, as the humidity is increased it leads to a significant reduction in this response. However, for the Ppy sensors which give a relatively small response at low humidity, the response to ethanol may dominate when the water vapour concentration is increased. Therefore, even though the response of both polymers to water vapour can be explained by a competitive binding model, the water sensitivity of Ppy is less severe and so it has a superior practical value in atmospheres of high and variable humidities. Details of the parameter values obtained for all of the parameters employed in this model are shown in Table 4.3.

Table 4.3 Parameter values obtained from a non-linear regression fit to the data obtained showing the effect of humidity on the sensors response to ethanol.

SENSOR	$a_e\Gamma/G_0$ (10^2)	$a_w\Gamma/G_0$ (10^2)	K_e $(10^{-4}\ ppm^{-1})$	K_w $(10^{-4}\ ppm^{-1})$
Ppy/PSA/H_2O(a)	-8.27 ± 0.56	-1.979 ± 2.62	0.973 ± 0.19	1.583 ± 0.93
Ppy/PSA/H_2O(b)	-7.41 ± 1.07	-2.249 ± 4.92	0.811 ± 0.35	1.985 ± 2.46
Ppy/PSA/H_2O(c)	-9.60 ± 0.69	-1.497 ± 2.63	1.137 ± 0.23	2.030 ± 1.05
Ppy/DSA/H_2O(a)	-43.67 ± 12.76	-3.054 ± 3.75	0.074 ± 0.03	0.216 ± 0.88
Ppy/DSA/H_2O(b)	-11.28 ± 0.79	-0.5638 ± 0.66	1.282 ± 0.22	2.037 ± 0.89
Ppy/DSA/H_2O(c)	-11.85 ± 0.42	-2.125 ± 1.46	1.277 ± 0.13	2.760 ± 0.65
Pan/DSA/H_2O(a)	36.92 ± 2.28	39.04 ± 1.57	1.283 ± 0.14	3.835 ± 0.68
Pan/DSA/H_2O(b)	28.42 ± 2.30	33.46 ± 1.81	1.396 ± 0.20	3.745 ± 0.77
Pan/DSA/H_2O(c)	30.76 ± 1.90	32.12 ± 1.23	1.564 ± 0.17	4.189 ± 0.73
Pan/PSA/H_2O(a)	82.34 ± 7.73	102.9 ± 7.47	0.888 ± 1.29	2.724 ± 6.00
Pan/PSA/H_2O(b)	95.75 ± 12.32	117.9 ± 11.56	0.771 ± 0.15	3.199 ± 0.82
Pan/PSA/H_2O(c)	63.22 ± 3.74	75.68 ± 3.61	0.695 ± 0.07	3.194 ± 0.43
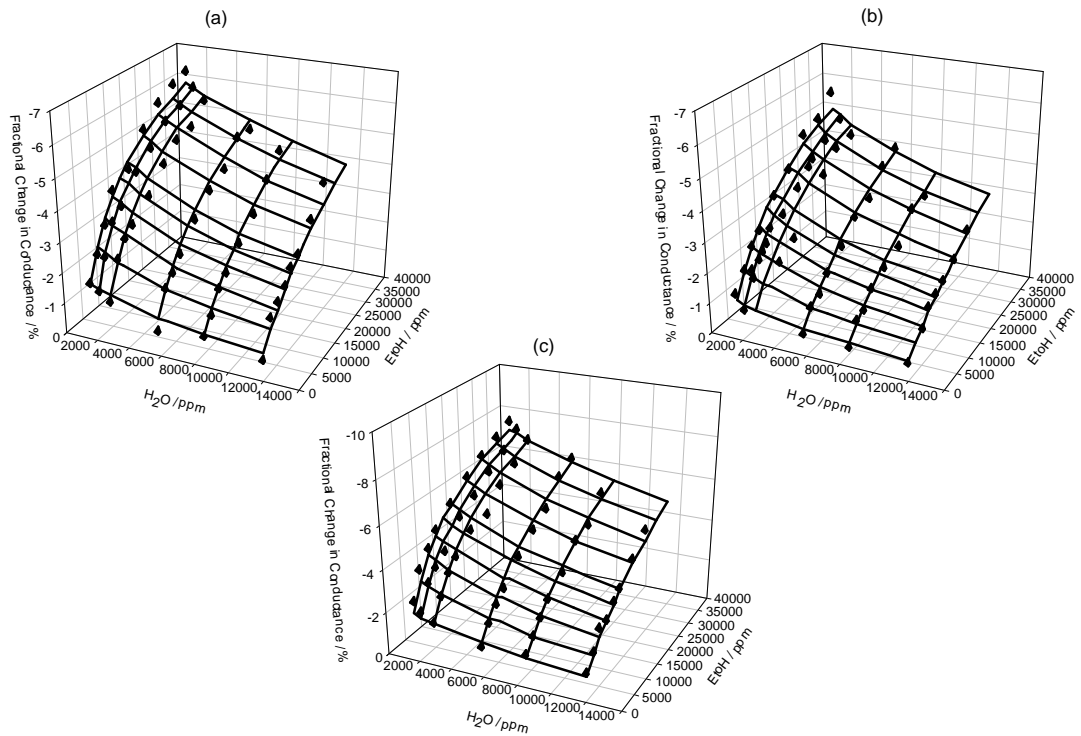
Figure 4.10 A plot showing the effect of water and ethanol vapour on the response of Ppy/PSA/H_2O gas sensors at 23.7°C. The solid mesh is a fit of the theory to the experimental data.
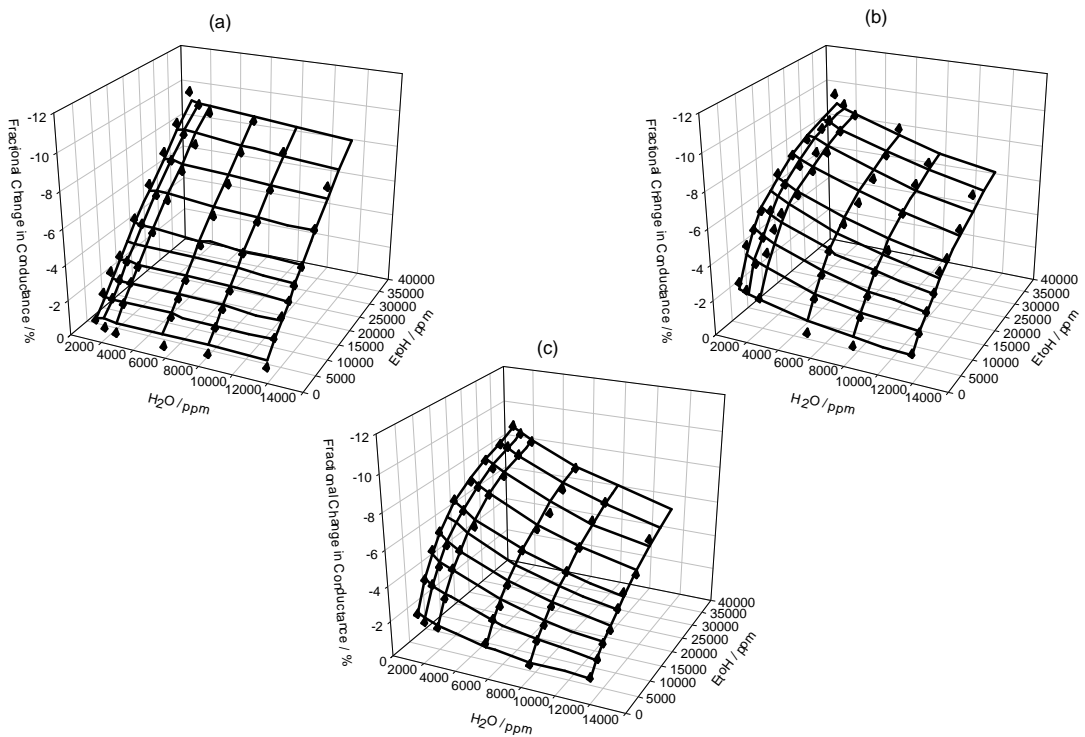
Figure 4.11 A plot showing the effect of water and ethanol vapour on the response of Ppy/DSA/H_2O gas sensors at 23.7°C. The solid mesh is a fit of the theory to the experimental data.
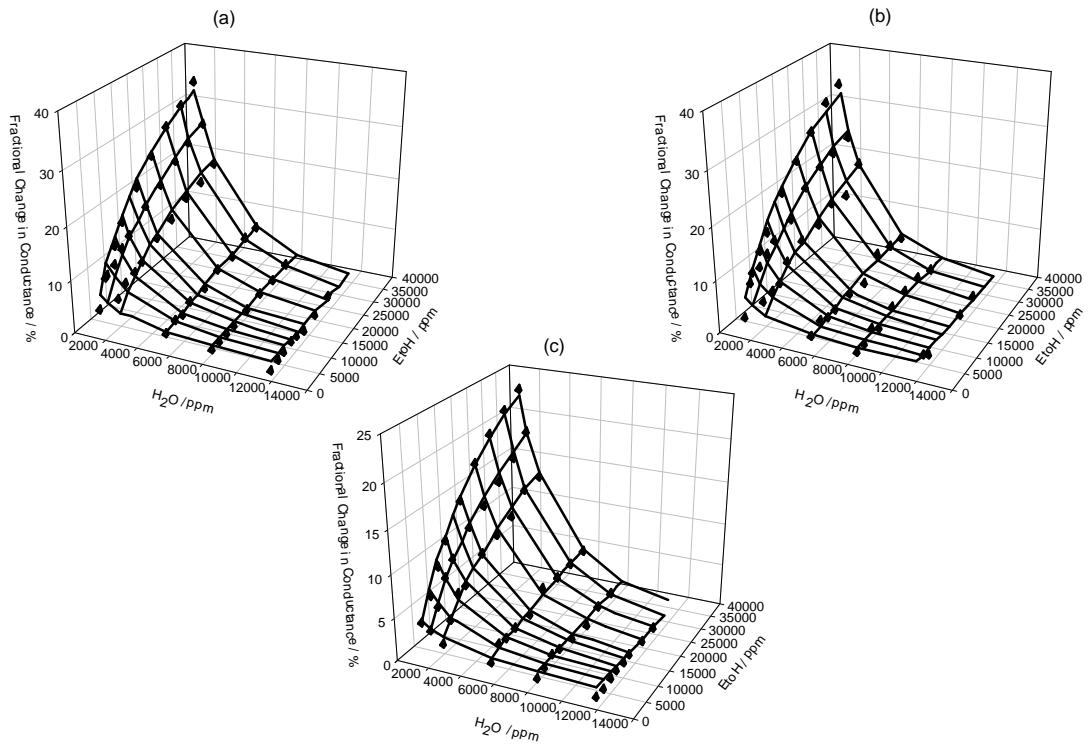
Figure 4.12 A plot showing the effect of water and ethanol vapour on the response of Pan/PSA/H$_2$O gas sensors at 23.7°C. The solid mesh is a fit of the theory to the experimental data.
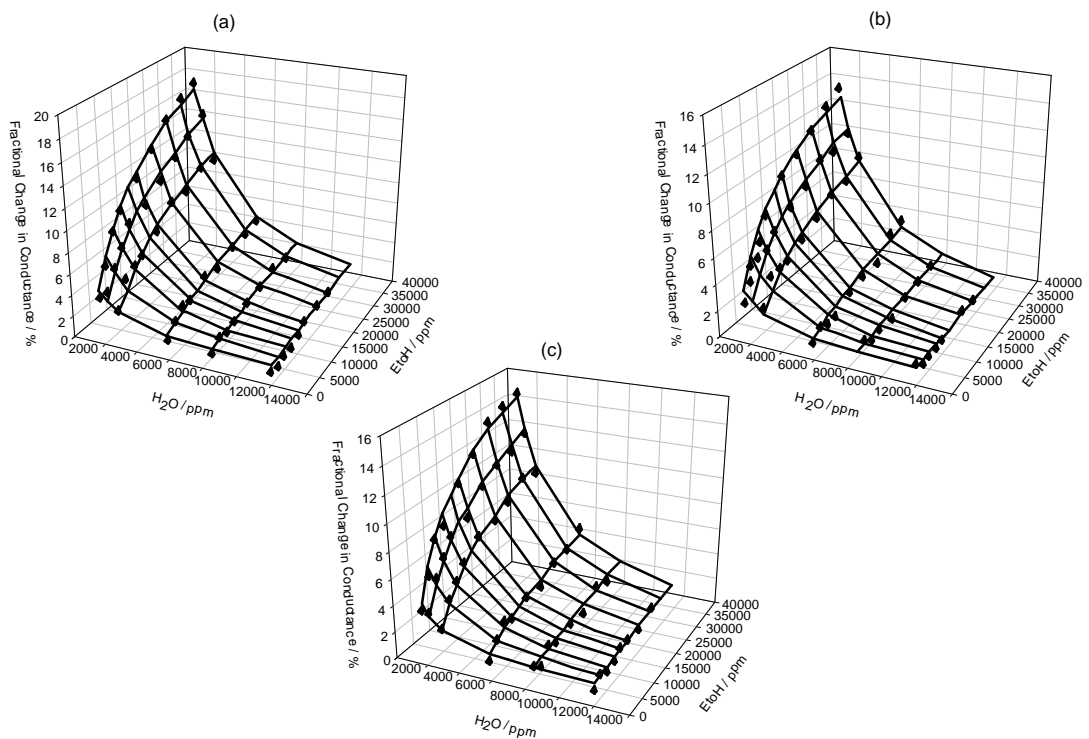
Figure 4.13 A plot showing the effect of water and ethanol vapour on the response of Pan/DSA/H$_2$O gas sensors at 23.7°C. The solid mesh is a fit of the theory to the experimental data.

The characteristics of the Pan sensors established by the independent models (Equations 4.6 and 4.7) were demonstrated again in the competitive model. The sensitivity parameter predicted for water (in this model expressed as $a_w\Gamma/G_0$) was consistently larger than the equivalent ethanol term ($a_e\Gamma/G_0$). The value obtained for the binding constant also followed the trend demonstrated by the earlier models with K_w being consistently larger than K_e for all of the Pan sensors. However, the tendency established by the Ppy sensors in the independent models was not consistent with the full competitive model. The values obtained for the binding constant in the competitive model were continually greater for water when compared with the ethanol. This is opposite to the trends demonstrated in the previous models. The sensitivity parameter also demonstrated the converse inclination in the competitive model, with the magnitude of the ethanol value now being greater than that shown by the water. It should also be noted that, although there is evidently competition occurring between the ethanol and water, the curves shown in figures 4.10 to 4.13 do not exhibit a smooth 'mirrored s–shape' that would normally be expected in a competitive binding model.

4.4 Effect of Temperature

4.4.1 Competitive Model

The effect of temperature on the model can now be investigated using results obtained from 5 temperatures between 30 ℃ and 57 °C. We can initially gain information about the temperature effect on the baseline conductance of the sensors by employing Equation 4.7. Applying this model to data describing the effect of humidity on the conductance of the polymers at different temperatures, allows a prediction of the effect of temperature on the baseline conductance of the polymers in the absence of

water vapour. Examples of the effect of temperature on the baseline (G_0) are shown in Figures 4.14 and 4.15. In order to investigate the competitive model, data were taken at each of the 5 temperatures, for eight different ethanol concentrations at three different humidities. These data can be employed to see how the parameter values predicted by the model vary as the temperature is changed. The non-linear regression fitting process at each temperature will be limited by the number of humidity tests completed. However, the modelling process has been performed and examples of the variation of parameter values with temperature for Ppy are shown in Figures 4.16 to 4.19 and Pan in Figures 4.20 to 4.23.

There are a number of conclusions that we can draw from this temperature analysis. Firstly there is good agreement between the parameter values obtained in the temperature range for the replicates of nominally identical polymer types. This was true for both Ppy and Pan sensors. The values obtained for the sensitivity parameters, $a_w\Gamma/G_0$ and $a_e\Gamma/G_0$, were similar for nominally identical sensors over the range of temperatures tested. Within the experimental error, the parameter values of individual sensors could be identical. The replacement of these two parameters in the model with a single sensitivity term was attempted in order to characterise any effects on the overall model. The consequence of this was a slight deterioration in the accuracy of the fit without any significant effect on the temperature characteristics.

The polymers demonstrated distinct differences in the values obtained for the sensitivity terms for Pan and Ppy. The trends discussed earlier (section 4.3.2) were again demonstrated with both the polarity and the magnitude of the sensitivity terms varying between the Pan and Ppy sensors. Although there were no definite variations between the $a_e\Gamma/G_0$ and $a_w\Gamma/G_0$ parameters for the two lengths of counter-ion of the
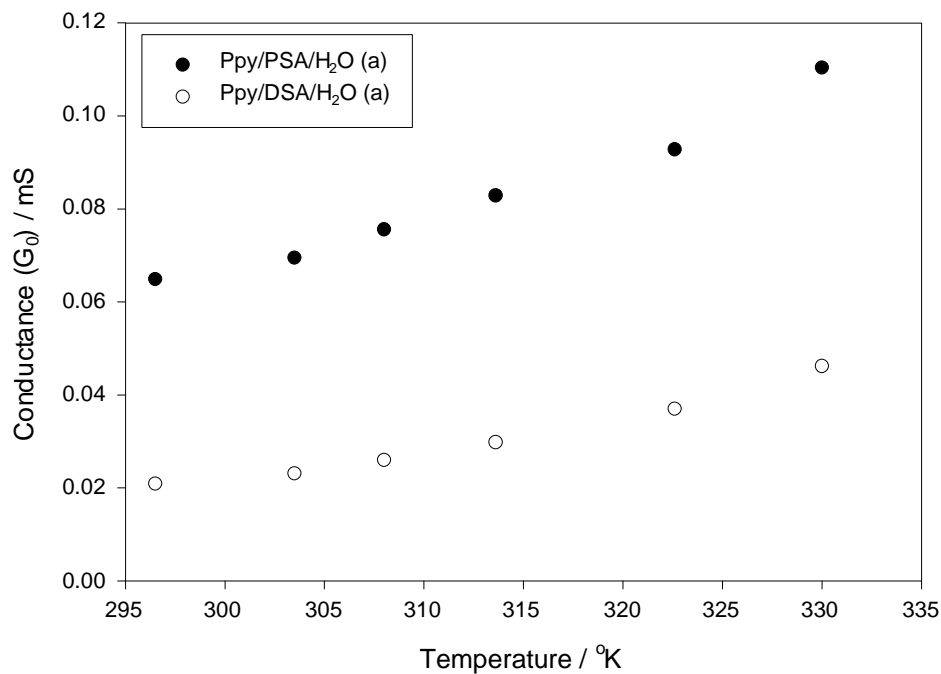
Figure 4.14 Examples of the effect of temperature on the baseline conductance (in the absence of water) of the Ppy sensors. Values were predicted at a range of temperatures using equation 4.7.
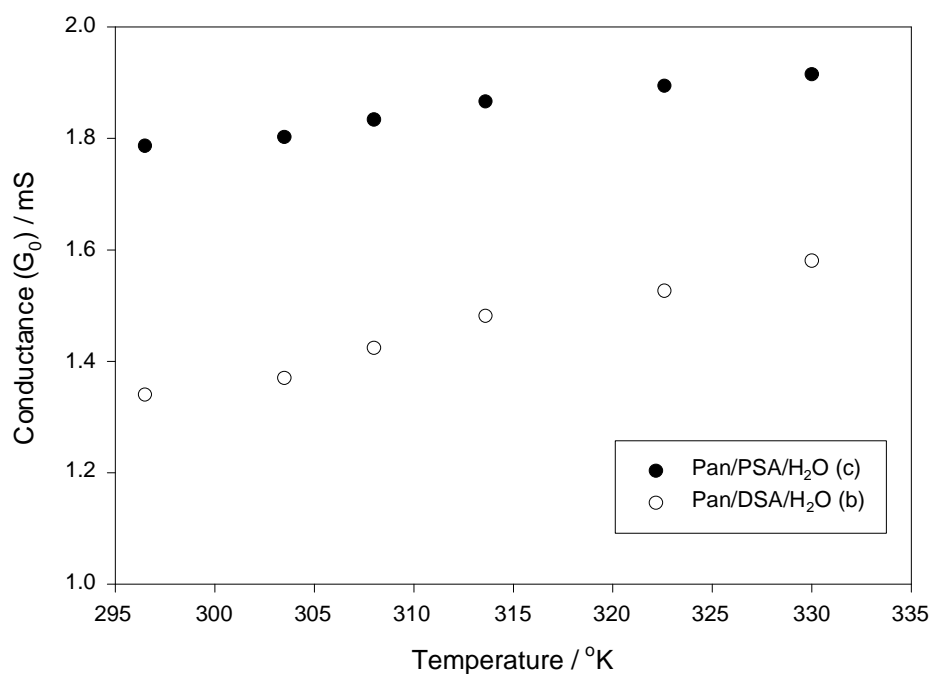
Figure 4.15 Examples of the effect of temperature on the baseline conductance (in the absence of water) of the Pan sensors. Values were predicted at a range of temperatures using equation 4.7.
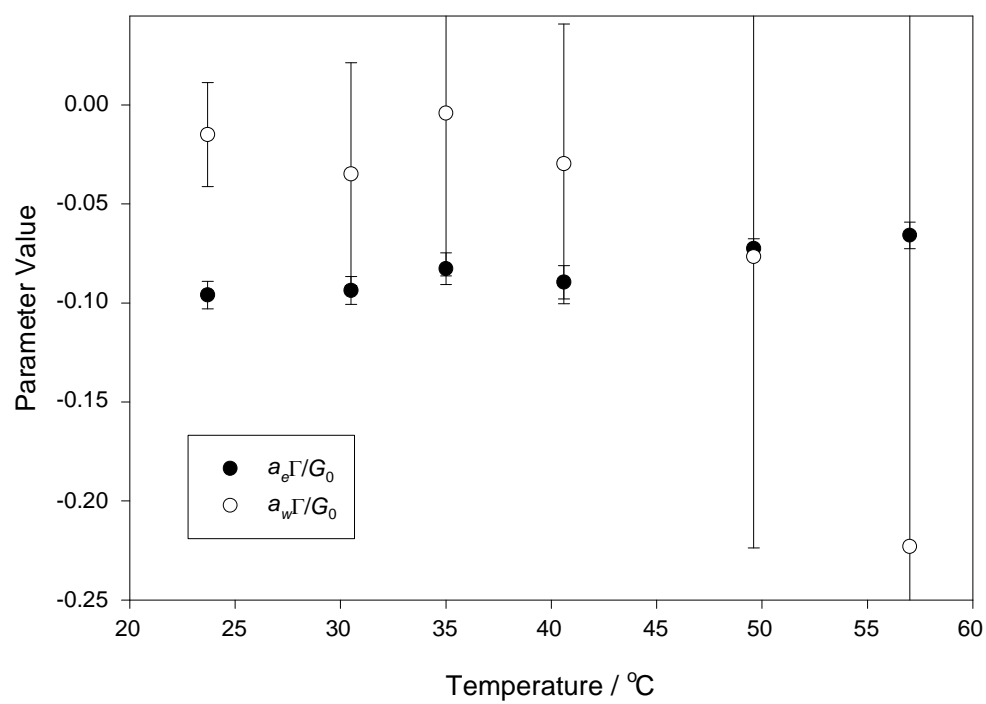
Figure 4.16 The typical temperature variation of the sensitivity parameters for Ppy/PSA/H$_2$O sensors.
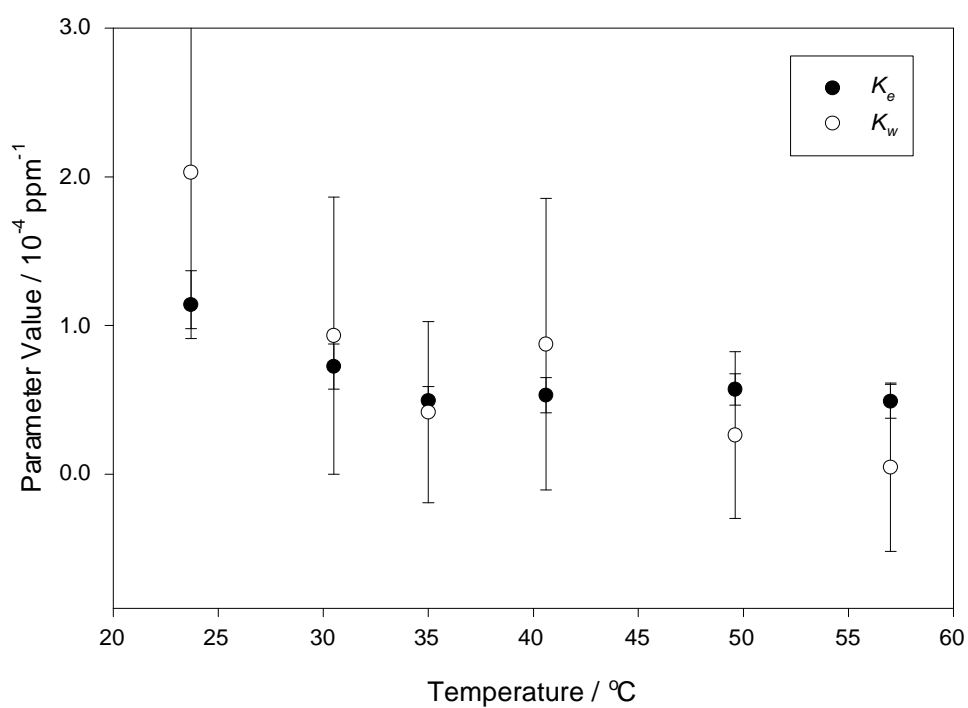
Figure 4.17 The typical temperature variation of the binding constants for Ppy/PSA/H$_2$O sensors.
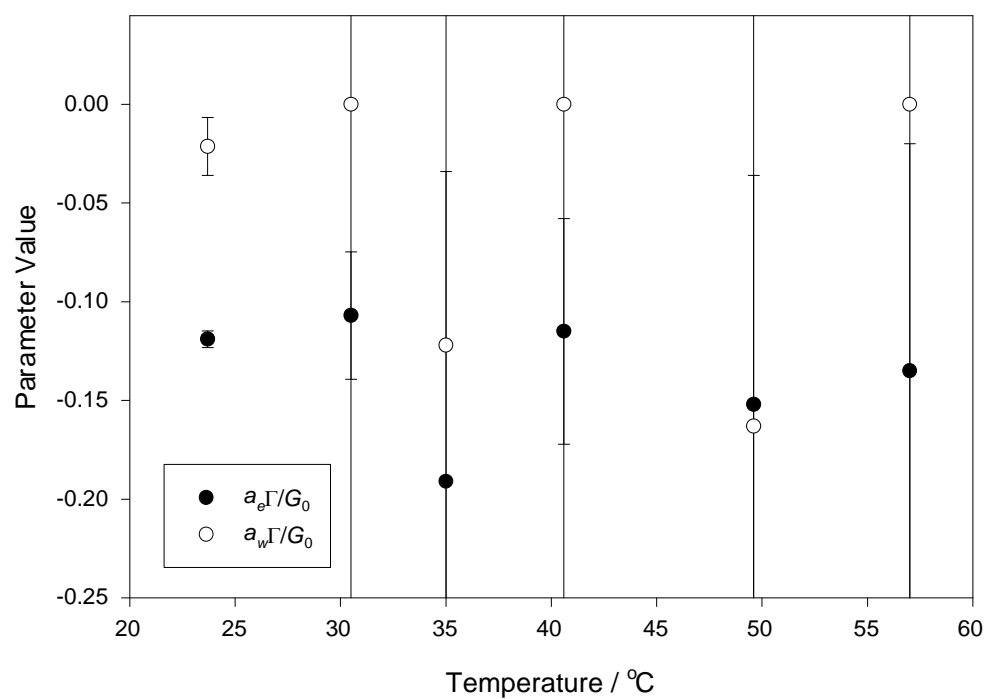
Figure 4.18 The typical temperature variation of the sensitivity parameters for Ppy/DSA/H$_2$O sensors.
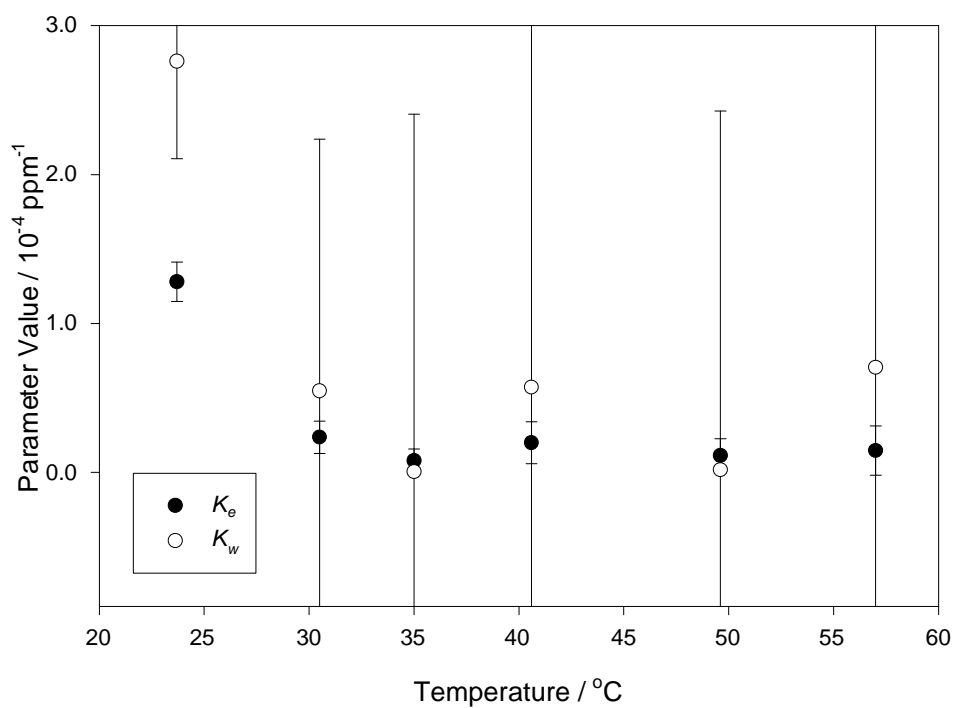
Figure 4.19 The typical temperature variation of the binding constants for Ppy/DSA/H$_2$O sensors.
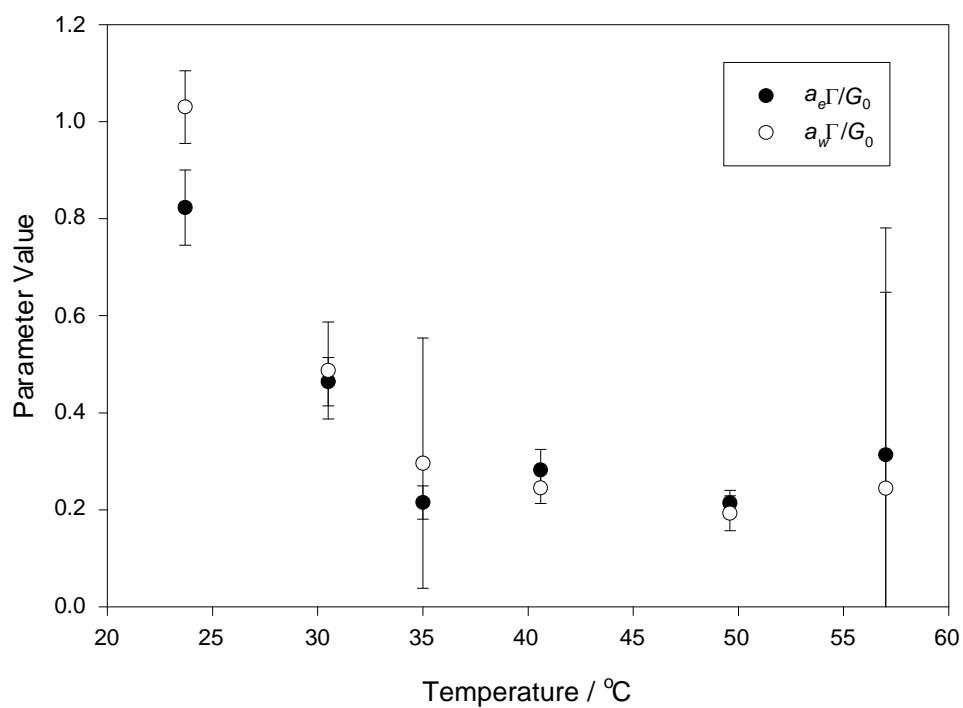
Figure 4.20 The typical temperature variation of the sensitivity parameters for Pan/PSA/H$_2$O sensors.
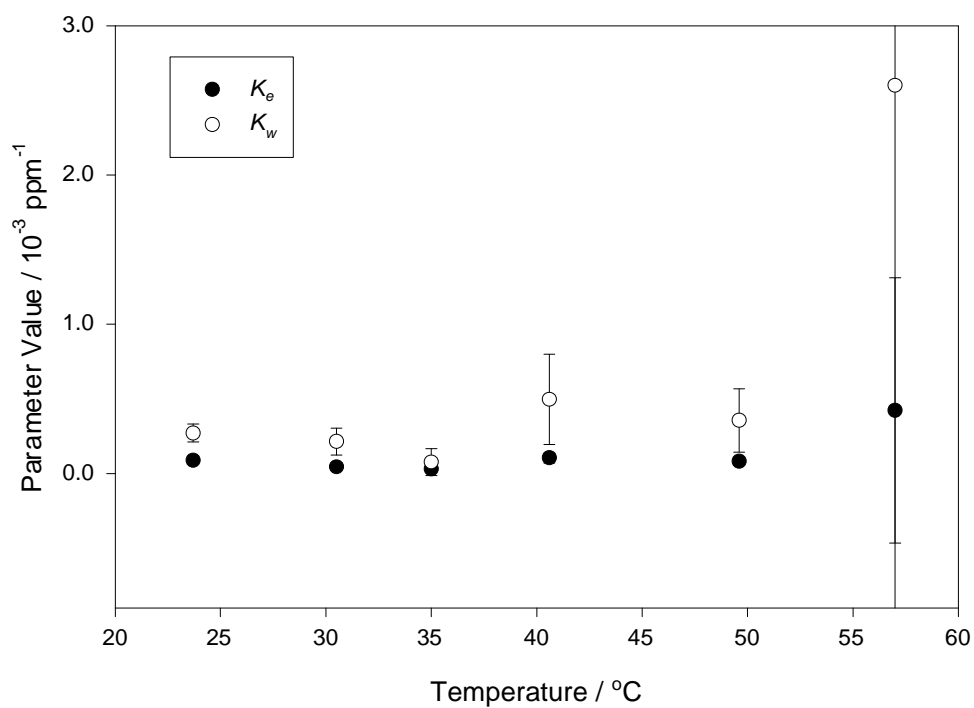
Figure 4.21 The typical temperature variation of the binding constants for Pan/PSA/H$_2$O sensors.
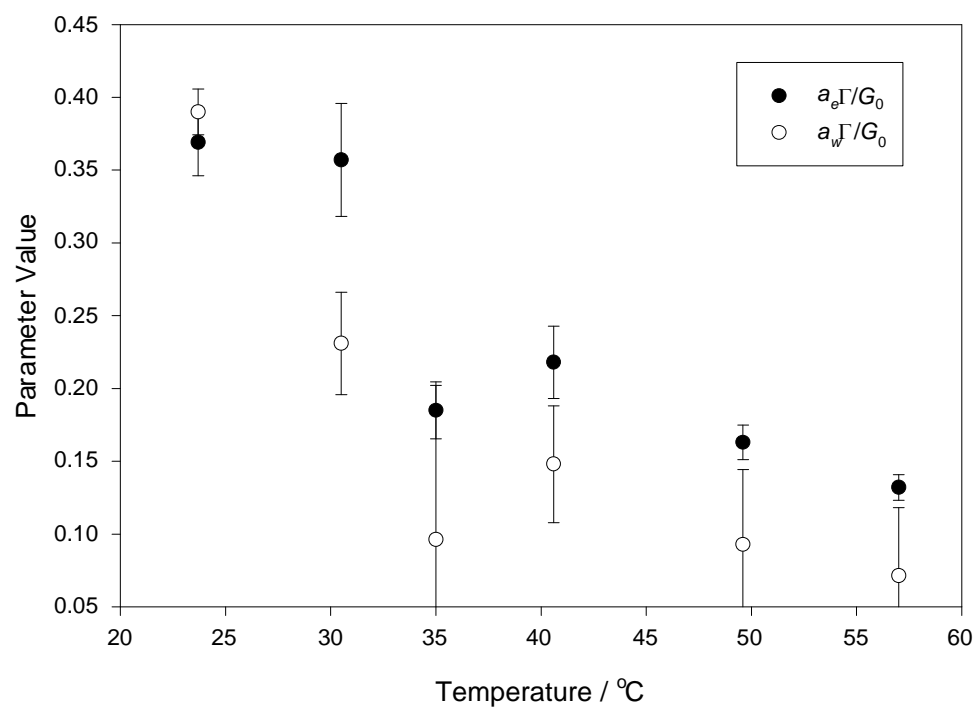
Figure 4.22 The typical temperature variation of the sensitivity parameters for Pan/DSA/H$_2$O sensors.
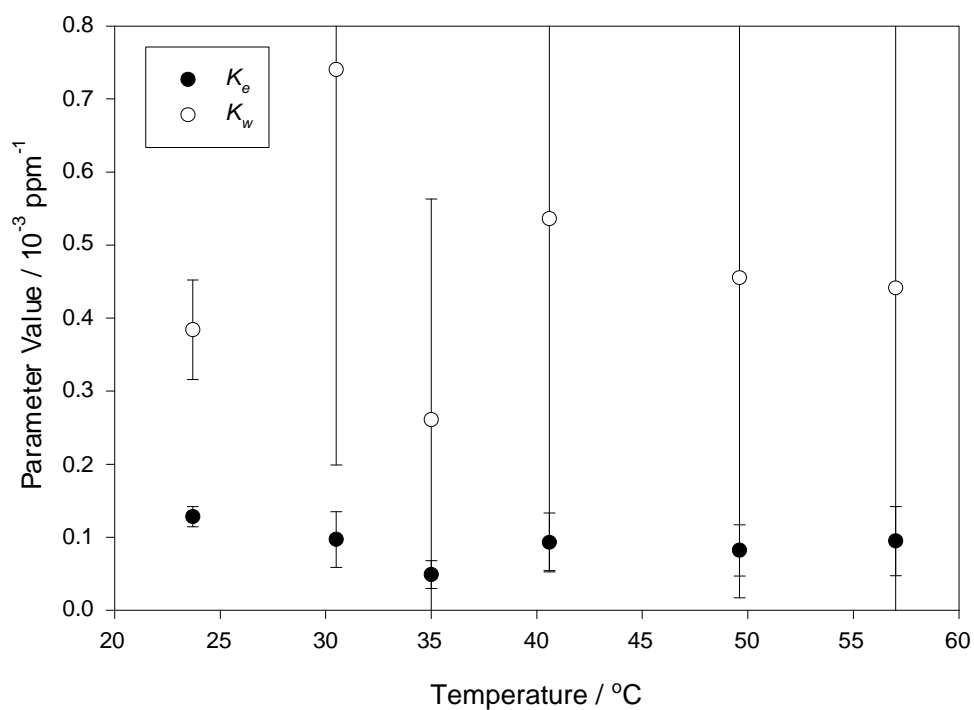
Figure 4.23 The typical temperature variation of the binding constants for Pan/DSA/H$_2$O sensors.

_____

Ppy sensors, the values obtained for Pan/PSA/H$_2$O were consistently greater over the temperature range than those found for Pan/DSA/H$_2$O. Although these parameter values do converge at higher temperatures the trend is still evident. Temperature effects on the sensitivity parameter of Ppy sensors seems to be negligible with no distinct trend developing over the range of temperatures tested. The Pan sensors, however, demonstrate a clear reduction in there magnitude as the temperature is increased. This indicates that, although the Pan sensors give larger responses to the ethanol vapour than the Ppy, that this response significantly reduces as the temperature is increased.

Using the model we can also investigate the effects of temperature on the ethanol and water binding constants, K_e and K_w, respectively. Firstly, the magnitude of the K_w parameter in the Pan sensors is consistently larger than the K_e. This trend was not demonstrated by the Ppy sensors which had far more variation in the values of the two parameters as the temperature was increased and therefore more disorder between the two. However, both types of polymer consistently gave larger standard errors for the K_w values. This again leads to the possibility that, within experimental error the two binding constants have the same value. For both the Pan and Ppy sensors there were no apparent differences between the parameter values obtained for the two lengths of counter-ion.

Finally, the trend demonstrated by the binding constants as the temperature of the sensors is increased should be consistent with the underlying thermodynamic characteristic of the polymers [4.9, 4.10]. These are defined by the Helmholtz Equation,

$$\Delta E = \Delta H - T\Delta S \tag{4.10}$$

where ΔE is the free energy of adsorption or Gibbs free energy (J mol^{-1}), ΔH is the enthalpy (J mol^{-1}), ΔS is the entropy (J mol^{-1} K^{-1}) and T is the temperature (K). The free energy of adsorption is defined by the binding constant [4.11] through the equation

$$\Delta G = -RT \ln K \qquad (4.11)$$

Combining these expressions allows us to predict that an increase in temperature should lead to a decrease in the value of the binding constant. This trend is clearly not evident in the analysis of the temperature effect on the value of K in our competitive binding model. The temperature seems to have a negligible effect (within experimental error) on the value of the K parameter and for some of the Pan/PSA/H$_2$O polymers the value increases with temperature. These trends were validated by using Equation 4.8 and using the final conductance data obtained from the polymer responses. Again the temperature dependence of the polymers seemed to be modelled by changes in the sensitivity terms $a_e\Gamma/G_0$ and $a_w\Gamma/G_0$ leaving negligible variations in the binding constants, K_e and K_w. This suggests that the model needs modifying with the conductance having its own temperature dependence.

4.4.2 Empirical Model

Although the temperature dependence of the parameters used in the competitive binding model were not consistent with the underlying thermodynamic behaviour of the polymers, the data obtained for the magnitude of the response of the sensors seemed

more consistent.   These data have therefore been used to predict an empirical relationship demonstrating the effect of temperature on the response to ethanol at a constant humidity. From section 4.3 we know that water has an effect on the base–line and response of conducting polymers. However, in order to simplify the empirical model we use a fundamental model of an ethanol response at a constant humidity. This response is based on a variable range hopping model of the Mott kind [4.12]. This basic model assumes that when a charge carrier within the polymer encounters a potential barrier it will hop to the nearest available site. This type of barrier–limited conduction mechanism can be modelled by an exponential equation when the temperature range is small so there is only nearest–neighbour hopping,

$$G \approx G_0 \exp\left(\frac{-\Phi}{kT}\right)$$
(4.12)

where Φ is the work function of the polymer, k is Boltzmann's constant, G_0 is a constant (as T tends to infinity) and T is the temperature of the experiment. A target vapour can now be modelled by how it affects the work function of the polymer [4.13]. Blackwood and Josowicz [4.14] have shown that the work function for Ppy and poly(phenylene) films can increase or decrease when exposed to organic vapours. The polarity of this change depends on whether the target vapour acts as a charge "donor" or "acceptor". Equation 4.12 can therefore be modified to include a work function modulation due to exposure of the polymers to ethanol vapour,

$$G \approx G_0 \exp\left[\frac{-\left(\Phi_0 + \Delta\Phi_e\right)}{kT}\right]$$
(4.13)

where $\Delta\Phi_e$ is the change in the work function due to the ethanol vapour and Φ_0 is the work function in air. Recent work on MOSFETs [4.15] shows that the chemically activated shift in the work function of the polymers follows a Langmuir isotherm,

$$\Delta\Phi \approx \frac{\alpha \times KC}{(1+KC)} \tag{4.14}$$

where α is the sensitivity of the work function to the target vapour and has a similar effect to $a_e\Gamma$ in the earlier competitive model. We can now rewrite Equation 4.13 as,

$$G \approx G_0 \exp\left(\frac{-\Phi_0}{kT}\right) \times \exp\left(\frac{-\alpha}{kT}\frac{KC}{(1+KC)}\right) \tag{4.15}$$

The fractional response can therefore be written,

$$\frac{\Delta G}{G} \approx \exp\left(\frac{-\alpha}{kT}\frac{KC}{(1+KC)}\right) - 1 \tag{4.16}$$

When using weakly interacting vapours such as ethanol it is reasonable to assume that the chemical shift $\Delta\Phi$ is small when compared to kT (~30 meV). Under these conditions Equation 4.16 can be approximated to,

$$\frac{\Delta G}{G} \approx \frac{-\alpha_e}{kT}\frac{K_e C_e}{(1+K_e C_e)} \tag{4.17}$$

Using data obtained at a constant humidity of 1238 ppm we can now employ Equation 4.17 and determine the effect of temperature changes on the values of both the binding constant, K_e, and the sensitivity term α_e. Empirical expressions can then be used to reproduce these effects and yield a thermal model of the response of ethanol vapour.

Figures 4.24 to 4.31 show how the parameters employed in Equation 4.17 vary with temperature between 295 °K and 335 °K. The empirical models used to describe these changes have also been included in these figures. The Pan sensors shown in Figures 4.24 to 4.27 show an decrease in their sensitivity as the temperature increases. This has been modelled using an exponential expression shown below,

$$\alpha = \alpha_0 \exp(\gamma T) \tag{4.18}$$

where γ is the temperature coefficient of the polymer's sensitivity. The binding constant showed an almost linear increase with temperature. Although this is not the response we would expect thermodynamically from our polymer model, the increase in the binding constants value may be accounted for by swelling within the membrane. The further development of a model to include both the chemical effect on the work function and the effect of swelling is beyond the scope of this thesis. However, the marked deviation of the binding constant from its thermodynamically predicted behaviour may be an indication of a large amount of swelling within the Pan films. The empirical model used for the binding constant take is shown in Equation 4.19,
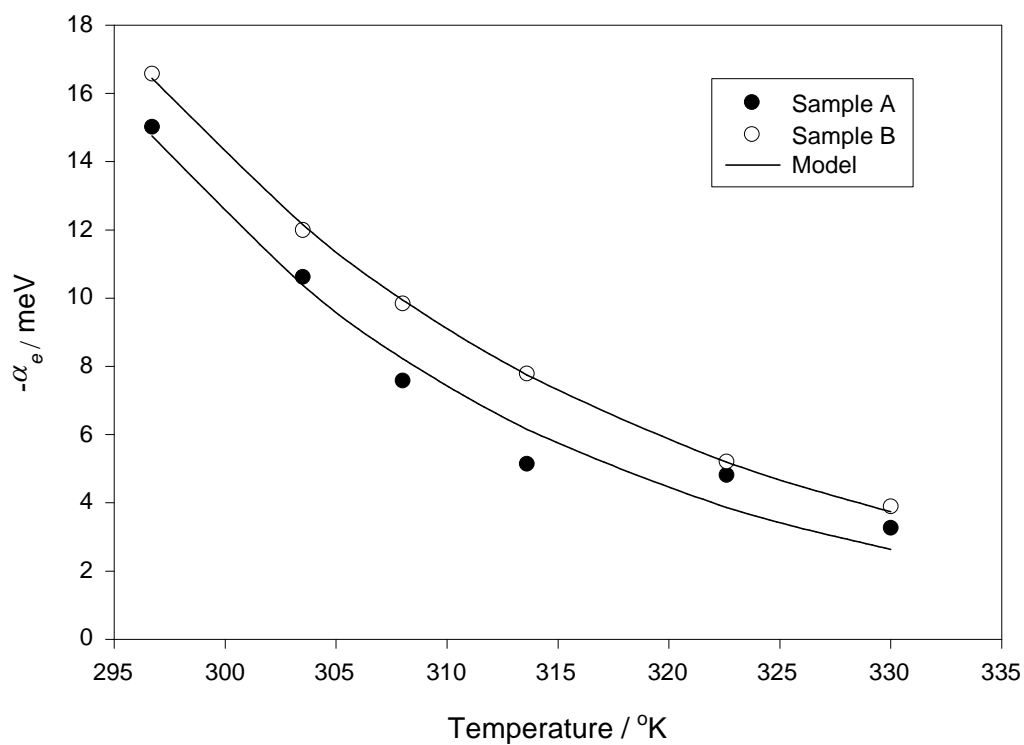
Figure 4.24 Two examples of the typical temperature variation of the sensitivity coefficient for Pan/PSA/H$_2$O sensors.
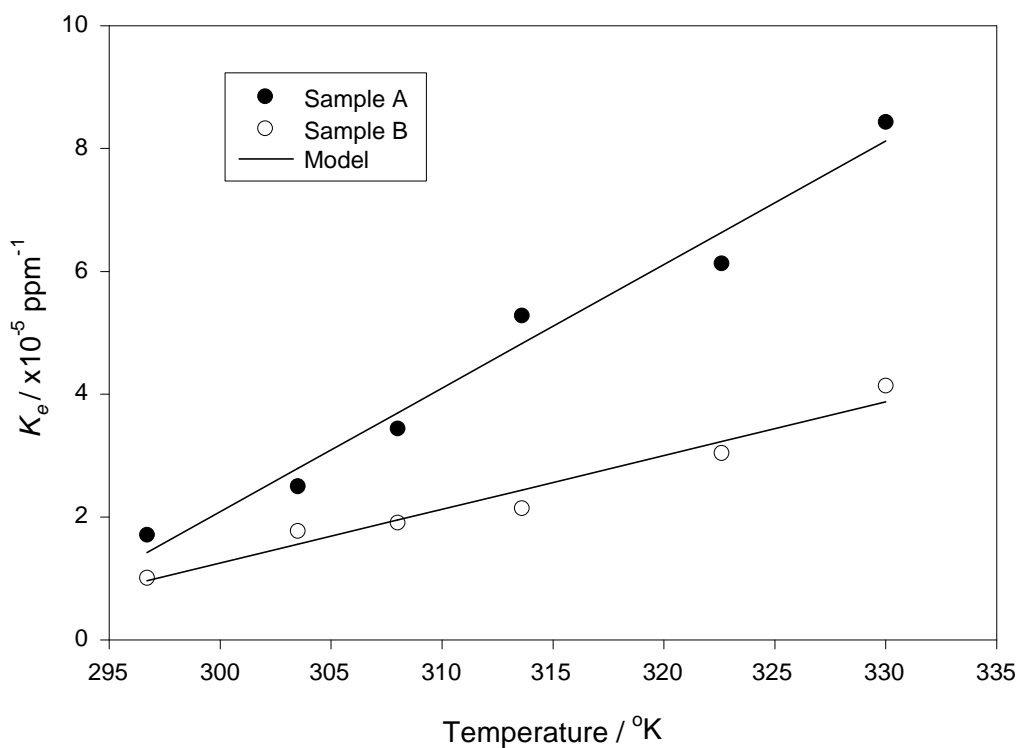
Figure 4.25 Two examples of the typical temperature variation of the binding constant for Pan/PSA/H$_2$O sensors.
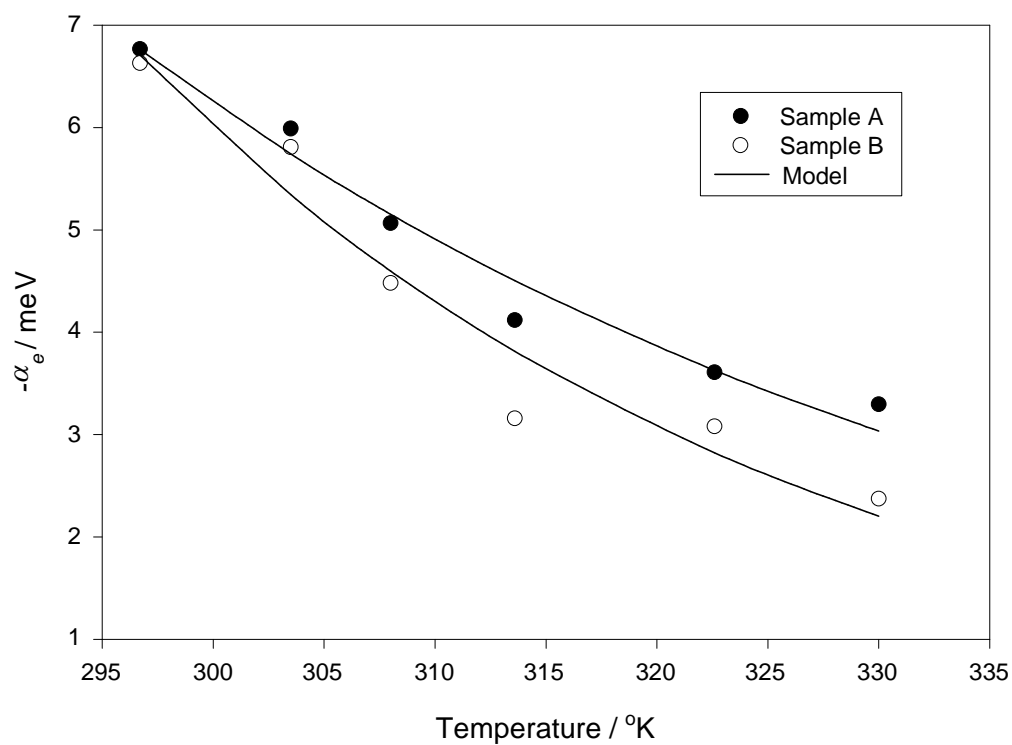
Figure 4.26 Two examples of the typical temperature variation of the sensitivity coefficient for Pan/DSA/H$_2$O sensors.
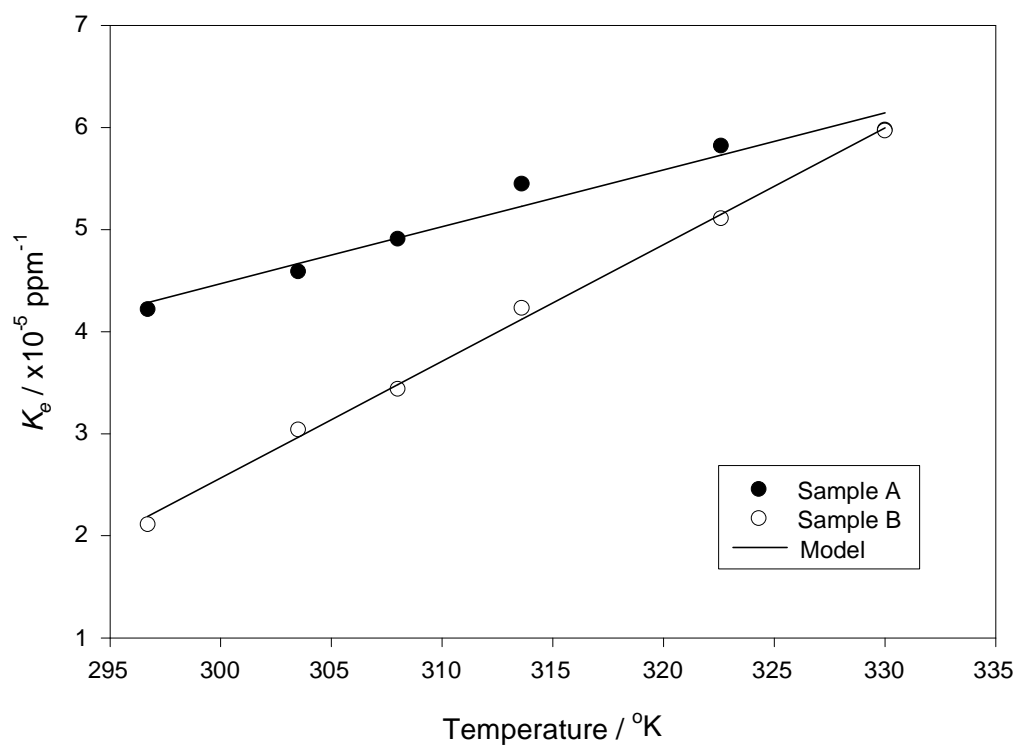
Figure 4.27 Two examples of the typical temperature variation of the binding constant for Pan/PSA/H$_2$O sensors.

$$K_e = K_{e0}(1 + \beta T)$$ (4.19)

The values obtained for the constant used in Equations 4.20 and 4.21 are shown in

Table 4.4.

Table 4.4 Parameter values employed in the empirical model of the temperature effects on the response of Pan sensors at an absolute humidity of 1238 ppm.

Sensor	α_0 (10^2 eV)	γ (10^{-2} K^{-1})	K_{e0} (10^{-4} ppm^{-1})	β (10^{-4})
Pan/PSA/H$_2$O (a)	67.9 ± 10.80	-5.171 ± 0.53	-5.828 ± 0.50	-3.453 ± 0.02
Pan/PSA/H$_2$O (b)	88.9 ± 18.57	-4.450 ± 0.07	-2.496 ± 0.28	-3.500 ± 0.04
Pan/PSA/H$_2$O (c)	8.9 ± 15.20	-3.687 ± 0.56	-3.128 ± 0.41	-3.559 ± 0.05
Pan/DSA/H$_2$O (a)	0.012 ± 0.006	-1.788 ± 0.17	-0.342 ± 0.10	-8.382 ± 1.55
Pan/DSA/H$_2$O (b)	0.085 ± 0.059	-2.406 ± 0.22	-1.228 ± 0.17	-4.547 ± 0.19
Pan/DSA/H$_2$O (c)	1.367 ± 1.820	-3.344 ± 0.44	-3.174 ± 0.09	-3.603 ± 0.01

The Ppy sensors demonstrated marginally different characteristics than the Pan.

Both the sensitivity and the binding constant were modelled using the exponential

expressions below,

$$\alpha_e = \alpha_{e0}(1 + \gamma_\alpha \exp \beta_\alpha T)$$ (4.20)

$$K_e = K_{e0}(1 + \gamma_K \exp \beta_K T)$$ (4.21)

The values of the parameters employed in these empirical expressions are shown in

Table 4.5. As expected, the polarity of the work function modulation as defined by the

sensitivity α_e was the opposite of the Pan sensors. However, for both types of polymer

the magnitude of this parameter reduced as the temperature was increased. The binding

constant for the Ppy sensors demonstrated characteristics that were consistent with the

thermodynamic predictions of Equations 4.10 and 4.11. This implies that swelling that

occurs in the Ppy does not dominate, allowing the real effects of the temperature on the

binding constant to emerge from the model. Further research would be required in

order to confirm this theory.

Table 4.5 Parameter values employed in the empirical model of the temperature effects on the response of Pan sensors at an absolute humidity of 1238 ppm.

Sensor	α_{e0} $(10^{-3}$ eV)	γ_{α} (10^{-5})	β_{α} (10^{-2})	K_{e0} $(10^{-9}$ eV)	γ_K (10^6)	β_K (10^{-2})
Ppy/PSA/H$_2$O (a)	-2.42 ± 0.05	-2.54 ± 5.86	4.72 ± 1.25	1.99 ± 2.06	95.46 ± 12.34	-4.52 ± 0.58
Ppy/PSA/H$_2$O (b)	-3.14 ± 0.92	-1.49 ± 6.60	3.12 ± 3.27	3.29 ± 0.22	58.72 ± 11.73	-6.14 ± 0.07
Ppy/DSA/H$_2$O (a)	-2.59 ± 0.02	-2.51 ± 4.58	8.57 ± 0.55	0.53 ± 0.46	172.0 ± 51.32	-7.87 ± 0.05
Ppy/DSA/H$_2$O (b)	-3.32 ± 0.18	-0.40 ± 0.85	3.59 ± 0.58	0.80 ± 0.17	150.0 ± 54.87	-6.08 ± 1.83

4.5 Conclusions

We have studied the response of Ppy pentane and decane sulfonic acid and Pan pentane

and decane sulfonic acid to ethanol vapour at varying levels of humidity and

temperature. A competitive binding model has been developed which gives a good fit

to all of the experimental data taken at a constant temperature. A number of

characteristics were demonstrated by the two types of monomer tested. Pan was found

to exhibit a greater sensitivity to both ethanol and water vapour when compared to Ppy.

The polarity of these responses was also different for the two monomer types. Values

of the binding constants for ethanol and water were observed to be similar for both

_____
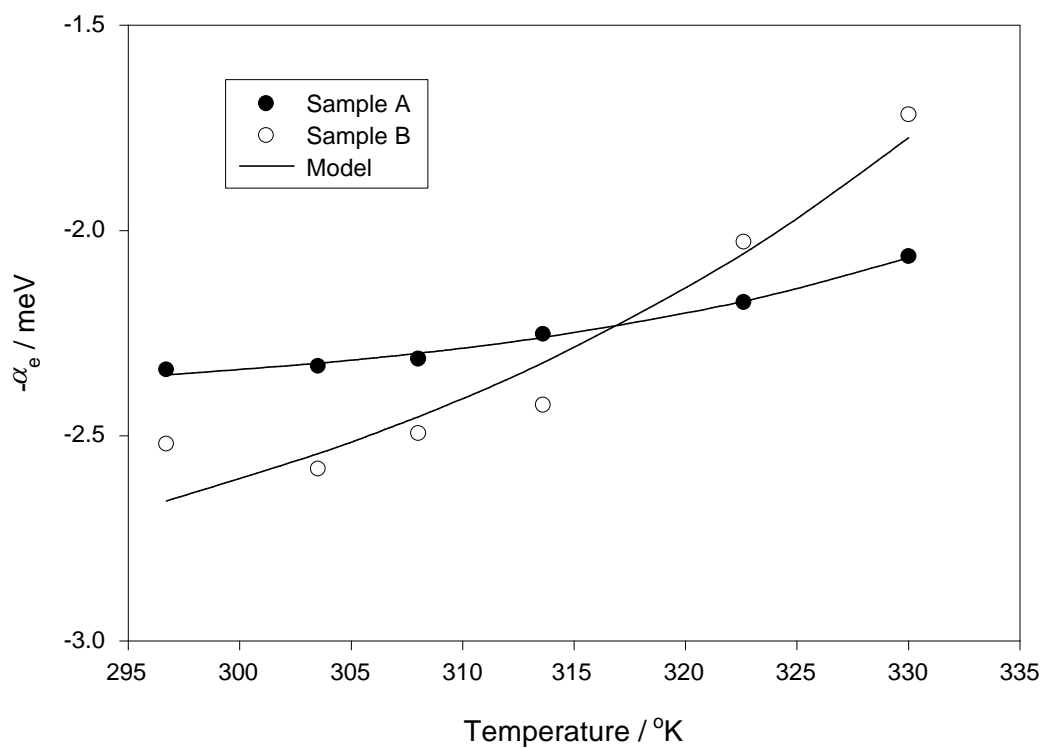
Figure 4.28 Two examples of the typical temperature variation of the sensitivity coefficient for Ppy/PSA/H$_2$O sensors.
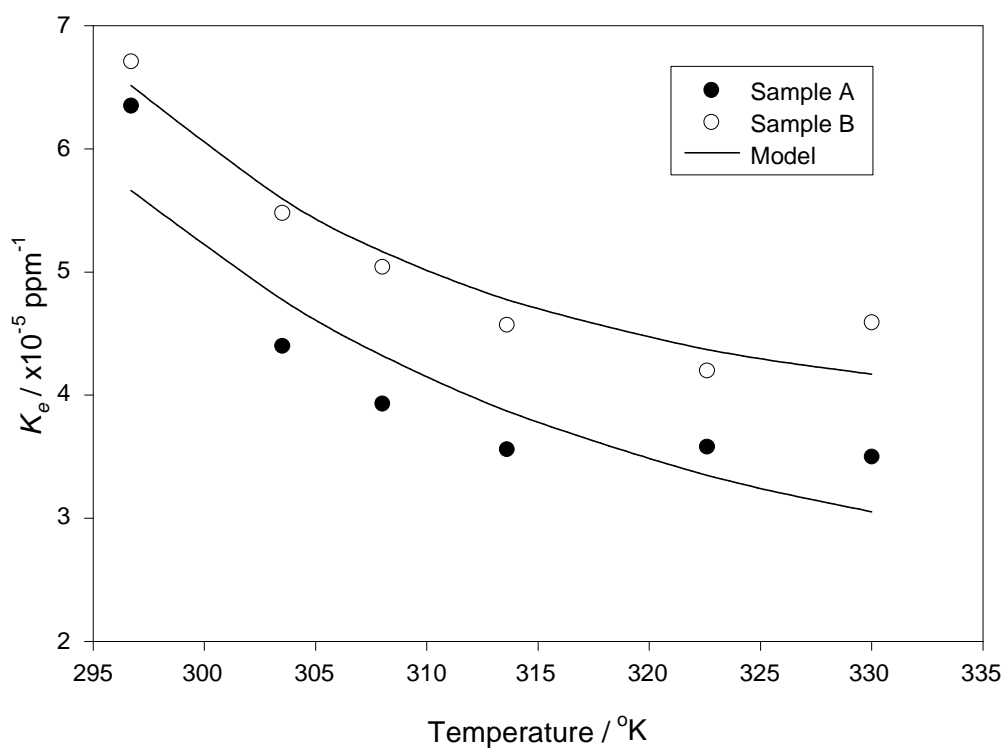
Figure 4.29 Two examples of the typical temperature variation of the binding constant for Ppy/PSA/H$_2$O sensors.

_____
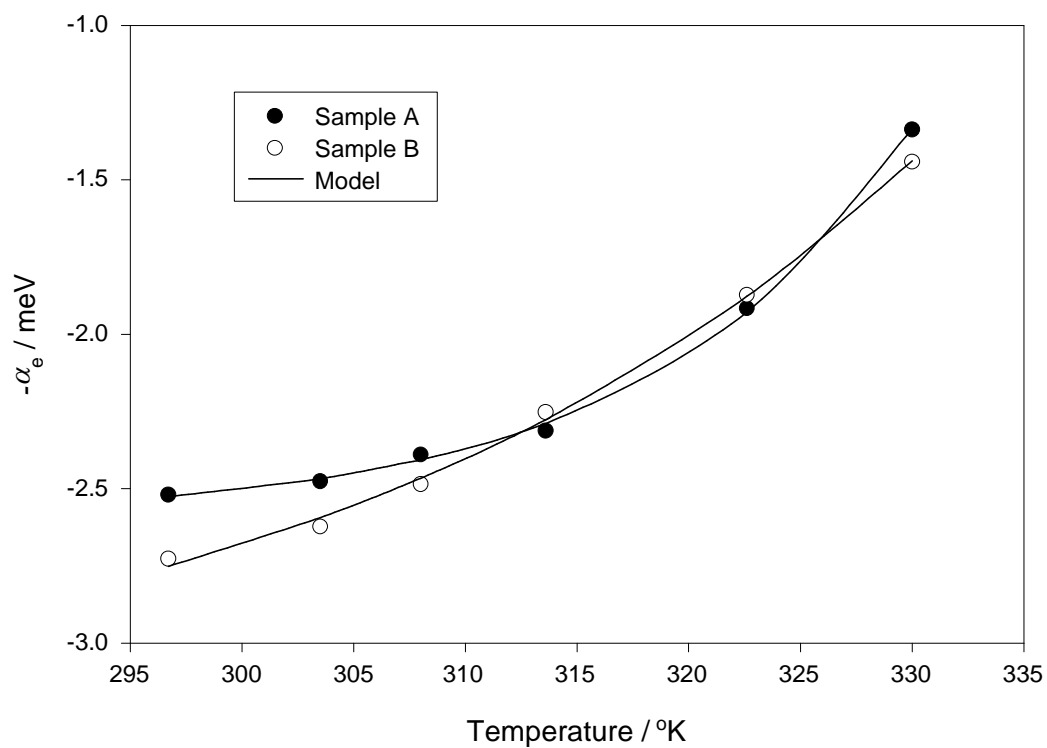
Figure 4.30 Two examples of the typical temperature variation of the sensitivity coefficient for Ppy/DSA/H$_2$O sensors.
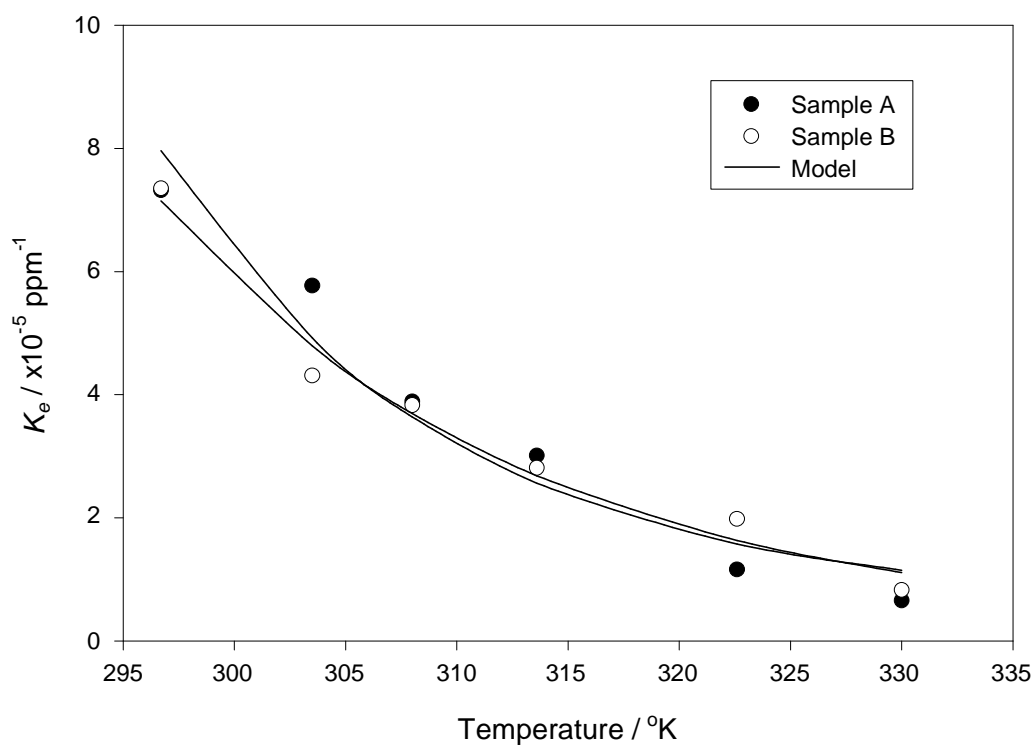
Figure 4.31 Two examples of the typical temperature variation of the binding constant for Ppy/PSA/H$_2$O sensors.

types of polymer. The sensitivity of the polymers to ethanol vapour was found to fall with increasing water vapour and temperature although this effect was more dramatic in the case of Pan. In general, it was found that the largest response of the sensors occurred at low humidity and low operating temperature. However the relative sensitivity of the polymers to fluctuations in humidity and temperature also increased under these conditions. The effect of the size of the counter-ion chain was small when compared with the choice of monomer, although the temperature-sensitivity and stability of the films with DSA counter-ions was better.

Extension of the competitive binding model to include the effects of temperature on the polymers was also explored. The values of the physical parameters extracted from the conductance model, particularly the binding constants, were not thermodynamically consistent with our basic model of the polymers. An empirical model was therefore constructed to describe the observed effect of temperature on the response of the polymers at a constant humidity. In order to achieve this goal, the modification of some of the basic premises from which the conductance model was developed may be required.

In conclusion, an isothermal competitive binding model seems to apply both to pyrrole and aniline based conducting polymer gas sensors and may be used to characterise their behaviour. However, further research is required in order to successfully extend this model to include temperature effects on the device conductance and on the competition between the two vapours.

4.6 References

4.1   P. N. Bartlett, P. B. M. Archer, and S. K. Ling-Chung, Conducting polymer gas sensors. Part I: Fabrication and characterisation, *Sensors and Actuators*, **19**, (1989), 125-140.

4.2   P. N. Bartlett and S. K. Ling-Chung, Conducting polymer gas sensors. Part II: Response of polypyrrole to methanol vapour, *Sensors and Actuators*, **19**, (1989), 141-150.

4.3   P. N. Bartlett and S. K. Ling-Chung, Conducting polymer gas sensors. Part III: Results for four different polymers and five different vapours, *Sensors and Actuators*, **20**, (1989), 287-292.

4.4   P. N. Bartlett, J. W. Gardner, and R. J. Whitaker, Electrochemical deposition of conducting polymers onto electronic substrates for sensor applications, *Sensors and Actuators A*, **23,** (1990), 911-915.

4.5   N. Blair, The Development and characterisation of conducting polymer based sensors for use in an electronic nose, *Ph.D. Thesis, University of Southampton, UK,* 1990.

4.6   T. A. Skotheim (ed.), *Handbook of conducting polymers*, Dekker, New York, 1986.

4.7   J. W. Gardner, P. N. Bartlett, and K. F. Pratt, Modelling of gas-sensitive conducting polymer devices, *IEE Proc.-Circuits Devices Syst.*, **142**, (1995), 321-333.

4.8   J. W. Gardner, *Personal communication*, 1998.

4.9   M. Haug, K. D. Schierbaum, G. Gauglitz and W. Göpel, Chemical sensors based upon polysiloxanes: comparison between optical, quartz microbalance, calorimetric, and capacitance sensors, *Sensors and Actuators B,* **11,** (1993), 383-391.

4.10   R. A. Bailey and K. C. Persaud, Application of inverse gas chromatography to characterisation of the Ppy surface, *Analytica Chimica Acta,* **363**, (1998), 147-156.

4.11   J. H. de Boer, *The dynamical character of adsorption*, Oxford University Press, London, 1953.

4.12   N. Mott, *Metal–Insulator transitions,* Taylor and Francis Ltd, London, 1974

4.13   J. Janata, *Microsensors based on modulation of work function, in Sensors and Sensory Systems for an Electronic Nose,* P. N. Bartlett and J. W. Gardner (eds), Kluwer Academic Publishers, Dordrecht, 1992, 103-116.

4.14   D. Blackwood and M. Josowicz, Work function and spectroscopic studies of interactions between conducting polymers and organic vapours, *J. Phys. Chem.,* **95,** (1991), 493-502.

4.15   J. V. Hatfield, J. A. Covington and J. W. Gardner, GasFETs incorporating conducting polymers as gate materials, *Technical Digest of the Seventh Int. Meeting on Chemical Sensors, Beijing, China,* (1998).

CHAPTER 5

Modelling the Effects of CO$_2$

5.1 Introduction

The detection of CO$_2$ has become an area of particular interest recently due to its role as a "greenhouse gas" and subsequent effects on the global warming of the earth. Redox active gases such as O$_2$, H$_2$, Cl$_2$, CO or NO$_x$ can be monitored by means of gas–solid reactions based on oxidation or reduction mechanisms such as those employed in Taguchi type gas sensors. However, gases such as CO$_2$ and NH$_3$ are inactive in terms of their reduction or oxidation processes. This makes sensors based on redox reactions either not sensitive or not selective in the detection of such gases [5.1]. However, gases that are not redox active sometimes exhibit a larger activity in acid–base reactions. This means that they react with the ions within a solid rather than with the electrons. This chapter concentrates on the detection and modelling of the effects of CO$_2$ with conducting polymer sensors.

The most common method for the detection of CO$_2$ is based on infrared spectroscopic analysers. However, this type of equipment is expensive and is not portable. There is therefore a need for a low–cost portable, reproducible CO$_2$ sensor. A number of researchers have developed CO$_2$ sensors based on solid electrolytes [5.2-5.6], and mixed oxide [5.7]. Shimizu et al. have developed CO$_2$ sensors based on polymers with carbonate solutions supported on porous alumina ceramics [5.8]. These

sensors demonstrated a linear relationship with CO_2 from 1 to 9% with good reproducibility and long–term stability.

This chapter reports on the effects of CO_2 concentrations in the range 0 to 500 ppm, on the response of resistive conducting polymer sensors. The sensors included in these tests were Ppy/PSA/H_2O, Pan/PSA/H_2O and a modified form of Pan butane sulfonic acid (BSA) grown in a sodium salt solution. The Pan/BSA sensors were modified after growth by soaking in a sodium hydrogen carbonate ($NaHCO_3$) solution. This process was aimed at increasing the sensitivity of the sensors by maximising the acid–base interactions occurring between the sensor material and the CO_2. A theoretical model of the interaction between the gas and the polymer is postulated and the effects of both humidity and temperature on an alternative empirical model is included.

5.2 Response of Polymers to CO_2

The automated exposure of the conducting polymer sensors to controlled concentrations of CO_2 was carried out using the Injection Flow Analysis Equipment (Chapter 3). For the purpose of these experiments the vessels containing the solutions of target analytes were by–passed in order to expose the sensors directly to the compressed gas source. Both the target gas and those employed for the dilution of the sample were supplied by BOC Special Gases Ltd. The cylinder of compressed target gas was confirmed by the supplier to contain 500 ± 5 ppm of CO_2 mixed with zero grade air. The dilution cylinders were also confirmed by the supplier to contain zero grade air with less than 1 ppm CO_2. By directly mixing these sources the sensors could be exposed to a range of CO_2 concentrations between 0 and 500 ppm. The humidity of the sample and

temperature of the sensors were also regulated. Examples of the type of results obtained from this experimental set–up are shown in Figure 5.1.
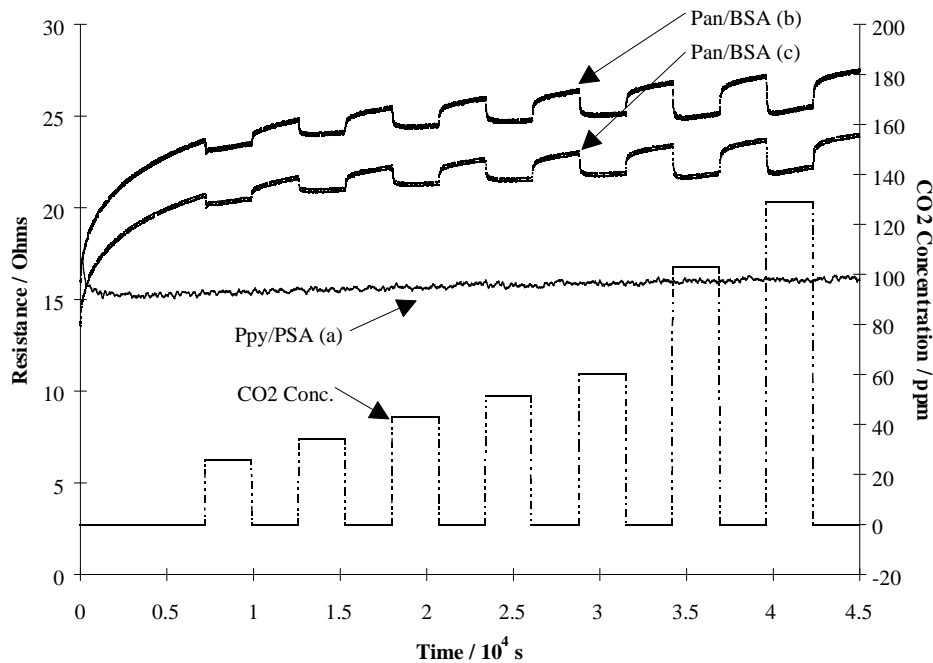
Figure 5.1 An example chart showing the form of the raw data as collected from the Injection Flow Analysis equipment. This graph shows two of the modified Pan/BSA sensors (b and c) and the example Ppy sensor in terms of their resistance versus the sampling time at 25 °C and 1238 ppm of water. The CO_2 concentration to which the sensors are exposed is also shown.

The sensors employed in the CO_2 testing comprised six of the modified Pan/BSA sensors, two Pan/PSA/H₂O sensors and a nominal Ppy/PSA/H₂O sensor. As expected, the Ppy sensor demonstrated negligible response to the range of CO_2 included in these experiments and has therefore been omitted from the data analysis and modelling (see Figure 5.1). Two of the modified sensors were found to have drifted off their resistance scales during testing and were also omitted from the modelling process. However, the remaining sensors still furnish us with a statistically valid array of four modified and two unmodified Pan sensors.

5.3 Physiochemical Model of the Response of Polymers to CO_2

The ionic interaction mechanisms between the polymer films, the water contained

within the polymer and the CO_2, and hence the rationale behind the development of the

CO_2 sensors has been postulated by Bartlett and Gardner [5.9]. We can now attempt to

develop a physiochemical model to describe the interaction of the CO_2 with the

polymer films. If we assume that within the films the following equilibrium is set–up.

$$CO_2(film) + H_2O \overset{K_A}{\Leftrightarrow} HCO_3^- + H^+ \tag{5.1}$$

where $CO_2(film)$ is the concentration of CO_2 that has been partitioned to the inside of

the polymer and is therefore related to the external gas concentration, $CO_2(gas)$,

through the relationship[1],

$$\left[CO_2(film)\right] = K_P\left[CO_2(gas)\right] \tag{5.2}$$

where K_P is the partition coefficient. K_A is the binding constant given by the expression,

$$K_A = \frac{\left[HCO_3^-\right]\left[H^+\right]}{\left[CO_2(film)\right]\left[H_2O\right]} \tag{5.3}$$

We can now assume that the film contains some concentration of HCO_3^- and H^+ prior

to the exposure of CO_2 due to the doping of the membrane. This ionic concentration

---

[1] Square brackets have been employed in these formulae to indicate the concentration of a substance.

accounts for the baseline characteristics of the sensors. A change in the CO_2 concentration ($\Delta[CO_2(gas)]$) will therefore modify the amount of HCO_3^- and H^+ present in the polymer. The change in the concentration of the two ions (ΔC_{ion}) is identical for the two cases due to the stoichiometry of the polymer. Equation 5.3 can now be written,

$$K_A = \frac{\left([HCO_3^-] + \Delta C_{ion}\right)\left([H^+] + \Delta C_{ion}\right)}{K_P\left(\Delta[CO_2(gas)]\right)[H_2O]}$$

(5.4)

Equation 5.4 can be re–arranged in terms of the change in the concentration of CO_2,

$$\Delta[CO_2(gas)] = \frac{\left(\Delta C_{ion}^2 + \Delta C_{ion}\left([HCO_3^-] + [H^+]\right)\right) + [HCO_3^-][H^+]}{K_P K_A [H_2O]}$$

(5.5)

This equation can be rewritten as the quadratic equation,

$$\Delta[CO_2(gas)] = a\Delta C_{ion}^2 + b\Delta C_{ion} + c$$

(5.6)

where the parameters a, b and c are given by Equations 5.7, 5.8 and 5.9, respectively.

$$a = \frac{1}{K_A K_P [H_2O]}$$

(5.7)

$$b = \frac{\left[HCO_3^-\right] + \left[H^+\right]}{K_A K_P \left[H_2O\right]} \tag{5.8}$$

$$c = \frac{\left[HCO_3^-\right] \times \left[H^+\right]}{K_A K_P \left[H_2O\right]} \tag{5.9}$$

We know that the protonation of Pan affects its conductivity (G) [5.10], therefore, for small changes, we can assume that,

$$\Delta C_{ion} \propto \frac{\Delta G}{G} \tag{5.10}$$

Therefore,

$$\Delta C_{ion} \approx \frac{\gamma \Delta G}{G} \tag{5.11}$$

where $\Delta G/G_i$ is the fractional change in conductance of the sensors and γ is a constant. Therefore, in this basic ionic model the concentration of CO₂ has a quadratic relationship to the fractional response of the sensors,

$$\Delta\left[CO_2\left(gas\right)\right] = a\left(\frac{\gamma \Delta G}{G_i}\right)^2 + b\left(\frac{\gamma \Delta G}{G_i}\right) + c \tag{5.12}$$

These basic assumptions formed the theoretical rationale for the development of the modified CO_2 sensors which have their properties tailored to take advantage of the acid–base interactions occurring within the polymers.

We can now compare the model described by Equation 5.12 with the results gained by exposing the sensors to concentrations of CO_2 at a constant absolute humidity (1164 ppm) and temperature (25 °C). Figure 5.2 shows the typical response of both modified and unmodified sensors to an exposure to CO_2. The values obtained for the model parameters for these fits are shown in Table 5.1.
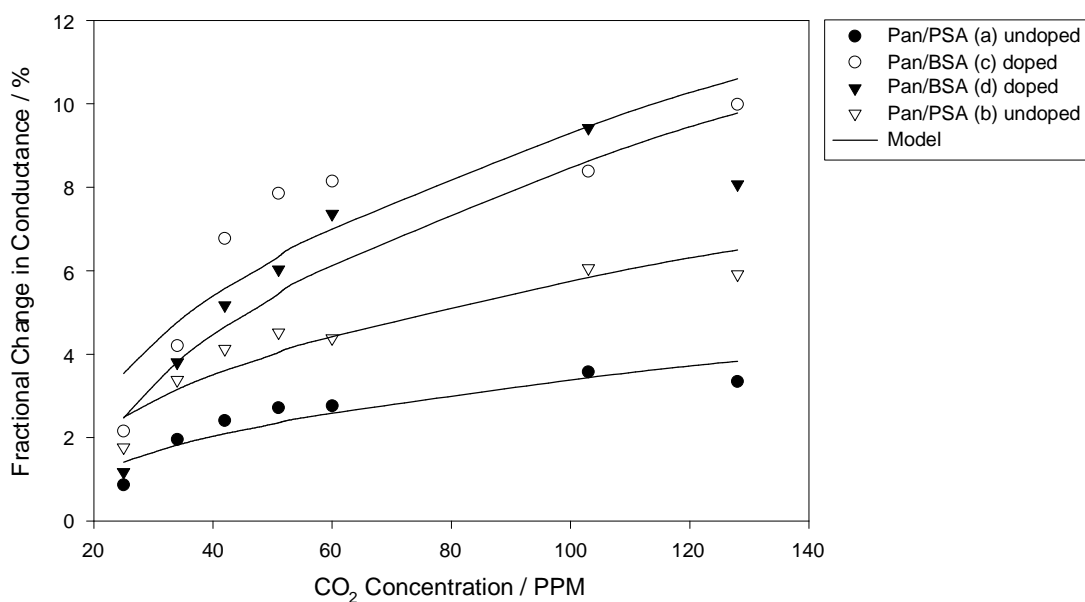
Figure 5.2 A graph showing the typical effect of CO_2 on the response of both modied and unmodified Pan sensors. The modified sensors have the suffix PSA and the unmodified have the suffix BSA. A theoretical model based on the ionic interaction between the polymer, water and the CO_2 is also shown.

Table 5.1 A table showing the model parameters a and b obtained from a non–linear regression fit between experimental data obtained at an absolute humidity of 1164 ppm and temperature of 25 °C and the physiochemical model described by Equation 5.12. The correlation coefficient between the experimental results and the model is also shown (*c* set to 20 ppm).

Sensor	a / ppm^{-1}	b	Correlation Coefficient
Pan/BSA (a)	2.13	-1.47	0.9332
Pan/BSA (b)	10.20	-10.90	0.9135
Pan/BSA (c)	1.24	-2.99	0.8949
Pan/BSA (d)	1.23	-1.03	0.9176
Pan/PSA (a)	1.82	-2.10	0.9654
Pan/PSA (b)	3.64	-7.05	0.9429

The value of the parameter *c* has been restricted to 20 ppm in all cases in order to achieve a reasonable fit to the experimental data. There are a number of points that are interesting from this analysis. Firstly, in all cases the response of the modified Pan/BSA sensors to the CO_2 was larger than the unmodified Pan/PSA. This would seem to indicate that the modification process employed on these sensors was increasing their sensitivity (in some cases the response of the modified sensor was three times greater than the unmodified). However, it is also important to note the poor fit between the model and the data, particularly at high concentrations or high responses. Although the correlation coefficient is typically between 0.8949 and 0.9654 the limited number of data points and the deviation of the data from the model at high concentrations make the model seem imprecise. The fragility of the model is compounded by the values obtained for the model parameter, *b*. For every sensor the value of *b* was found to be negative. However, the relationship between this parameter and the physical properties of the polymer, related by Equation 5.8, cannot be negative.

This flaw in the model can only be explained by assuming that there is a secondary mechanism occurring within the polymer which is dominating the sensor response.

This secondary mechanism can be confirmed by exploring the effect of humidity on the response of the sensors to a CO_2 concentration at a constant temperature (Figure 5.3). From the basic model it can be seen that an increase in the water concentration within the polymer, [H_2O], results in a reduction of the parameters a, b and c (Equations 5.7, 5.8 and 5.9). The magnitude of the fractional change in conductance due to exposure to a specific CO_2 concentration must therefore be greater at higher water concentrations (Equation 5.12). We would therefore expect an increase in the humidity of a testing sequence to result in an increase in the magnitude of the sensor's response to a CO_2 concentration. Figure 5.3 clearly shows that this trend is not observed.

We can therefore conclude that a different chemical mechanism is dominating the response of the polymers to CO_2. There is a range of possible interactions that could be affecting the polymer response. These include the affects of swelling due to the CO_2 exposure on both the electron mobility or the water content within the film, or the effects of CO_2 on the work function of the polymer. Further work is therefore required in order to develop a satisfactory model based on the chemistry of the interaction between the CO_2 and the polymers that is consistent with the experimental data. At this stage we will employ an empirical model to yield an enhanced correlation between the experimental data and the model.
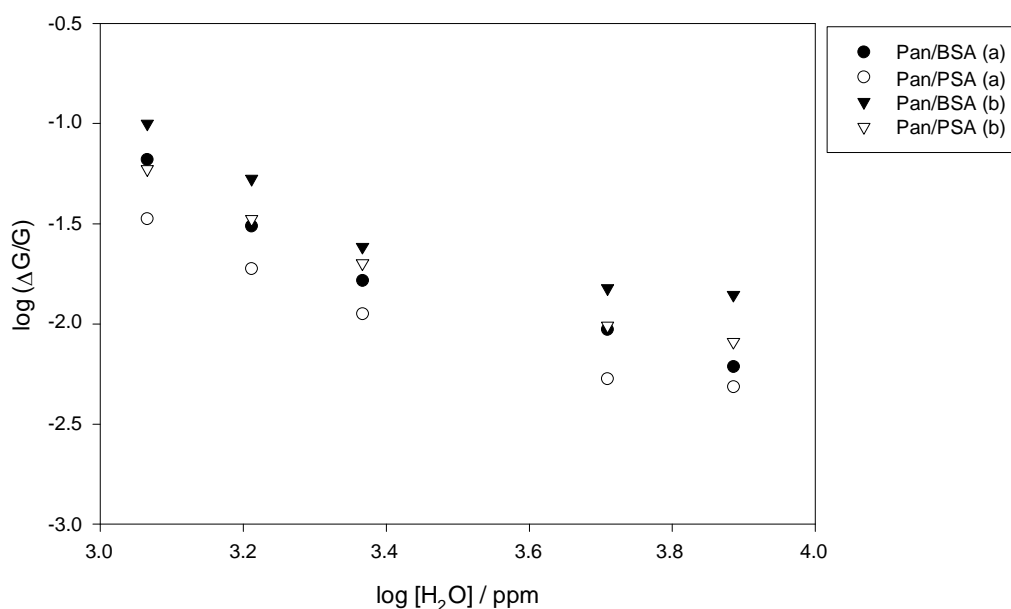
Figure 5.3 A graph showing the effect of absolute humidity on the fractional response of the sensors at a constant CO_2 exposure concentration (128 ppm) and temperature (25 °C). Two modified (Pan/BSA) and two unmodified sensors (Pan/PSA) are shown.

5.4 Empirical Model of the effects of CO_2

The response of the polymer sensors to CO_2 can be accurately modelled using expressions based on a Langmuir isotherm similar to that employed in Chapters 3 and 4. However, in this case the Langmuir equations are used as purely empirical relationships and are not based on any theory of the interactions occurring within the film. A basic Langmuir expression would only predict the absence of a response from the sensors when there was no CO_2 present in their environment. As can be seen in Figure 5.4, the polymer's response to CO_2 appears to be buffered resulting in a negligible response from the sensors at a range of low concentrations. In order to model this effect the basic Langmuir equation has to be modified, giving the expression,

_____

$$\frac{\Delta G}{G_i} = \frac{S_{CO2} K_{CO2} \left([CO_2] - \alpha \right)}{1 + K_{CO2} \left([CO_2] - \alpha \right)}$$

(5.13)

where S_{CO2} is the magnitude of the curve and is therefore related to the sensitivity, K_{CO2} is the curvature of the response and α is the buffer concentration required before the sensors begin to respond. The values obtained for each of the model parameters at an absolute humidity of 1164 ppm and temperature of 25 °C are shown in Table 5.2, with typical responses shown in Figure 5.4. Comparison of the correlation coefficients obtained for the empirical and physiochemical expressions demonstrates that a definite improvement in the accuracy of the model has been achieved.

Table 5.2 A table showing the model parameters S_{CO2}, K_{CO2}, and α obtained from a non–linear regression fit between experimental data obtained at an absolute humidity of 1164 ppm and temperature of 25 °C and the empirical model described by Equation 5.13. The correlation coefficient between the experimental results and the model is also shown.

Sensor	S_{CO2}	K_{CO2} / 10^{-2} ppm^{-1}	α / ppm	Correlation Coefficient
Pan/BSA (a)	7.91	5.67	22.94	0.9967
Pan/BSA (b)	10.84	7.17	21.89	0.9913
Pan/BSA (c)	10.54	5.26	22.79	0.9758
Pan/BSA (d)	9.71	3.69	19.34	0.9805
Pan/PSA (a)	3.89	7.56	21.14	0.9916
Pan/PSA (b)	6.96	5.63	18.61	0.9916
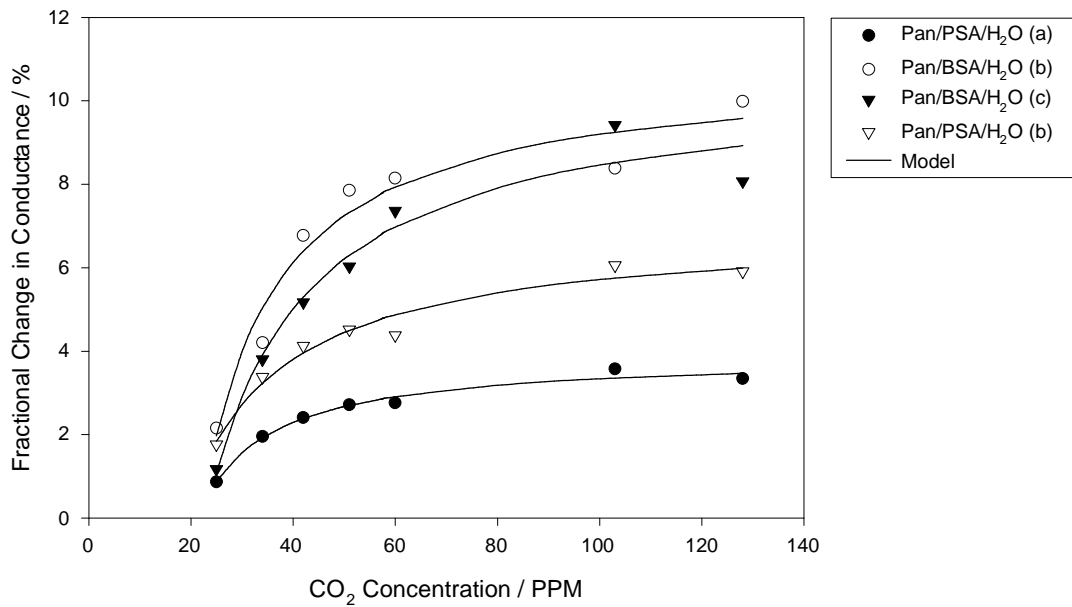
Figure 5.4 A graph showing the typical effect of CO_2 on the response of both modied and unmodified Pan sensors at an absolute humidity of 1164 ppm and temperature of 25 °C. The modified sensors have the suffix PSA and the unmodified have the suffix BSA. An empirical model of the CO_2 response is also shown.

5.5 Effects of Humidity and Temperature on Polymer Sensors

An extension of the basic empirical model to include the effects of humidity and temperature on the polymer's response to CO_2 will now be postulated. The effect of water on the polymers was predicted by the chemical model to enhance the response of the sensors (i.e.: an increase in the humidity would result in an increase in the sensor's response). This was inconsistent with the results obtained from the sensors where the fractional response of the polymers reduced significantly as the humidity of the experiments were increased (Figure 5.3). The extension of the empirical model to include this effect was completed by modelling the response of the sensors using Equation 5.13 at a range of humidities. Expressions describing the effect of the water concentration on each of the model parameters can then be developed. These

expressions would themselves be empirical relationships between each of the parameters and the water. The expressions employed for each of the parameters are shown in Equations 5.14 to 5.16 with the values for each of the humidity parameters shown in Tables 5.3 to 5.5.

$$S = \frac{\beta_S}{[H_2O]} - \chi_S \tag{5.14}$$

$$K = \frac{\beta_K}{[H_2O]} + \chi_K \tag{5.15}$$

$$\alpha = \beta_\alpha \ln[H_2O] + \chi_\alpha \tag{5.16}$$

Table 5.3 The values of parameters employed in Equation 5.14 in order to model the effect of humidity on the parameter S in the empirical model (Equation 5.13).

Sensor	$\beta_S / 10^3$	$\chi_S / 10^{-1}$
Pan/BSA (a)	8.33	4.56
Pan/BSA (b)	11.14	5.43
Pan/BSA (c)	10.37	6.32
Pan/BSA (d)	10.89	4.95
Pan/PSA (a)	6.78	3.32
Pan/PSA (b)	8.24	2.75

Table 5.4 The values of parameters employed in Equation 5.15 in order to model the effect of humidity on the parameter K in the empirical model (Equation 5.13).

_____

Sensor	β_K	χ_K / 10^{-3} ppm^{-1}
Pan/BSA (a)	55.89	8.94
Pan/BSA (b)	65.66	12.41
Pan/BSA (c)	62.79	10.32
Pan/BSA (d)	71.97	9.53
Pan/PSA (a)	76.90	4.49
Pan/PSA (b)	46.92	9.00

Table 5.5 The values of parameters employed in Equation 5.16 in order to model the effect of humidity on the parameter α in the empirical model (Equation 5.13).

Sensor	β_α	χ_α / 10^2 ppm
Pan/BSA (a)	-31.96	2.44
Pan/BSA (b)	-26.23	2.04
Pan/BSA (c)	-33.47	2.74
Pan/BSA (d)	-28.52	1.94
Pan/PSA (a)	-66.82	4.88
Pan/PSA (b)	-59.78	4.32

We can now explore the effects of temperature on the response of the sensors. In this model the humidity is restricted to 1164 ppm and the effect of temperature on the parameter values in the empirical model (Equation 5.13) is explored. Empirical models of the effect of temperature on the parameters S and K are shown in Equations 5.17 and 5.18. The parameter α in the empirical model does not demonstrate a consistent trend within the temperature range studied. Within experimental error we can say that this parameter does not change within this range.
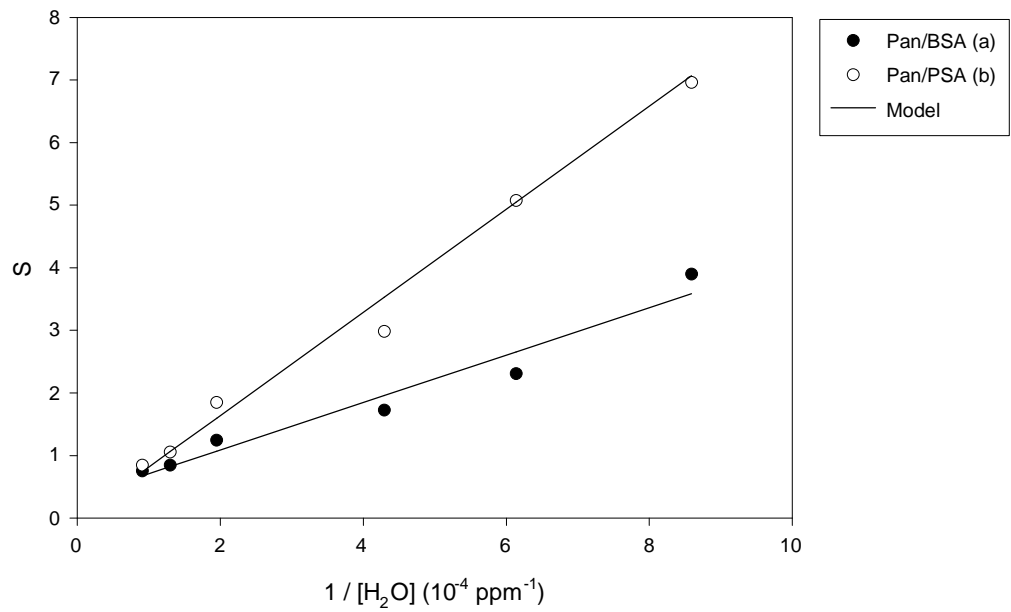
Figure 5.5 A graph showing the typical effect of absolute humidity on the value of parameter *S* employed in the empirical model (Equation 5.13) at a constant temperature of 25 °C. One modified and one unmodified sensor are shown with a model of this effect is also displayed.
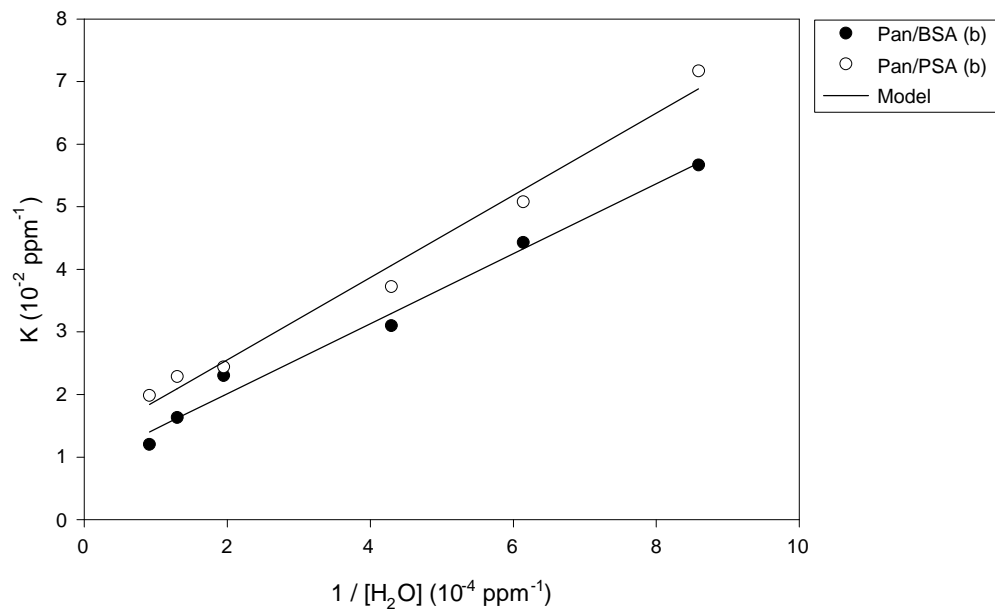
Figure 5.6 A graph showing the typical effect of absolute humidity on the value of parameter *K* employed in the empirical model (Equation 5.13) at a constant temperature of 25 °C. One modified and one unmodified sensor are shown with a model of this effect is also displayed.
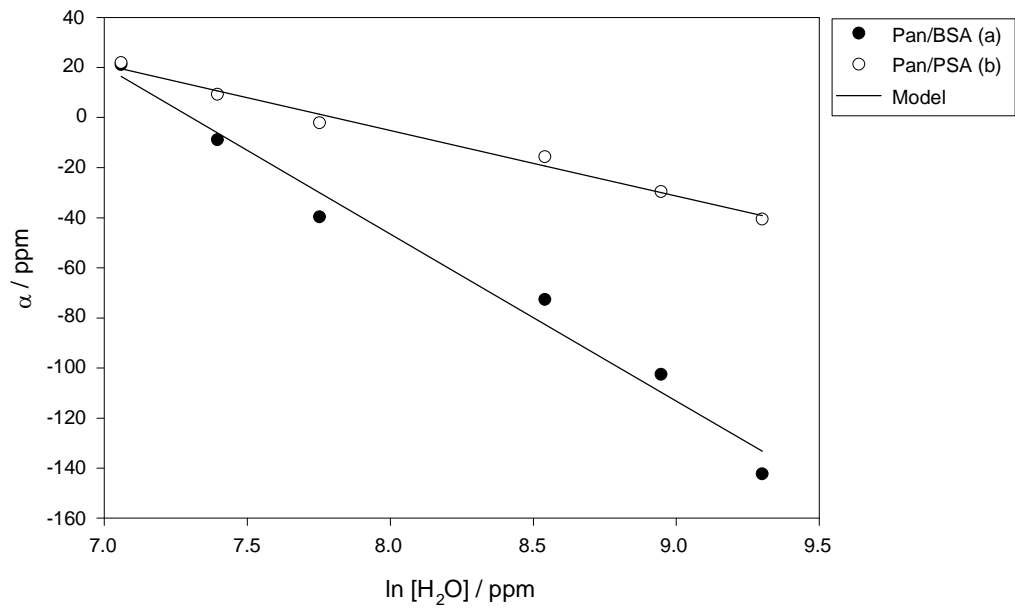
Figure 5.7 A graph showing the typical effect of absolute humidity on the value of parameter α employed in the empirical model (Equation 5.13) at a constant temperature of 25 °C. One modified and one unmodified sensor are shown with a model of the effect also displayed.

Tables 5.6 and 5.7 show the values of the parameters obtained in this empirical temperature model for Equations 5.17 and 5.18. Figures 5.8 to 5.10 show the effect of temperature on the empirical model parameters.

$$S(T) = \beta_S T^2 + \chi_S T + S_0 \qquad (5.17)$$

$$K(T) = \beta_K T + K_0 \qquad (5.18)$$

Table 5.6 A table showing the value of the parameters employed in Equation 5.17 demonstrating the effect of temperature on the value of S in the response model (Equation 5.13).

Sensor	β_S / 10^{-2} K^{-2}	χ_S / K^{-1}	S_0 / 10^3
Pan/BSA (a)	1.643	-10.44	1.659
Pan/BSA (b)	2.895	-18.35	2.907
Pan/BSA (c)	2.894	-18.31	2.896
Pan/BSA (d)	2.267	-14.38	2.281
Pan/PSA (a)	0.762	-4.83	0.765
Pan/PSA (b)	1.474	-9.37	1.491

Table 5.7 A table showing the value of the parameters employed in Equation 5.17 demonstrating the effect of temperature on the value of K in the response model (Equation 5.13).

Sensor	β_K / 10^{-3} $ppm^{-1}K^{-1}$	K_0 / ppm^{-1}
Pan/BSA (a)	8.332	-2.430
Pan/BSA (b)	7.675	-2.234
Pan/BSA (c)	9.190	-2.696
Pan/BSA (d)	6.244	-1.812
Pan/PSA (a)	0.271	-8.046
Pan/PSA (a)	0.213	-6.329

5.6 Conclusion

In this chapter we have examined the effects of CO_2 on Ppy, Pan and a modified form

of Pan sensors. The Ppy sensors showed no response to CO_2 and were therefore

omitted from the modelling of the effects of the gas. Both the modified and unmodified

Pan sensors demonstrated large fractional responses (up to 10%) at low concentrations
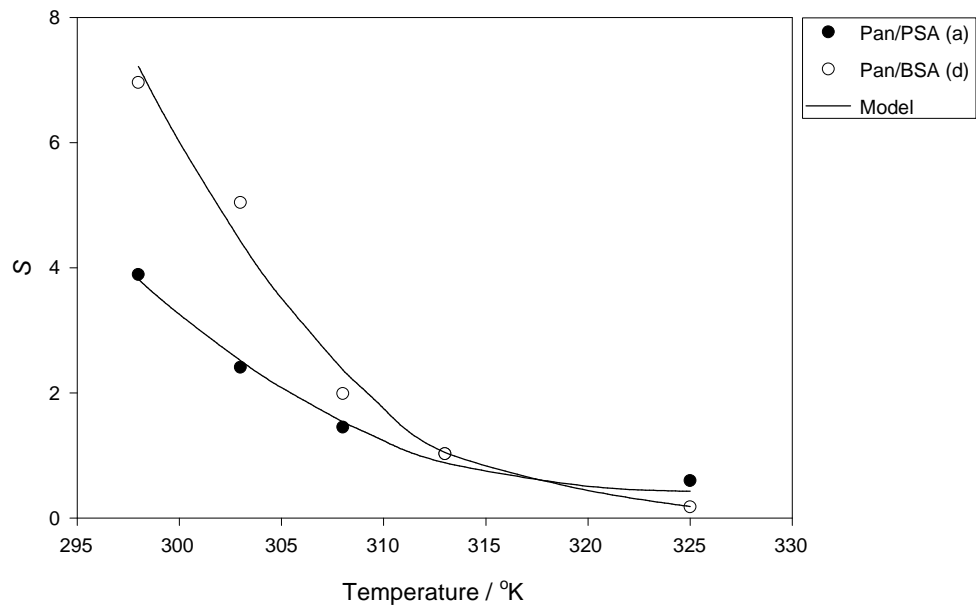
Figure 5.8 A graph showing the typical effect of temperature on the parameter *S* from the empirical model (Equation 5.13) at a constant absolute humidity of 1164 ppm. Examples of both modified and unmodified sensors are shown with an empirical model of the data.
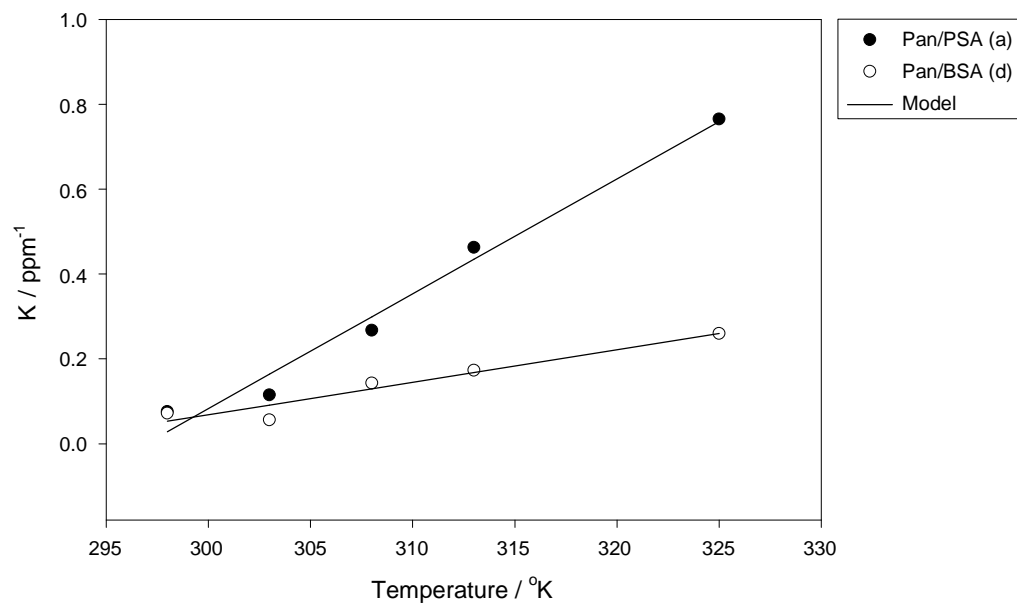
Figure 5.9 A graph showing the typical effect of temperature on the parameter *K* from the empirical model (Equation 5.13) at a constant absolute humidity of 1164 ppm. Examples of both modified and unmodified sensors are shown with an empirical model of the data.
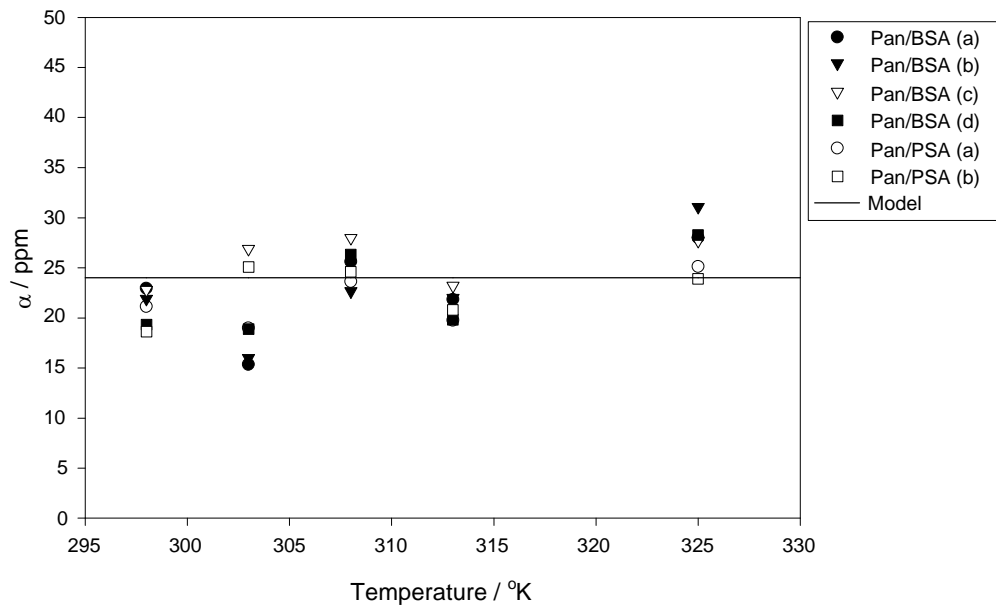
Figure 5.10 A graph showing the typical effect of temperature on the parameter α from the empirical model (Equation 5.13) at a constant absolute humidity of 1164 ppm. No clear trend is demonstrated within the temperature range examined. Both modified and unmodified sensors are shown.

of CO_2. The modified sensors were generally more sensitive than the unmodified with responses as much as 3 times greater to similar concentrations. An initial model of the ionic interaction between the sensors and the CO_2 proved unsuccessful for two reasons. Firstly, the experimental data predicted values of parameters associated with properties of the polymer that were physically impossible. Secondly, the effect of humidity on the response of the polymers was inconsistent with the trend that was predicted by the model. Clearly, a different mechanism is dominating the response of the polymers. There are a number of other ways in which the CO_2 can react with the polymers to produce this second reaction mechanism. These alternatives could include swelling within the polymer or modulation of the polymer's work function. Further work is required in order to investigate these effects fully.

_____

An empirical model has therefore been developed which gives a more accurate fit than the chemical model to the experimental data. The empirical model has also been extended to include the effects of temperature and humidity on the response of both the modified and unmodified Pan sensors.

5.7 References

5.1   M. Holzinger, J. Maier and W. Sitte, Potentiometric detection of complex gases: Application to CO$_2$, *Solid State Ionics,* **94**, (1997), 217-225.

5.2   M. Gauthier and A. Chamberland, Solid–state detectors for the potentiometric determination of gaseous oxides 1. Measurements in air, *Journal of the Electrochemical Society,* **124**, (1977), 1579-1583.

5.3   R. Cote, C. W. Bale and M. Gauthier, K$_2$CO$_3$ solid electrolyte as a CO$_2$ probe: Decomposition measurements of CaCO$_3$, *Journal of the Electrochemical Society,* **131**, (1984), 63-67.

5.4   T. Maruyama, S. Sasaki and Y. Saito, Potentiometric gas sensors for carbon dioxide using solid electrolytes, *Solid State Ionics,* **23**, (1987), 107-112.

5.5   N. Miura, S. Yao, Y. Shimizu, and N. Yamazoe, High–performance solid–electrolyte carbon dioxide sensor with a binary carbonate electrode, *Sensors and Actuators B,* **B9**, 165-170.

5.6   S. Yao, Y. Shimizu, N. Miura and N. Yamazoe, Solid–electrolyte carbon dioxide sensor using sodium ionic conductor and lithium carbonate based auxiliary phase, *Applied Physics A Materials Science and Processing,* **57**, 25-29.

_____

5.7   T. Ishihara, K. Kometani, M. Hashida and Y. Takita, Application of mixed

        oxide capacitor to the selective carbon dioxide sensor. I. Measurement of carbon

        dioxide sensing characteristics, *Journal of the Electrochemical Society,* **138**,

        (1991), 173-180.

5.8   Y. Shimizu, K. Komori and M. Egashira, Carbon dioxide sensor consisting of

        K$_2$CO$_3$ polyethylene glycol solution supported on porous ceramics 1:

        Measurements of carbon dioxide sensing characteristics, *Journal of the*

        Electrochemical Society, **136**, (1989), 2256-2260.

5.9   P. N. Bartlett and J. W. Gardner, *Personal communications,* 1998.

5.10   P. M. McManus, R. J. Cushman and S. C. Yang, Influence of oxidation and

        protonation on the electrical conductivity of polyaniline, *Journal of Physical*

        Chemistry, **91**, (1987), 744-747.

CHAPTER 6

Dynamic Modelling of Conducting Polymers

6.1 Introduction

This chapter describes the development of a transient model to characterise the response of Ppy and Pan films to a ethanol vapour at a variety of temperatures and humidities. Using such a model, information about the effects of electrode geometry on the response of conducting polymers can be determined. The work is an extension of earlier investigations into the effect of the electrode geometry in lead phthalocyanine gas sensors [6.1], and semiconducting oxide gas sensors [6.2, 6.3]. Models of both the transient and steady–state responses are developed and compared with results obtained by exposing the sensors to different concentrations of ethanol vapour in air at different humidities (0 to 12,000 ppm). As in Chapter 4, due to the similarity between the two types of polar molecule, the model assumes that there is competition for one set of available binding sites within the polymer film. The results are compared with the analytical expressions developed by Gardner and Bartlett [6.4] for six limiting cases describing the site occupancy and sorbate distribution within the polymer. From the data we are able to determine the dominating mechanism affecting the response of the polymers, such as whether it is diffusion–rate or reaction–rate limited. We can then determine the position of the polymers in the proposed diffusion–reaction case diagram [6.4].

To be consistent with the steady–state characterisation carried out in Chapter 4, the types of polymer chosen for the transient analysis represented each of the two major classes of monomer, pyrrole and aniline, with two types of counter-ion representing a five unit chain (pentane sulfonic acid) and a ten unit chain (decane sulfonic acid). This type of acid was chosen due to its hydrophobic properties and also because it has previously produced polymers with good long term stability [6.5].

6.2 Diffusion and Binding in Conducting Polymers

A model has been developed elsewhere in which it is assumed that a species, A, diffuses into a homogeneous thin film of thickness, L, and undergoes a Langmuir adsorption [6.6]. In other words, we assume that the film contains a uniform distribution, N, of immobile sites, S, with which the species can reversibly react. The reaction being described by the Langmuir adsorption isotherm, that is

$$A + \langle S \rangle \underset{k_b}{\overset{k_f}{\Longleftrightarrow}} \langle A \rangle \tag{6.1}$$

where k_f and k_b are the forward and backward reaction rate constants, respectively. Exploiting the geometry of a planar film allows the use of a one dimensional model in which the sorbate concentration, a, and site occupancy, θ, profiles are only a function of distance, x, into the film and time t. We can therefore write a diffusion reaction equation for the species A,

$$D \frac{\partial^2 a}{\partial x^2} - k_f a (1 - \theta) N + k_b \theta N = \frac{\partial a}{\partial t} \tag{6.2}$$

_____

Assuming that the species A is present in the external phase at a constant concentration, a_∞, then the boundary conditions for the adsorption transient are,

at $t = 0$: $\theta = 0$ and $0 \leq x \leq L$

$\forall$ $t > 0$: $\left.\dfrac{da}{dx}\right|_{x=0} = 0$ and $a = a_\infty$ at $x = L$

This assumes that the partition coefficient for the species A into the film is unity and that there is no kinetic barrier at the film surface to the passage of A into the film. It should be noted that the effect of the partition coefficient can be taken into account by replacing a_∞ by $K_a a_\infty$, where K_a is the partition coefficient. We also know from consideration of the kinetics of the reaction sites that,

$$N \frac{\partial \theta}{\partial t} = k_f a(1 - \theta)N - k_b \theta N \tag{6.3}$$

Combining equations 6.2 and 6.3 gives,

$$D \frac{\partial^2 a}{\partial x^2} - \frac{\partial a}{\partial t} = N \frac{\partial \theta}{\partial t} \tag{6.4}$$

The process described in Equation 6.4 can be rewritten in dimensionless form,

$$\frac{\partial^2 \gamma}{\partial \chi^2} - \frac{\partial \gamma}{\partial \tau} = \frac{\eta}{\lambda} \frac{\partial \theta}{\partial \tau}$$

(6.5)

where χ is the dimensionless distance parameter (x/L), L is the depth of the polymer, τ is the dimensionless time parameter (Dt/L^2), γ the normalised gas concentration (a/a_∞) and a_∞ is the external gas concentration. η and λ are dimensionless parameters given by KN and Ka_∞, respectively, and therefore depend on the material properties such as the binding constant K (κ_f / κ_b) and the density of sites N [6.7], see Figure 6.1. The corresponding boundary conditions for the adsorption transient become,

at $\tau = 0$: $\theta = 0$ and $\gamma = 0$, $0 \leq \chi \leq 1$

$\forall$ $\tau > 0$: $\left. \dfrac{d\gamma}{d\chi} \right|_{\chi=0} = 0$ and $\gamma = 1$ at $\chi = 1$
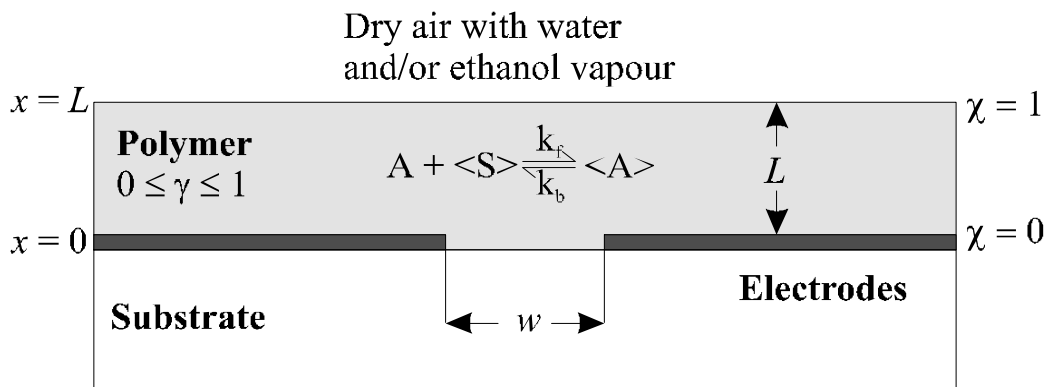
Figure 6.1 Schematic diagram of a polymer chemoresistor with model parameters defined.

We can also rewrite Equation 6.3 in terms of the dimensionless parameters,

$$\eta \frac{\partial \theta}{\partial \tau} = \kappa \lambda \gamma (1 - \theta) - \kappa \theta \qquad (6.6)$$

where κ describes the balance between the adsorption ($k_f N$) and diffusion (D/L^2) kinetics within the film and is given by,

$$\kappa = \frac{k_f N L^2}{D} \qquad (6.7)$$

Equations 6.5 and 6.6 are coupled non–linear partial differential equations and do not have an exact analytical solution. However it is possible to identify a number of limiting cases for which we can develop approximate analytical expressions for the site occupancy $\theta(\chi, \tau)$ profiles. Figure 6.2 shows the case diagram that contains the full solution space defined by κ, λ and η with the six limiting cases I to VI marked on it. Case I ($\lambda < 1$, $\eta < 1$, $\kappa > \eta$) describes a pure diffusion process where the diffusion rate is far slower than the reaction rate and there are few adsorption sites to modify the diffusion process. Case II ($\lambda < 1$, $\eta > 1$, $\kappa > 1$) is again a diffusion–limited case. However in this case there are a significant number of sites which slow the diffusion process (by a factor of ~ $1/\eta$ [6.8]). In Case III ($\lambda < 1$, $\kappa < 1$, $\kappa < \eta$) the reaction–rate is far slower than the diffusion–rate and therefore the process is reaction–rate limited. The reaction kinetics are in the linear (unsaturated) region of the isotherm, i.e.: most of
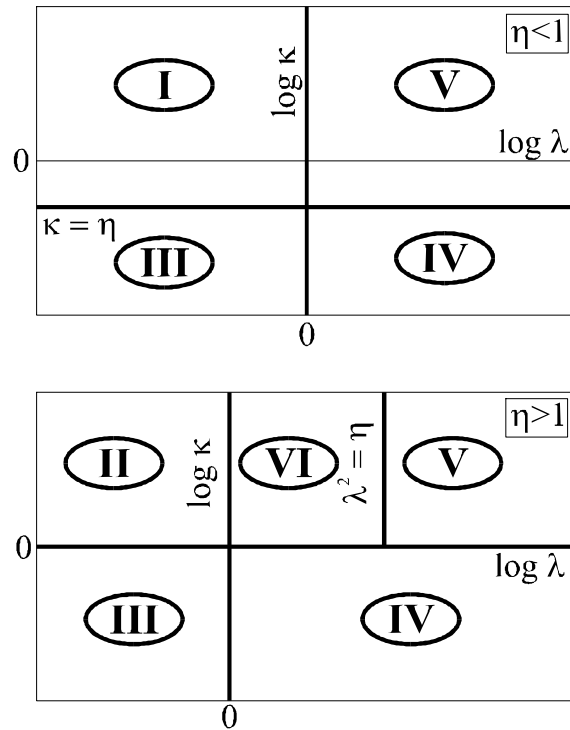
Figure 6.2 Case diagram showing solutions to the diffusion reaction problem: I – pure diffusion; II – slow diffusion; III – unsaturated (linear) reaction kinetics; IV – saturated reaction kinetics; V – saturated (non–linear) reaction kinetics; VI – mixed diffusion reaction process.

the sites within the polymer are unoccupied. Case IV ($\lambda > 1$, $\kappa < 1$, $\kappa < \eta$) is also a reaction–rate limited process. However, this case describes the saturated region of the isotherm i.e.: most of the sites within the polymer are occupied. Case V ($\lambda > 1$, $\lambda^2 > \eta$, $\kappa > 1$, $\kappa > \eta$) describes the saturated region of the isotherm where the kinetics are fast so that equilibrium is maintained between free and bound species. Finally, in Case VI ($\lambda > 1$, $\lambda^2 < \eta$, $\eta > 1$, $\kappa > 1$) neither diffusion nor reaction dominates the process and a moving boundary problem is encountered [6.9].

6.3 Device Conductance Model

The transient and steady-state conductance of polymeric devices can be fully described by combining the site occupancy profiles described in section 6.2, with the electric field distribution within the polymer. For a pair of semi-infinite thin electrodes with a separation of w and a length b (ie: $b \gg w$) the electric field, E, has been determined using Schwartz-Christoffel transformations [6.10] to be,

$$E(\chi, 0) = \frac{V}{L\pi} \Bigg/ \sqrt{\chi^2 + w^2 / 4L^2} \tag{6.8}$$

where V is the voltage applied across the electrodes. This equation assumes that there is a homogeneous medium in the semi-infinite region above the electrodes. The difference in the dielectric permittivities of the polymer, substrate or air/vapour will have an effect on the distribution of the displacement field lines. We believe the device's response is not very sensitive to this phenomenon because the device conductance is calculated by integrating the electric field along a line through the structure. The parametric form of Equation 6.8 has been verified experimentally by data reported by Bartlett *et al.* [6.11].

In this model we assume that the local conductivity of the polymeric film is given by,

$$\sigma(\chi, \tau) = \sigma_{00} \big[1 - S_h \theta_h - S_e \theta_e \big] \tag{6.9}$$

where S_e and S_h are the sensitivity to ethanol and water, respectively, and σ_{00} is the conductance of the device when neither water nor ethanol vapour are present.

The current passing through a device can therefore be calculated by integrating the product of the local conductivity, Equation 6.9, and the electric field, Equation 6.8, over a closed surface. Hence we can then write the fractional response of the device as,

$$\frac{G(\tau)-G_0}{G_0} = \frac{1}{1-S_h\theta_h} \times \left[S_h\Delta\theta_h - \frac{S_e\int_0^1 \theta_e(\chi,\tau)/\sqrt{\chi^2+w^2/4L^2}\,d\chi}{\ln\left[\frac{1+\sqrt{(1+w^2/4L^2)}}{w/2L}\right]} \right] \qquad (6.10)$$

Where G_0 is the steady–state baseline conductance of the device at a constant absolute humidity and $\Delta\theta_h$ is the change in the proportion of sites occupied by water when the ethanol vapour is introduced. Equation 6.9 is tailored specifically for the manner in which the polymers are tested in the injection flow analysis equipment (Chapter 3). This means that we have a set humidity in which the baseline conductance of the polymer is dependent on the fractional site occupancy of water. The introduction of ethanol vapour will then change this water site occupancy by a factor, $\Delta\theta_h$. The model therefore assumes that the water and ethanol vapour are absorbed by the same sites, i.e. a <u>competitive</u> single–site binding model. The proportion of sites occupied by water when no ethanol vapour is present, θ_h', can then be given by,

$$\theta_h' = \frac{K_h a_h}{1 + K_h a_h} \qquad (6.11)$$

and when ethanol is present the proportion occupied by water and ethanol are given by,

$$\theta_h'' = \frac{K_h a_h}{1 + K_h a_h + K_e a_e} \qquad\qquad \theta_e = \frac{K_e a_e}{1 + K_h a_h + K_e a_e} \tag{6.12}$$

The steady–state response (in terms of device conductance) is defined here in terms of the fractional site occupancy by

$$\frac{G(\tau = \infty) - G_0}{G_0} = \frac{S_h\left(\theta_h' - \theta_h''\right) - S_e \theta_e}{(1 - S_h \theta_h')} \tag{6.13}$$

The size of the steady–state response for homogeneous conducting polymer films with a uniform distribution of absorbent and sites therefore depends on the magnitude of the sensitivity terms but not on the device geometry. Equations 6.10 and 6.13 fully define the transient and steady–state response of the polymer sensors. The effect of the competitive binding model on the steady–state response of the polymers has been examined in Chapter 4. We can now investigate predictions made by these models and relate them to the properties of our polymer films

6.4 Physical Characteristics of Polymer Films

In order to investigate the dynamic properties of the polymers, we require a knowledge of various physical properties of the film. Firstly, we need to know the thickness of the polymers deposited across different electrode gaps. The effect of the polymers thickness, particularly in diffusion–rate limited cases, is significant. In order to confirm that the electrode geometry does not greatly effect the thickness of the polymer, surface profiles of the devices employed during testing were carried out using a Taylor–Hobson

form talysurf. The profiles for Pan and Ppy sensors are shown in Figures 6.3 and 6.4, respectively.

These results show that the thickness of the film does not vary significantly over the range of gap sizes used for each polymer. It is interesting to note that although the electrode separation does not seem to significantly modify the thickness of the films, each of the different types of polymer have been grown to different thickness. This can been attributed to the different growth solutions and possible differences in the number of potential cycles employed during the electrochemical deposition process (Chapter 2).
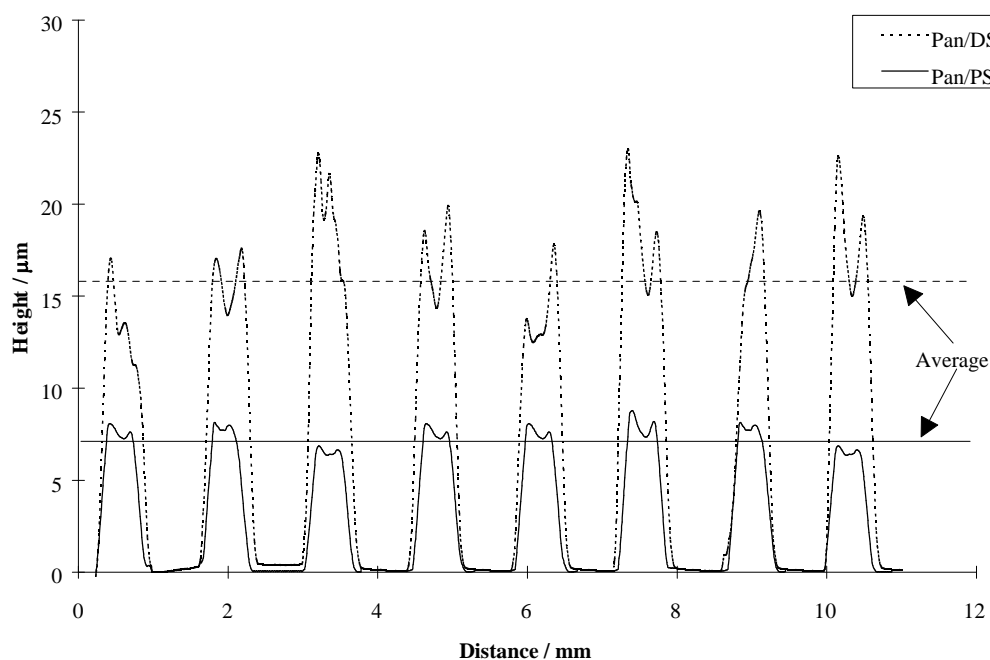
Figure 6.3 A talysurf profile of Pan/DSA/H_2O and Pan/PSA/H_2O sensors.
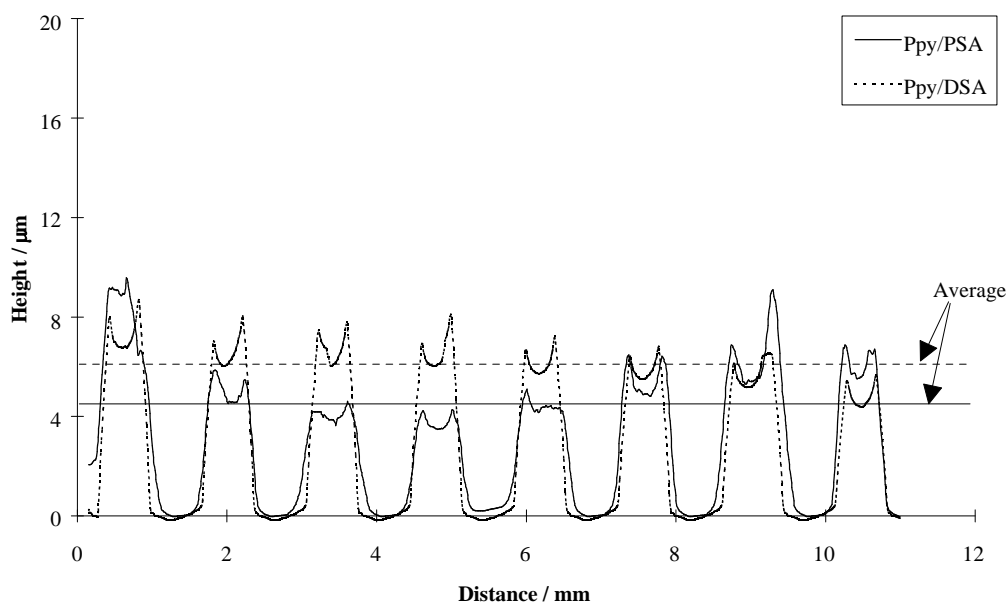
Figure 6.4 A talysurf profile of Ppy/DSA/H_2O and Ppy/PSA/H_2O sensors.

For accurate modelling of the effects of electrode gap separation it was also important to measure the gaps etched in the gold substrate. This was done using an optical microscope (MU-214B, Sociëte Genëvoise). The gap dimensions varied greatly between the devices with the smallest separation 11 μm and the largest 64 μm. Table 6.1 shows the gap dimensions for each of the devices employed. Although the gap dimensions do differ significantly from the nominal values (Chapter 2), each device did demonstrate a general increase in the electrode separation for each of the deposition areas.

Table 6.1 The electrode separations employed for each of the four polymer devices. The dimensions were measured using an optical microscope.

Gap	Pan/DSA/H_2O (μm)	Pan/PSA/H_2O (μm)	Ppy/DSA/H_2O (μm)	Ppy/PSA/H_2O (μm)

A	18	11	20	25
B	22	22	23	27
C	34	26	28	37
D	42	35	32	41
E	50	45	45	48
F	53	54	45	44
G	64	55	54	58

In order to confirm that the response we observe for the polymer films is not greatly affected by the capacitance of the device, we have also ascertained the RC time–constant of the membranes. The resistance and capacitance of the polymers were measured using a universal precision LCR bridge (Ranger 1000, Lloyd Instruments plc.) to an accuracy of ±0.1% with the values shown in Table 6.2. Although these values were measured in laboratory air and not under experimental conditions, the very small values of the time–constant (i.e. 0.8 to 3.6 μs) allow us to be confident that the dynamic response of the polymers will not be greatly effected by charging or discharging of the membrane.

Finally, in order to gain information about the microstructure of the polymers and how this may effect the diffusion–reaction model, scanning electron microscope pictures of each of the different types of polymer are shown in Figures 6.5 to 6.8. The morphologies of the Ppy sensors[1] (Figures 6.5 and 6.6) consist of a dense base structure consisting of close packed micro–spheres. Conversely, the composition of the Pan sensors (Figures 6.7 and 6.8) seems to consist of strands forming an almost coral structure. The Pan structure also seems to be a more porous membrane which may affect the diffusion process when compared to the Ppy membranes.

---

[1] Courtesy of Dr. N. Blair [6.5]

Table 6.2 The capacitance, resistance and associated time–constant for each of the polymer types and gap sizes employed.

Polymer	Gap	Resistance / Ω	Capacitance / nF	Time–constant / μs
Pan/DSA/H_2O	A	90.3	11.4	1.0
	B	118.0	9.0	1.0
	C	92.5	9.2	0.8
	D	113.3	12.1	1.3
	E	131.4	8.9	1.2
	F	117.8	2.4	0.3
	G	187.3	2.7	0.5
Pan/PSA/H_2O	A	3.1×10^3	0.500	1.5
	B	2.2×10^3	0.600	1.3
	C	1.9×10^3	0.700	1.3
	D	2.2×10^3	0.400	0.9
	E	3.0×10^3	0.400	1.2
	F	5.1×10^3	0.150	0.8
	G	4.9×10^3	0.100	0.5
Ppy/DSA/H_2O	A	102.7	9.1	0.9
	B	483.1	1.3	0.6
	C	780.38	1.8	1.4
	D	-	-	-
	E	-	-	-
	F	398.0	2.5	1.0
	G	221.3	4.8	1.1
Ppy/PSA/H_2O	A	8.1×10^3	0.450	3.6
	B	3.08×10^3	0.300	0.9
	C	1.8×10^3	0.500	0.9
	D	2.4×10^3	0.300	0.7
	E	6.3×10^3	0.100	0.6
	F	4.0×10^3	0.200	0.8
	G	5.2×10^3	0.450	2.3

_____
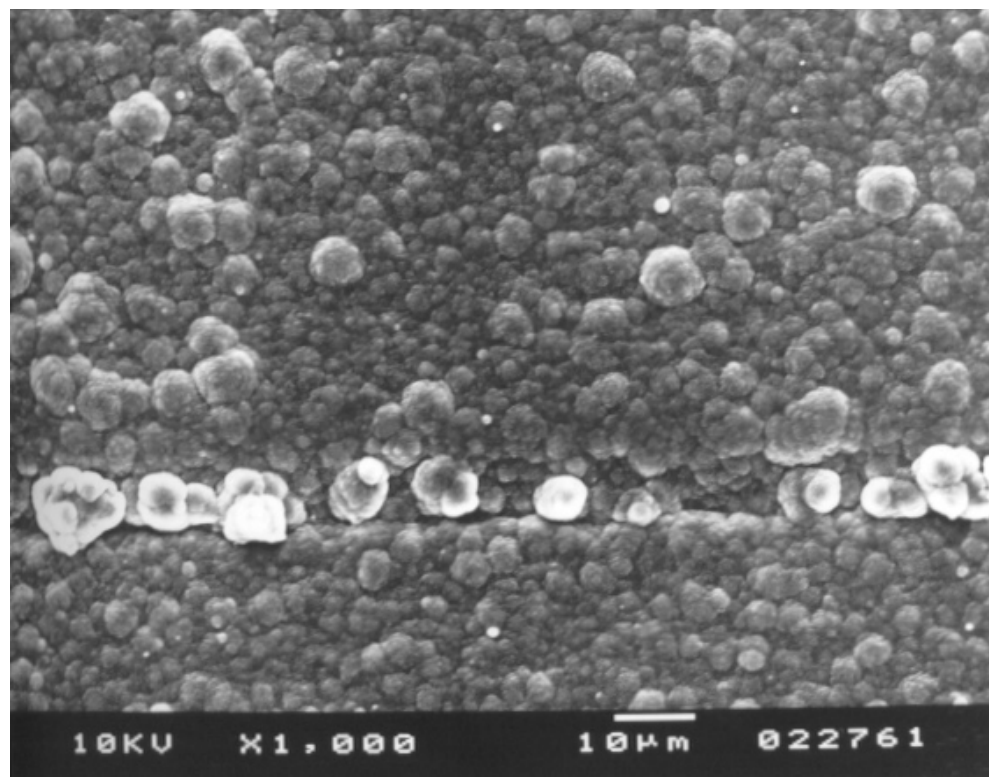
Figure 6.5 Scanning electron micrograph of Ppy/DSA/H_2O film. Shown at a magnification of 1000 times.
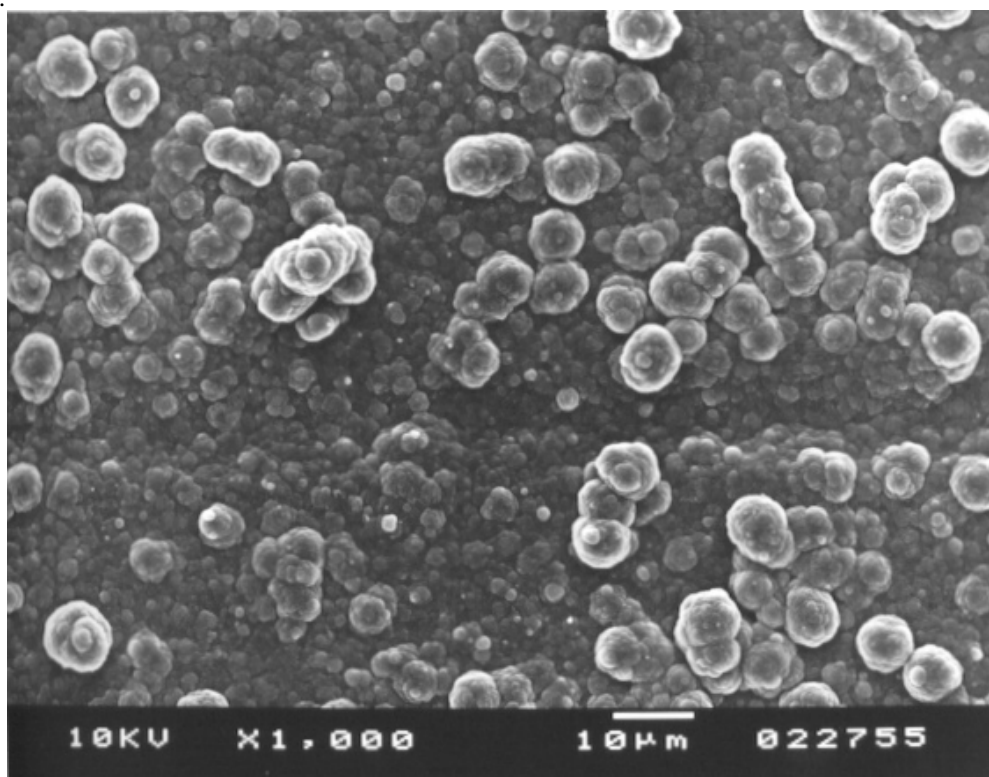
Figure 6.6 Scanning electron micrograph of Ppy/PSA/H_2O film. Shown at a magnification of 1000 times.
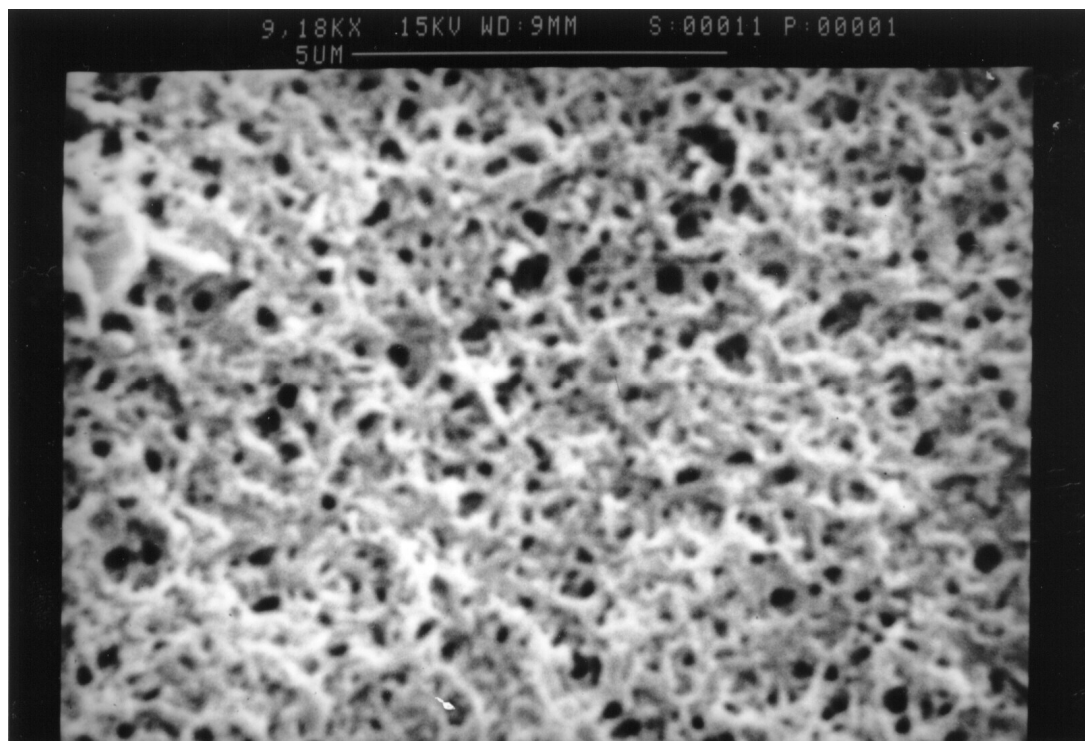
Figure 6.7 Scanning electron micrograph of Pan/DSA/H_2O film. Shown at a magnification of 9180 times.
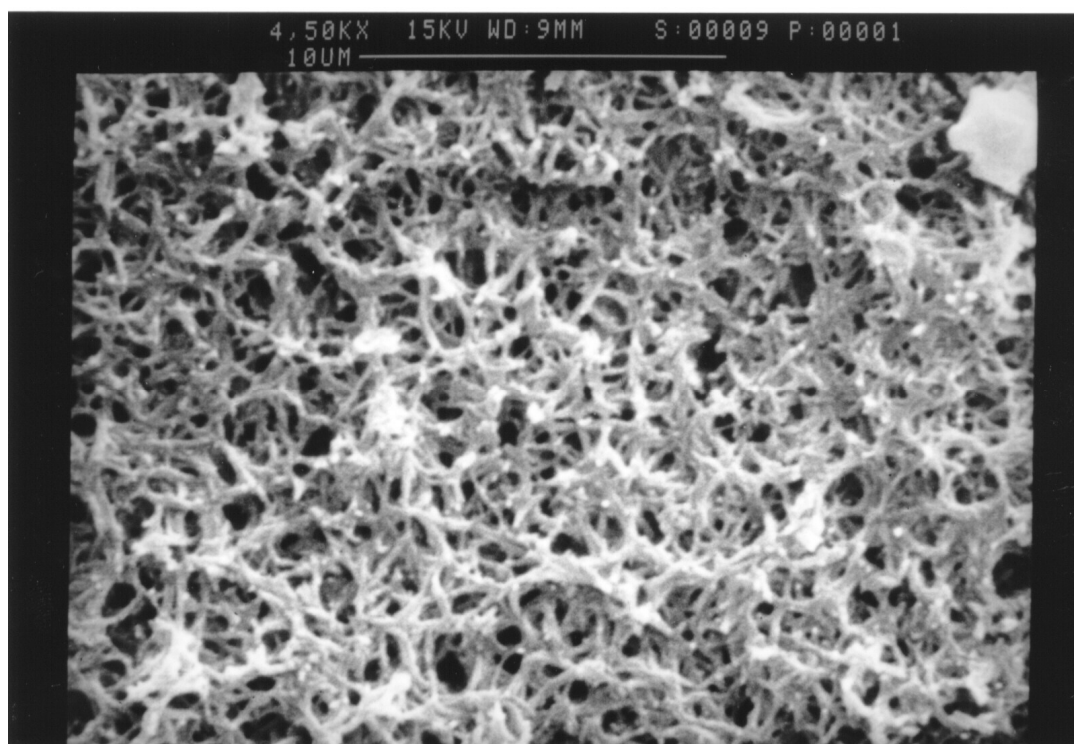
Figure 6.8 Scanning electron micrograph of Pan/PSA/H_2O film. Shown at a magnification of 9180 times.

6.5 Empirical Model of Transient Responses

In order to explore the effects of gap size, analyte concentration etc. on the transient responses of conducting polymer sensors, we first need to develop an empirical expression that can rapidly identify the time–constant characteristics of the sensors. The expressions employed to describe the Pan on and off transients are given in Equations 6.14 and 6.15 respectively, and are consistent with the kinetics of a pure reaction–rate limited case (Case III) [6.12]

$$G(t) - G_0 = \Delta G - \Delta G \exp\left(\frac{-t}{\tau_{on}}\right) \tag{6.14}$$

$$G(t) - G_0 = \Delta G \exp\left(\frac{-t}{\tau_{off}}\right) - \Delta G \tag{6.15}$$

where $G(t)$ is the conductance of the polymer at time t, G_0 is the baseline conductance of the polymer i.e.: in the absence of ethanol vapour, ΔG is the change in conductance of the sensor due to the ethanol concentration and τ_{on} and τ_{off} are the time–constants for the on and off responses, respectively. Figures 6.9 and 6.10 show examples of the on and off transients for Pan/DSA/H_2O. The empirical model is also shown on these diagrams. This demonstrates an excellent fit to the experimental data with the correlation coefficient for both the on and off transients greater than 0.99.
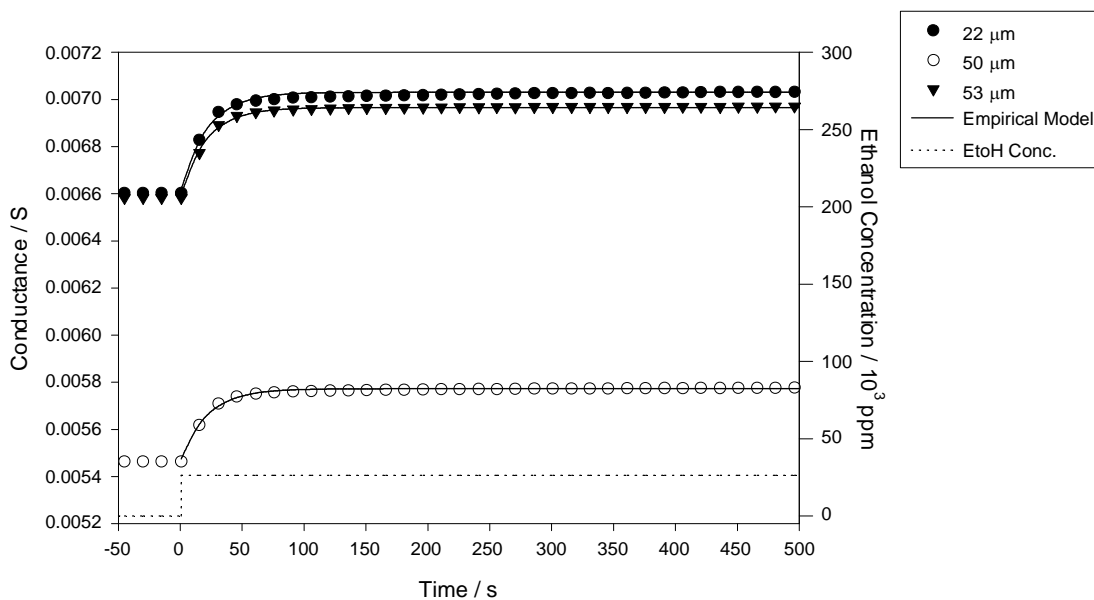
Figure 6.9 A diagram showing the on transient for Pan/DSA/H_2O when exposed to an ethanol concentration of 26336 ppm at a constant humidity of 2328 ppm and temperature of 35.3 ^{0}C. Three electrode separations 22, 50 and 53 μm are shown.

Figure 6.10 A diagram showing the off transient for Pan/DSA/H_2O when ethanol at a concentration of 26336 ppm is removed at a constant humidity of 2328 ppm and temperature of 35.3 ^{0}C. Three electrode separations 22, 50 and 53 μm are shown.

The empirical expressions employed to model the transients for the Pan sensors did not give satisfactory correlation for Ppy. For this type of polymers a <u>double–exponential</u> expression was used to model the generally longer time responses. The double–exponential expression is more consistent with the kinetics of a competitive binding model where the response would be limited by both ethanol adsorption and water desorption from the available reaction sites. Equations 6.16 and 6.17 were used for the two sets of on and off transients respectively,

$$G(t) - G_0 = \Delta G_1 \left(\exp\left(\frac{-t}{\tau_{on1}} \right) - 1 \right) + \Delta G_2 \left(\exp\left(\frac{-t}{\tau_{on2}} \right) - 1 \right) \qquad (6.16)$$

$$G(t) - G_0 = \Delta G_1 \left(1 - \exp\left(\frac{-t}{\tau_{off1}} \right) \right) + \Delta G_2 \left(1 - \exp\left(\frac{-t}{\tau_{off2}} \right) \right) \qquad (6.17)$$

These expressions divide the response of the Ppy sensors into two components: the first is an initial response due to the exposure of the ethanol vapour; and the second component is a long–term response either due to the ethanol vapour or due to drift within the polymer. The value of the time–constants for the second component of both the on and off transients (τ_{on2} and τ_{off2}) were very large, generally greater than 3000 seconds, and also seemed to be independent of the ethanol concentration. This second component may be due to the competition occurring within the polymer between the species reacting with reaction sites and the species that has to relinquish the reaction sites. It is also possible that the heterogeneity of the Ppy microstructure may produce a double–exponential expression. Figures 6.5 and 6.6 show that the structure of the Ppy

sensors consists of a micro–sphere configuration. This may produce two diffusion processes where the species has to diffuse into the bulk and then into the micro–spheres. Again this may contribute to a double–exponential expression in the modelling of the sensor response. Figures 6.11 and 6.12 show examples of the on and off transients for three gaps coated with Ppy/PSA/H_2O. The empirical model of the responses is also shown. Although the correlation between this model and the data is not as good as that demonstrated for the Pan sensors, a reasonable fit was still obtained with the correlation coefficient generally greater than 0.71. The symmetry of the on and off transients shown in Figures 6.9 to 6.12 can now be employed to determine some of the physical properties of these polymers. In Cases IV and V the boundary conditions assume that the polymers are reaction–rate limited and that saturation is reached ($\theta \approx 1$). This means that there is a larger concentration of the target vapour and only a few sites with which it can react. Therefore the sites fill quickly but upon desorption a large amount of the vapour has to leave before the sites are emptied. This means that the off transient for the exposure should take far longer than the on (i.e.: the on and off transients are asymmetric). Case VI also assumes that the sites become saturated. Although in this case neither the reaction or diffusion kinetics dominate the response we should still observe differences between the on and off transients. Figures 6.9 to 6.12 show that the transients observed for both Pan and Ppy are almost perfectly symmetric with typical on and off time–constants varying by less than 2%. We can therefore deduce that, at equilibrium most of the sites in the polymers tested are unoccupied ($\lambda < 1$) and we can conclude that we are not working in Cases IV, V or VI.
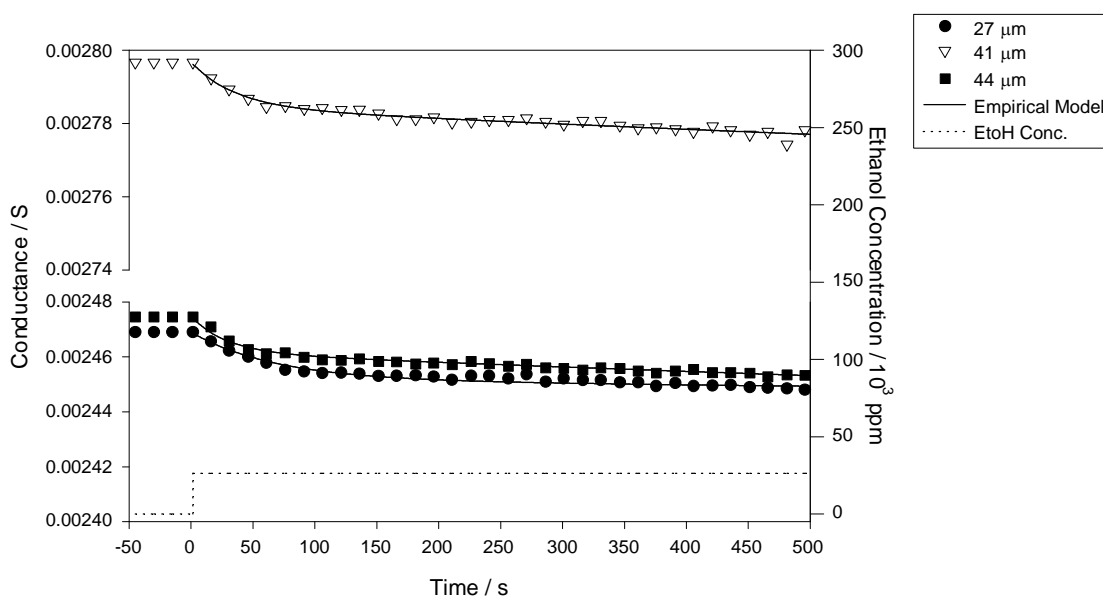
Figure 6.11 A diagram showing the on transient for Ppy/PSA/H_2O when exposed to ethanol at a concentration of 26336 ppm at a constant humidity of 2328 ppm and temperature of 35.8 ^{0}C. Three electrode separations 27, 41 and 44 μm are shown.

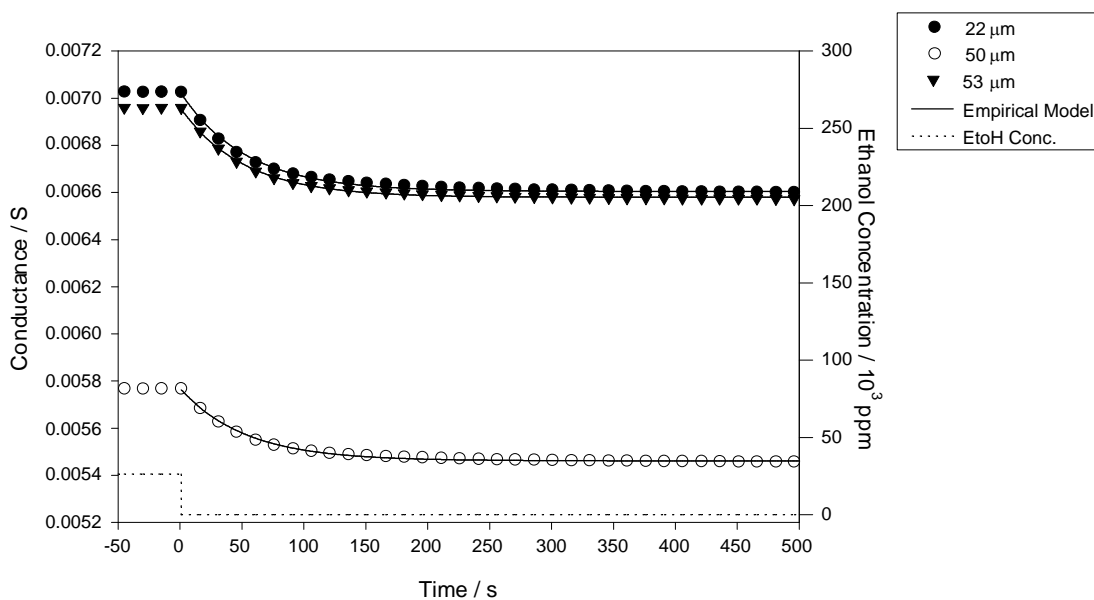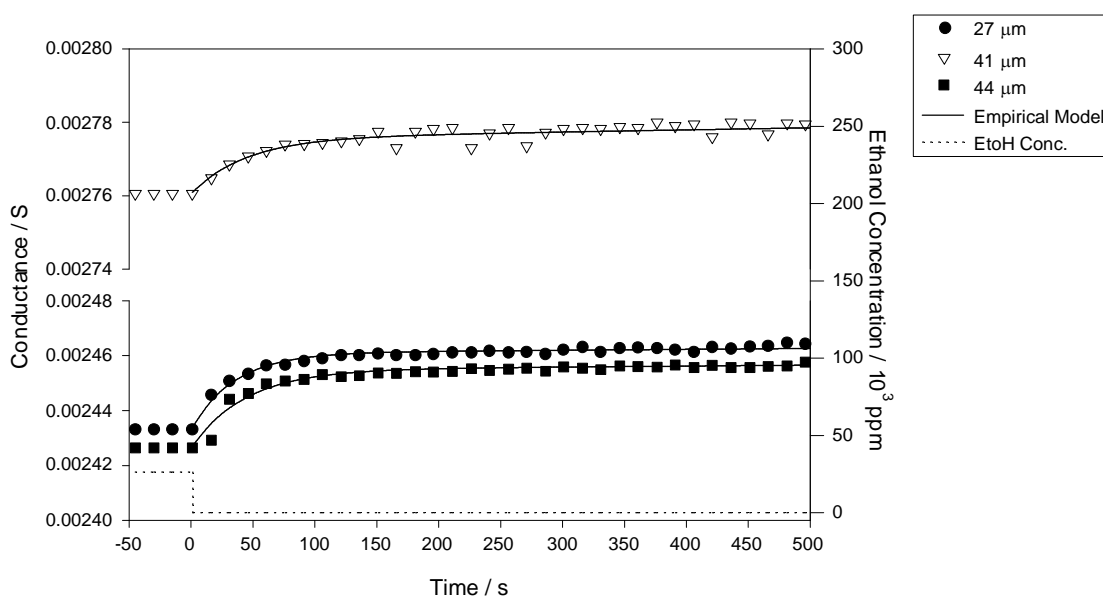**Figure 6.12** A diagram showing the on transient for Ppy/PSA/H_2O when ethanol at a concentration of 26336 ppm is removed at a constant humidity of 2328 ppm and temperature of 35.8 ^{0}C. Three electrode separations 27, 41 and 44 μm are shown.

_____

In order to distinguish between the remaining cases we need to determine if the polymers are limited by their diffusion or reaction rate. If the reaction of the vapour with the available sites was almost instantaneous when compared with its diffusion through the film (diffusion–rate limited), we would expect to see a significant dependence of the time constant on the electrode separation at constant film thickness. This is due to the electric field distribution within the membrane altering as the electrode separation changes, i.e.: the inner part of the films has a more significant effect on the conductance for the narrow electrode spacing than for the wider spacing. Both the diffusion–rate limited cases also include the postulate that the diffusion coefficient is independent of the vapour concentration. Therefore, we would expect the time constant to be independent of the analyte concentration. In Case III (reaction–rate limited) we would expect to see a large dependence of the time constant on the vapour concentration as the Langmuir reaction kinetics, defined by Equation 6.1, would be dominating the response. However, for this type of case we would not expect to observe a dependence of the time constant on the electrode separation. Figures 6.13 to 6.16 show the time constant for different gap sizes against ethanol concentration for all four types of polymer tested. These results show that, within experimental error, the electrode geometry has little or no effect on the time constant of the polymers, and that the vapour concentration has a large influence. We can therefore postulate that the polymers are reaction–rate limited in the linear portion of the isotherm (Case III).

For a purely reaction–rate limited case where the Langmuir isotherm dominates the response time, it has been shown [6.12] that,

$$\theta_t = \frac{\left[1 - \exp(-kt)\right]}{(1 + K)} \tag{6.18}$$

where θ_t is the fraction of occupied sites after time t, K is the ratio of the forward and backward reaction–rate constants and k is given by,

$$k = k_f C + k_b \tag{6.19}$$

The effect of the time–constant predicted by the empirical expressions 6.14 to 6.17 can therefore be modelled by the equation,

$$\tau = \frac{1}{k_f C + k_b} \tag{6.20}$$

Although this equation is valid for a purely reaction–rate limited case, it should be noted that the expression is based on a non–competitive model where a target vapour simply fills the available reaction sites. In a competitive binding model the introduction of the ethanol vapour will not only fill any empty sites, but will also be competitive with the sites containing water. The dynamics of the competitive model are therefore complicated by the inclusion of the desorption of water from occupied sites due to the ethanol vapour. We would expect the kinetics in such a competitive process to fit a double–expontential model. In order to simplify the dynamic model at this stage we will assume that the adsorption of ethanol is not greatly slowed by desorption of water from the occupied sites and that Equation 6.20 is therefore a valid model. This model has been included in Figures 6.13 and 6.14 for the Pan sensors. However, for the Ppy sensors where, as the concentration tended to infinity, the value of the time–constant

_____

did not tend to zero, Equation 6.20 clearly was not valid.   Although the Ppy sensors

demonstrate characteristics consistent with a purely reaction–rate limited model (i.e. no

effect of electrode geometry and large concentration effect on the time–constant), the

basic model of the effect of concentration on the time–constant has to be modified to,

$$\tau = \tau_{offset} + \frac{1}{k_b + k_f C} \tag{6.21}$$

where τ_{offset} is the value of the time–constant as the concentration tends to infinity. This

model is shown in Figures 6.15 and 6.16 with the values of the parameters for both

types of polymer shown in Table 6.3.

Table 6.3 Model parameter values for Pan and Ppy sensors using equations 6.20 and 6.21, respectively.

Polymer	$\tau_{offset} \times 10^{-3}$ / s	$k_f \times 10^{-3}$ / ppm^{-1}s^{-1}	$k_b \times 10^{-3}$ / s^{-1}
Pan/DSA/H$_2$O	-	1.534	1.104
Pan/PSA/H$_2$O	-	2.658	1.223
Ppy/DSA/H$_2$O	100.6	-6.621	2.485
Ppy/PSA/H$_2$O	54.34	-9.312	4.065
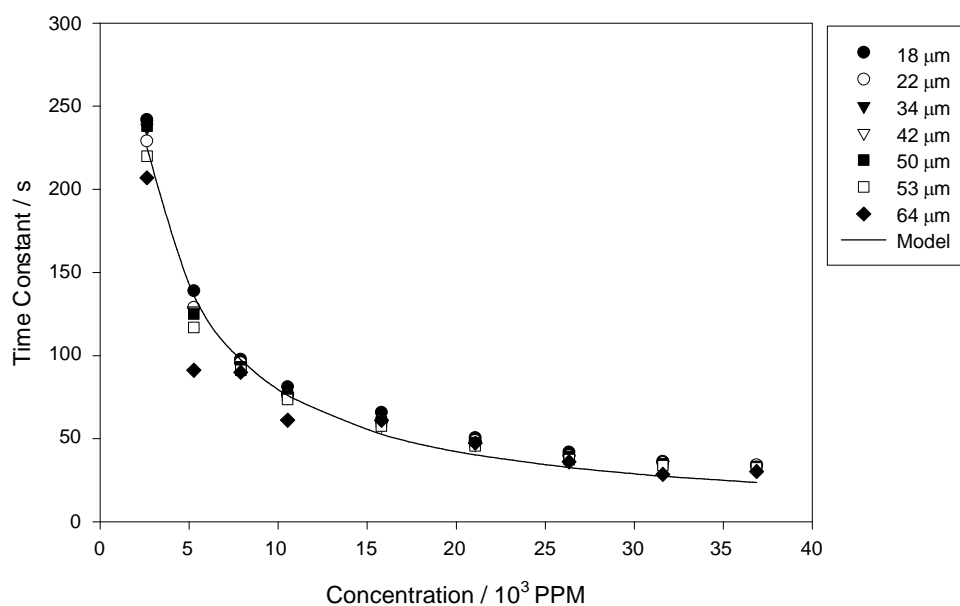
Figure 6.13 A graph showing the effect of ethanol concentration on the time constant of Pan/DSA/H$_2$O at constant humidity (2328 ppm) and temperature (35.3 °C). A range of electrode separations are shown.
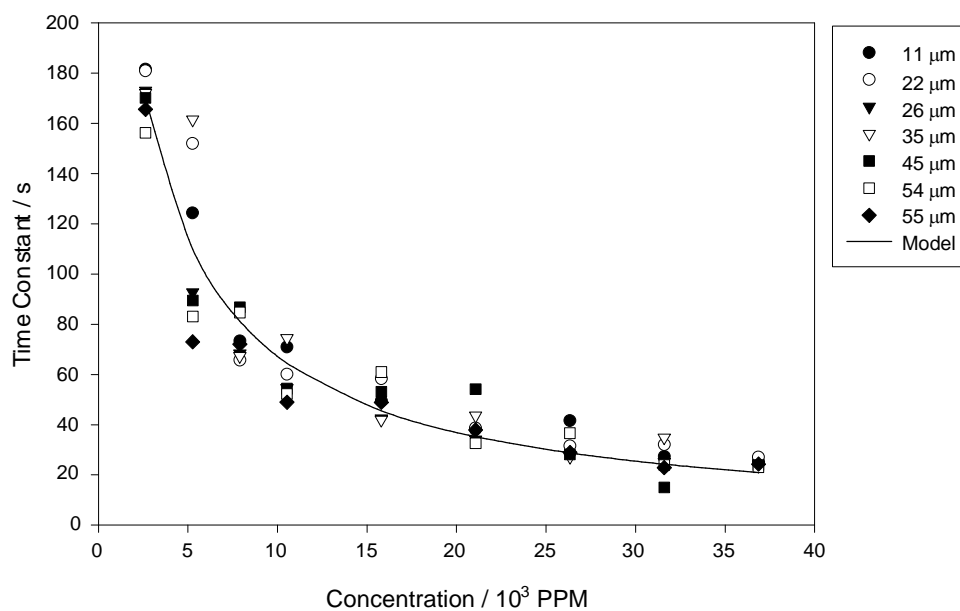
Figure 6.14 A graph showing the effect of ethanol concentration on the time constant of Pan/PSA/H$_2$O at constant humidity (2328 ppm) and temperature (35.3 °C). A range of electrode separations are shown.
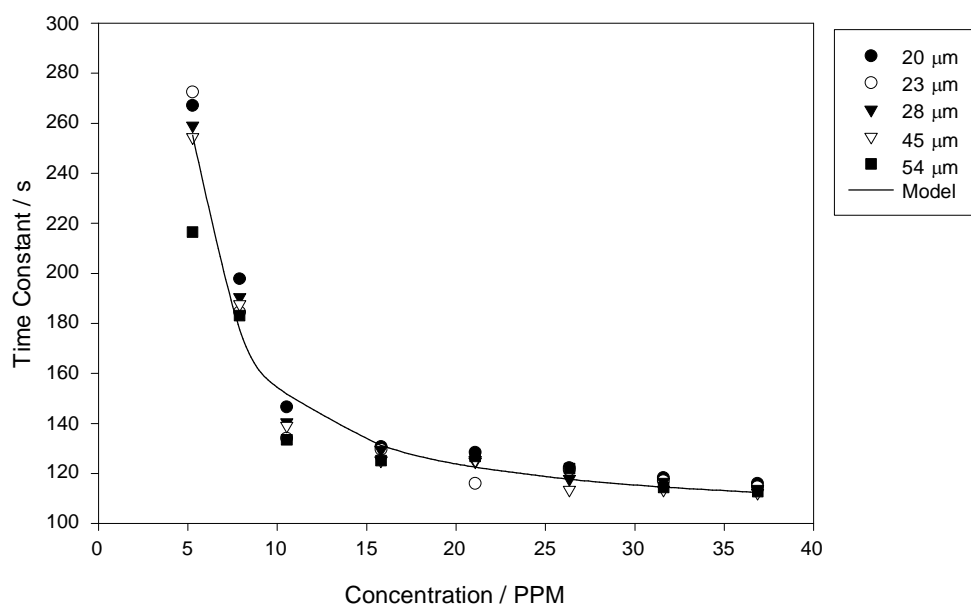
Figure 6.15 A graph showing the effect of ethanol concentration on the time constant of Ppy/DSA/H$_2$O at constant humidity (2328 ppm) and temperature (35.8 °C). A range of electrode separations are shown.
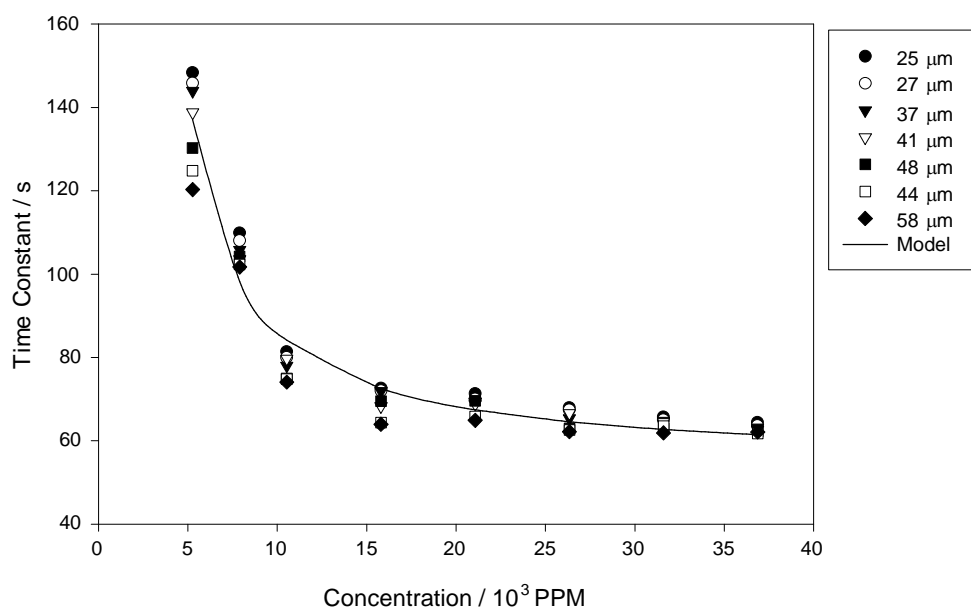
Figure 6.16 A graph showing the effect of ethanol concentration on the time constant of Ppy/PSA/H$_2$O at constant humidity (2328 ppm) and temperature (35.8 °C). A range of electrode separations are shown.

_____

There are a number of possible reasons explaining the deviation of the Ppy sensors from the basic reaction–rate limited equation describing the effect of concentration on the time–constant. Two possible explanations are:

1. the basic model, which assumes that there is no competition between the water and ethanol vapour, is not valid for the Ppy sensors. This possibility seems doubtful as the Pan sensors, which demonstrate a far greater level of competition, are accurately modelled by Equation 6.20. This suggests that this expression is valid for a simplified competitive model where the rate constants for forward and backward reaction are matched.

2. although the Ppy sensors are dominated by the reaction–rate of the polymer, there is also a diffusion process which is having an effect, perhaps due to the polymers structural heterogeneity. If this is the case, we can conclude that the Pan sensors can be modelled by a pure reaction–rate limited process (Case III), however the Ppy sensors are on the border between a pure reaction–rate limited and diffusion–rate limited case (see Figure 6.17).

6.6 Humidity and Temperature Effects on Transient Responses

We can now examine the effects of both humidity and temperature on the transient response of the polymer membranes. The humidity effect on the time–constant of the response has been modelled for one electrode separation, at one temperature and ethanol concentration. The effect of changing the humidity on the time–constant of the response of the polymers is shown in Figures 6.18 to 6.21. An increase in the level of
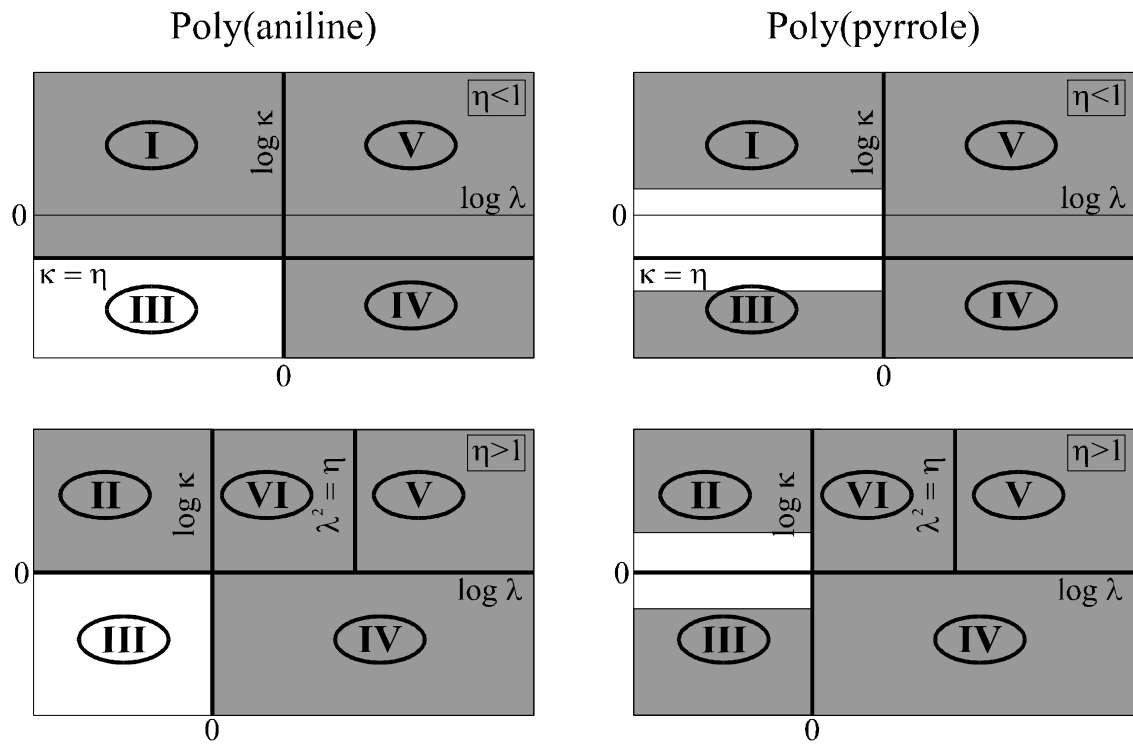
Figure 6.17 Case diagram showing solutions to the diffusion reaction problem: I – pure diffusion; II – slow diffusion; III – unsaturated (linear) reaction kinetics; IV – saturated reaction kinetics; V – saturated (non–linear) reaction kinetics; VI – mixed diffusion reaction process. The unshaded areas show the probable positions for each of the polymer types.

water vapour appears to slow the response time of both Ppy and Pan sensors. This effect can be explained by the reduced number of sites with which the ethanol vapour can react with quickly upon exposure. In a competitive polymer, as the humidity level is increased there are less free sites available for the ethanol to occupy (i.e. the level of competition is increased). If we assume that it takes longer for ethanol to occupy the sites when it is in direct competition with water vapour, we can we can postulate that an increase in water concentration should slow the response of reaction–rate limited polymer films.

The effect of humidity on the time–constant has been modelled using a purely empirical expression, Equation 6.22, where C_h is the water concentration, τ_0 is the time–constant in dry air and A and B are constants defined by the model.

$$\tau = \tau_0 + AC_h + BC_h^2 \qquad\qquad (6.22)$$

The values obtained for the three model parameters are shown in Table 6.4.

Table 6.4 Parameter values obtained for the empirical model of the effect of water on the time–constant. The sensors were exposed to an ethanol concentration of 10534 ppm at a temperature of 23.6 °C

Polymer	τ_0 / s	$A \times 10^{-3}$ / ppm^{-1}s	$B \times 10^{-6}$ / ppm^{-1}s
Pan/DSA/H$_2$O	96.36	5.60	0.97
Pan/PSA/H$_2$O	59.09	5.68	3.53
Ppy/DSA/H$_2$O	190.49	10.82	0.26
Ppy/PSA/H$_2$O	109.04	4.44	0.37
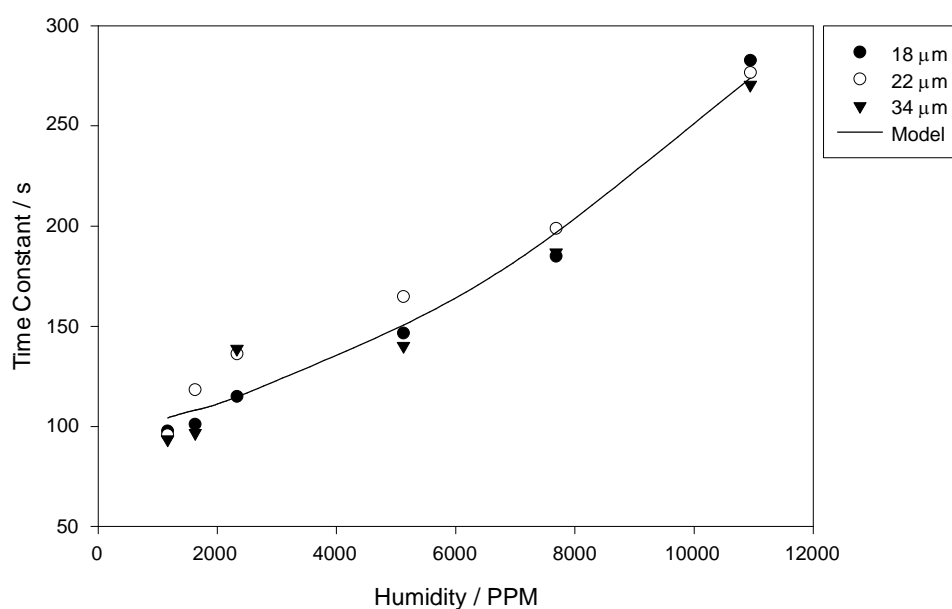
Figure 6.18 A graph showing the effect of humidity on the time–constant of Pan/DSA/H$_2$O. The sensors were exposed to an ethanol concentration of 10534 ppm and temperature of 23.6 °C. Three electrode separations (18, 22, and 34 μm) are shown.
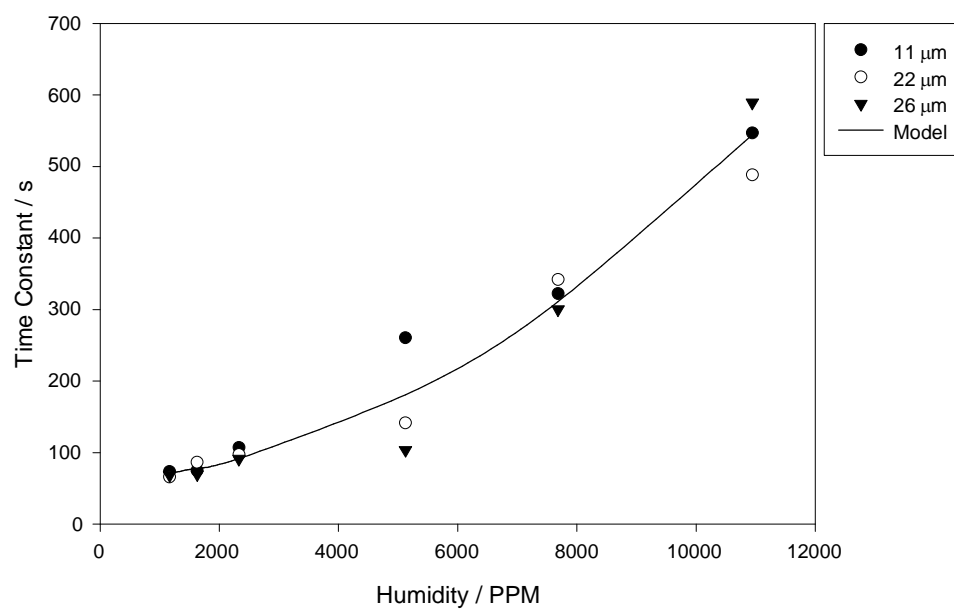
Figure 6.19 A graph showing the effect of humidity on the time–constant of Pan/PSA/H$_2$O. The sensors were exposed to an ethanol concentration of 10534 ppm and temperature of 23.6 ºC. Three electrode separations (11, 22, and 26 µm) are shown.
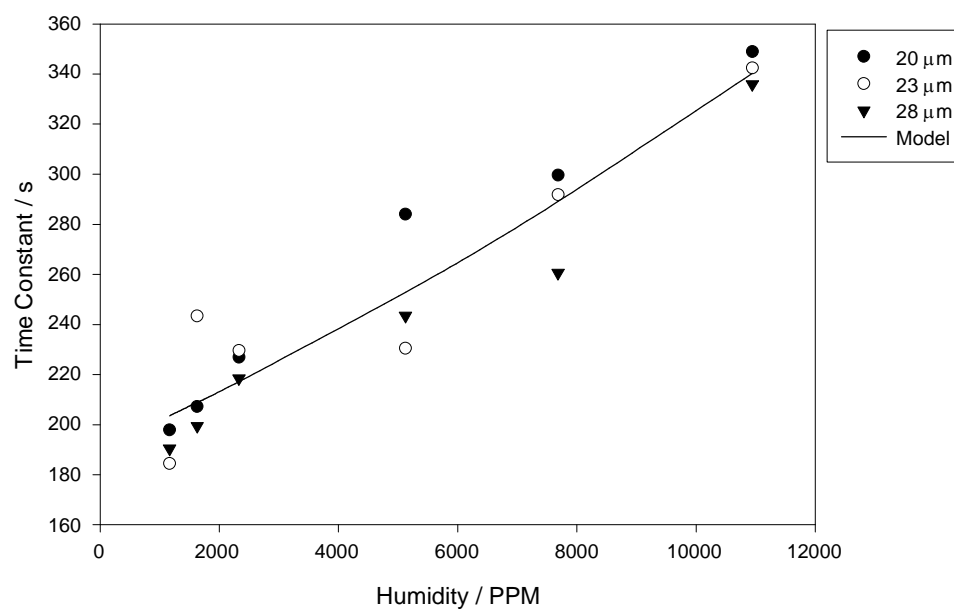
Figure 6.20 A graph showing the effect of humidity on the time–constant of Ppy/DSA/H$_2$O. The sensors were exposed to an ethanol concentration of 10534 ppm and temperature of 23.6 ºC. Three electrode separations (20, 23, and 28 µm) are shown.
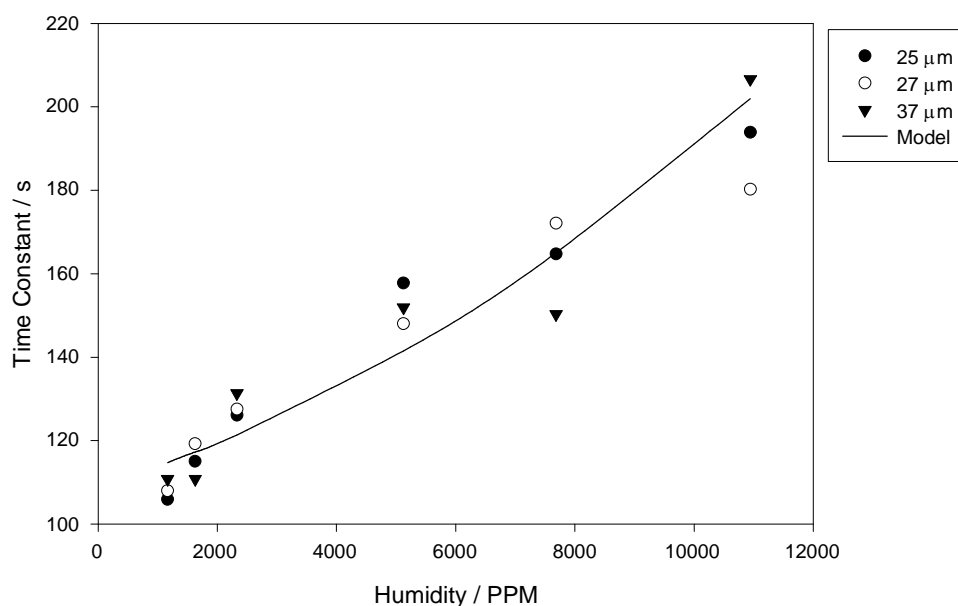
Figure 6.21 A graph showing the effect of humidity on the time–constant of Ppy/DSA/H$_2$O. The sensors were exposed to an ethanol concentration of 10534 ppm and temperature of 23.6 ºC. Three electrode separations (25, 27, and 37 μm) are shown.

Finally, based on the assumption that the polymers are reaction–rate limited we can model the effects of temperature on the value of the time–constant. An empirical observation is that many reactions have rate constants that follow the Arrhenius equation [6.13]. If we therefore assume that the time–constant of the polymers follows a similar equation,

$$\ln \tau = \ln A - \frac{E_a}{RT} \qquad (6.23)$$

where E_a is the activation energy and A is the frequency factor. If we now plot the log of our time–constant data against the inverse of the temperature we can extract the values of E_a/R (gradient of the plot) and $\ln A$. The Arrhenius plots for each of the

_____

sensors are shown in Figures 6.22 to 6.25 at a constant humidity of 2328 ppm and an

ethanol concentration of 26386 with the extracted values in Table 6.5.

It is interesting to note from Table 6.4 that the size of the counter–ion seems to

have a large effect on the value of the activation energy predicted by the empirical

equation. For both types of polymer the values of the PSA counter–ion were far higher

than for the DSA. This can be seen clearly on in the figures with a notable reduction in

the slope of the plot. It is also important to note that the change in sign of the activation

energy predicted for Ppy/PSA/H_2O is due to a reduction in the effect of temperature on

the time–constant to a point where experimental error dominates the extracted

parameters.

Table 6.5 Parameters extracted from the Arrhenius plots for the temperature coefficients for conducting
polymer sensors at an absolute humidity of 2328 ppm for responses to ethanol at 26386 ppm.

Polymer	E_a / JK^{-1}mol^{-1}	ln A / s
Pan/DSA/H_2O	2734.35	4.489
Pan/PSA/H_2O	445.73	3.491
Ppy/DSA/H_2O	2476.52	5.733
Ppy/PSA/H_2O	-181.66	4.079
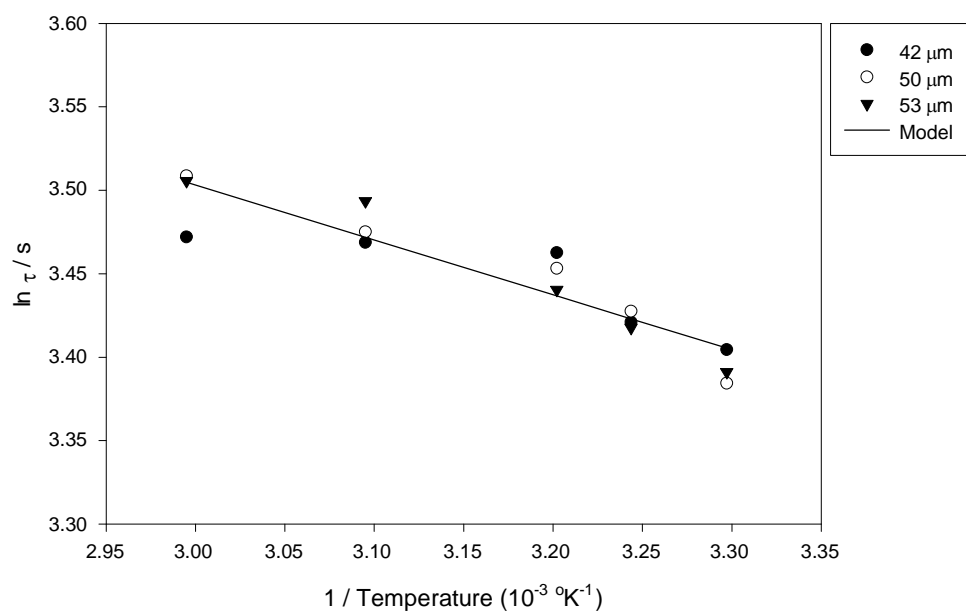
Figure 6.22 An Arrhenius plot showing the effect of temperature on the time–constant of Pan/DSA/H$_2$O at a humidity of 2328 ppm when exposed to ethanol at 26386 ppm. Three electrode separations (42, 50 and 53 μm) are shown for comparison.
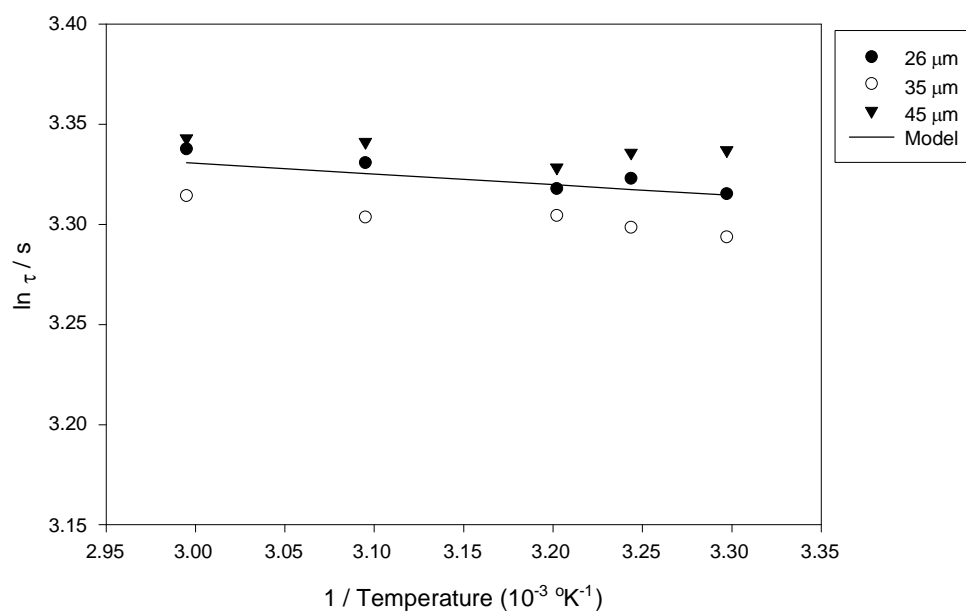
Figure 6.23 An Arrhenius plot showing the effect of temperature on the time–constant of Pan/PSA/H$_2$O at a humidity of 2328 ppm when exposed to ethanol at 26386 ppm. Three electrode separations (26, 35 and 45 μm) are shown for comparison.
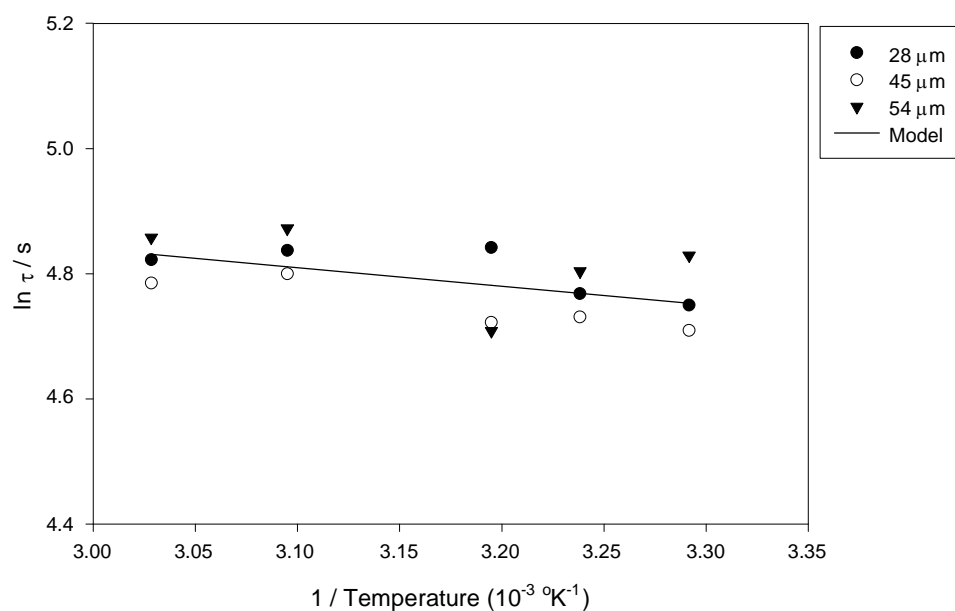
Figure 6.24 An Arrhenius plot showing the effect of temperature on the time–constant of Ppy/DSA/H$_2$O at a humidity of 2328 ppm when exposed to ethanol at 26386 ppm. Three electrode separations (28, 45 and 54 μm) are shown for comparison.
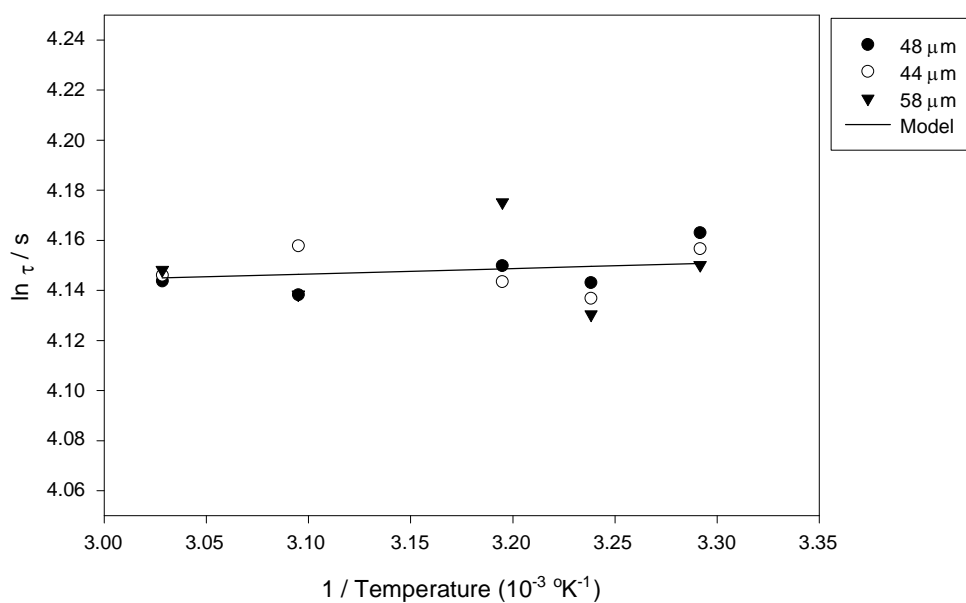
Figure 6.25 An Arrhenius plot showing the effect of temperature on the time–constant of Ppy/PSA/H$_2$O at a humidity of 2328 ppm when exposed to ethanol at 26386 ppm. Three electrode separations (48, 44 and 58 μm) are shown for comparison.

6.7 Steady–State Responses

Finally, we can investigate the steady–state responses of the polymers when the time, t, tends to infinity (i.e. $t \gg \tau$). Equation 6.13 predicts that the response of the polymers will be independent of the electrode separation at a constant humidity and temperature. This effect is demonstrated within experimental error and can be seen in Figures 6.26 to 6.29. These figures show the effect of ethanol concentration on the fractional change in conductance of the polymer sensors at a constant absolute humidity (2328 ppm) and at a constant temperature (35.3 °C). Each figure contains a range of electrode separations and it can be seen that, within experimental error, the responses are not effected by the electrode geometries. A basic Langmuir isotherm has been employed to model the response of the sensors (Chapter 4).
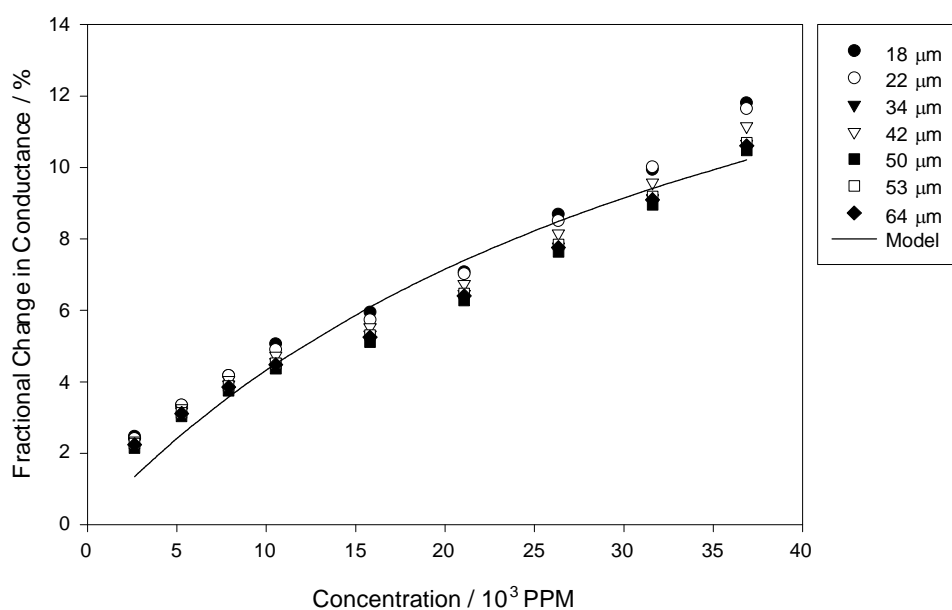
Figure 6.26 A graph showing the effect of ethanol concentration on the magnitude of the fractional response of a Pan/DSA/H_2O gas sensor at constant humidity (1164 ppm) and temperature (35.3°C). A range of electrode separations is shown.
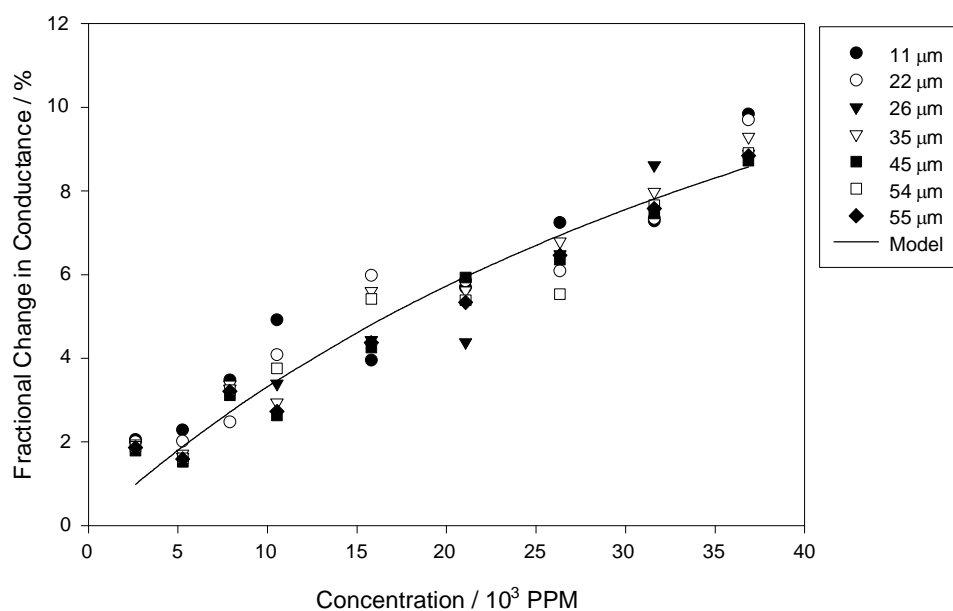
Figure 6.27 A graph showing the effect of ethanol concentration on the magnitude of the fractional response of a Pan/PSA/H$_2$O gas sensor at constant humidity (1164 ppm) and temperature (35.3°C). A range of electrode separations is shown.
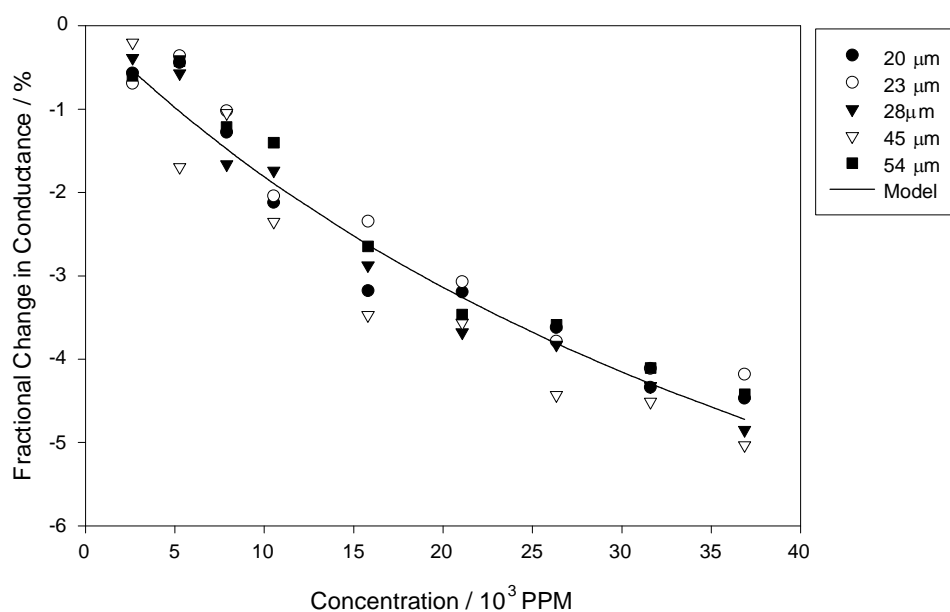
Figure 6.28 A graph showing the effect of ethanol concentration on the magnitude of the fractional response of a Ppy/DSA/H$_2$O gas sensor at constant humidity (1164 ppm) and temperature (35.8°C). A range of electrode separations is shown.
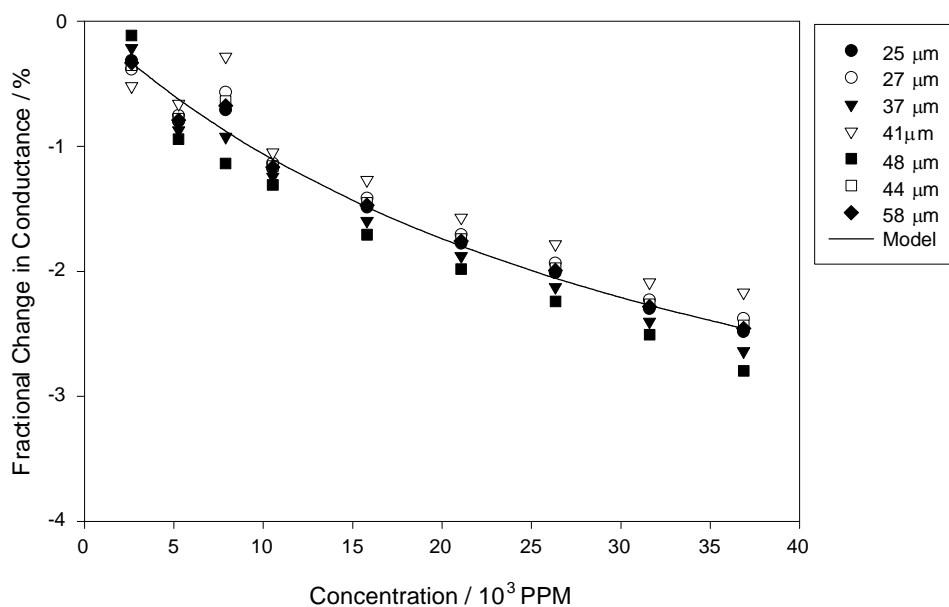
Figure 6.29 A graph showing the effect of ethanol concentration on the magnitude of the fractional response of a Ppy/PSA/H$_2$O gas sensor at constant humidity (1164 ppm) and temperature (35.8°C). A range of electrode separations is shown.

6.8 Conclusion

In this chapter we have studied the dynamic response of Ppy decane and pentane sulfonic acid, and Pan decane and pentane sulfonic acid films when exposed to ethanol vapour at varying levels of humidity and temperature. A diffusion and reaction theory used to describe conducting polymer membranes has been combined with a device conductance model describing a pair of semi–infinite thin electrodes. An empirical model of the transient responses has been presented in order to extract the time–constant for each of the polymers. Using the symmetry of the polymer responses and the effects of electrode separation and ethanol concentration on the time–constant, we have been able to determine that the Pan sensors have characteristics consistent with a pure reaction–rate limited model (Case III). Although the Ppy sensors also possesses

attributes that conform to a reaction–rate limited model, the effect of ethanol concentration on the time–constant suggests that there is also a diffusion effect for this type of polymer possibly due to the different structure. We can therefore conclude that these sensors are approaching the boundary between a reaction–rate limited and diffusion–rate limited model (Cases I/III or II/III).

An empirical model of the effects of both humidity and temperature on the time–constant has then been developed. Increasing the level of humidity in the analyte appears to significantly slow the response of both Ppy and Pan sensors. A temperature increase also seems to slow the response of the sensors, however, this effect was reduced for both types of polymer as the counter–ion length was increased. Finally, the predictions of the transient model on the magnitude of the steady–state response of the polymers has been confirmed using experimental results.

6.9 References

6.1   J. W. Gardner, M. Z. Iskandarani and B. Bott, Effect of electrode geometry on gas sensitivity of lead phthalocyanine thin films, *Sensors and Actuators B,* **9** (1992) 133-142.

6.2   U. Jain, A. H. Harker, A. M. Stoneham and D. E. Williams, Effect of electrode geometry on sensor response, *Sensors and Actuators B,* **2** (1990) 111-114.

6.3   J. W. Gardner, Electrical conduction in solid–state gas sensors, *Sensors and Actuators,* **18** (1989) 373-387.

6.4   J. W. Gardner, P. N. Bartlett and K. Pratt, Modelling of gas–sensitive conducting polymer devices, *IEE Proc.: Circuits, devices & systems,* **142** (1995) 321-333.

6.5   N. Blair, The Development and characterisation of conducting polymer based sensors for use in an electronic nose, *Ph.D. Thesis, University of Southampton, UK,* 1990.

6.6   P. N. Bartlett and J. W. Gardner, Diffusion and binding of molecules to sites within homogeneous thin films, *Trans. Roy. Soc. London A*, **354**, (1996), 35-57.

6.7   J. W. Gardner, P. N. Bartlett and K. F. E. Pratt, Modelling of gas–sensitive conducting polymer devices, *IEE Proc.: Circuits, devices and systems,* **142**, (1995), 321-333.

6.8   J. W. Gardner, A diffusion–reaction model of electrical conduction in tin oxide gas sensors, *Semicond. Sci. Technol.*, **4**, (1989), 345-350

6.9   J. Crank, *Mathematics of diffusion*, Oxford University Press, 1975.

6.10   J. W. Gardner, Electrical conduction in solid state gas sensors, *Sensors and Actuators*, **18**, (1989), 373-387.

6.11   P. N. Bartlett, P. B. M. Archer and S. K. Ling–Chung, Conducting polymer gas sensors, Part I: Fabrication and characterisation, *Sensors and Actuators,* **19** (1989) 125-140.

6.12   P. N. Bartlett and S. K. Ling–Chung, Conducting polymer gas sensors, Part II: Response of polypyrrole to methanol vapour, *Sensors and Actuators,* **19**, (1989), 141-150.

6.13   P. W. Atkins, *Physical Chemistry (Fifth Edition),* Oxford University Press, London, 1994.

_____

CHAPTER 7

Final Model of Conducting Polymer Sensors

7.1 Introduction

The aim of this chapter is to summarise and, where possible, combine the models developed in Chapters 4, 5 and 6 to deliver a final model of the interaction between polymer sensors and their environment. This model will include descriptions of the effects of both vapour and gases on the polymers and will also characterise the effects of humidity and temperature on the response. A brief summary of the static and dynamic models will also be included to give an overview each of the sections developed in previous chapters. These expressions will then be combined in order to produce a general model of both Ppy and Pan devices. The final model will be separated into four sections describing: the effect of organic vapours at constant humidity and temperature; the effect of humidity on the response of the polymers when exposed to an unchanging organic vapour concentration at a constant temperature; the effects of temperature on the response of the polymers when exposed to an unchanging organic vapour concentration at a constant humidity; response of polymers to a target gas.

The final model will describe the magnitude of the sensor response and also the transient characteristics on exposure to a target analyte. Such a model could be employed in a gas–monitoring instrument in the determination of gas or vapour

concentration through the employment of a pre–calibrated mathematical look–up table (LUT). Theoretical models may also assist in the improvement of the accuracy of gas sensing equipment, such as electronic noses, in the selection of appropriate sensors for different types of application and in the selection of pre–processing techniques.

7.2 Synopsis of Static Vapour Model

The static model of the interaction of conducting polymers with ethanol vapour was developed in Chapter 4. This model included the effects of humidity on the characteristics of the membranes in isothermal conditions by assuming competition between the available reaction sites within the polymer and the water and ethanol vapour. The model assumes that a polymer film contains a uniform distribution of immobile sites, concentration Γ, with which the species, A, can reversibly react. The reaction is described by the Langmuir adsorption isotherm [7.1],

$$A + \left\{ \ \right\}_{site} \underset{k_b}{\overset{k_f}{\Longleftrightarrow}} \left\{ A \right\}_{site} \tag{7.1}$$
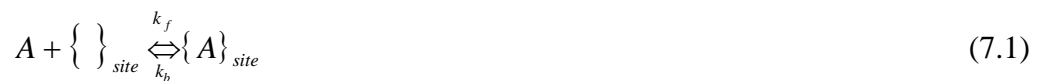
where k_f and k_b are the forward and backward reaction rate constants, respectively. From this basic premise the fractional site occupancy, θ, of the polymer can be defined by the equation,

$$\theta_{\infty} = \frac{K_a c_a}{\left(1 + K_a c_a \right)} \tag{7.2}$$

where c_a is the concentration of species A, and the binding constant, K_a, is the ratio of the forward and backward reaction rate constants (k_f / k_b). By making the assumption that the conductance of the device is related linearly to the concentration of the bound species, a model has been developed that defines the change in conductance of the device at a constant humidity and temperature.

$$\Delta G = \left(G_f - G_i\right) \approx \frac{K_a c_a a_a \Gamma}{1 + K_a c_a} \tag{7.3}$$

This model was tested against results obtained from the Dynamic Headspace Testing equipment (see Chapter 3) and showed good agreement with the data.

The effects of water vapour on the response of the polymers to ethanol vapour was then postulated. The initial conductance of the polymer at a constant humidity before the exposure of the ethanol vapour is approximately given by,

$$G_i \approx G_0 + \frac{K_w c_w a_w \Gamma}{\left(1 + K_w c_w\right)} \tag{7.4}$$

where G_0 is the conductance of the polymer in dry air, K_w is the water binding constant, a_w is the sensitivity coefficient for water vapour and Γ is again the concentration of sites within the film. This model was also tested against experimental results with the theory and data showing good agreement. The combined effect of both water and ethanol in air can be given by,

$$G_f \approx G_0 + \frac{\left(K_w c_w a_w \Gamma + K_e c_e a_e \Gamma\right)}{\left(1 + K_w c_w + K_e c_e\right)} \tag{7.5}$$

Assuming that only water and ethanol are reacting with the available sites and that these vapours are directly competitive, the fractional response of a conducting polymer film was shown to be,

$$\frac{\Delta G}{G_i} \approx \frac{\dfrac{\left(K_w c_w a_w \Gamma + K_e c_e a_e \Gamma\right)}{\left(1 + K_w c_w + K_e c_e\right)} - \dfrac{K_w c_w a_w \Gamma}{\left(1 + K_w c_w\right)}}{G_0 + \dfrac{K_w c_w a_w \Gamma}{\left(1 + K_w c_w\right)}} \tag{7.6}$$

where K_e is the ethanol binding constant, c_e is the ethanol concentration and a_e describes the sensitivity of the polymer to ethanol vapour. This model demonstrated satisfactory correlation with the experimental results under isothermal conditions. Unfortunately, extension of the model to include the effects of temperature on the physical parameters of the model was inconsistent with the thermodynamics of the polymer membranes. For this reason, a second model had to be developed in order to model the effects of temperature on the response of conducting polymers to ethanol vapour.

The empirical temperature model was developed at a constant humidity and based on a variable range hopping model of the Mott kind [7.2]. This basic model assumes that when a charge carrier within the polymer encounters a potential barrier it will hop to the nearest available site. This type of barrier−limited conduction

mechanism can be modelled by an exponential equation when the temperature range is small so there is only nearest–neighbour hopping,

$$G \approx G_0 \exp\left(\frac{-\Phi}{kT}\right)$$

(7.7)

where Φ is the work function of the polymer, k is Boltzmann's constant, G_0 is a constant (as T tends to infinity) and T is the temperature of the experiment. A target vapour can now be modelled by how it affects the work function of the polymer [7.3]. The effect of vapours on the response of the polymers can therefore be modelled through a modulation of the work function,

$$G \approx G_0 \exp\left[\frac{-\left(\Phi_0 + \Delta\Phi_e\right)}{kT}\right]$$

(7.8)

where $\Delta\Phi_e$ is the change in the work function due to the ethanol vapour and Φ_0 is the work function in air. Recent work on MOSFETs [7.4] shows that the chemically activated shift in the work function of the polymers follows a Langmuir isotherm. The fractional response of the polymer can therefore be written,

$$\frac{\Delta G}{G_i} \approx \exp\left(\frac{-\alpha}{kT} \frac{Kc_e}{\left(1 + Kc_e\right)}\right) - 1$$

(7.9)

When the chemical shift, $\Delta\Phi$, is small compared to kT, Equation 7.9 can be approximated to,

$$\frac{\Delta G}{G} \approx \frac{-\alpha}{kT} \frac{Kc_e}{\left(1 + Kc_e\right)}$$
                                                                                     (7.10)

Equation 7.10 was the basic model used to describe the response of the polymer sensors at constant humidity. The temperature effect on the response was modelled empirically through variations in the values of the parameters α and K due to temperature changes. It should be noted at this point that Equation 7.10 is identical to the basic Langmuir isotherm employed to describe the effects of ethanol on the response of a polymer at a constant humidity. However, in this equation the sensitivity term ($a_e\Gamma$) has been replaced with a temperature dependent term ($-\alpha/kT$).

The variation of the binding constant, K, and the sensitivity, α, with temperature were modelled using different expressions for the two basic types of polymer. The expressions employed for the Pan sensors are shown below,

$$\alpha = \alpha_0 \exp(\gamma T)$$
                                                                                     (7.11)

$$K_e = K_{e0}\left(1 + \beta T\right)$$
                                                                                     (7.12)

where γ and β are the temperature coefficient of the polymers sensitivity and binding constant respectively. For Ppy sensors the sensitivity and binding constant were both modelled using the exponential expressions shown below,

$$\alpha_e = \alpha_{e0}\left(1 + \gamma_\alpha \exp \beta_\alpha T\right)$$
                                                                                     (7.13)

$$K_e = K_{e0}\left(1 + \gamma_K \exp \beta_K T\right) \tag{7.14}$$

In summary two models have been developed for the description of the response of the polymer films. The first describes the effects of humidity on the response of the sensors to ethanol vapour through the application of a competitive binding model. The second expression describes the effects of temperature on the response to the same vapour at a constant humidity employing a work function view of the polymers. Due to the independent way in which each of these models were developed, a combination of the expressions to form a single model of the response of polymers and the effects of both humidity and temperature is problematic. At this stage we will have to be satisfied with two models which describe these environmental effects on the response of the devices to our target vapour.

7.3 Synopsis of Static Gas Model

Chapter 5 was dedicated to the development of a model describing the response of polymer sensors to CO_2 concentrations up to 500 ppm. An initial model based on the chemistry of the interaction between the gas, water and the polymer was unsuccessful for a number of reasons. Firstly, the value of one of the parameters included in the model was found to be negative. As this parameter was linked to concentrations within the polymer, a value less than zero was physically impossible. Secondly, the effect of water on the response of the polymers was predicted by the model to increase the magnitude of the response to the CO_2. The polymers demonstrated characteristics completely opposite to this with their response reducing significantly as the humidity of

the testing sequence was increased. Finally, the correlation between the data and the model could be improved for every sensors by employing a simple empirical expression of the response.

An empirical model based on equations similar to those employed in a Langmuir isotherm was therefore employed to model the response of the polymers to the CO_2. The basic model is given by Equation 7.15.

$$\frac{\Delta G}{G_i} = \frac{S_{CO2}\, K_{CO2}\left(c_{CO2} - \alpha\right)}{1 + K_{CO2}\left(c_{CO2} - \alpha\right)}$$
(7.15)

where S_{CO2} is the magnitude of the curve and is therefore related to the sensitivity, K_{CO2} is the curvature of the response, c_{CO2} is the concentration of CO_2 and α is the buffer concentration required before the sensors begin to respond. This basic model gave correlation coefficients of greater than 0.97 for all the sensors. Extension of the model to include the effects of both humidity and temperature was completed by creating empirical expressions of the variation of the parameters S_{CO2}, K_{CO2} and α. The effect of humidity is modelled by Equations 7.16 to 7.18 and the effect of temperature by Equations 7.19 and 7.20. The effect of temperature on the parameter α in Equation 7.15 was found to be inconclusive within the temperature range studied. Within experimental error we can conclude that this parameter was constant.

$$S = \frac{\beta_S}{c_w} - \chi_S$$
(7.16)

$$K = \frac{\beta_K}{c_w} + \chi_K \tag{7.17}$$

$$\alpha = \beta_\alpha \ln c_w + \chi_\alpha \tag{7.18}$$

$$S(T) = \beta_S T^2 + \chi_S T + S_0 \tag{7.19}$$

$$K(T) = \beta_K T + K_0 \tag{7.20}$$

7.4 Synopsis of Dynamic Model

In Chapter 6 the dynamic response of the polymer films to ethanol vapour has been investigated.   Much of the analysis in this chapter was aimed at determining the physical properties of the polymer derived by the effects of ethanol concentration, electrode geometry etc. on the time–constant of the polymer response. For the purpose of this final model the expressions employed in the extraction of the time–constant have to be used to describe the transient response of the devices. The on and off transients (switching at $t = 0$ in each case) for Pan are shown in Equations 7.21 and 7.22 and are consistent with the kinetics of a pure reaction–rate limited case [7.5]. The expressions employed for Ppy are shown in Equations 7.23 and 7.24.

$$G(t) - G_0 = \Delta G \left[1 - \exp\left(\frac{-t}{\tau_{on}} \right) \right] \tag{7.21}$$

$$G(t) - G_0 = \Delta G \exp\left(\frac{-t}{\tau_{off}}\right) - \Delta G \tag{7.22}$$

$$G(t) - G_0 = \Delta G_1 \left(\exp\left(\frac{-t}{\tau_{on1}}\right) - 1 \right) + \Delta G_2 \left(\exp\left(\frac{-t}{\tau_{on2}}\right) - 1 \right) \tag{7.23}$$

$$G(t) - G_0 = \Delta G_1 \left(1 - \exp\left(\frac{-t}{\tau_{off1}}\right) \right) + \Delta G_2 \left(1 - \exp\left(\frac{-t}{\tau_{off2}}\right) \right) \tag{7.24}$$

where $G(t)$ is the conductance of the polymer at time t, G_0 is the baseline conductance of the polymer i.e.: in the absence of ethanol vapour, ΔG is the change in conductance of the sensor due to the ethanol concentration and τ_{on} and τ_{off} are the time–constants for the on and off responses, respectively.

The second component of the ethanol response associated with the parameters ΔG_2 and τ_{off2} demonstrated a small change in conductance which typically occurred over an extremely long exposure period (with a time–constant greater than 3000 s). This period was greater than the time of exposure employed during the acquisition of the data employed in the static modelling. The initial response of the Ppy sensors, within the period employed for the competitive binding model (2700 s) can therefore be approximated to a single exponential expression. If the data employed in the static modelling of the Ppy sensors had been gathered over a much greater period the second component of the response would also have to be included in this analysis. The final model of the Ppy sensors is therefore limited to responses gathered during to the initial

_____

response of the sensors upon exposure. In the case of the sensors employed in this study the model would be limited to approximately the first 3000 seconds.

We can now explore the effects of ethanol concentration, humidity and temperature on the time–constants defined by the dynamic models. The effect of ethanol concentration on the time–constants for Pan sensors [7.5] was defined by the equation,

$$\tau = \frac{1}{k_f c_e + k_b} \tag{7.25}$$

and for Ppy sensors,

$$\tau = \tau_{offset} + \frac{1}{k_f c_e + k_b} \tag{7.26}$$

where k_f and k_b are the forward and backward reaction rate constants, c_e is the ethanol concentration and τ_{offset} is the offset time–constant employed for the Ppy sensors. The humidity effect on the time–constant was modelled using the purely empirical expression,

$$\tau = \tau_0 + Ac_w + Bc_w^2 \tag{7.27}$$

where c_w is the water concentration, τ_0 is the time–constant in dry air and A and B are constants defined by the model. The temperature effects on the sensor response was modelled using the Arrenhius equation [7.6],

_____

$$\ln \tau = \ln A - \frac{E_a}{RT} \qquad\qquad (7.28)$$

where E_a is the activation energy and A is the frequency factor. This can be written,

$$\tau = Ae^{\frac{-E_a}{RT}} \qquad\qquad (7.29)$$

We therefore have expressions defining the transient response of the polymer sensors and the effects of vapour concentration, humidity and temperature on the time–constant.

7.5 Final Model of Polymers Chemoresistors

Due to the limitations of the models derived in Chapters 4 to 6, the final model of the response of conducting polymer sensors both to ethanol vapour and CO_2 will be separated into four sections. Firstly, the basic response of conducting polymers to a target vapour at a constant humidity and temperature will be derived. The subsequent two sections will derive the effects of humidity on the vapour response, where the target concentration and temperature are kept constant, and the effects of temperature on the vapour response where the target concentration and humidity are constant. Finally, a model describing the effects of CO_2 on both modified and un–modified sensors will be presented.

a) Final model of vapour effects at constant humidity and temperature.

The expression that models fractional change in conductance under static conditions using a competitive binding model is given by Equation 7.6. This is our fundamental relationship between humidity and the response of conducting polymer sensors to an organic vapour. This expression must therefore be combined with expressions for the transient responses of the sensors in order to achieve a final model. The basic transient responses to ethanol is given by Equations 7.21 and 7.22 for Pan sensors, and by Equations 7.23 and 7.24 for Ppy sensors. As discussed earlier (Section 7.4), under most data acquisition conditions, the second component of the Ppy response can be omitted in order to obtain a final model. To re–introduce this second component, further work on the effects of ethanol concentration, humidity and temperature on the time–constant of the second term would have to be carried out.

We can now derive our final model of the effects of ethanol on the conducting polymer sensors at a constant humidity and temperature. Firstly, the transient equations (7.21 to 7.24) have to be combined with the expressions modelling the effects of ethanol concentration on the on and off transients (Equations 7.25 and 7.26 for Pan and Ppy, respectively). These combined equations then have to be re–arranged so that they are expressed as functions of the fractional change in conductance of the sensors. This can be achieved by deriving the conductance when the time is equal to zero ($G_{t=0}$) for the on and off transients. For the on transient, the value of $G_{t=0}$ is identical to the initial conductance term, G_i in the static model. For the off transient response the conductance at time zero is equal to the final conductance (G_f) of the static model. However, in order to simplify the final model it is useful to express the value of $G_{t=0}$ for the off transient in terms of initial conductance and the change in conductance due to the target

_____

vapour. This gives us different expressions for Pan (Equation 7.30) and Ppy (Equation 7.31)[1].

$$G_{t=0}^{off} = G_f = G_i + \Delta G \qquad (7.30)$$

$$G_{t=0}^{off} = G_f = G_i - \Delta G \qquad (7.31)$$

We can now derive our final models of the effects of ethanol concentration on the normalised response of conducting polymer sensors at constant humidity (c_w) and temperature (T). For Pan sensors the on transient is modelled by a combination of Equations 7.6, 7.21 and 7.25. This gives,

$$\left.\frac{G(t) - G_{t=0}}{G_{t=0}}\right|_{T,c_w} \approx + \left[\left(\frac{\dfrac{\left(K_w c_w a_w \Gamma + K_e c_e a_e \Gamma\right)}{\left(1 + K_w c_w + K_e c_e\right)} - \dfrac{\left(K_w c_w a_w \Gamma\right)}{\left(1 + K_w c_w\right)}}{G_0 + \dfrac{K_w c_w a_w \Gamma}{\left(1 + K_w c_w\right)}}\right) \times \left(1 - \exp\left(-t\left(k_f c_e + k_b\right)\right)\right)\right] \qquad (7.32)$$

The off transients for Pan are modelled employing Equations 7.6, 7.22, 7.25 and 7.30 giving,

$$\left.\frac{G(t) - G_{t=0}^{off}}{G_{t=0}^{off}}\right|_{T,c_w} \approx + \left[\left(\frac{\dfrac{\left(K_w c_w a_w \Gamma + K_e c_e a_e \Gamma\right)}{\left(1 + K_w c_w + K_e c_e\right)} - \dfrac{\left(K_w c_w a_w \Gamma\right)}{\left(1 + K_w c_w\right)}}{G_0 + \dfrac{K_w c_w a_w \Gamma}{\left(1 + K_w c_w\right)}}\right) \times \exp\left(-t\left(k_f c_e + k_b\right)\right)\right] \qquad (7.33)$$

_____

[1] It is important to note that G_0 is the conductance of the polymers in the absence of water and ethanol, and $G_{t=0}$ is the conductance at time zero (i.e. prior to the exposure of an analyte).

For Ppy sensors the on transient is derived by combining Equations 7.6, 7.23 and 7.26, which gives,

$$\frac{G(t)-G_{t=0}}{G_{t=0}}\bigg|_{T,c_w} \approx -\left[\left(\frac{\left(\dfrac{\left(K_w c_w a_w \Gamma + K_e c_e a_e \Gamma\right)}{\left(1+K_w c_w + K_e c_e\right)} - \dfrac{\left(K_w c_w a_w \Gamma\right)}{\left(1+K_w c_w\right)}\right)}{G_0 + \dfrac{K_w c_w a_w \Gamma}{\left(1+K_w c_w\right)}}\right) \times \left(1-\exp\left(\frac{-t}{\tau_{offset} + \left(1\Big/ k_f c_e + k_b\right)}\right)\right)\right] \quad (7.34)$$

Finally, the off transient for Ppy is a combination of Equations 7.6, 7.24, 7.26 and 7.31 and is given by the expression,

$$\frac{G(t)-G^{off}_{t=0}}{G^{off}_{t=0}}\bigg|_{T,c_w} \approx -\left[\left(\frac{\left(\dfrac{\left(K_w c_w a_w \Gamma + K_e c_e a_e \Gamma\right)}{\left(1+K_w c_w + K_e c_e\right)} - \dfrac{\left(K_w c_w a_w \Gamma\right)}{\left(1+K_w c_w\right)}\right)}{G_0 + \dfrac{K_w c_w a_w \Gamma}{\left(1+K_w c_w\right)}}\right) \times \exp\left(\frac{-t}{\tau_{offset} + \left(1\Big/ k_f c_e + k_b\right)}\right)\right] \quad (7.35)$$

b) The effects of humidity at a constant vapour concentration and temperature.

The effects of the water concentration on the response of the polymers to an organic vapour will take a similar form to Equations 7.32 to 7.35. However, in this case the ethanol concentration (c_e) and temperature (T) remain constant, and the effect of the water concentration on the time–constant is given by Equation 7.27 for both Pan and Ppy sensors. The models for the on and off transients for Pan are shown in Equations 7.36 and 7.37 respectively.

$$\left.\frac{G(t) - G_{t=0}}{G_{t=0}}\right|_{T,c_e} \approx + \left[\left(\frac{\dfrac{\left(K_w c_w a_w \Gamma + K_e c_e a_e \Gamma\right)}{\left(1 + K_w c_w + K_e c_e\right)} - \dfrac{\left(K_w c_w a_w \Gamma\right)}{\left(1 + K_w c_w\right)}}{G_0 + \dfrac{K_w c_w a_w \Gamma}{\left(1 + K_w c_w\right)}}\right) \times \left(1 - \exp\left(\frac{-t}{\left(\tau_0 + Ac_w + Bc_w^2\right)}\right)\right)\right] \quad (7.36)$$

$$\left.\frac{G(t) - G_{t=0}^{off}}{G_{t=0}^{off}}\right|_{T,c_e} \approx + \left[\left(\frac{\dfrac{\left(K_w c_w a_w \Gamma + K_e c_e a_e \Gamma\right)}{\left(1 + K_w c_w + K_e c_e\right)} - \dfrac{\left(K_w c_w a_w \Gamma\right)}{\left(1 + K_w c_w\right)}}{G_0 + \dfrac{K_w c_w a_w \Gamma}{\left(1 + K_w c_w\right)}}\right) \times \exp\left(\frac{-t}{\tau_0 + Ac_w + Bc_w^2}\right)\right] \quad (7.37)$$

The on and off transients for the Ppy sensors are shown in Equations 7.38 and 7.39, respectively.

$$\left.\frac{G(t) - G_{t=0}}{G_{t=0}}\right|_{T,c_e} \approx - \left[\left(\frac{\dfrac{\left(K_w c_w a_w \Gamma + K_e c_e a_e \Gamma\right)}{\left(1 + K_w c_w + K_e c_e\right)} - \dfrac{\left(K_w c_w a_w \Gamma\right)}{\left(1 + K_w c_w\right)}}{G_0 + \dfrac{K_w c_w a_w \Gamma}{\left(1 + K_w c_w\right)}}\right) \times \left(1 - \exp\left(\frac{-t}{\tau_0 + Ac_w + Bc_w^2}\right)\right)\right] \quad (7.38)$$

$$\left.\frac{G(t) - G_{t=0}^{off}}{G_{t=0}^{off}}\right|_{T,c_e} \approx - \left[\left(\frac{\dfrac{\left(K_w c_w a_w \Gamma + K_e c_e a_e \Gamma\right)}{\left(1 + K_w c_w + K_e c_e\right)} - \dfrac{\left(K_w c_w a_w \Gamma\right)}{\left(1 + K_w c_w\right)}}{G_0 + \dfrac{K_w c_w a_w \Gamma}{\left(1 + K_w c_w\right)}}\right) \times \exp\left(\frac{-t}{\tau_0 + Ac_w + Bc_w^2}\right)\right] \quad (7.39)$$

c) The effects of temperature at a constant vapour concentration and humidity.

We can now derive expressions that describe the effects of temperature on the vapour response of the polymer sensors. For this purpose the temperature effects on the magnitude of the fractional response of the polymers to ethanol vapour has to be

_____

derived. This can be achieved for Pan by combining Equation 7.10 with 7.11 and 7.12, and for Ppy by combining Equation 7.10 with 7.13 and 7.14. This gives us two expressions that model the effect of temperature on the response of Pan (Equation 7.40) and Ppy (Equation 7.41) sensors to an organic vapours,

$$\left.\frac{G_f - G_i}{G_i}\right|_{T,c_e} \approx \left(\frac{-\alpha_0 \exp(\gamma T)}{kT}\right) \times \left(\frac{K_{e0}(1+\beta T)}{1+K_{e0}c_e(1+\beta T)}\right) \tag{7.40}$$

$$\left.\frac{G_f - G_i}{G_i}\right|_{T,c_e} \approx \left(\frac{-\alpha_{e0}(1+\gamma_\alpha \exp(\beta_\alpha T))}{kT}\right) \times \left(\frac{K_{e0}(1+\gamma_K \exp(\beta_K T))}{1+K_{e0}c_e(1+\gamma_K \exp(\beta_K T))}\right) \tag{7.41}$$

These expressions will replace Equation 7.6 as our fundamental model in this section. We can combine these equations with the transient equations (7.21 to 7.24) and Equation 7.29 deriving the effect of temperature on the time–constant of the polymers response. This gives us final models of the effect of temperature on the response of the polymers at a constant humidity and ethanol concentration. The on and off transients for Pan are shown in Equations 7.42 and 7.43, respectively, with the on and off for Ppy shown in Equations 7.44 and 7.45.

$$\left.\frac{G(t) - G_{t=0}}{G_{t=0}}\right|_{c_e,c_w} \approx +\left[\left(\left(\frac{-\alpha_0 \exp(\gamma T)}{kT}\right) \times \left(\frac{K_{e0}(1+\beta T)}{1+K_{e0}c_e(1+\beta T)}\right)\right) \times \left(1 - \exp\left(\frac{-t}{Ae^{-E_a/RT}}\right)\right)\right] \tag{7.42}$$

$$\left.\frac{G(t) - G_{t=0}^{off}}{G_{t=0}^{off}}\right|_{c_e,c_w} \approx +\left[\left(\left(\frac{-\alpha_0 \exp(\gamma T)}{kT}\right) \times \left(\frac{K_{e0}(1+\beta T)}{1+K_{e0}c_e(1+\beta T)}\right)\right) \times \left(\exp\left(\frac{-t}{Ae^{-E_a/RT}}\right)\right)\right] \tag{7.43}$$

$$\left.\frac{G(t)-G_{t=0}}{G_{t=0}}\right|_{c_e,c_w} \approx -\left[\left(\left(\frac{-\alpha_{e0}\left(1+\gamma_\alpha \exp(\beta_\alpha T)\right)}{kT}\right)\times\left(\frac{K_{e0}\left(1+\gamma_K \exp(\beta_K T)\right)}{1+K_{e0}c_e\left(1+\gamma_K \exp(\beta_K T)\right)}\right)\right)\times\left(1-\exp\left(\frac{-t}{Ae^{-E_a/RT}}\right)\right)\right] \quad (7.44)$$

$$\left.\frac{G(t)-G_{t=0}^{off}}{G_{t=0}^{off}}\right|_{c_e,c_w} \approx -\left[\left(\frac{-\alpha_{e0}\left(1+\gamma_\alpha \exp(\beta_\alpha T)\right)}{kT}\right)\times\left(\frac{K_{e0}\left(1+\gamma_K \exp(\beta_K T)\right)}{1+K_{e0}c_e\left(1+\gamma_K \exp(\beta_K T)\right)}\right)\times\exp\left(\frac{-t}{Ae^{-E_a/RT}}\right)\right] \quad (7.45)$$

d) The effects of CO₂.

In the absence of a dynamic model of the response of the Pan sensors employed in the modelling of CO_2 to gases of this type, we can only conclude this model by combining the static expressions documented in section 7.3. The basic model is given by Equation 7.15, can be combined the Equations 7.16, 7.17 and 7.18 defining the effect of humidity on values of the parameters included in the model. The resultant expression models the effect of CO_2 and humidity on the response of Pan conducting polymer sensors,

$$\left.\frac{G_f-G_i}{G_i}\right|_{T,c_{co2}} = \frac{\left(\frac{\beta_S}{c_w}-\chi_S\right)\left(\frac{\beta_K}{c_w}+\chi_K\right)\left[c_{co2}-\beta_\alpha \ln c_w - \chi_\alpha\right]}{1+\left[\left(\frac{\beta_K}{c_w}+\chi_K\right)\left(c_{co2}-\beta_\alpha \ln c_w - \chi_\alpha\right)\right]} \quad (7.46)$$

The effect of temperature can be modelled by combining Equations 7.15, 7.19 and 7.20. This gives us the expression,

$$\left.\frac{G_f-G_i}{G_i}\right|_{c_{co2},c_w} = \frac{\left(\beta_S T^2+\chi_S T+S_0\right)\times\left(\beta_K T+K_0\right)\times\left(c_{co2}-\alpha\right)}{1+\left[\left(\beta_K T+K_0\right)\times\left(c_{co2}-\alpha\right)\right]} \quad (7.47)$$

_____

Equations 7.46 and 7.47 therefore model the effects of CO_2, humidity and temperature on Pan sensors.

7.6 Conclusion

In this chapter I have summarised the models of the response of conducting polymers to both an organic vapour and a gas. Where possible the models have been combined in order to produce final expressions describing the response of the conducting polymers. The final expressions for the response to ethanol vapour have been defined under different boundary conditions where two out of the three variables (i.e. temperature, humidity and ethanol concentration) have been kept constant. The effects of ethanol vapour on the response of the sensors at a constant humidity and temperature is described by Equations 7.32 to 7.35. Equations 7.36 to 7.39 describe the effects of humidity on the response of the polymers when exposed to a constant concentration of ethanol at a constant temperature. In order to combine these equations into a final model of the effects of both ethanol and humidity on the polymer response at a constant temperature, the models describing the effect of humidity and ethanol concentration on the time–constant of the sensors would have to be combined. The effect of temperature on the response of the sensors to a constant ethanol concentration at a constant humidity is given by Equations 7.40 to 7.45.

Due to some problems associated with the production of a chemical model of the interaction of Pan sensors and CO_2, an empirical model of this response has been postulated (Equation 7.15). This model gives good correlation to the experimental data and has been extended to include the effects of both humidity and temperature through

Equations 7.46 and 7.47. The development of a theoretical rather than empirical model will form the basis of some future research.

7.7 References

7.1   T. A. Skotheim (ed.), *Handbook of conducting polymers*, Dekker, New York, 1986.

7.2   N. Mott, *Metal–Insulator transitions,* Taylor and Francis Ltd, London, 1974.

7.3   J. Janata, *Microsensors based on modulation of work function, in Sensors and Sensory Systems for an Electronic Nose,* P. N. Bartlett and J. W. Gardner (eds.), Kluwer Academic Publishers, Dordrecht, 1992, 103-116.

7.4   J. V. Hatfield, J. A. Covington and J. W. Gardner, GasFETs incorporating conducting polymers as gate materials, *Proc. Int. Conf. Chemical Sensors, Beijing, China,* (1998).

7.5   P. N. Bartlett and S. K. Ling–Chung, Conducting polymer gas sensors, Part II: Response of polypyrrole to methanol vapour, *Sensors and Actuators,* **19**, (1989), 141-150.

7.6   P. W. Atkins, *Physical Chemistry (Fifth Edition),* Oxford University Press, London, 1994.

CHAPTER 8

Conclusions and Future Work

8.1 Research Procedure and Objectives

The general aim of the research undertaken for this study was the development of mathematical models that could be used in the characterisation of conducting polymer gas and vapour sensors. The modelling procedure has been divided into three sections: static modelling of the effect of vapours on polymers; static modelling of the effect of gases on polymers; and dynamic modelling of the effects of vapours on conducting polymer sensors. A final model of the response of the sensors combining all the research carried out in these areas has also been presented.

In order to systematically test the sensors an injection flow system was developed (Chapter 3). This system was modified from existing equipment that was designed specifically for the analysis of beers [8.1]. The modified system had a novel layout designed specifically for the controlled exposure of conducting polymer chemoresistive sensors to gases and vapours. The system was controlled using a high level graphical programming language, Labview® for Windows, Version 4.0. (National Instruments®). This was also a novel application of this type of Virtual Instrumentation.

A full analysis of a wide range of vapours and gases was beyond the scope of this thesis. Therefore examples of typical vapours and gases were employed for the

development of the mathematical models. An in–depth analysis of the effects of different types of gases and vapours is an area of particular interest and may form part of a future research initiative. Ethanol was chosen as the target vapour as it had previously demonstrated quick and reversible responses to the conducting polymers of interest [8.2, 8.3 and 8.4] and, being a polar molecule, its response may be related to water sensitivity. Ethanol is also an example of a Volatile Organic Compound. This group of environmental pollutants are of particular interest when monitoring air quality and have previously been detected using sophisticated and expensive Gas Chromatography (GC) equipment. A sensor system which can reproducibly detect, identify and quantify this type of pollutant without the use of GC equipment would be a significant improvement in this technology. Carbon dioxide (CO_2) was chosen as the example gas because of its importance as a greenhouse gas and also the difficulties associated with its detection. It was postulated that this gas would not effect the polymers in the same way as the vapour as it does not posses a polar structure. Therefore, other methods of interaction such as swelling or titration effects have to be postulated.

A full investigation into the range of polymers available cannot be undertaken in this study. Therefore the polymers investigated during the vapour experiments represented one of each of the available types of monomer: aniline; and pyrrole. The counter–ions were chosen to represent a five unit and ten unit chain length i.e.: pentane and decane sulfonic acid. The same types of polymer were employed during both the static and dynamic analysis of the ethanol response. During the static CO_2 experiments some examples of the types of polymers employed in the ethanol tests were used. However, the main polymers of interest in these tests were based on Pan butane sulfonic acid devices that had been grown in a mixture of sodium salt and sulphuric

acid. These polymers had then been soaked in a sodium hydrogen carbonate ($NaHCO_3$) solution. This was aimed at encouraging titration within the membrane, thus causing an ionic change the structure of the polymer on exposure to CO_2 resulting in a change in conductance. A summary of the number and type of sensor used in each of the experiments is shown in Table 8.1.

Table 8.1 A summary of the numbers and types of polymers employed for each of the experiments carried out during this study.

Polymer	Ethanol (Static Model)	Ethanol (Dynamic Model)	Carbon Dioxide (Static Model)
Ppy/PSA/H_2O	6 off	8 off	2 off
Ppy/DSA/H_2O	6 off	8 off	N/A
Pan/PSA/H_2O	6 off	8 off	2 off
Pan/DSA/H_2O	6 off	8 off	N/A
Pan/BSA (modified)	N/A	N/A	6 off

The static evaluation of the polymers was carried out using discrete silicon sensors [8.5]. This type of substrate and the manufacturing processes that are employed for sensor production achieved reproducible devices with extremely uniform electrode geometries. The steady–state model developed in Chapter 4 was based on a Langmuir adsorption isotherm which was employed to describe the reaction of a vapour with sites within the polymer membrane. This basic premise was extended to include the effects of both absolute humidity and temperature on the sensor characteristics. The effect of humidity was modelled by assuming direct competition between the target vapour and the water molecules for the available sites. However, extension of this competitive

_____

model to include temperature effects was found to be problematic. Alternative expressions that could be used for describing the effects of temperature were therefore developed. These were based on a variable range hopping model of the Mott kind [8.6] and purely empirical equations used to describe the responses obtained from the polymer. From this work we can therefore conclude that an isothermal competitive binding model can be applied to both pyrrole and aniline based conducting polymer sensors. However, further research is required in order to extend this model to include temperature effects on the device conductance and on the competition between the two types of vapour.

The static modelling of the effects of CO_2 was carried out on examples of both Ppy and Pan sensors. Modified Pan polymers that had been soaked in sodium hydrogen carbonate solution were also included in these experiments. The Ppy sensors demonstrated no response to the CO_2. However, the Pan and modified Pan sensors both showed large responses to low gas concentrations. A theoretical model examining the interaction between the polymers, water and the CO_2 was investigated. Although this model was based on the chemistry of the interaction between the species, fundamental inconsistencies between the model and the experimental data were observed. An empirical model of the response was therefore developed. This model demonstrated an improved correlation to the gathered data. The empirical model was then extended to include the effects of humidity and temperature on the response of the polymers to the CO_2.

The dynamic model of the effects of ethanol (Chapter 6), was based on the results obtained from experiments carried out on nominally identical polymers deposited over a range of electrode separations. From the data we were able to develop purely mathematical expressions that modelled the dynamic response characteristics of

the polymer membranes. Using these expressions we were able to investigate the dominating mechanisms of the polymers response, concluding that the Pan sensors were purely reaction–rate limited, but the Ppy sensors had a combination of reaction kinetics and diffusion that effected there response. The model was then used to predict that the electrode separation should have no effect of the magnitude of the static response of the membranes. This theory was tested against experimental results and demonstrated good agreement. The effects of both humidity and temperature on the dynamic response were also investigated with empirical models of their effect on the time–constant of the response postulated.

Finally, in Chapter 7 the static and dynamic models were combined in order to produce a final model of conductance in polymer membranes. This final model was separated into four sections: the effects of an organic vapour at a constant humidity and temperature; the effect of humidity on the response of the polymers when exposed to a consistent concentration of organic vapour at a constant temperature; the effect of temperature on the response of the polymers when exposed to a consistent concentration of organic vapour at a constant humidity; and the effects of a target gas on the response of conducting polymer films. Although parts of this model are based on purely empirical expressions the research objectives have been achieved with the development of this final model.

8.2 Application of Models in Gas/Vapour Sensing

The main application of this type of conducting polymer sensor is in electronic nose vapour and odour detection systems. Such a system would employ an array of sensors in order to detect and identify vapours, gases or odours using pattern recognition

techniques (electronic noses are discussed in more detail in Chapter 1). In general a gas identification or detection system would have to collect sensor outputs from a testing regime, execute any data processing algorithms required and then compare this information with a look–up table derived during the calibration of the instrument.

The calibration and data processing sections of the equipment therefore play an important role in the success or failure of instruments such as electronic noses. The calibration of each sensor element is usually carried out using a known gas or vapour under laboratory conditions controlling both the humidity and temperature of the samples. However, when an instrument is in use in the field, the target sample is rarely delivered in such a regulated manner. A wide variety of analyte concentrations can be encountered at a variety of temperatures and humidities all of which vary the response of the sensor elements from those demonstrated during calibration. This problem can be combated in three ways. Firstly, the sensor elements could be modified to reduce the effects of both water vapour and temperature on their response to the target component. This modification could be either in the chemistry of the active element, the design and layout of the sensors or by the employment of coatings and heaters on the sensors to manage their responses. A second option is to regulate the delivery of the test species so that the sensors always receive the gases or vapours at the same temperature and humidity. These conditions could be exactly the same as those employed during sensor calibration. In order to achieve this an odour delivery system would have to be incorporated with every electronic nose, making the advent of completely portable, hand–held instruments unlikely. Finally, the temperature and humidity could be measured using dedicated sensors. This information could be used in the data processing stage of the detection equipment to compensate the response of the sensors for comparison with the pre–calibrated look–up tables.

_____

Models such as those developed in this study can be used in all three of these stages for humidity and temperature compensation of the sensors. It is only through a better understanding of the mechanisms of interaction between the active membrane and vapours, gases or odours, particularly with reference to the effects of humidity and temperature, that improved sensors can be developed or modifications to existing technology can be achieved. The production of controlled delivery systems can be optimised to achieve the most appropriate responses from the sensors where such methods are employed. Finally, the most direct application of the models developed in this study is in the data processing stage of electronic noses. If the parameters associated with the physical characteristics of the polymers (such as binding constants and sensitivities) were discovered during the calibration of the active element, the mathematical expressions developed by this research could be employed to compensate for any variations of temperature or humidity of the samples being tested. This would be particularly useful in the application of electronic noses in areas such as on–line monitoring in factories, environmental pollution observations or any application where the system is likely to encounter variations in operating conditions.

8.3 Future Work

The possibilities for future work related to modelling the characteristics of conducting polymer sensors are immense. There are a variety of polymer types and deposition conditions that make a full characterisation of all those currently available an enormous task. A few of the areas that stimulate the most interest include the effects of different counter–ion lengths on the response of electrochemically deposited films. This subject has only briefly been covered in this study and requires far more attention. The

significance of varying the types of solution used during growth also requires some investigation, particularly with the advent of sensors specifically modified by their growth solution or by post–growth treatment (such as the CO_2 sensors discussed in Chapter 5).

Modelling the consequences of changing the physical properties of the polymers through their deposition conditions etc. is only one area of future interest. The effects of different types of vapour or gas on the polymers also requires further research. This study has only discussed the effects of ethanol vapour, water vapour and CO_2 on conducting polymer sensors. The interaction of a wide variety of other types of vapours and gases with the polymers must also be investigated. It is only through a knowledge of how different classes of gas and vapour effect conducting polymers and how this response can best be modelled that improvements in the application of this type of sensor technology to gas and vapour detection can be achieved.

From this work it has been shown that the response of conducting polymers to ethanol vapour can be modelled using a simple competitive binding theory. However, the extension of this work to include the temperature effects on the model has been problematic. There is certainly scope for further research into successful modelling of the characteristics of this type of polymer, particularly with the development of a model describing the effects of temperature on polymers. Ideally this model would be based on a physical or chemical theory rather than consisting of purely empirical expressions derived from experimental results.

It seems likely that future models of conduction will be based on modulations of the polymer's work function due to the exposure of gases and vapours. This type of theory will benefit from the interest currently being shown in the development of GasFET sensors [8.7 and 8.8]. However, the opportunities for the development of

_____

sensors that will provide an insight into the mechanisms of gas and vapour interaction are not only limited to this transistor technology. Transducers that probe a variety of the polymers physical characteristics during exposure to a range of gases and vapours can also be employed in the modelling process. Two particular attributes of interest are the mass and swelling of the membranes when exposed to a target analyte. Both of these characteristics of the polymer may provide further ammunition for the development of theoretical models of the interaction between the gas or vapour and the conducting membrane.

The research presented in my thesis has provided a theoretical insight into the mechanisms of gas and vapour interaction with conducting polymer films. A basic theory describing the interaction of a gas or vapour with the membrane has been proposed and tested using data obtained under a variety of conditions. The resulting expressions defining both the static and transient responses of the polymers can be employed in two fields. Firstly, the theory is a useful step in the continued research into the mechanisms of interaction between polymer sensors and their environment. This research will ultimately lead to models based on physiochemical properties of the polymers, not on purely empirical expressions. Secondly, models such as those developed in this research can be used in the application of conducting polymers to the identification and measurement of vapours or odours by compensating for changes in the test environment. Such expressions can be used to ameliorate the problems of temperature and humidity interference on the data processing algorithms and identification techniques employed by systems such as electronic noses.

8.4 References

_____

8.1   T. C. Pearce, Sensor–based machine olfaction: Instrumentation for the analysis

of beer, *Ph.D. Thesis, University of Warwick, UK,,* 1997.

8.2   P. N. Bartlett, P. B. M. Archer, and S. K. Ling–Chung, Conducting polymer gas

sensors. Part I: Fabrication and characterisation, *Sensors and Actuators*, **19**,

(1989), 125-140.

8.3   P. N. Bartlett and S. K. Ling–Chung, Conducting polymer gas sensors. Part II:

Response of polypyrrole to methanol vapour, *Sensors and Actuators*, **19**, (1989),

141-150.

8.4   P. N. Bartlett and S. K. Ling–Chung, Conducting polymer gas sensors. Part III:

Results for four different polymers and five different vapours, *Sensors and

Actuators*, **20**, (1989), 287-292.

8.5   A. C. Pike, Design of chemoresistive silicon sensors for applications in gas

monitoring, *PhD Thesis, University of Warwick, UK,* 1996

8.6   N. Mott, *Metal–Insulator transitions,* Taylor and Francis Ltd, London, 1974.

8.7   D. Blackwood and M. Josowicz, Work function and spectroscopic studies of

interactions between conducting polymers and organic vapours, *J. Phys. Chem.,*

95, (1991), 493-502.

8.8   J. V. Hatfield, J. A. Covington and J. W. Gardner, GasFETs incorporating

conducting polymers as gate materials, *Technical Digest of the Seventh Int.

Meeting on Chemical Sensors, Beijing, China,* (1998).

APPENDIX

Published Papers

1. *Eurosensors X, 8–11 September, 1996, Leuven, Belguim,* Dual resistance–mass polymeric sensor for improved gas sensing, P. Ingleby, J. A. Covington, J. W. Gardner and P. N. Bartlett.

2. *Eurosensors XII, 13–16 September, 1998, Southampton, UK,* Effect of micro–electrode geometry on the response of thin–film poly(pyrrole) and poly(aniline) chemoresistive sensors, P. Ingleby, J. W. Gardner and P. N. Bartlett.

3. J. W. Gardner, M. Vidic, P. Ingleby, A. C. Pike, J. E. Brignell, P. Scivier, P. N. Bartlett, A. J. Duke and J. M. Elliott, Response of a poly(pyrrole) resistive micro–bridge to ethanol vapour, *Sensors and Actuators B,* **48**, (1998) 289-295.